DEFECTS IN MUSCLE DIFFERENTIATION AND MATURATION AS PATHOGENIC CONTRIBUTORS TO MUSCULAR DYSTROPHY CAUSED BY LAMIN A/C MUTATIONS

A Dissertation

Presented to the Faculty of the Graduate School of

Cornell University

In Partial Fulfillment of the Requirements for the Degree of

Doctor of Philosophy

by

Ashley Joan Earle

May 2019

DEFECTS IN MUSCLE DIFFERENTIATION AND MATURATION AS PATHOGENIC CONTRIBUTORS TO MUSCULAR DYSTROPHY CAUSED BY LAMIN A/C MUTATIONS

Ashley Joan Earle, Ph. D.

Cornell University 2019

Laminopathies, a broad class of diseases that primarily impact mechanically active tissues such as cardiac and skeletal muscle, are caused by genetic mutations in the *LMNA* gene, which encodes for the Lamin A/C protein. Lamins A/C form a dense protein network on the inside of the inner nuclear membrane and perform diverse roles in the cell, ranging from structural support of the nucleus to chromatin organization and transcriptional regulation. Many of the *LMNA* mutations result in Emery-Dreifuss muscular dystrophy, which presents with muscle weakness, muscle wasting, and cardiac conduction defects that lead to pre-mature death. To date, Emery-Dreifuss muscular dystrophy remains incurable, and the disease mechanism incompletely understood.

In my doctoral work, I investigated three non-mutually exclusive hypotheses regarding the disease mechanism of Emery-Dreifuss muscular dystrophy: 1) disease causing *LMNA* mutations render the nuclear more susceptible to mechanical damage, resulting in cell death; 2) misregulation of myogenic differentiation leads to ineffective regeneration of muscle in response to injury; and 3) altered extracellular matrix structure

and composition, possibly due to disturbed gene expression, leads to exacerbation of the phenotype through a positive mechanotransduction feedback loop. Using *in vitro* and *in vivo* models of Emery-Dreifuss muscular dystrophy, I found that the nuclear damage hypothesis is a major contributor to disease progression. Functional loss of lamins A/C resulted in increased nuclear fragility and nuclear envelope rupture, leading to DNA damage and activation of DNA damage response pathways. Additional defects in later stages of muscle development, including muscle fiber maturation and hypertrophy, may further contribute to disease phenotype.

These insights provide important information on the impact of disease causing *LMNA* mutations and highlight DNA damage response pathways and muscle hypertrophy as key areas for potential treatment development.

BIOGRAPHICAL SKETCH

Ashley Earle (nee Kaminski), never one to choose a single focus, obtained her Bachelor of Science in Chemical Engineering and a Bachelor of Arts in International Studies from the Lafayette College in 2013. During her time there, she actively participated in research in cell-material interactions with Dr. Lauren Anderson. Growing up, Ashley was an avid dancer, but despite all her efforts, was constantly injured and had to have numerous rounds of surgeries. She decided in high school that she wanted to study diseases that negatively impacted the ability of kids, and adults, to walk, run and dance. She found the perfect fit in Dr. Jan Lammerding's laboratory at Cornell studying Emery-Dreifuss muscular dystrophy. Ashley's scientific research helped to show that later stages of muscle differentiation are severely disrupted in muscular dystrophy models. Through numerous fellowships, Ashley discovered her true passion was found in the classroom. She's participated actively in designing and developing a new Biomolecular Thermodynamics course with Dr. Jan Lammerding, as well as numerous teaching interventions aimed to enhance student participation with challenging material. After her PhD studies, Ashley will serve as a lecturer at York College of Pennsylvania in the Mechanical Engineering department.

Dedicated to Gloria Kaminski – who was planning my PhD before I could read or write.

ACKNOWLEDGMENTS

This work would not have been possible without the unwavering support of my advisor, Dr. Jan Lammerding. His dedication to his student's advancement in all areas: scientific, professional and personal have been instrumental to my success in more ways than I have comprehended at this moment. Jan, thank you for always reminding me that "work will be here when I get back," for letting me take chances and make mistakes in the classroom, and being my biggest advocate.

I would also like to thank my committee, Dr. Ben Cosgrove and Dr. Eve Donnelly for their support, advice, and encouragement throughout my PhD. All of the labs in the Weill Institute for Cell and Molecular Biology as well as the Meinig School of Biomedical Engineering have also helped greatly through scientific discussion and collaborations – especially the Bretscher lab, Schaffer-Nishimura lab, and Butcher lab, and of course the entire Lammerding lab. I specifically would like to acknowledge that this work would not have been possible without the help of Dr.'s Tyler Kirby and Greg Fedorchak. It has been a pleasure and joy to work with two dedicated and collaborative scientists – I have learned so much from both of you and thank you. To all of my undergraduate students: Felicia Sadikin, Jean Kwon, Rebecca Mount, Shweta Modi, Sushruta Iruvanti, Holly Zheng, and Alex Corbin – you have given me your time, and your trust, and I am forever grateful. My PhD, and the most important lessons I've learned from it, would not have been possible without you.

My educational research, and deep passion for teaching innovation, was sparked through my involvement with the NSF GK12 fellowship, the DOE GAANN fellowship, and the support and advice of the Cornell Center for Teaching Innovation, specifically Dr. Kim Williams. Thank you.

My husband, Greg, entered the crazy of PhD life after my candidacy exam and has stood by my side through all the ups and downs. I'll be trying to pay him back my whole life. My family has been my biggest cheerleaders though all my education – my parents, Walt and Paige, my brother Ben, my grandparents Walt and Gloria, and especially my Aunt Joan, who introduced me to science when I was just a kid. And to all of my friends, near and far, but especially Greg (and soon to be!) Krista Fedorchak, Jim and Liz Nichols, Emily Allen, and the members of Cornell's GCF, this journey would have not been the same without your love and constant prayer.

Glory to God for all things!

The end of a matter is better than its beginning;

a patient spirit is better than a proud spirit. – Ecc 7:8

TABLE OF CONTENTS

SUMMARY PAGE

Chapter 1: Mechanosensing and the Nucleus

The nucleus is the central hub of the genome, but is also involved in many cellular processes such as mechanotransduction, cellular migration, and others. Underlying the nuclear envelope is the nuclear lamina, a meshwork of intermediate filament proteins that binds to chromatin, transcription factors, and forms the foundation of the nucleus' connection to the cytoskeleton and extracellular matrix. Mutations in the nuclear lamina and other nuclear envelope proteins lead to multiple types of diseases that often effect mechanically active cells and tissues. This chapter explores the specific role of the nucleus in mechanotransduction and disease.

Chapter 2: Mutant lamins cause mechanically-induced nuclear envelope rupture and DNA damage due to forces of nuclear migration in muscle cells

Using three mouse models of muscle laminopathies, we found that *Lmna* mutations reduced nuclear stability and caused widespread nuclear damage in skeletal muscle cells *in vitro* and *in vivo*, including the formation of chromatin protrusions, transient rupture of the nuclear envelope, DNA damage, and activation of DNA damage response pathways. *In vitro*, nuclear damage resulted from nuclear movement in maturing myotubes, and could be reversed by depletion of kinesin-1 or stabilization of microtubules surrounding the myonuclei. Increased DNA damage, which is also increased in human patient samples, appears to be primarily due to continued damage events and not from major defects in repair.

Chapter 3: The *Lmna* H222P mutation causes severe fiber size misregulation in response to injury but normal myogenic transcription factor signaling

We conducted both short and long term studies of differentiation and regeneration of *Lmna* H222P myoblasts *in vitro* and *in vivo* using an injury model. Short term differentiation *in vitro* indicated only very minor defects in myogenic transcription factor signaling and nuclear positioning. To verify effective regeneration at long time scales, we performed muscle injury in *Lmna* H222P mice which showed no overt phenotype in Pax7+ cell self-renewal or muscle regeneration but did show a significant fiber diameter defect that could explain the muscle wasting phenotype in these mice.

Chapter 4: Investigating the role of extracellular matrix on disease progression in Emery-Dreifuss muscular dystrophy

We optimized a decellularization protocol to achieve whole, optically clear muscle tissues. Proteomic analysis showed some changes in ECM composition between *Lmna* null and WT tissue, but multi-photon imaging showed no overt changes in architecture. Growing cells on solubilized tissue derived muscle matrix highlighted cell intrinsic defects that were not rescuable by ECM.

Chapter 5: Evaluating Student Response and Efficacy of a Two-Stage Homework System using a Paper Based and Online Grading System

As part of BME 2110, Biomolecular Thermodynamics, I designed and implemented a two submission homework system that focused students on conceptual foundation

behind each problem and then provided feedback for them to submit a full mathematical solution. Most students felt that this system enhanced their understanding of the material, even though a transition to online grading and adding additional undergraduate teaching assistants and graders. Based on conceptual knowledge scores, students showed improvement between homework submissions that was sustained on the first exam but was less effective as the semester progressed. Introducing additional grader highlighted the need for clearer and stricter grading strategies to prevent student frustration from style and consistency issues among graders.

Chapter 6: A How to Guide and Template for Designing a Puzzle Based Escape Room Game

Designing valuable educational games takes extensive time and preparation. Most escape rooms that have been published require laboratory activities, making them suitable only for certain classes. This chapter describes and provides the materials that I developed for use in BME 2110 as a template for other educators to use to design their own games.

CHAPTER 1
MECHANOSENSING AND THE NUCLEUS[1]

The nucleus, often considered the "brain" of the cell, contains the cell's vast genome. The nucleus is primarily responsible for regulating gene expression, which in turn controls the instructions for protein synthesis. This transcriptional and translational mechanism enables cells to respond to mechanical, and other, stimuli. Initiating the appropriate mechano-response necessitates the nucleus correctly interpreting the type, duration, and magnitude of the signals it receives. Thanks to groundbreaking research conducted over the past three decades, much is known about how integrins and focal adhesions respond to substrate stiffness, strain, and other mechanical stimuli. For the nucleus, such insights are only beginning to emerge.

Although the specific function(s) of the nucleus in cellular mechanotransduction is still incompletely understood, it is well established that mutations in numerous nuclear envelope proteins cause both defects in mechanotransduction signaling and force transmission [1, 2]. These mutations can cause muscular dystrophy, dilated cardiomyopathy, partial familial lipodystrophy, cancer, and the accelerated aging disease Hutchinson-Gilford progeria syndrome, among others. Many of these diseases

[1]This chapter is a compilation of the following two published manuscripts:
Kaminski A*, Fedorchak GR*, Lammerding J. 2014, The cellular mastermind(?) - mechanotransduction and the nucleus, *Prog Mol Biol Transl Sci.* 126: 157-203. * these authors contributed equally.

Fedorchak GR, **Kaminski A**, Lammerding J. 2014, Cellular mechanosensing: Getting to the nucleus of it all, *Prog Biophys Mol Biol*. 115(2-3): 76-92.

are caused by mutations in a nuclear envelope protein, lamin A/C, which is encoded by the *LMNA* gene. To date, more than 450 disease-causing mutations have been discovered in the *LMNA* gene alone, with the vast majority of mutations affecting striated muscle, i.e., mechanically stressed tissues (http://www.umd.be/LMNA). In the case of the *LMNA* gene, the specific effects of subtle differences between these mutations on the resulting disease are fascinating. For instance, changing a single amino acid in lamin A/C at position 528 from threonine to lysine causes muscular dystrophy, while changing the identical amino acid position to methionine results in lipodystrophy symptoms [3, 4]. Equally interesting is the fact that similar disease phenotypes can often be caused by mutations in one of multiple proteins (e.g., mutations in either lamins, emerin, nesprins, or the cytoskeletal protein dystrophin all cause muscular dystrophy). This suggests that these proteins are all involved in similar cellular functions, e.g., force transmission, mechanical stability, or mechanotransduction, and highlights the importance of intact force transmission and mechanotransduction pathways in cellular function. An improved understanding of the role of the nucleus in mechanotransduction would not only lead to better insights into normal cell biology but may also pave the way for novel therapies for the many diseases caused by mutations in nuclear (envelope) proteins.

Overview of nuclear structure and organization

As the age old maxim goes, structure imparts function. Like a mechanic fixing a car without understanding how the engine is built and connected to the rest of the car, trying to decipher the role of the nucleus in mechanotransduction and disease necessitates an

understanding of nuclear structure and its connection to the cytoskeleton. Given the relevance to human disease, we restrict our discussion to mammalian cells. In eukaryotic cells, the nucleus not only houses the genome, but also transcriptional machinery, thus allowing it to act as the central processing center of incoming signals. The nucleus is typically the largest cellular organelle. It is separated from the surrounding cytoplasm by two lipid membranes and the underlying nuclear lamina meshwork which provides structural support. Together the membranes, lamina, and associated proteins make up the nuclear envelope, which also mechanically connects the cytoskeleton to the nuclear interior [5]. As the nucleus is substantially stiffer than the surrounding cytoplasm, the mechanical properties of the nucleus significantly contribute to the overall cell deformability and the transmission of forces across the cell. In the following, we provide a brief description of the structural and mechanical components of the cell nucleus, from the nuclear interior to the outer nuclear membrane and the proteins linking the nucleus to the cytoskeleton. These sections will illustrate that the nucleus is connected to the cellular environment by a continuous physical chain via the cytoskeleton, focal adhesions, and cell-cell junctions (**Figure 1.1**). Consequently, forces from the extracellular matrix, neighboring cells, and the cytoskeleton can be transmitted directly to the nucleus, where they can induce substantial structural changes [6].

Chromatin and chromosome territories

Long, contiguous DNA polymers are packaged into discrete units called chromosomes, which are made of chromatin, a fibrous combination of DNA and DNA-binding proteins. The most prominent of these proteins are histones; histone polypeptides

facilitate the efficient packing of two meters of human DNA into a ≈10 μm-diameter nucleus [7]. This stunning packaging is achieved by winding the DNA like thread around a histone spool. Histones H2A and H2B, and H3 and H4, unite as heterodimers to form octamer "beads" that are—together with the wound DNA—called nucleosomes. The odd-histone out, histone H1, helps link nucleosomes together and stabilize higher-order structures. Histones are well suited to transmit signals directly to the genome through a plethora of covalent biochemical modifications such as acetylation, phosphorylation, methylation, poly-ADP-ribosylation, ubiquination, and SUMOylation which affect the structure and transcriptional activity of chromatin without altering the DNA sequence [8, 9]. Broadly speaking, chromatin exists in two states, (1) the more transcriptionally active, more loosely organized euchromatin, which typically localizes to central regions of the nucleus, and (2) the transcriptionally inactive, more densely packed heterochromatin, which inhabits the nuclear periphery and the area surrounding nucleoli [10]. DNA-binding dyes such as DAPI or Hoechst stain compact heterochromatin brighter than its euchromatic counterpart. Euchromatin and heterochromatin can also be easily distinguished in transmission electron micrographs [7].

The differences in chromatin compaction have important implications for deformation under force. Studies on isolated nuclei have shown that the nuclear interior, chromatin in particular, substantially contributes to the mechanical property of the nucleus [11]. Both condensed and non-condensed chromatin behave as complex viscoelastic fluids but demonstrate plastic changes after ≈10 seconds of stress in micropipette aspiration experiments [12].

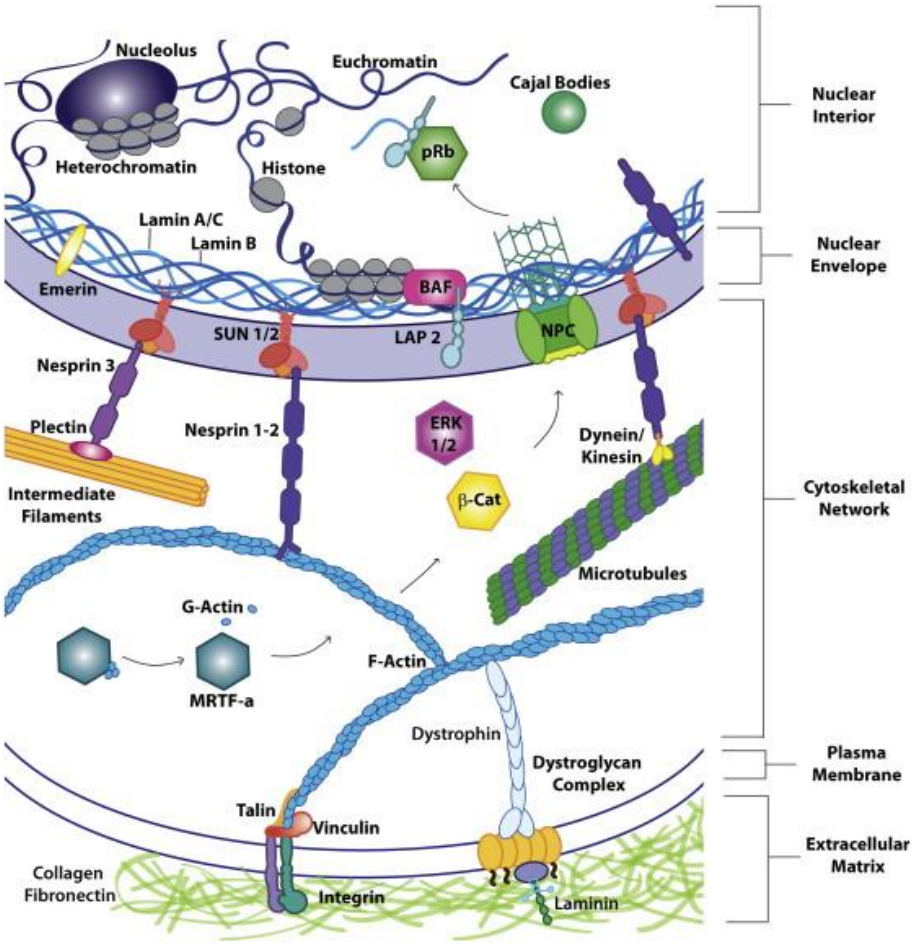

Figure 1.1 A 'direct connection' from the extracellular matrix (ECM) to the genome. Schematic illustration highlighting the (protein) elements that maintain the structural integrity of the cell, as well as some of the important signaling molecules and transcriptional regulators (ERK 1/2, β-catenin, nuclear, pRb) and intranuclear domains (nucleolus, Cajal bodies). Integrins at the plasma membrane connect the ECM to cytoskeletal filaments, which bind the nucleus through LINC complex proteins (nesprins and SUN proteins) and the nuclear lamina. The outer nuclear membrane (ONM), along with the 30–50 nm wide luminal space enclosed between the inner nuclear membrane (INM) and ONM, is continuous with the endoplasmic reticulum. Bridging the nuclear membranes are nuclear pores that allow for transport of large molecules, such as transcription factors or RNA, between the nucleus and the cytoplasm. Composed of both A- and B-type lamins, the lamina helps to tether heterochromatin, transcription factors, and nuclear membrane proteins to the nuclear periphery (Ho and Lammerding, 2012, Lin et al., 2000, Wilson and Foisner, 2010, Zuleger et al., 2012). This physical connectivity between nesprins, SUN-proteins, and the nuclear interior allows a direct route for mechanical signals to reach the nucleus and also impacts how biochemical signals traverse the cytoplasm and the nuclear envelope or interact with nuclear proteins once inside the nucleus. It is important to note that emerin and some nesprin isoforms can be found on both the INM and ONM (Salpingidou et al., 2007, Zhang et al., 2002); however, it remains unclear whether they fulfill distinct functions depending on their localization. Within the nesprin families, there are wide variations in size due to alternative splicing and transcriptional initiation, with the largest isoforms, referred to as nesprin1/2-giant, reaching ~800–1000 kD in size, which may enable them to reach as far as 1 μm into the cytoplasm (Rajgor et al., 2012).

In addition, condensed chromatin is substantially less deformable than non-condensed chromatin, [12] suggesting that the higher packing density limits further compaction. Importantly, the nucleoplasm is ≈2-to 10-times stiffer than the cytoplasm and resists further compression after being compacted more than 60% [13, 14], [15]. The "compression limit" is one contributor to chromatin's, and especially heterochromatin's, ability to bear up to 50% of the load applied to the nucleus, [12, 16] and may become highly relevant when cells must deform during migration through tight interstitial spaces [17]. These findings illustrate the interrelation between chromatin and nuclear mechanics, and may hint at mechanisms by which force induced changes in chromatin structure could contribute to nuclear mechanosensing.

The nucleoskeleton

For decades, researchers have sought to characterize the putative nucleoskeleton as either an active framework, a passive framework, or an artifact [18, 19]. The existence of simple, cell-free technologies to replicate and transcribe DNA proves that many of the quintessential functions of the nucleus can be carried out without higher order structures (i.e. nucleoskeletal elements). At the same time, a nucleoskeletal framework or scaffold could help organize chromosome territories as well as position the transcriptional machinery and regulatory complexes. Relating back to mechanosensing, a dynamic, well-networked nucleoskeleton has the potential to directly couple extracellular forces to the genome. A prominent class of nucleoskeletal proteins are lamins, which exist as both a solid-like meshwork at the periphery and may form stable structures with transcription factors and other molecules in the interior [20]. Lamins and their interaction

partners will be discussed in detail later.

In addition to specialized nuclear proteins, recent findings suggest that many proteins traditionally found in the cytoskeleton, such as spectrin II-alpha, titin, 4.1R, myosin, and actin, have roles in the nucleus as well [21, 22]. The organization of these proteins in the nucleus remains uncertain – they may form a structural scaffold throughout the nuclear interior, or they may form a peripheral network supporting the nuclear envelope [23]. Spectrin II-alpha and titin are cross-linking proteins known for their large size and elasticity. Consistent with these characteristics, nuclei that lack spectrin II-alpha have difficulty recovering from swelling and stretching [22]. Beyond its mechanical function, spectrin II-alpha is also important for DNA repair, [24] demonstrating how structural and regulatory roles often overlap in the nucleus [10, 22]. Titin, normally found in muscle sarcomeres, has been shown to also interact with lamins both *in vitro* and *in vivo*. Structurally, loss of titin results in large nuclear blebs [25]. The presence of actin in the nucleus, a once hotly-contested subject, is now widely accepted [26, 27]. Actin exists as either monomeric G-actin or polymeric F-actin and is ubiquitously-expressed in virtually all eukaryotic cells. In the nucleus, monomeric actin is highly active throughout transcription and has many interaction partners, including RNA polymerase I-III and certain transcription factors [26]. Exciting new fluorescent probes can now distinguish between monomeric (RPEL1 motif-probes) and filamentous (Lifeact-NLS and Utr230-based probes) nuclear actin in living cells, showing distinct localization patterns and kinetics of these molecules [26, 28]. Regardless of its structural role, F-actin assembly by formins or other actin nucleators [26] can control gene expression by freeing G-actin from

the transcription factor MKL1 and enabling it to activate serum response factor (SRF) target genes, or alternatively, through modulating histone-acetyltransferases [26].

Lamins, the nuclear lamina, and nuclear mechanics

Lamins and their associated proteins form a dense meshwork (nuclear lamina) along the inner nuclear membrane. The lamina interacts with inner nuclear membrane proteins, nuclear pore complexes, and the nuclear interior. Lamins are type V intermediate filaments that can be grouped into two classes: (1) A-type lamins, which are generated by alternatively splicing of the *LMNA* gene into lamin A and C and some less abundant isoforms, and (2) B-type lamins, which are encoded by the *LMNB1* and *LMNB2* genes, which produce lamin B1 and B2/B3, respectively [20]. While A-type lamins and lamins B1 and B2 are expressed in almost all somatic cells, lamin B3 expression is restricted to germ cells. Lamin A and B-type lamins undergo extensive posttranslational processing at the C-terminus, including farnesylation and endoproteolytic cleavage. B-type lamins remain permanently farnesylated and thus attached to the inner nuclear membrane, even during mitosis [29]. In contrast, lamin A undergoes an additional modification, where the protein Zmpste24 removes the farnesylated tail, resulting in mature lamin A. Lamin C, which has a distinct C-terminus, does not undergo the same processing and is not farnesylated [8]. Mature lamin A and lamin C, which lack the hydrophobic farnesyl tail, can be found both in the nucleoplasm and the nuclear lamina [30].

Lamins, which have a half-life of ≈13 hours, assemble into stable filaments [31]. They form parallel dimers through coiled-coil interaction of their central rod domains [20]. The

dimers associate head-to-tail and then laterally assemble in an anti-parallel fashion into non-polar filaments with a final diameter of about 10 nm. In transmission electron micrographs of mammalian cells, the nuclear lamina is visible as a 25–50 nm thick dense protein layer underneath the inner nuclear membrane [15, 32]. The higher order structure of lamins in somatic cells is not completely understood due to the tight association of the lamina with chromatin, which makes high resolution imaging challenging [33]. However, *Xenopus* oocytes do not pose the same challenges; electron micrographs in these cells show a lamin structure composed of a square lattice of ≈10-nm thick cross-linked filaments [33, 34]. Because of this, lateral interactions between dimers and proto-filaments are thought to be critical for maintaining the correct higher order structure. Based on mathematical modeling, correct coiling direction of the heptads appears to be important to allow for "unzipping" and subsequent attachment to adjacent strand [35]. Mutations could result in increased or decreased stability due to incorrect assembly and/or binding [36]. It is important to note that these ideas await experimental confirmation. Intriguingly, although different lamin isoforms can all interact and form heteropolymers *in vitro*, they typically segregate into homopolymers and form distinct, but overlapping, networks *in vivo* [37-40].

Although there are still some questions about the filament and structural assembly of the lamina *in vivo*, the importance of nuclear lamins in contributing to nuclear stiffness and stability has been unequivocally established. Based on micropipette aspiration experiments on isolated *Xenopus* oocyte nuclei, which can be osmotically swollen to separate the chromatin from the nuclear lamin, the lamin network has an elastic modulus

of ≈25 mN/m [41]. For comparison, the plasma membrane of neutrophils has an elastic modulus of ≈0.03 mN/m and chondrocyte and endothelial cell membranes have a modulus of ≈0.5 mN/m [42]. Using a variety of experimental approaches, the stiffness of the nucleus has been determined to be 2- to 10-times stiffer than the surrounding cytoplasm, depending on the particular cell-type and measurement method [14, 43, 44]. When comparing the lysis strain of the nuclear envelope (i.e., the the nuclear lamina and the nuclear membranes) with that of a simple double lipid membrane to distinguish the contribution of the nuclear lamina, the lysis strain of the nuclear envelope was 12-fold higher than that of the standard double membrane system, highlighting the stabilizing impact of the nuclear lamina [41]. Similarly, when a fluorescent dye is injected into the nucleus of living cells, cells that lack lamins A/C show dramatically increased rates of nuclear rupture compare to wild-type cells [45].

Given this important role of lamins in conferring structural integrity to the nucleus, what is the contribution of the different types of lamins to nuclear mechanics? While B-type lamins are nearly ubiquitously and uniformly expressed among different cell-types and tissues, lamin A/C expression is highly tissue-specific. For instance, muscle cells and other mesenchymal cells typically are among the highest in A-type lamin expression levels [46, 47]. A recent study found that the ratios of A-type to B-type lamins in different tissues closely correlates with the tissue stiffness suggesting a mechanosensitive regulation of lamin levels,[46] which could help protect the nucleus from mechanical stress by increasing mechanical stability [45]. In cells that express both A-type and B-type lamins, lamins A and C are the major contributors to nuclear stability, with B-type

lamins having a smaller role in overall nuclear stiffness [48]. Nonetheless, there may be some functional redundancy between lamins regarding mechanical properties. For instance, introducing lamin B into lamin A-null cells can partially rescue mechanical defects [38, 49]. Furthermore, B-type lamins are important for nuclear anchoring to the cytoskeleton, particularly during neuronal migration/development in the brain, as these cells lack A-type lamins [50-53].

Similarly, embryonic stem cells do not express A-type lamins until they begin to differentiate. Once they decrease their stemness, their nuclear stiffness increases up to 6-fold compared to the undifferentiated state. This is most likely due to the increased levels of lamins A/C in the new lineage and possibly changes in chromatin configuration [12, 47]. A few specialized differentiated cells, notably neutrophils and neurons, hardly express any A-type lamins even after differentiation [52, 54]. The lack of A-type lamins in embryonic stem cells, neutrophils, and neurons may facilitate migration, enabling these cells to travel through dense tissues and interstitial spaces during development and inflammation [55]. For example, the decrease in lamin A/C levels along with the concomitant increase in expression of lamin B receptor (LBR) during granulopoiesis promotes the distinct highly lobulated nuclear shape of mature neutrophils [13]. In addition, the low levels of lamin A result in a highly deformable nucleus allowing neutrophils to easily squeeze through small spaces [13]. Similarly, regulation of lamin A/C levels may also regulate trafficking and lineage maturation of other hematopoietic cells types [56].

In addition to changes in lamin expression, posttranslational modifications of lamins may further affect nuclear mechanics. Lamins are phosphorylated during mitosis, causing them to become soluble and disperse into the cytoplasm [30, 57]. Because farnesylation and phosphorylation of lamins changes their solubility, interaction, and localization, these posttranslational modification may also offer cells a way to dynamically adjust their nuclear stiffness in response to mechanical stimuli [46].

Lamin Binding Proteins

Beyond their direct structural role, lamins bind many different proteins, including transcriptional regulator, histones, and several inner nuclear membrane proteins (**Figure 1.2**). Lamin binding partners include LBR, nesprins, SUN proteins, and members of the LEM-domain protein family, which comprises LAP2, Emerin, and MAN1 proteins [58, 59]. In the absence of lamins, many of the lamin binding proteins become mislocalized. This has severe consequences for force propagation across the nuclear envelope (see below) and mechanotransduction signaling. The LEM-domain proteins share a conserved ~40 amino acid sequence that allows them to bind BAF (Barrier to Autointegration Factor), a protein with roles in nuclear organization and DNA bridging [60, 61]. BAF helps to recruit lamin A and stabilize emerin at the nuclear envelope in addition to maintaining heterochromatin [62, 63]. The LEM-domain proteins have additional binding partners that could affect mechanotransduction signaling. Broadly, LAP2, emerin, and MAN1 all interact with GCL, a transcriptional repressor. Emerin is particularly interesting in this regard because it competitively binds BAF and GCL [64]. Mutations in LEM domain proteins can cause changes in downstream BAF signaling,

but can also disrupt additional signaling pathways such as TGF-β and Wnt signaling, as will be discussed in detail later [65, 66].

Lamins can also directly connect to the genome by binding DNA and histones [59, 67]. The areas of the genome that are bound to the nuclear lamina are called Lamina-Associated Domains (LADs) and are often transcriptionally repressed heterochromatin. In addition, lamins also directly bind to numerous transcriptional factors such as extracellular-signal-regulated kinases 1 and 2 (ERK1/2), retinoblastoma protein pRb (RB1), Fos, sterol regulatory element-binding protein-1 (SREBP1) and MOK2, among others [67-70]. Of note is that phosphorylated Rb, one proposed regulator of lamin expression, can also directly bind lamins (together with LAP2α), suggesting a potential feedback loop. Some of these factors, such as ERK1/2 and c-Fos, have well established roles in mechanotransduction signaling. For a detailed discussion of lamin binding partners and their function, we refer to a recent review by Simon and Wilson [8].

Nuclear Membranes and nuclear pore complexes

Adjacent to the nuclear lamina and forming a barrier to the surrounding cytoplasm are the inner nuclear membrane and the outer nuclear membrane. The latter is continuous with the endoplasmic reticulum (ER), a large intracellular membrane system. The space enclosed by the inner and outer nuclear membranes is the ≈30–50 nm wide luminal or perinuclear space. Proteins in the inner nuclear membrane can interact with, and be retained, by the underlying lamina and nuclear interior. In the absence of these

interactions, as in the case of lamin A/C-deficient cells, the inner nuclear membrane proteins can diffuse into the outer nuclear membrane at the nuclear pores, where the membranes converge, and then further into the ER. Similarly, proteins in the outer nuclear membrane are often retained there by their interaction with inner nuclear membrane proteins and can be mislocalized to the ER if this interaction is lost [71]. At least 74 membrane proteins specific to the nuclear envelope have been identified to date, conferring a variety of often tissue-specific functions from import and export, chromatin anchoring and regulation, and nucleo-cytoskeletal coupling [72, 73].

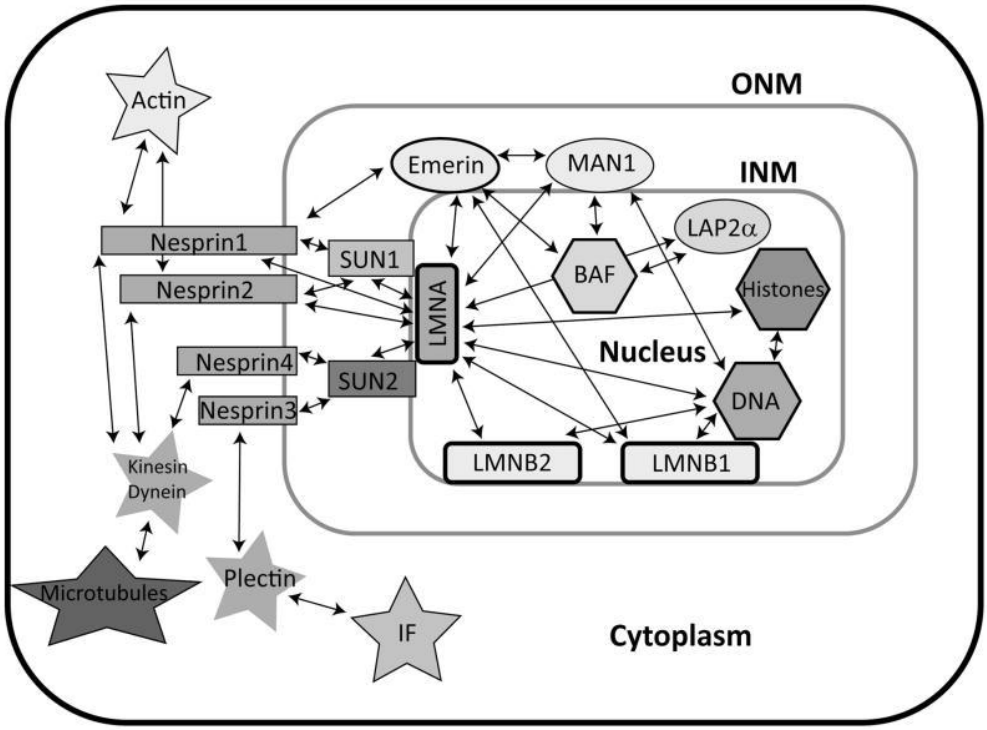

Figure 1.2 Nuclear envelope protein binding partners. Lamins associate with numerous proteins/structures in the nuclear interior and the nuclear membranes, thereby modulating intracellular force propagation and mechanotransduction signaling. Many of the lamin-binding proteins also bind to each other, creating a complex network of interactions. Please note that additional interactions may exist. In addition, many of the nuclear envelope proteins also bind a variety of transcriptional regulators not included in the figure. Stars = cytoskeletal elements; rectangles = LINC complex proteins; rounded rectangles = lamins; ellipses = LEM-domain proteins; hexagons = chromatin-associated elements. IF: Intermediate Filaments.

Nuclear pores help to regulate the active transport of large molecules (larger than ≈40 kDa) into and out of the nucleus. Ions and small molecules can passively diffuse through the membranes or the nuclear pores. Nuclear pore complexes are highly structured, symmetric channels that are regularly spaced along the nuclear envelope. This spatial regulation is likely due to interactions with the nuclear lamina, because loss of lamins can result in clustering of nuclear pore complexes [74]. Nuclear pore complex components interact with a larger number of proteins at the nuclear envelope (e.g., lamins, SUN proteins) and the nuclear interior [75, 76]. Recent evidence suggests that proteins typically associated with the nuclear pore complex proteins can also be found deep inside the nuclear interior, where they may play a role in transcriptional regulation [9, 10].

LINC Complex

The lamina is connected to the cytoskeleton by the Linker of Nucleoskeleton and Cytoskeleton (LINC) complex, which spans both the inner and outer nuclear membrane to transmit forces across the nuclear envelope (**Figure 1.1**). LINC complex consists of SUN proteins at the inner nuclear membrane and KASH-domain proteins at the outer nuclear membrane. The LINC complex proteins are highly conserved across organisms and their vertebrate names are a combination of the names originally given in *C. elegans*, *D. melanogaster*, and *S. pombe*. The SUN (Sad-1/UNC-84) proteins bind to the lamina and the SUN domain occupies the perinuclearspace. There are two SUN proteins in somatic cells, SUN1 and SUN2, which have distinct but overlapping functions.[77] Three additional SUN proteins, SUN3–5, are only expressed in male germline cells [78]. All SUN proteins are composed of an N-terminal nucleoplasmic

domain, a transmembrane domain, and a luminal coiled-coil rod domain that ends in a trimeric, SUN-domain head [79]. The main difference between SUN1 and -2 and the germline SUN proteins is the length of the rod domain [79].

The trimeric C-terminal of the SUN proteins binds up to three KASH (Klarsicht/ANC-1/Syne homology) peptides, which make up the luminal C-terminus (and the transmembrane domain) of the aptly named KASH-domain proteins. The first four KASH-domain family members are referred to as nesprins (nuclear envelope spectrin repeat proteins), each consisting of several isoforms resulting from alternative splicing or initiation [80]. Historically, nesprin-1 and -2 were named Enaptin and NUANCE, respectively. Some nesprins were also referred to as SYNEs (synaptic nuclear envelope proteins), because of their presence in myonuclei at neuromuscular junctions [81]. A fifth family member, KASH5, is germ cell specific and lacks the name-sake spectrin repeats of nesprins [82]. Nesprins-1, -2, and -3 are generally widely expressed, and at least one nesprin isoform is found in all cell-types [83]. In contrast, nesprin-4 expression is specific to secretory epithelial cells. On the cytoplasmic side, nesprins can interact with all major cytoskeletal structures. The largest isoforms of nesprin-1 and -2 directly bind to actin and nesprins-1 and -2 also bind to kinesin and dynein; nesprin-3 engages intermediate filaments via plectin; nesprin-4 connects to the microtubule network via kinesin-1 (**Figure 1.1**) [84-87]. The large, "giant", nesprin isoforms are found on the outer nuclear membrane, while smaller nesprin isoforms like nesprin-1α and nesprin-2β also localize to the inner nuclear membrane and bind lamins [86, 88, 89].

The integrity of the LINC complex and cytoskeletal filaments is needed to support intracellular force transmission to the nucleus. LINC complex disruption causes changes in both the nuclear and cytoskeletal morphology, including loss of the actin and vimentin network surrounding the nucleus [90, 91]. Depletion of LINC complex components, or expression of dominant negative nesprin constructs, results in altered nuclear cross-sectional area and an increase in nuclear height. This is presumably due to loss of cytoskeletal tension or compression acting on the nucleus [92]. In additional to changes in nuclear morphology, down regulation of nesprin-1 also increases focal adhesion strength, potentially in an attempt to balance the forces normally distributed to the nucleus. In addition to these findings, many other groups have demonstrated the effect of the LINC complex on nuclear morphology based on substrate stiffness, 2-D versus 3-D microenvironment, and under strain [93-97].

In many ways, the LINC complexes appear analogous to the focal adhesion complexes at the plasma membrane, which help transmit forces from the cellular environment to the cytoskeleton and are also involved in mechanosensing [98]. Comparing the current view of the simple LINC complex structure with the complex structure and interaction of focal adhesion complexes and the many associated proteins, it becomes apparent that there is still much work that needs to done to better understand nucleo-cytoskeletal coupling. As of now, there are a few other proteins that are known to help control the interaction between nesprins and SUN-proteins. Samp1 was recently identified as a LINC complex-associated protein that interacts with SUN1 and aids in nuclear positioning [99, 100]. Torsin-A appears to be another potential regulator of SUN-nesprin

interaction, [101] but much remains to be uncovered about how binding between SUN-proteins and nesprins is controlled. Furthermore, there are still many questions regarding the formation, maintenance, and regulation of LINC complexes, especially in response to mechanical stimuli. For example, does the same principle of concurrent inside-out and outside-in signaling that governs cell adhesion also apply to the LINC complex? And which other proteins could be involved in such regulation or potential mechanosensing?

Mechanotransduction signaling in the nucleus

When force is exerted on a cell, it is propagated through the various intracellular structural scaffolds. Along the way, the force causes mechanosensitive proteins to change conformation, resulting in exposure of cryptic binding sites, phosphorylation of specific residues, and/or altered binding affinities and interaction partners. Ultimately, many of the mechanically induced signaling pathways converge on the nucleus and involve the import/export of transcription factors, their interaction with co-factors, and changes in chromatin organization (**Figure 1.3**) [102]. Recent findings suggest that many of the involved pathways directly or indirectly interact with nuclear (envelope) proteins, as discussed in detail below. Consequently, the role of the nucleus in mechanotransduction is not limited to direct mechanosensing; it also includes the modulation of biochemical signals arriving at the nucleus.

MAPK/ERK/Fos

One of the most prevalent and best characterized responses to mechanical stress is the

phosphorylation of proteins, which leads to changes in their binding affinities and often triggers further downstream signaling. The mitogen activated protein kinase (MAPK) pathway mediates cellular reactions to stress and growth factors by regulating differentiation, apoptosis and inflammation [103]. There are multiple distinct MAP kinases, including ERK1/2, p38, JNK, and ERK3-5. The first three constitute particularly important branches of the MAPK pathway in cellular mechanotransduction [104]. Intriguingly, recent findings have implicated lamins A/C and emerin in causing impaired MAPK signaling resulting in cardiac and skeletal muscle disease. Patient samples carrying different *LMNA* mutations responsible for dilated cardiomyopathy have an increase in phosphorylated ERK and JNK in the nucleus [105]. Cardiomyocytes from mouse models that have either a lamin A/C mutation (*Lmna* H222P) or lack emerin also have enhanced ERK1/2 signaling [106, 107]. Surprisingly, emerin and lamin mutations appear to have somewhat different effects. While the Lmna H222P mutation affects the JNK branch, loss of emerin does not[89,90]. Both, however, have similar effects on the ERK1/2 branch. In addition, p38 phosphorylation is shown to be increased in cardiac tissue samples from laminopathy patients [108, 109]. Lastly, lamin A/C- and emerin-deficient fibroblasts subjected to cyclic strain respond with decreased expression of the mechanosensitive genes *egr-1* and *iex-1*, which are downstream targets of the MAPK pathway [45, 110].

At least some of the effects of lamin mutations on MAPK signaling may be attributed to the direct interaction of lamin A/C with c-Fos; when ERK1/2 enters the nucleus, it displace c-Fos by binding to lamins and becomes transcriptionally active (**Figure 1.3**)

[111]. Although this mechanism had not been definitively confirmed, there are multiple reports supporting it. For instance, cells with mutated lamins have normal activation of ERK1/2 in the cytoplasm but decreased expression of downstream genes [45, 112, 113].

Wnt signaling

Wnt signaling is important for multiple developmental processes such as axis patterning, as well as differentiation, proliferation and migration.[114] Wnt has been shown to be modulated by mechanical forces in bone cell differentiation [115]. There are three Wnt pathways, the canonical Wnt pathway, which involves translocation of the transcriptional co-activator β-catenin from the cytoplasm and cell-cell adhesions to the nucleus, and two non-canonical pathways. Importantly, β-catenins can directly interact with several nuclear envelope proteins. At the nuclear envelope, emerin is responsible for nuclear export of β-catenin, so cells lacking emerin or lamins A/C show enhanced growth and proliferation due to β-catenin accumulation in the nucleus (**Figure 1.3**) [66]. Furthermore, nesprin-2 can interact with α-catenin, together with emerin and β-catenin [116]. Recently, it has been proposed that nesprin-2, α-catenin, emerin and β-catenin form a complex that recruits β-catenin to the perinuclear region and facilitates its nuclear import, as β-catenin lacks a nuclear localization sequence [117]. This mechanism could explain why depletion of nesprin-2 reduces levels of nucleoplasmic β-catenin [116]. Other potential effects of altered Wnt signaling include impaired fibronectin and Col11A1 synthesis, which could affect cellular mechanosensing at the plasma membrane [118].

TGF-β and Smad signaling

Transforming growth factor beta (TGF-β) stimulates cell proliferation, extracellular matrix synthesis and degradation, as well as aspects of embryogenesis and wound healing [117, 119]. TGF-β expression levels have been shown to directly correlate with mechanical loading in tendons and to be activated downstream of integrin-mediated contraction in myofibroblasts [120, 121]. Binding of TGF-β to its receptor on the plasma membrane induces formation of a receptor ligand complex and activation of the cytoplasmic receptor kinase domain, which results in phosphorylation of Smads, transcription factors that translocate from the cytoplasm into the nucleus, where they activate transcription of TGF-β target genes. There are three different kinds of Smads; regulating Smads (R-Smads), Co-Smads, and inhibitory Smads. The nuclear envelope LEM domain protein MAN1 binds R-smads in a manner that also regulates BMP and activin signaling in addition to TGF-β [122]. R-Smads bound to Co-Smads are transcriptionally active and enter the nucleus. MAN1 breaks this complex apart by selectively binding to R-Smads, promoting nuclear export of the Smads and resulting in attenuation of TGF-β signaling (**Figure 1.3**) [123]. In addition to MAN1, lamin A/C regulates TGF-β signaling by modulating the phosphorylation of Smads in a mechanism that involves lamin-bound PP2, a nuclear phosphatase [124, 125]. The role of lamins A/C and emerin in modulating Smad activity may be particularly relevant for muscle tissue, because TGF-β1 stimulates satellite cell differentiation. Disruption of this pathway by lamin or emerin mutation may contribute to impaired muscle regeneration.

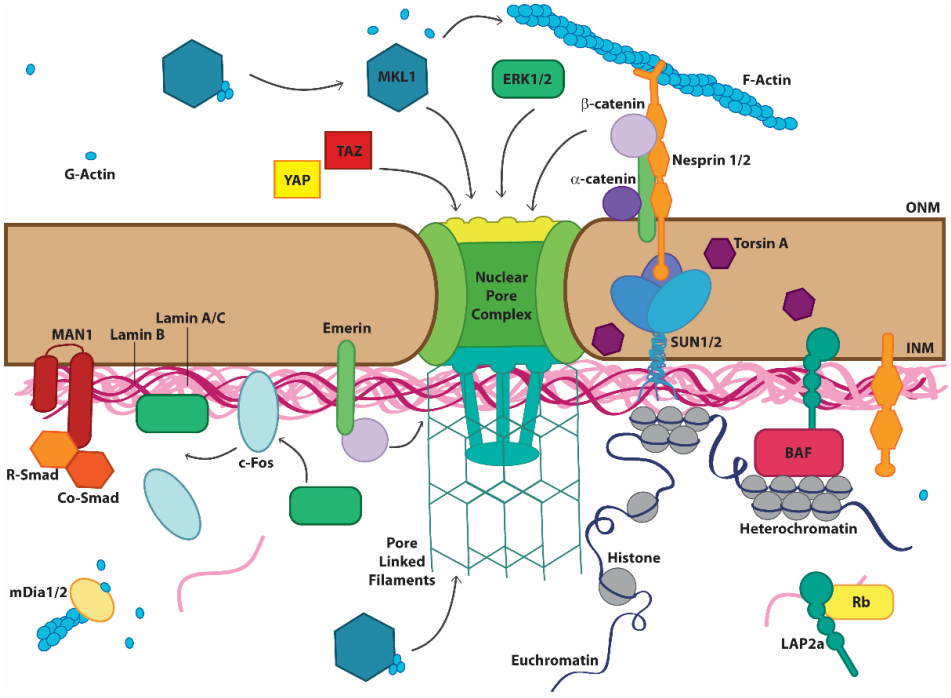

Figure 1.3. **Nuclear envelope connectivity and signaling**. Schematic overview of signaling pathways (MKL1/SRF, MAPK and ERK1/2, YAP/TAZ, TGF-β, and Wnt) associated with nuclear envelope proteins.

MKL1/SRF signaling

The serum response factor (SRF) transcription factor and its co-factor, megakaryocytic acute leukemia (MKL1, also known as MAL or myocardin-related transcription factor-A (MRTF-A)), control a large number of genes involved in growth factor response, cytoskeletal remodeling (e.g., vinculin, actin, and actin binding proteins), and muscle-specific functions such as myoblast fusion and differentiation [126]. The MKL1/SRF pathway is highly sensitive to changes in actin dynamics [127]. MKL1 is normally sequestered in the cytoplasm through interactions with G-actin's three RPEL motifs. This prevents importin dimers from binding with a bipartite NLS signal in the regulatory domain of MKL1 [126, 128]. Serum- or mechanically induced polymerization of actin

releases G-actin from MKL1 and allows the translocation of MKL1 to the nucleus, where it, together with SRF, activates SRF/MKL1 target genes (**Figure 1.3**). Recent studies illustrate the importance of this pathway in diseases affecting mechanically-stressed tissues, particularly cardiac and skeletal muscle. For example, MKL regulates the fibrotic repair gene program in injured cardiac tissue following myocardial infarction, [129] and SRF-null mice develop severe cardiac defects [129].

A recent study revealed a novel mechanism by which nuclear envelope proteins can affect actin dynamics and MKL1/SRF signaling.[130] Lamin A/C mutations are shown to displace emerin from the inner nuclear membrane, thereby leading to disturbed actin polymerization and impaired nuclear import and increased nuclear export of MKL1. This causes decreased nuclear localization of MKL1 and reduced expression of MKL1/target genes *in vitro* and *in vivo.*[130] This effect was attributed to the ability of emerin to bind and polymerize actin,[131] but it remains unclear to what extent emerin at the inner nuclear membrane and its effect on nuclear actin, versus emerin on the outer nuclear membrane and its effect on cytoskeletal actin[132] contributes to this mechanism.

YAP/TAZ signaling

Recent findings indicate that the YAP/TAZ pathway, traditionally considered to be a component of the Hippo pathway, can operate independently to mediate the cellular response to mechanical cues [133, 134]. YAP/TAZ activation is particularly sensitive to substrate stiffness and cytoskeletal tension, resulting in an increased presence of YAP/TAZ in the nucleus when cells are grown on stiffer substrates that promote cell

spreading [133, 134]. Unlike the SRF pathway discussed above, YAP/TAZ shows nuclear accumulation in response to cell spreading, whereas SRF shows a decrease in activity [133]. In addition, SRF is responsive to F-/G-actin ratios, but this metric has no effect on YAP/TAZ activity. While lamin A/C overexpression decreases YAP1 levels and nuclear localization, the exact interplay between lamins and YAP/TAZ signaling remains unresolved. Interestingly, expression of YAP1 and its binding partners did not scale with the stiffness of the corresponding tissue [46].

Interaction of Retinoblastoma protein, lamins A/C, and LAP2α

Retinoblastoma protein (Rb) is part of the E2F pathway and helps to regulate cell cycle progression and differentiation [135]. Nuclear accumulation of Rb is present in proliferating cells. LAP2α and lamin A/C bind to RB and halt cell cycle progression; when LAP2α is depleted, cells continue to proliferate, preventing differentiation of stem cells [136, 137]. Similarly, lamin A/C has been shown to play a role in cell cycle regulation; lamin A/C null cells show decreased proliferation with impacts in tissue regeneration [138]. This defect is rescued by LAP2α knockdown [138]. Recently, Rb has been proposed to act as a potential regulator of lamin expression levels, but the mechanistic details remain to be determined [46].

Functional consequences of impaired mechanotransduction and disease

As illustrated by the above sections, proper mechanosensing and mechanotransduction signaling is essential for numerous cellular functions. Both the external mechanical input, as well as the integrity of the internal connectivity, can affect nuclear morphology,

mechanosensing, and transcription. Mutations in nuclear envelope proteins and disturbed expression of nuclear proteins can thus have severe functional consequences, resulting in a variety of human diseases. Therefore, it is crucial to understand how mechanical forces affect the cell, both the structurally and by rerouting its signaling pathways. This is especially true for mechanically active tissue such as skeletal and cardiac muscle which is primarily affected in many of the pathologies resulting from defects in nuclear (envelope) proteins. Beyond the immediate effects of disturbed protein function, the mechanical microenvironment is implicated in several other diseases, such as cancer, where changes in the mechanical environment are thought to contribute to the disease progression, or vascular disease, where plaques often form at sites of perturbed fluid shear stress [104]. An improved understanding of the underlying disease mechanisms is critical for developing therapeutic approaches. In particular, it is important to distinguish which of the following scenarios constitutes the primary disease driver: (1) changes in the mechanical environment, in which cellular mechanotransduction signaling functions normally but responds to an altered input; (2) physical defects in cellular structure, resulting in altered force transmission, mechanosensing, and/or direct physical damage in response to mechanical stress; or (3) altered mechanotransduction signaling. Only the third scenario is readily amenable to pharmaceutical intervention with small molecules to restore normal signaling.

In the following, we highlight some of the diseases that can be caused by mutations in nuclear envelope proteins such as lamins A/C and emerin as examples of how defects in nuclear envelope proteins can affect cellular mechanics and mechanotransduction.

What is particularly perplexing about the large number of diseases resulting from mutations in nuclear envelope proteins is that although the implicated proteins are almost ubiquitously expressed throughout the body, many of the diseases primarily affect skeletal and cardiac muscle and tendons. Several hypotheses have been proposed to explain these tissue-specific effects. One hypothesis is the 'structural hypothesis' – loss of protein function causes nuclear fragility, rupture and death. This mechanism helps to explain the progressive nature of many of the laminopathies, especially in mechanically stressed tissues. Another hypothesis is that of disturbed gene regulation – mutations in nuclear envelope proteins affect their (tissue-specific) binding partners and lead to altered gene expression. Another, related hypothesis is that the mutations alter the ability for stem cells to differentiate and decrease their self-renewal capacity, thereby causing defects in the maintenance and repair of tissues [139]. Importantly, these hypotheses are not mutually exclusive, and the specific disease mechanism probably lies at an intersection of these propositions.

Muscular Dystrophy

The discovery that mutations in the nuclear envelope protein emerin cause Emery-Dreifuss muscular dystrophy was one of the main motivators for studying nuclear structure and mechanics [140]. To date, the nuclear envelope proteins lamin A/C, emerin, nesprin1/2, and SUN1 have all been linked to Emery-Dreifuss muscular dystrophy [3, 89, 140]. Emery-Dreifuss muscular dystrophy presents with early contractures, humero-peroneal weakness, and cardiac conduction defects, although overall the disease is less severe than Duchenne muscular dystrophy, which is caused by mutations in the

dystrophin gene [141]. Muscle biopsies from patients with Emery-Dreifuss muscular dystrophy often show highly fragmented nuclei [66]. Another signature of muscular dystrophy is the mislocalization of the nucleus in muscle fibers, with cells lacking lamins or nesprins showing loss of myonuclei from the neuromuscular junction, suggestive of defects in anchoring of the nucleus to the cytoskeleton [142-144]. Impaired nucleo-cytoskeletal coupling and disrupted force transmission between the cytoskeleton and nucleus has also been reported in fibroblasts expressing lamin A/C mutations responsible for muscular dystrophies [36, 145]. A detailed analysis comparing a large set of lamin A/C mutations found that mutations that cause striated muscle disease often lead to impaired lamin assembly, reduced nuclear stability, and impaired nucleo-cytoskeletal coupling, while mutations that cause familial partial lipodystrophy have no effect on nuclear stability [36].

Importantly, cells lacking lamins A/C or emerin have severe defects in several mechanotransduction pathways *in vitro* and *in vivo*, including failure to adequately activate expression of the mechanosensitive genes *Egr-1* and *Iex-1* [45, 48, 146] and in the translocation of MKL1 to the nucleus [130, 131]. However, it remains to be established whether the defects in mechanotransduction signaling are caused by altered nuclear mechanics and impaired force transmission to the nucleus or primarily represent disturbed interactions between lamins/emerin and binding partners involved in transcriptional regulation. Regardless of the mechanism, the impaired mechanotransduction signaling may not only weaken muscle adaptation to mechanical stress [146] but could also affect appropriate stem cell differentiation, as lineage commitment is strongly modulated by cells sensing their mechanical environment [147].

Dilated Cardiomyopathy

While dilated cardiomyopathy is often associated with muscular dystrophy, some lamin A/C mutations also cause cardiomyopathies without affecting skeletal muscle [1]. Dilated cardiomyopathy is characterized by progressive weakening of the heart muscles, thinning of the left ventricle wall, and insufficient pumping that typically leads to heart failure [148]. Dilated cardiomyopathy is the most prevalent disease caused by mutations in *LMNA* but can also be caused by mutations in emerin, nesprin-1 and -2, LUMA, an inner nuclear membrane protein that binds emerin, and LAP2α [1, 149]. Many of the disease mechanisms may mirror those for muscular dystrophy described above, and it remains unclear why/how some mutations specifically affect cardiac but not skeletal muscle. Possible explanations include cell-type specific differences in (mechanotransduction) signaling pathways or the fact that skeletal muscle has a higher potential for repair and regeneration compared to cardiac tissue. Recently, animal studies have produced promising evidence that blocking hyperactive MAPK signaling can significantly delaying the development of cardiomyopathy and prolong survival in mice expressing lamin or emerin mutations [108, 109, 150-152].

Hutchinson-Gilford progeria syndrome

Hutchinson-Gilford progeria syndrome (HGPS) is a premature aging disease that results from the build-up of progerin, a mutant form of lamin A with a 50 amino acid deletion in the tail domain that leads to permanent farnesylation and membrane accumulation [153]. Children with HGPS appear normal at birth, but soon begin to present with stunted growth, thinned skin, hair loss, atherosclerosis and cardiac defects; patients typically

die from heart attacks and strokes in their early teens [154, 155] HGPS cells have stiffer nuclei and are more prone to mechanically induced damage when stretched or squeezed through narrow constrictions [156-158]. In addition to increased sensitivity to mechanical stress, cells from HGPS patients display impaired proliferation in response to strain, altered extracellular matrix synthesis, and disturbed Wnt signaling, which may provide a mechanism explaining the predominance of vascular disease in HGPS [118, 157]. Currently, clinical trials aimed at blocking accumulation of progerin at the nuclear envelope by treatment with farnesylatransferase inhibitors, statins, and bisphosphonates are ongoing and have provided some encouraging findings, but it remains to be seen whether the beneficial results can be attributed to the drugs' effects on lamin farnesylation or other molecular targets [159].

Conclusions

Since the discovery of the first mutations in nuclear envelope proteins as cause for muscular dystrophy 20 years ago, research on nuclear mechanics and nuclear mechanotransduction has been a rapidly growing field (**Figure 1.4**). In the last decade alone, many details have emerged on the role of lamins in conferring nuclear stability, the 3-D organization of chromatin, and the molecular details involved in transmitting forces between the cytoskeleton and nuclear interior, not to mention the growing number of mutations, diseases, and binding partners associated with nuclear envelope proteins. Nonetheless, the opening question—what exactly is the role of the nucleus in mechanosensing and mechanotransduction signaling—has not yet been completely answered.

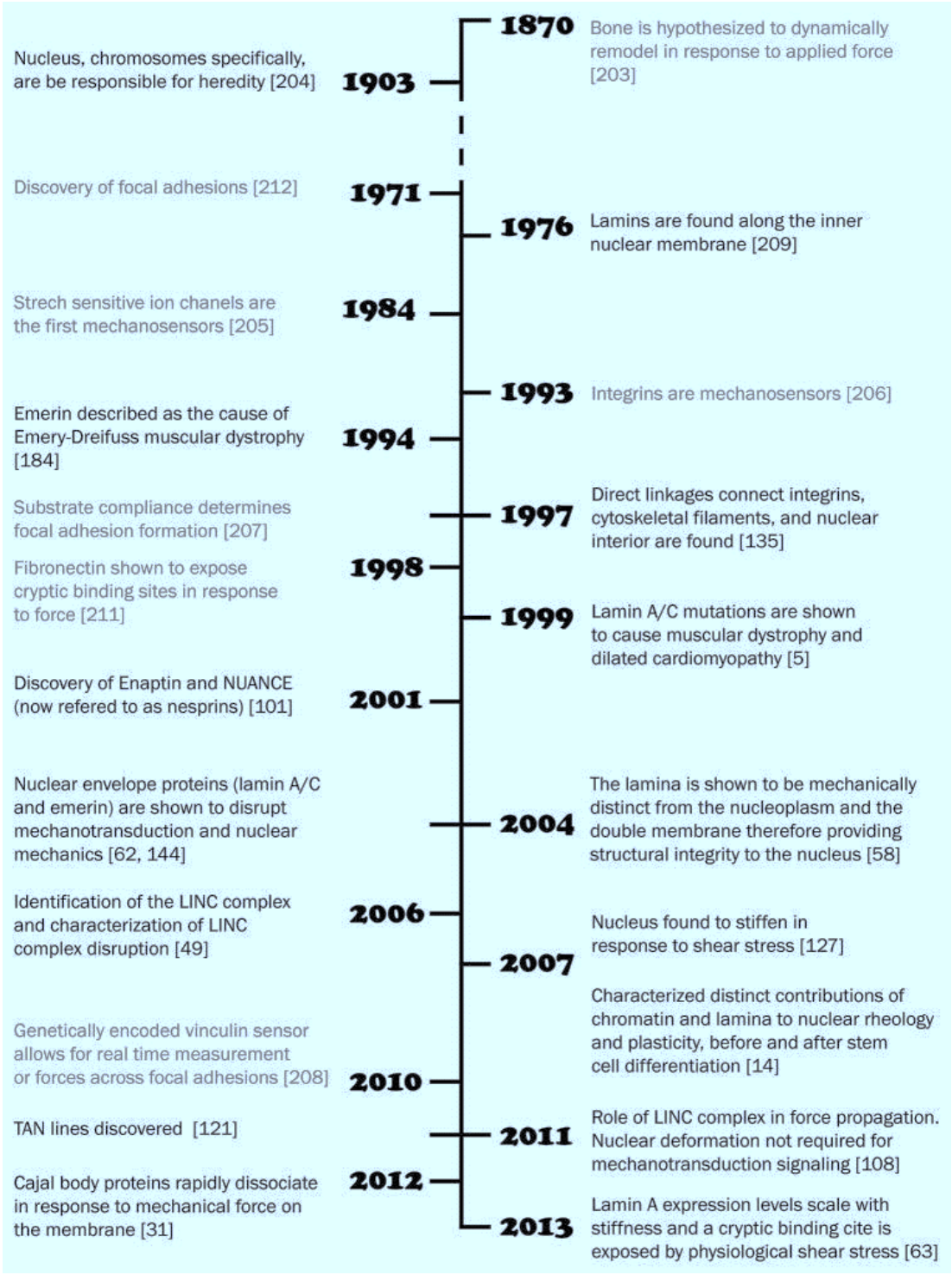

Figure 1.4: **Timeline of (nuclear) mechanotransduction discoveries.** Roadmap of selected milestones in the field of mechanobiology that have paved the way for our current understanding of the role of the nucleus in mechanotransduction. Discoveries most relevant to nuclear mechanotransduction are printed in bold.

Increasing evidence suggests that external force application can lead to direct changes in chromatin organization and dissociation of protein complexes in subnuclear structures, but insights into mechanistic details and functional consequences are still lacking. Undoubtedly, the direct physical connection of the nucleus to the cytoskeleton and the cellular exterior provides a means for physical forces to propagate through the cell and results in nuclear deformation, which may ultimately cause changes in chromatin organization and mediate transcriptional regulation. Concurrently, many nuclear envelope proteins play a crucial role in correctly interpreting mechanically induced biochemical signals that originated in the cytoplasm. Mutations in these proteins, including lamins, emerin, and nesprin, therefore not only affect force transmission to the nucleus and potential nuclear mechanosensing, but also disturb biochemical pathways independent of immediate structural changes to the nucleus, which may further affect gene expression, differentiation, and proliferation. Lastly, the example of impaired MKL1 activity in lamin A/C-deficient cells due to emerin mislocalization illustrates how tightly some of these ideas are interconnected. Going forward, new experimental techniques to probe deeper into associations between the nuclear envelope, the nucleoskeleton and the genome are expected to elicit many of the mechanistic details currently lacking. Ultimately, insights gained from these studies will not only enhance our understanding of normal cellular processes and mechanotransduction but may also provide important novel therapeutic targets for diseases ranging from deafness to muscular dystrophy, heart disease, and cancer.

REFERENCES

1. Schreiber, K.H. & Kennedy, B.K. When Lamins Go Bad: Nuclear Structure and Disease. *Cell* **152**, 1365-1375 (2013).
2. Zwerger, M., Ho, C.Y. & Lammerding, J. Nuclear mechanics in disease. *Annual review of biomedical engineering* **13**, 397-428 (2011).
3. Bonne, G. *et al.* Mutations in the gene encoding lamin A/C cause autosomal dominant Emery-Dreifuss muscular dystrophy. *Nature Genetics* **21**, 285-288 (1999).
4. Savage, D.B. *et al.* Familial partial lipodystrophy associated with compound heterozygosity for novel mutations in the LMNA gene. *Diabetologia* **47**, 753-756 (2004).
5. Crisp, M. *et al.* Coupling of the nucleus and cytoplasm role of the LINC complex. *The Journal of cell biology* **172**, 41-53 (2006).
6. Wang, N., Tytell, J.D. & Ingber, D.E. Mechanotransduction at a distance: mechanically coupling the extracellular matrix with the nucleus. *Nature Reviews Molecular Cell Biology* **10**, 75-82 (2009).
7. Martins, R.P., Finan, J.D., Guilak, F. & Lee, D.A. Mechanical regulation of nuclear structure and function. *Annual review of biomedical engineering* **14**, 431 (2012).
8. Simon, D.N. & Wilson, K.L. Partners and post-translational modifications of nuclear lamins. *Chromosoma*, 1-19 (2013).
9. Kouzarides, T. Chromatin modifications and their function. *Cell* **128**, 693-705 (2007).
10. Simon, D.N. & Wilson, K.L. The nucleoskeleton as a genome-associated dynamic'network of networks'. *Nature Reviews Molecular Cell Biology* **12**, 695-708 (2011).
11. Dahl, K.N., Engler, A.J., Pajerowski, J.D. & Discher, D.E. Power-law rheology of isolated nuclei with deformation mapping of nuclear substructures. *Biophysical journal* **89**, 2855-2864 (2005).
12. Pajerowski, J.D., Dahl, K.N., Zhong, F.L., Sammak, P.J. & Discher, D.E. Physical plasticity of the nucleus in stem cell differentiation. *Proceedings of the National Academy of Sciences* **104**, 15619-15624 (2007).
13. Rowat, A.C. *et al.* Nuclear envelope composition determines the ability of neutrophil-type cells to passage through micron-scale constrictions. *Journal of Biological Chemistry* **288**, 8610-8618 (2013).
14. Guilak, F. & Mow, V.C. The mechanical environment of the chondrocyte: a biphasic finite element model of cell-matrix interactions in articular cartilage. *Journal of Biomechanics* **33**, 1663-1673 (2000).
15. Versaevel, M., Riaz, M., Grevesse, T. & Gabriele, S. Cell confinement: putting the squeeze on the nucleus. *Soft Matter* (2013).
16. Mazumder, A. & Shivashankar, G.V. Emergence of a prestressed eukaryotic nucleus during cellular differentiation and development. *Journal of the Royal Society Interface* **7**, S321-S330 (2010).

17. Wolf, K. *et al.* Physical limits of cell migration: Control by ECM space and nuclear deformation and tuning by proteolysis and traction force. *Journal of Cell Biology* **201**, 1069-1084 (2013).
18. Cook, P.R. THE NUCLEOSKELETON - ARTIFACT, PASSIVE FRAMEWORK OR ACTIVE-SITE. *Journal of Cell Science* **90**, 1-6 (1988).
19. Dahl, K.N. & Kalinowski, A. Nucleoskeleton mechanics at a glance. *Journal of cell science* **124**, 675-678 (2011).
20. Ho, C.Y. & Lammerding, J. Lamins at a glance. *Journal of cell science* **125**, 2087-2093 (2012).
21. Castano, E. *et al.* Actin complexes in the cell nucleus: new stones in an old field. *Histochemistry and Cell Biology* **133**, 607-626 (2010).
22. Zhong, Z.X., Wilson, K.L. & Dahl, K.N. Beyond Lamins: Other Structural Components of the Nucleoskeleton, in *Nuclear Mechanics and Genome Regulation*, Vol. 98. (ed. G.V. Shivashankar) 97-119 (Elsevier Academic Press Inc, San Diego; 2010).
23. Dahl, K.N., Ribeiro, A.J. & Lammerding, J. Nuclear shape, mechanics, and mechanotransduction. *Circulation research* **102**, 1307-1318 (2008).
24. McMahon, L.W., Sangerman, J., Goodman, S.R., Kumaresan, K. & Lambert, M.W. Human alpha spectrin II and the FANCA, FANCC, and FANCG proteins bind to DNA containing psoralen interstrand cross-links. *Biochemistry* **40**, 7025-7034 (2001).
25. Zastrow, M.S., Flaherty, D.B., Benian, G.M. & Wilson, K.L. Nuclear titin interacts with A- and B-type lamins in vitro and in vivo. *Journal of Cell Science* **119**, 239-249 (2006).
26. Grosse, R. & Vartiainen, M.K. To be or not to be assembled: progressing into nuclear actin filaments. *Nature Reviews Molecular Cell Biology* **14**, 693-697 (2013).
27. Nürnberg, A., Kitzing, T. & Grosse, R. Nucleating actin for invasion. *Nature Reviews Cancer* **11**, 177-187 (2011).
28. Belin, B.J., Cimini, B.A., Blackburn, E.H. & Mullins, R.D. Visualization of actin filaments and monomers in somatic cell nuclei. *Molecular Biology of the Cell* **24**, 982-994 (2013).
29. Rober, R.A., Weber, K. & Osborn, M. DIFFERENTIAL TIMING OF NUCLEAR LAMIN A/C EXPRESSION IN THE VARIOUS ORGANS OF THE MOUSE EMBRYO AND THE YOUNG ANIMAL - A DEVELOPMENTAL-STUDY. *Development* **105**, 365-378 (1989).
30. Ottaviano, Y. & Gerace, L. PHOSPHORYLATION OF THE NUCLEAR LAMINS DURING INTERPHASE AND MITOSIS. *Journal of Biological Chemistry* **260**, 624-632 (1985).
31. Eden, E. *et al.* Proteome Half-Life Dynamics in Living Human Cells. *Science* **331**, 764-768 (2011).
32. Crisp, M. *et al.* Coupling of the nucleus and cytoplasm: role of the LINC complex. *The Journal of Cell Biology* **172**, 41-53 (2006).

33. Aebi, U., Cohn, J., Buhle, L. & Gerace, L. THE NUCLEAR LAMINA IS A MESHWORK OF INTERMEDIATE-TYPE FILAMENTS. *Nature* **323**, 560-564 (1986).
34. Goldberg, M.W., Huttenlauch, I., Hutchison, C.J. & Stick, R. Filaments made from A- and B-type lamins differ in structure and organization. *Journal of Cell Science* **121**, 215-225 (2008).
35. Gangemi, F. & Degano, M. Disease-associated mutations in the coil 2B domain of human lamin A/C affect structural properties that mediate dimerization and intermediate filament formation. *Journal of Structural Biology* **181**, 17-28 (2013).
36. Zwerger, M. *et al.* Myopathic lamin mutations impair nuclear stability in cells and tissue and disrupt nucleo-cytoskeletal coupling. *Human Molecular Genetics* (2013).
37. Kapinos, L.E. *et al.* Characterization of the head-to-tail overlap complexes formed by human lamin A, B1 and B2 "half-minilamin" dimers. *Journal of molecular biology* **396**, 719-731 (2010).
38. Zuela, N., Bar, D.Z. & Gruenbaum, Y. Lamins in development, tissue maintenance and stress. *EMBO reports* (2012).
39. Shimi, T. *et al.* The A-and B-type nuclear lamin networks: microdomains involved in chromatin organization and transcription. *Genes & development* **22**, 3409-3421 (2008).
40. Kolb, T., Maass, K., Hergt, M., Aebi, U. & Herrmann, H. Lamin A and lamin C form homodimers and coexist in higher complex forms both in the nucleoplasmic fraction and in the lamina of cultured human cells. *Nucleus-Austin* **2**, 425-433 (2011).
41. Dahl, K.N., Kahn, S.M., Wilson, K.L. & Discher, D.E. The nuclear envelope lamina network has elasticity and a compressibility limit suggestive of a molecular shock absorber. *Journal of cell science* **117**, 4779-4786 (2004).
42. Hochmuth, R.M. Micropipette aspiration of living cells. *Journal of Biomechanics* **33**, 15-22 (2000).
43. Caille, N., Thoumine, O., Tardy, Y. & Meister, J.J. Contribution of the nucleus to the mechanical properties of endothelial cells. *Journal of Biomechanics* **35**, 177-187 (2002).
44. Kha, H.N., Chen, B.K., Clark, G.M. & Jones, R. Stiffness properties for Nucleus standard straight and contour electrode arrays. *Medical Engineering & Physics* **26**, 677-685 (2004).
45. Lammerding, J. *et al.* Lamin A/C deficiency causes defective nuclear mechanics and mechanotransduction. *Journal of Clinical Investigation* **113**, 370-378 (2004).
46. Swift, J. *et al.* Nuclear lamin-A scales with tissue stiffness and enhances matrix-directed differentiation. *Science* **341**, 1240104 (2013).
47. Stewart, C. & Burke, B. TERATOCARCINOMA STEM-CELLS AND EARLY MOUSE EMBRYOS CONTAIN ONLY A SINGLE MAJOR LAMIN POLYPEPTIDE CLOSELY RESEMBLING LAMIN-B. *Cell* **51**, 383-392 (1987).

48. Lammerding, J. *et al.* Lamins A and C but not lamin B1 regulate nuclear mechanics. *Journal of Biological Chemistry* **281**, 25768-25780 (2006).
49. Chen, H., Chen, X. & Zheng, Y. The nuclear lamina regulates germline stem cell niche organization via modulation of EGFR signaling. *Cell stem cell* **13**, 73-86 (2013).
50. Ji, J.Y. *et al.* Cell nuclei spin in the absence of lamin B1. *Journal of Biological Chemistry* **282**, 20015-20026 (2007).
51. Jung, H.J. *et al.* Farnesylation of lamin B1 is important for retention of nuclear chromatin during neuronal migration. *Proceedings of the National Academy of Sciences of the United States of America* **110**, E1923-E1932 (2013).
52. Jung, H.J., Lee, J.M., Yang, S.H., Young, S.G. & Fong, L.G. Nuclear Lamins in the Brain - New Insights into Function and Regulation. *Molecular Neurobiology* **47**, 290-301 (2013).
53. Coffinier, C., Fong, L.G. & Young, S.G. LINCing lamin B2 to neuronal migration Growing evidence for cell-specific roles of B-type lamins. *Nucleus-Austin* **1**, 407-411 (2010).
54. Olins, A.L. *et al.* Nuclear envelope and chromatin compositional differences comparing undifferentiated and retinoic acid- and phorbol ester-treated HL-60 cells. *Experimental Cell Research* **268**, 115-127 (2001).
55. Friedl, P., Wolf, K. & Lammerding, J. Nuclear mechanics during cell migration. *Current opinion in cell biology* **23**, 55-64 (2011).
56. Shin, J.-W. *et al.* Lamins regulate cell trafficking and lineage maturation of adult human hematopoietic cells. *Proceedings of the National Academy of Sciences* **110**, 18892-18897 (2013).
57. Kuga, T., Nozaki, N., Matsushita, K., Nomura, F. & Tomonaga, T. Phosphorylation statuses at different residues of lamin B2, B1, and A/C dynamically and independently change throughout the cell cycle. *Experimental Cell Research* **316**, 2301-2312 (2010).
58. Wilson, K.L. & Berk, J.M. The nuclear envelope at a glance. *Journal of cell science* **123**, 1973-1978 (2010).
59. Lin, F. *et al.* MAN1, an inner nuclear membrane protein that shares the LEM domain with lamina-associated polypeptide 2 and emerin. *Journal of Biological Chemistry* **275**, 4840-4847 (2000).
60. Lee, K.K. & Wilson, K.L. in Symposia of the Society for Experimental Biology 329-339 (2003).
61. Margalit, A., Brachner, A., Gotzmann, J., Foisner, R. & Gruenbaum, Y. Barrier-to-autointegration factor - a BAFfling little protein. *Trends in Cell Biology* **17**, 202-208 (2007).
62. Haraguchi, T. *et al.* BAF is required for emerin assembly into the reforming nuclear envelope. *Journal of Cell Science* **114**, 4575-4585 (2001).
63. Margalit, A., Segura-Totten, M., Gruenbaum, Y. & Wilson, K.L. Barrier-to-autointegration factor is required to segregate and enclose chromosomes within the nuclear envelope and assemble the nuclear lamina. *Proceedings of the National Academy of Sciences of the United States of America* **102**, 3290-3295 (2005).

64. Dorner, D., Gotzmann, J. & Foisner, R. Nucleoplasmic lamins and their interaction partners, LAP2 alpha, Rb, and BAF, in transcriptional regulation. *Febs Journal* **274**, 1362-1373 (2007).
65. Lin, F., Morrison, J.M., Wu, W. & Worman, H.J. MAN1, an integral protein of the inner nuclear membrane, binds Smad2 and Smad3 and antagonizes transforming growth factor-beta signaling. *Human Molecular Genetics* **14**, 437-445 (2005).
66. Markiewicz, E. *et al.* The inner nuclear membrane protein Emerin regulates beta-catenin activity by restricting its accumulation in the nucleus. *Embo Journal* **25**, 3275-3285 (2006).
67. Wilson, K.L. & Foisner, R. Lamin-binding Proteins. *Cold Spring Harbor Perspectives in Biology* **2**, 17 (2010).
68. Rodriguez, J. *et al.* ERK1/2 MAP kinases promote cell cycle entry by rapid, kinase-independent disruption of retinoblastoma-lamin A complexes. *Journal of Cell Biology* **191**, 967-979 (2010).
69. Moiseeva, O., Bourdeau, V., Vernier, M., Dabauvalle, M.C. & Ferbeyre, G. Retinoblastoma-independent regulation of cell proliferation and senescence by the p53-p21 axis in lamin A/C-depleted cells. *Aging Cell* **10**, 789-797 (2011).
70. Lloyd, D.J., Trembath, R.C. & Shackleton, S. A novel interaction between lamin A and SREBP1: implications for partial lipodystrophy and other laminopathies. *Human Molecular Genetics* **11**, 769-777 (2002).
71. Zuleger, N., Kerr, A.R.W. & Schirmer, E.C. Many mechanisms, one entrance: membrane protein translocation into the nucleus. *Cellular and Molecular Life Sciences* **69**, 2205-2216 (2012).
72. Schirmer, E.C., Florens, L., Guan, T.L., Yates, J.R. & Gerace, L. Nuclear membrane proteins with potential disease links found by subtractive proteomics. *Science* **301**, 1380-1382 (2003).
73. de las Heras, J.I., Batrakou, D.G. & Schirmer, E.C. Cancer biology and the nuclear envelope: A convoluted relationship. *Seminars in Cancer Biology* **23**, 125-137 (2013).
74. Sullivan, T. *et al.* Loss of A-type lamin expression compromises nuclear envelope integrity leading to muscular dystrophy. *Journal of Cell Biology* **147**, 913-919 (1999).
75. Lu, W.S. *et al.* Sun1 forms immobile macromolecular assemblies at the nuclear envelope. *Biochimica Et Biophysica Acta-Molecular Cell Research* **1783**, 2415-2426 (2008).
76. Lombardi, M.L. & Lammerding, J. Keeping the LINC: the importance of nucleocytoskeletal coupling in intracellular force transmission and cellular function. *Biochemical Society Transactions* **39**, 1729-1734 (2011).
77. A., R., T., S. & U., K. LINCing complex functions at the nuclear envelope: What the molecular architecture of the LINC complex can reveal about its function. Nucleus 2013; 4:11 - 10; PMID: 23324460; http://dx.doi.org10.4161/nucl.23387. *Nucleus* **4** (2013).

78. Fridkin, A., Penkner, A., Jantsch, V. & Gruenbaum, Y. SUN-domain and KASH-domain proteins during development, meiosis and disease. *Cellular and Molecular Life Sciences* **66**, 1518-1533 (2009).
79. Sosa, B.A., Kutay, U. & Schwartz, T.U. Structural insights into LINC complexes. *Current Opinion in Structural Biology* **23**, 285-291 (2013).
80. Mellad, J.A., Warren, D.T. & Shanahan, C.M. Nesprins LINC the nucleus and cytoskeleton. *Current Opinion in Cell Biology* **23**, 47-54 (2011).
81. Apel, E.D., Lewis, R.M., Grady, R.M. & Sanes, J.R. Syne-1, a dystrophin- and klarsicht-related protein associated with synaptic nuclei at the neuromuscular junction. *Journal of Biological Chemistry* **275**, 31986-31995 (2000).
82. Morimoto, A. *et al.* A conserved KASH domain protein associates with telomeres, SUN1, and dynactin during mammalian meiosis. *Journal of Cell Biology* **198**, 165-172 (2012).
83. Rajgor, D. & Shanahan, C.M. Nesprins: from the nuclear envelope and beyond. *Expert reviews in molecular medicine* **15**, e5 (2013).
84. Zhang, Q.P. *et al.* Nesprins: a novel family of spectrin-repeat-containing proteins that localize to the nuclear membrane in multiple tissues. *Journal of Cell Science* **114**, 4485-4498 (2001).
85. Wilhelmsen, K. *et al.* Nesprin-3, a novel outer nuclear membrane protein, associates with the cytoskeletal linker protein plectin. *The Journal of cell biology* **171**, 799-810 (2005).
86. Zhang, Q.P., Ragnauth, C., Greener, M.J., Shanahan, C.M. & Roberts, R.G. The nesprins are giant actin-binding proteins, orthologous to Drosophila melanogaster muscle protein MSP-300. *Genomics* **80**, 473-481 (2002).
87. Roux, K.J. *et al.* Nesprin 4 is an outer nuclear membrane protein that can induce kinesin-mediated cell polarization. *Proceedings of the National Academy of Sciences of the United States of America* **106**, 2194-2199 (2009).
88. Wheeler, M.A. *et al.* Distinct functional domains in nesprin-1 alpha and nesprin-2 beta bind directly to emerin and both interactions are disrupted in X-linked Emery-Dreifuss muscular dystrophy. *Experimental Cell Research* **313**, 2845-2857 (2007).
89. Zhang, Q.P. *et al.* Nesprin-1 and -2 are involved in the pathogenesis of Emery-Dreifuss muscular dystrophy and are critical for nuclear envelope integrity. *Human Molecular Genetics* **16**, 2816-2833 (2007).
90. Lu, W. *et al.* Nesprin interchain associations control nuclear size. *Cellular and Molecular Life Sciences* **69**, 3493-3509 (2012).
91. Lombardi, M.L. *et al.* The interaction between nesprins and sun proteins at the nuclear envelope is critical for force transmission between the nucleus and cytoskeleton. *Journal of Biological Chemistry* **286**, 26743-26753 (2011).
92. Chancellor, T., Lee, J., Thodeti, C.K. & Lele, T. Actomyosin tension exerted on the nucleus through nesprin-1 connections influences endothelial cell adhesion, migration, and cyclic strain-induced reorientation. *Biophysical journal* **99**, 115-123 (2010).

93. Lovett, D.B., Shekhar, N., Nickerson, J.A., Roux, K.J. & Lele, T.P. Modulation of Nuclear Shape by Substrate Rigidity. *Cellular and Molecular Bioengineering*, 1-9 (2013).
94. Tamiello, C. *et al.* Soft substrates normalize nuclear morphology and prevent nuclear rupture in fibroblasts from a laminopathy patient with compound heterozygous LMNA mutations. *Nucleus* **4**, 61-73 (2013).
95. Khatau, S.B. *et al.* The distinct roles of the nucleus and nucleus-cytoskeleton connections in three-dimensional cell migration. *Scientific reports* **2** (2012).
96. Anno, T., Sakamoto, N. & Sato, M. Role of nesprin-1 in nuclear deformation in endothelial cells under static and uniaxial stretching conditions. *Biochemical and Biophysical Research Communications* **424**, 94-99 (2012).
97. Houben, F., Ramaekers, F., Snoeckx, L. & Broers, J. Role of nuclear lamina-cytoskeleton interactions in the maintenance of cellular strength. *Biochimica et Biophysica Acta (BBA)-Molecular Cell Research* **1773**, 675-686 (2007).
98. Geiger, B., Bershadsky, A., Pankov, R. & Yamada, K.M. Transmembrane extracellular matrix-cytoskeleton crosstalk. *Nature Reviews Molecular Cell Biology* **2**, 793-805 (2001).
99. Gudise, S., Figueroa, R.A., Lindberg, R., Larsson, V. & Hallberg, E. Samp1 is functionally associated with the LINC complex and A-type lamina networks. *Journal of Cell Science* **124**, 2077-2085 (2011).
100. Gomes, E.R., Jani, S. & Gundersen, G.G. Nuclear movement regulated by Cdc42, MRCK, myosin, and actin flow establishes MTOC polarization in migrating cells. *Cell* **121**, 451-463 (2005).
101. Nery, F.C. *et al.* TorsinA binds the KASH domain of nesprins and participates in linkage between nuclear envelope and cytoskeleton. *Journal of Cell Science* **121**, 3476-3486 (2008).
102. Maraldi, N.M., Capanni, C., Cenni, V., Fini, M. & Lattanzi, G. Laminopathies and Lamin-Associated Signaling Pathways. *Journal of Cellular Biochemistry* **112**, 979-992 (2011).
103. Peti, W. & Page, R. Molecular basis of MAP kinase regulation. *Protein Science* **22**, 1698-1710 (2013).
104. Jaalouk, D.E. & Lammerding, J. Mechanotransduction gone awry. *Nature reviews Molecular cell biology* **10**, 63-73 (2009).
105. Emerson, L.J. *et al.* Defects in cell spreading and ERK1/2 activation in fibroblasts with lamin A/C mutations. *Biochimica et Biophysica Acta (BBA)-Molecular Basis of Disease* **1792**, 810-821 (2009).
106. Muchir, A., Pavlidis, P., Bonne, G., Hayashi, Y.K. & Worman, H.J. Activation of MAPK in hearts of EMD null mice: similarities between mouse models of X-linked and autosomal dominant Emery-Dreifuss muscular dystrophy. *Human Molecular Genetics* **16**, 1884-1895 (2007).
107. Muchir, A. *et al.* Activation of MAPK pathways links LMNA mutations to cardiomyopathy in Emery-Dreifuss muscular dystrophy. *Journal of Clinical Investigation* **117**, 1282-1293 (2007).

108. Muchir, A. *et al.* Abnormal p38 mitogen-activated protein kinase signaling in dilated cardiomyopathy caused by lamin A/C gene mutation. *Human Molecular Genetics* **21**, 4325-4333 (2012).
109. Muchir, A. *et al.* Treatment with selumetinib preserves cardiac function and improves survival in cardiomyopathy caused by mutation in the lamin A/C gene. *Cardiovascular Research* **93**, 311-319 (2012).
110. Lammerding, J. *et al.* Abnormal nuclear shape and impaired mechanotransduction in emerin-deficient cells. *The Journal of cell biology* **170**, 781-791 (2005).
111. Gonzalez, J.M., Navarro-Puche, A., Casar, B., Crespo, P. & Andres, V. Fast regulation of AP-1 activity through interaction of lamin A/C, ERK1/2, and c-Fos at the nuclear envelope. *Journal of Cell Biology* **183**, 653-666 (2008).
112. Muchir, A., Wu, W. & Worman, H.J. Reduced expression of A-type lamins and emerin activates extracellular signal-regulated kinase in cultured cells. *Biochimica Et Biophysica Acta-Molecular Basis of Disease* **1792**, 75-81 (2009).
113. Ivorra, C. *et al.* A mechanism of AP-1 suppression through interaction of c-Fos with lamin A/C. *Genes & Development* **20**, 307-320 (2006).
114. Gordon, M.D. & Nusse, R. Wnt signaling: Multiple pathways, multiple receptors, and multiple transcription factors. *Journal of Biological Chemistry* **281**, 22429-22433 (2006).
115. Robinson, J.A. *et al.* Wnt/beta-catenin signaling is a normal physiological response to mechanical loading in bone. *Journal of Biological Chemistry* **281**, 31720-31728 (2006).
116. Neumann, S. *et al.* Nesprin-2 interacts with α-catenin and regulates Wnt signaling at the nuclear envelope. *Journal of Biological Chemistry* **285**, 34932-34938 (2010).
117. Fagotto, F., Gluck, U. & Gumbiner, B.M. Nuclear localization signal-independent and importin/karyopherin-independent nuclear import of beta-catenin. *Current Biology* **8**, 181-190 (1998).
118. Hernandez, L. *et al.* Functional Coupling between the Extracellular Matrix and Nuclear Lamina by Wnt Signaling in Progeria. *Developmental Cell* **19**, 413-425 (2010).
119. Bengtsson, L. What MAN1 does to the smads - TGF beta/BMP signaling and the nuclear envelope. *Febs Journal* **274**, 1374-1382 (2007).
120. Maeda, T. *et al.* Conversion of Mechanical Force into TGF-beta-Mediated Biochemical Signals. *Current Biology* **21**, 933-941 (2011).
121. Wipff, P.J., Rifkin, D.B., Meister, J.J. & Hinz, B. Myofibroblast contraction activates latent TGF-beta 1 from the extracellular matrix. *Journal of Cell Biology* **179**, 1311-1323 (2007).
122. Pan, D. *et al.* The integral inner nuclear membrane protein MAN1 physically interacts with the R-Smad proteins to repress signaling by the transforming growth factor-beta superfamily of cytokines. *Journal of Biological Chemistry* **280**, 15992-16001 (2005).

123. Osada, S.I., Ohmori, S. & Taira, M. XMAN1, an inner nuclear membrane protein, antagonizes BMP signaling by interacting with Smad1 in Xenopus embryos. *Development* **130**, 1783-1794 (2003).
124. Van Berlo, J.H. *et al.* A-type lamins are essential for TGF-beta 1 induced PP2A to dephosphorylate transcription factors. *Human Molecular Genetics* **14**, 2839-2849 (2005).
125. Worman, H.J. Inner nuclear membrane and regulation of Smad-mediated signaling. *Biochimica Et Biophysica Acta-Molecular and Cell Biology of Lipids* **1761**, 626-631 (2006).
126. Mouilleron, S., Langer, C.A., Guettler, S., McDonald, N.Q. & Treisman, R. Structure of a pentavalent G-actin* MRTF-A complex reveals how G-actin controls nucleocytoplasmic shuttling of a transcriptional coactivator. *Science signaling* **4**, ra40 (2011).
127. Miralles, F., Posern, G., Zaromytidou, A.I. & Treisman, R. Actin dynamics control SRF activity by regulation of its coactivator MAL. *Cell* **113**, 329-342 (2003).
128. Pawlowski, R., Rajakyla, E.K., Vartiainen, M.K. & Treisman, R. An actin-regulated importin alpha/beta-dependent extended bipartite NLS directs nuclear import of MRTF-A. *Embo Journal* **29**, 3448-3458 (2010).
129. Small, E.M. *et al.* Myocardin-related transcription factor-a controls myofibroblast activation and fibrosis in response to myocardial infarction. *Circulation research* **107**, 294-304 (2010).
130. Ho, C.Y., Jaalouk, D.E. & Lammerding, J. Novel insights into the disease etiology of laminopathies. *Rare Diseases* **1**, e27002 (2013).
131. Ho, C.Y., Jaalouk, D.E., Vartiainen, M.K. & Lammerding, J. Lamin A/C and emerin regulate MKL1-SRF activity by modulating actin dynamics. *Nature* (2013).
132. Chang, W., Folker, E.S., Worman, H.J. & Gundersen, G.G. Emerin Organizes Actin Flow for Nuclear Movement and Centrosome Orientation in Migrating Fibroblasts. *Molecular biology of the cell*, mbc. E13-06-0307 (2013).
133. Halder, G., Dupont, S. & Piccolo, S. Transduction of mechanical and cytoskeletal cues by YAP and TAZ. *Nature reviews Molecular cell biology* (2012).
134. Dupont, S. *et al.* Role of YAP/TAZ in mechanotransduction. *Nature* **474**, 179-183 (2011).
135. Andres, V. & Gonzalez, J.M. Role of A-type lamins in signaling, transcription, and chromatin organization. *Journal of Cell Biology* **187**, 945-957 (2009).
136. Dorner, D. *et al.* Lamina-associated polypeptide 2 alpha regulates cell cycle progression and differentiation via the retinoblastoma-E2F pathway. *Journal of Cell Biology* **173**, 83-93 (2006).
137. Markiewicz, E., Dechat, T., Foisner, R., Quinlan, R.A. & Hutchison, C.J. Lamin A/C binding protein LAP2 alpha is required for nuclear anchorage of retinoblastoma protein. *Molecular Biology of the Cell* **13**, 4401-4413 (2002).

138. Naetar, N. *et al.* Loss of nucleoplasmic LAP2α–lamin A complexes causes erythroid and epidermal progenitor hyperproliferation. *nature cell biology* **10**, 1341-1348 (2008).
139. Scaffidi, P. & Misteli, T. Lamin A-dependent misregulation of adult stem cells associated with accelerated ageing. *Nature Cell Biology* **10**, 452-U167 (2008).
140. Bione, S. *et al.* IDENTIFICATION OF A NOVEL X-LINKED GENE RESPONSIBLE FOR EMERY-DREIFUSS MUSCULAR-DYSTROPHY. *Nature Genetics* **8**, 323-327 (1994).
141. Emery, A.E.H. Emery-Dreifuss muscular dystrophy - a 40 year retrospective. *Neuromuscular Disorders* **10**, 228-232 (2000).
142. Tifft, K.E., Bradbury, K.A. & Wilson, K.L. Tyrosine phosphorylation of nuclear-membrane protein emerin by Src, Abl and other kinases. *Journal of Cell Science* **122**, 3780-3790 (2009).
143. Mejat, A. *et al.* Lamin A/C-mediated neuromuscular junction defects in Emery-Dreifuss muscular dystrophy. *Journal of Cell Biology* **184**, 31-44 (2009).
144. Zhang, X.C. *et al.* Syne-1 and Syne-2 play crucial roles in myonuclear anchorage and motor neuron innervation. *Development* **134**, 901-908 (2007).
145. Folker, E.S., Ostlund, C., Luxton, G.W.G., Worman, H.J. & Gundersen, G.G. Lamin A variants that cause striated muscle disease are defective in anchoring transmembrane actin-associated nuclear lines for nuclear movement. *Proceedings of the National Academy of Sciences of the United States of America* **108**, 131-136 (2011).
146. Cupesi, M. *et al.* Attenuated hypertrophic response to pressure overload in a lamin A/C haploinsufficiency mouse. *Journal of molecular and cellular cardiology* **48**, 1290-1297 (2010).
147. Engler, A.J., Sen, S., Sweeney, H.L. & Discher, D.E. Matrix elasticity directs stem cell lineage specification. *Cell* **126**, 677-689 (2006).
148. Nikolova, V. *et al.* Defects in nuclear structure and function promote dilated cardiomyopathy in lamin A/C-deficient mice. *Journal of Clinical Investigation* **113**, 357-369 (2004).
149. Bengtsson, L. & Otto, H. LUMA interacts with emerin and influences its distribution at the inner nuclear membrane. *Journal of Cell Science* **121**, 536-548 (2008).
150. Muchir, A., Shan, J., Bonne, G., Lehnart, S.E. & Worman, H.J. Inhibition of extracellular signal-regulated kinase signaling to prevent cardiomyopathy caused by mutation in the gene encoding A-type lamins. *Human Molecular Genetics* **18**, 241-247 (2009).
151. Wu, W., Iwata, S., Homma, S., Worman, H.J. & Muchir, A. Depletion of extracellular signal-regulated kinase 1 in mice with cardiomyopathy caused by lamin A/C gene mutation partially prevents pathology before isoenzyme activation. *Human Molecular Genetics* **23**, 1-11 (2014).
152. Wu, W., Muchir, A., Shan, J.A., Bonne, G. & Worman, H.J. Mitogen-Activated Protein Kinase Inhibitors Improve Heart Function and Prevent

Fibrosis in Cardiomyopathy Caused by Mutation in Lamin A/C Gene. *Circulation* **123**, 53-61 (2011).
153. Qin, Z., Kalinowski, A., Dahl, K.N. & Buehler, M.J. Structure and stability of the lamin A tail domain and HGPS mutant. *Journal of Structural Biology* **175**, 425-433 (2011).
154. Merideth, M.A. *et al.* Phenotype and course of Hutchinson-Gilford progeria syndrome. *New England Journal of Medicine* **358**, 592-604 (2008).
155. Al-Shali, K.Z. & Hegele, R.A. Laminopathies and atherosclerosis. *Arteriosclerosis Thrombosis and Vascular Biology* **24**, 1591-1595 (2004).
156. Booth-Gauthier, E.A., Alcoser, T.A., Yang, G. & Dahl, K.N. Force-Induced Changes in Subnuclear Movement and Rheology. *Biophysical journal* **103**, 2423-2431 (2012).
157. Verstraeten, V., Ji, J.Y., Cummings, K.S., Lee, R.T. & Lammerding, J. Increased mechanosensitivity and nuclear stiffness in Hutchinson-Gilford progeria cells: effects of farnesyltransferase inhibitors. *Aging Cell* **7**, 383-393 (2008).
158. Dahl, K.N. *et al.* Distinct structural and mechanical properties of the nuclear lamina in Hutchinson-Gilford progeria syndrome. *Proceedings of the National Academy of Sciences of the United States of America* **103**, 10271-10276 (2006).
159. Young, S.G., Yang, S.H., Davies, B.S.J., Jung, H.J. & Fong, L.G. Targeting Protein Prenylation in Progeria. *Science Translational Medicine* **5**, 6 (2013).

CHAPTER 2

MUTANT LAMINS CAUSE NUCLEAR ENVELOPE RUPTURE AND DNA DAMAGE IN SKELETAL MUSCLE CELLS[2]

Mutations in the human *LMNA* gene, which encodes the nuclear envelope proteins lamins A and C, cause autosomal dominant Emery-Dreifuss muscular dystrophy, congenital muscular dystrophy, limb-girdle muscular dystrophy, and other diseases collectively known as laminopathies. The molecular mechanisms responsible for these diseases remain incompletely understood, but the muscle-specific defects suggest that mutations may render nuclei more susceptible to mechanical stress. Using three mouse models of muscle laminopathies, we found that *Lmna* mutations caused extensive nuclear envelope damage, consisting of chromatin protrusions and transient rupture of the nuclear envelope, in skeletal muscle cells *in vitro* and *in vivo*. The nuclear envelope damage was associated with progressive DNA damage, activation of DNA damage response pathways, and reduced viability. Intriguingly, nuclear envelope damage resulted from nuclear movement in maturing skeletal muscle cells, rather than actomyosin contractility, and was reversed by either depletion of kinesin-1 or stabilization of microtubules. Depletion of kinesin-1 also rescued DNA damage, indicating that DNA damage is the result of nuclear envelope damage. The extent of

[2] Manuscript in revision at Nature Materials. Earle AJ*, Kirby TJ*, Fedorchak GR*, Isermann P, Patel J, Iruvanti S, Moore SA, Bonne G, Walwrath LL, Lammerding J. * these authors contributed equally.

AE contributed to experiment conception, design, and writing. Myoblast isolation, characterization of H222P cell lines, all *in vivo* work, and γH2AX quantification.

nuclear envelope damage and DNA damage in the different *Lmna* mouse models strongly correlated with the disease onset and severity *in vivo*, and inducing DNA damage in wild-type muscle cells was sufficient to phenocopy the reduced cell viability of lamin A/C-deficient muscle cells, suggesting a causative role of DNA damage in disease pathogenesis. Corroborating the mouse model data, muscle biopsies from patients with *LMNA* associated muscular dystrophy similarly revealed significant DNA damage compared to age-matched controls, particularly in severe cases of the disease. Taken together, these findings point to a new and important role of DNA damage as a pathogenic contributor for these skeletal muscle diseases.

Introduction

The nuclear envelope (NE) proteins lamin A and C, together with the B-type lamins B1 and B2, are the major components of the nuclear lamina, which line the inner nuclear membrane. Lamins A/C play important roles in providing structural support to the nucleus and connecting the nucleus to the cytoskeleton[1]. In addition, they participate in transcriptional regulation, genome organization, and DNA damage and repair[1-4]. The majority of the over 450 *LMNA* mutations identified to date are responsible for autosomal dominant Emery-Dreifuss muscular dystrophy (AD-EDMD)[5], characterized by slowly progressive skeletal muscle wasting, contractures of the elbow, neck, and Achilles tendons, a rigid spine, abnormal heart rhythms, heart block, and cardiomyopathy[6]. Other *LMNA* mutations cause congenital muscular dystrophy (*LMNA*-CMD), a particularly severe form of muscular dystrophy with onset in early childhood[7], and limb girdle muscular dystrophy[8]. It remains unclear how *LMNA* mutations result in muscle-specific defects, and the incomplete understanding of the

disease pathogenesis presents a major hurdle in the development of effective treatment approaches.

One potential explanation, the 'mechanical stress' hypothesis, states that *LMNA* mutations linked to muscular phenotypes result in structurally impaired nuclei that become damaged in mechanically active tissue, such as cardiac and skeletal muscle[4]. This hypothesis is supported by findings of decreased nuclear stiffness in fibroblasts expressing *LMNA* mutations linked to striated muscle laminopathies, impaired assembly of mutant lamins *in vitro*, and anecdotal reports of NE damage in skeletal and cardiac muscle cells of individuals with AD-EDMD and *LMNA*-related dilated cardiomyopathies[1, 4, 9, 10]. However, striated muscle laminopathies involve progressive muscle wasting, and analysis of fixed tissues and cells provides only a snapshot in time, often when the disease has already advanced substantially. Thus, the functional relevance of NE damage, particularly whether the NE damage is a cause or consequence of muscle dysfunction, remains unclear.

To better understand the mechanistic link between NE damage and muscle dysfunction, we employed three laminopathy mouse models with varying degrees of disease severity, along with a recently developed long-term *in vitro* muscle differentiation platform[11]. Using high resolution time lapse microscopy, we tracked myonuclear shape and integrity over time and recorded structural and functional changes during the differentiation of primary mouse myoblasts into multinucleated myotubes and subsequent formation of mature, contractile myofibers (**Fig. 2.1a, b**). Combining these models with novel, fluorescent nuclear damage reporters[12], both *in vitro* and *in vivo*, we obtained unprecedented systematic and detailed temporal and mechanistic information

of disease progression in mouse models of laminopathies, and corroborated key findings in skeletal muscle biopsies from human individuals with muscular dystrophy resulting from *LMNA* mutations.

We found that myonuclei in *Lmna* mutant muscle cells exhibited progressive NE damage *in vitro* and *in vivo*, including extensive chromatin protrusions into the cytoplasm and transient NE rupture. Intriguingly, the NE rupture was associated with progressive DNA damage and DNA damage response activation. Moreover, inducing DNA damage in wild-type muscle cells was sufficient to provoke defects in cell viability similar to those observed in the lamin A/C-deficient cells. Together, our findings indicate a causative role of DNA damage in the progressive muscle decline and provide a novel explanation for how lamin mutations lead to a muscle weakness and wasting.

Results

Lmna mutations cause progressive decline in myofiber health *in vitro* and *in vivo*

To examine the effect of *Lmna* mutations on nuclear mechanics and muscle function *in vitro*, we isolated myoblasts from three established mouse models of striated muscle laminopathies, representing a spectrum of disease severity (**Fig. 2.1a**): Lamin A/C-deficient ($Lmna^{-/-}$) mice[13], subsequently referred to as lamin A/C-knock-out mice (*Lmna* KO); knock-in mice carrying the $Lmna^{N195K/N195K}$ mutation (*Lmna* N195K)[14]; knock-in mice carrying the $Lmna^{H222P/H222P}$ mutation (*Lmna* H222P)[15]; and wild-type littermates. While the *Lmna* N195K mice were originally described as a model for dilated cardiomyopathy[14], in the C57BL/6 background used in our studies, the mice developed pronounced skeletal muscular dystrophy in addition to cardiac defects

(Suppl. Fig. S2.1). For *in vitro* studies, we utilized a recently developed, three-dimensional culture protocol to differentiate primary myoblasts into mature, contractile myofibers over the course of ten days (**Fig. 2.1b**)[16, 17]. The resulting myofibers display the highly organized sarcomeric structure and evenly spaced peripheral myonuclear positioning characteristic of mature skeletal muscle fibers *in vivo* (Suppl. Fig. S2.2).

All myoblasts, including the *Lmna* KO, *Lmna* N195K and *Lmna* H222P mutant cells, successfully completed myoblast fusion, differentiated into myotubes, formed sarcomeric structures, and matured into myofibers (**Fig. 2.1c**), consistent with previous studies on differentiation of *Lmna* KO myoblasts into myotubes[18, 19]. Wild-type myofibers remained healthy and highly contractile up to ten days of differentiation. In contrast, the *Lmna* KO myofibers showed a decline in cell contractility and viability, starting at day five of differentiation (**Fig. 2.1c,d**; Suppl. Fig. S2.3). The *Lmna* N195K myofibers had a similar decline in cell viability at day ten, albeit to lesser extent than the *Lmna* KO cells (**Fig. 2.1d**, Suppl. Fig S2.3). The reduction in cell viability at day ten in the *Lmna* KO and *Lmna* N195K myofibers was associated with an increase in activated caspase-3 (**Fig. 2.1e,f**), indicating that reduced viability was due at least in part to cell-intrinsic apoptosis. Unlike the *Lmna* KO and *Lmna* N195K models, the *Lmna* H222P myofibers exhibited no significant decrease in viability or contractility within ten days of differentiation. Taken together, the long-term differentiation assay revealed a striking correlation among the defects observed *in vitro*, including loss of muscle cell viability and presence of apoptotic markers, with the severity of the disease in the corresponding mouse models, suggesting that defects in the *in vitro* model may serve as prognostic markers for disease progression.

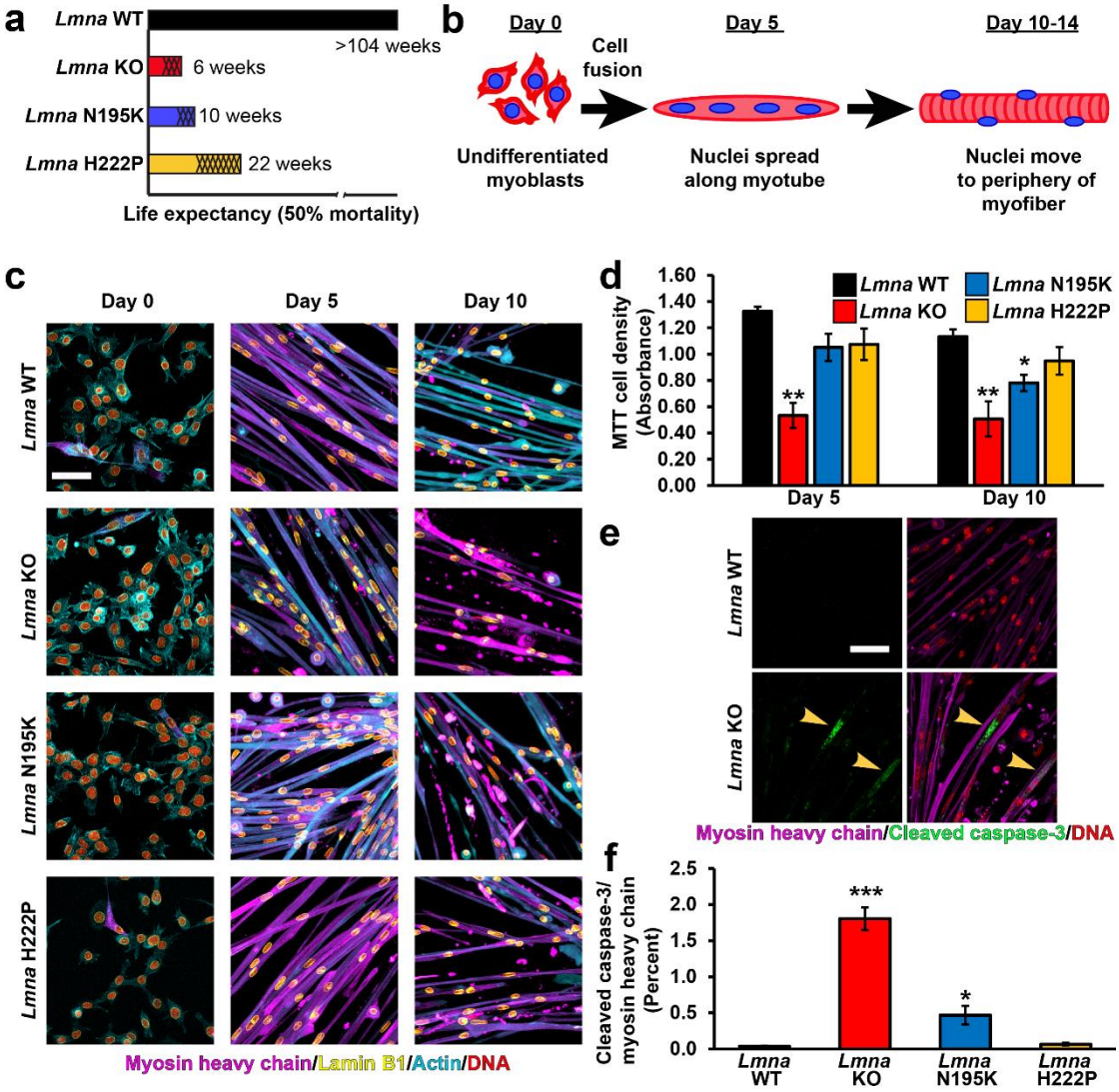

Figure 2.1. *In vitro* differentiated primary myoblasts from *Lmna* KO, *Lmna* N195K, and *Lmna* H222P mice recapitulates disease severity. (**a**) Graphical representation of the three *Lmna* mutant models used in the study, indicating the published 50% mortality rates of *Lmna* KO, *Lmna* N195K, and *Lmna* H222P mice, as well as wild-type (*Lmna* WT) controls. Shading represents the onset of disease symptoms in the mouse models. (**b**) Schematic for the stages of differentiation from primary myoblasts into mature myofibers in the *in vitro* system. (**c**) Representative images of *Lmna* WT, *Lmna* KO, *Lmna* N195K and *Lmna* H222P primary skeletal muscle cells at days 0, 5 and 10 of differentiation. Scale bar: 100 µm. (**d**) Quantification of cell viability using MTT assay at days 5, 10 of differentiation. n = 3-6 independent cell lines for each genotype. **, $p < 0.01$ vs. *Lmna* WT; *, $p < 0.05$ vs. *Lmna* WT. (**e**) Representative image of cleaved caspase-3 immunofluorescence in *Lmna* WT and *Lmna* KO myofibers at day 10 of differentiation. Scale bar: 20 µm (**f**) Quantification of cleaved caspase-3 relative to myosin heavy chain immunofluorescence area in *Lmna* WT, *Lmna* KO, *Lmna* N195K and *Lmna* H222P myofibers after 10 days of differentiation ***, $p < 0.001$ vs. *Lmna* WT; *, $p < 0.05$ vs. *Lmna* WT. n = 3 independent cell lines for each genotype.

Lmna mutant muscle cells exhibit defective nuclear stability that corresponds with disease severity

We hypothesized that the progressive deterioration of *Lmna* mutant myofibers may result from damage to mechanically weakened myonuclei exposed to cytoskeletal forces. Therefore, we measured the nuclear deformability in primary myoblasts from the three laminopathy models using a novel microfluidics-based cell aspiration assay (**Fig. 2.2a**). This assay is a higher throughput variation of the traditional micropipette aspiration technique commonly used to study nuclear mechanics[20, 21]. Nuclei from *Lmna* KO and *Lmna* N195K myoblasts were substantially more deformable than nuclei from wild-type controls (**Fig. 2.2b,c**). Intriguingly, myoblasts from *Lmna* H222P mice, which have a much later disease onset and less severe muscle defects than the other two *Lmna* mutant models (**Fig. 2.1a**), had only a modest increase in nuclear deformability relative to wild-type controls (**Fig. 2.2b,c**; Supp. Fig. S2.4a). Ectopic expression of lamin A significantly reduced the nuclear deformability defect in primary *Lmna* KO myoblasts (Suppl. Fig. S2.4b-d), confirming that the impaired nuclear stability was a direct consequence of altering the nuclear lamina. In addition, primary myoblasts from *Mdx* mice, which develop mild muscular dystrophy due to loss of dystrophin, a cell membrane protein, had nuclear deformation indistinguishable from wild-type controls (Suppl. Fig. 2.S5), indicating that the defects in nuclear stability are specific to *Lmna* mutations and not muscular dystrophy in general.

To assess whether the observed defects in nuclear stability also occur in more mature, multinucleated myofibers, we subjected *Lmna* KO and wild-type myofibers to a

'microharpoon' assay, in which precise strain is exerted on the perinuclear cytoskeleton, and the induced nuclear deformation and displacement are used to infer nuclear stability and nucleo-cytoskeletal coupling, respectively[22, 23]. *Lmna* KO myofibers had significantly more deformable nuclei than wild-type controls (**Fig. 2.2d,e**), consistent with the micropipette aspiration results in the myoblasts. Furthermore, analysis of *Lmna* mutant and wild-type myofibers at day five of *in vitro* differentiation revealed that *Lmna* KO, *Lmna* N195K, and *Lmna* H222P myofibers had significantly elongated myonuclei compared to wild-type controls (**Fig. 2.2f,g**), consistent with decreased nuclear stability in the *Lmna* mutant cells and with previous reports of elongated nuclei in muscle biopsies from laminopathy patients[24]. Taken together, these findings suggest that myopathic *Lmna* mutations result in mechanically weaker myonuclei.

Lmna mutant myonuclei display chromatin protrusions across the nuclear lamina

Physical stress on the nucleus during external compression or confined migration can induce chromatin protrusions across the NE into the cytoplasm, particularly in lamin-deficient cells[12, 25]. To test whether the mechanically weaker *Lmna* mutant myonuclei are prone to mechanically induced damage in muscle cells, we analyzed nuclear structure and morphology over the ten-day time course of differentiation and maturation of primary myoblasts from laminopathy mouse models and healthy controls. Despite their mechanically weaker nuclei (**Fig. 2.2**), the *Lmna* mutant myoblasts show no nuclear abnormalities prior to differentiation (**Fig. 2.3b**). Following the onset of differentiation, however, *Lmna* KO, *Lmna* N195K, and *Lmna* H222P myofibers exhibited striking chromatin protrusions that were completely absent in wild-type fibers.

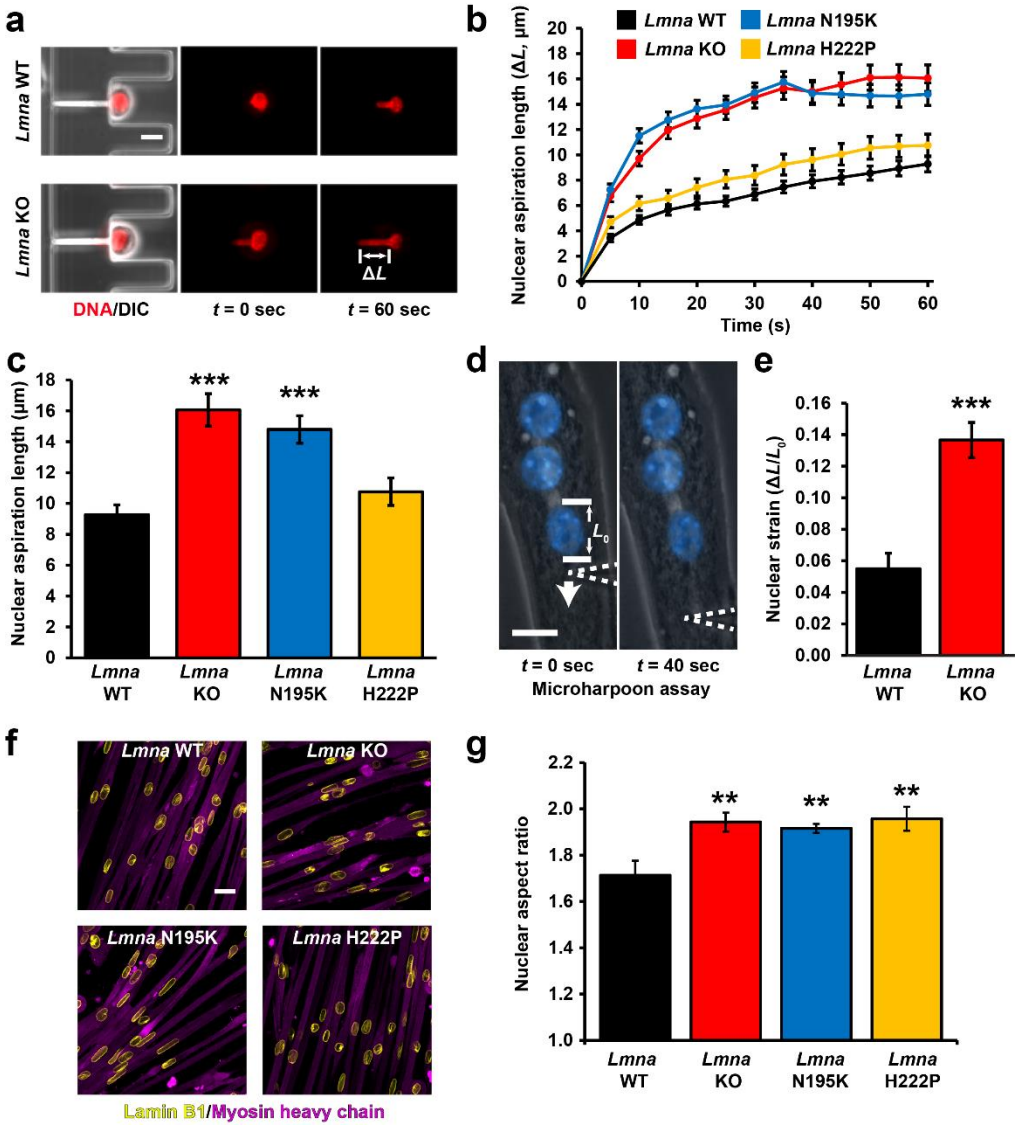

Figure 2.2. *Lmna* mutant muscle cells display defects in nuclear stability. (**a**) Representative images of *Lmna* WT and *Lmna* KO nuclei deforming in a microfluidic micropipette aspiration device. Scale bar: 10 μm. (**b**) Measurement for nuclear deformation at 5 second intervals for *Lmna* WT, *Lmna* KO, *Lmna* N195K, and *Lmna* H222P myoblasts during 60 seconds of aspiration. (**c**) Quantification of the nuclear deformation after 60 seconds of aspiration. n = 41-67 nuclei per genotype from 3 independent experiments. ***, $p < 0.001$ *vs*. *Lmna* WT. (**d**) Microharpoon assay to measure nuclear deformability ($\Delta L/L_0$) in myofibers, showing representative images before and at the end of perinuclear cytoskeletal strain application with a microneedle (dashed line). Scale bar: 15 μm. (**e**) Quantification of nuclear strain induced by microharpoon assay in *Lmna* WT and *Lmna* KO myotubes at day 5 of differentiation. n = 19-22 nuclei per genotype from 3 independent experiments. ***, $p < 0.001$ *vs*. *Lmna* WT myotubes. (**f**) Representative image of nuclear morphology in *Lmna* WT, *Lmna* KO, *Lmna* N195K and *Lmna* H222P myotubes after 5 days of differentiation. Scale bar: 20 μm (**g**) Nuclear aspect ratio

(length/width) in *Lmna* WT, *Lmna* KO, *Lmna* N195K and *Lmna* H222P myotubes after 5 days of differentiation. $n = 3$ - 4 independent cell lines per genotype with >100 nuclei counted per image. *, $p < 0.05$ *vs*. *Lmna* WT.

These protrusions extended beyond the (B-type) nuclear lamina up to tens of microns into the cytoplasm (**Fig. 2.3a,b**). The protrusions were enclosed by nuclear membranes, as indicated by the frequent presence of the nuclear membrane protein emerin, and occasionally nesprin-1 (Suppl. Fig. S2.6a); however, these NE proteins were often concentrated in punctae inside the protrusions and myonuclei. Other NE proteins, such as nuclear pore complex proteins, were largely absent from the protrusions (Supp. Fig. S2.6b), suggesting an altered membrane composition in the chromatin protrusion, similar to what has been reported in analogous structures in cancer cells[26, 27].

The frequency of chromatin protrusion was highest in *Lmna* KO myofibers, followed by *Lmna* N195K and then *Lmna* H222P myofibers (**Fig. 2.3b**), correlating with the increased nuclear deformability *in vitro* (**Fig. 2.2**) and the disease severity *in vivo* (**Fig. 2.1a**). Intriguingly, while *Lmna* KO and *Lmna* N195K myofibers had extensive chromatin protrusions at day five of differentiation, the frequency of chromatin protrusions in the *Lmna* H222P cells was initially very low, but increased significantly from five to ten days of differentiation (**Fig. 2.3b**), matching the delayed disease onset and progressive phenotype of the *Lmna* H222P model *in vivo.* Ectopic expression of lamin A in *Lmna* KO myoblasts significantly reduced the occurrence of chromatin protrusions at ten days of differentiation (**Fig. 2.3b**), confirming that the protrusions were caused by loss of lamin A/C expression.

To confirm the results of the *in vitro* studies *in vivo*, we isolated single muscle fibers from the hindlimbs of *Lmna* KO and wild-type mice. Chromatin protrusions were not detectable in muscle fibers from wild-type mice (**Fig. 2.3c,d**). In contrast, nuclei in muscle fibers from *Lmna* KO mice had similar chromatin protrusions as observed in the *in vitro* differentiated myofibers (**Fig. 2.3c,d**). Interestingly, the prevalence of chromatin protrusions in the *Lmna* KO myonuclei strongly depended on the location within the muscle. Myonuclei at the myotendinous junctions (MTJ) had significantly higher rates of chromatin protrusions than nuclei in the muscle fiber body (**Fig. 2.3d**), consistent with a previous report of nuclear abnormalities at the MTJ in *Lmna* KO mice[28], and possibly reflecting increased mechanical stress at the MTJ.

Nuclear damage is intrinsic to lamin A/C-deficient nuclei

To address whether the observed NE defects in *Lmna* mutant muscle cells are nucleus-intrinsic or arise from altered signaling pathways or other cytoplasmic changes in the mutant cells, we generated "hybrid" myofibers by combining wild-type and *Lmna* KO myoblasts prior to differentiation. Following myoblast fusion, these cells formed multinucleated myotubes and myofibers that contained both wild-type and *Lmna* KO nuclei with a shared cytoplasm (**Fig. 2.3e**). Importantly, in skeletal muscle cells, each nucleus is thought to provide mRNA transcripts for the nearby cytoplasm (referred to as myonuclear domain), so that the local RNA and protein content primarily stems from the nearest myonucleus[29], and the genotype of each myonucleus can be determined by antibody staining against lamin A (**Fig. 2.3e**).

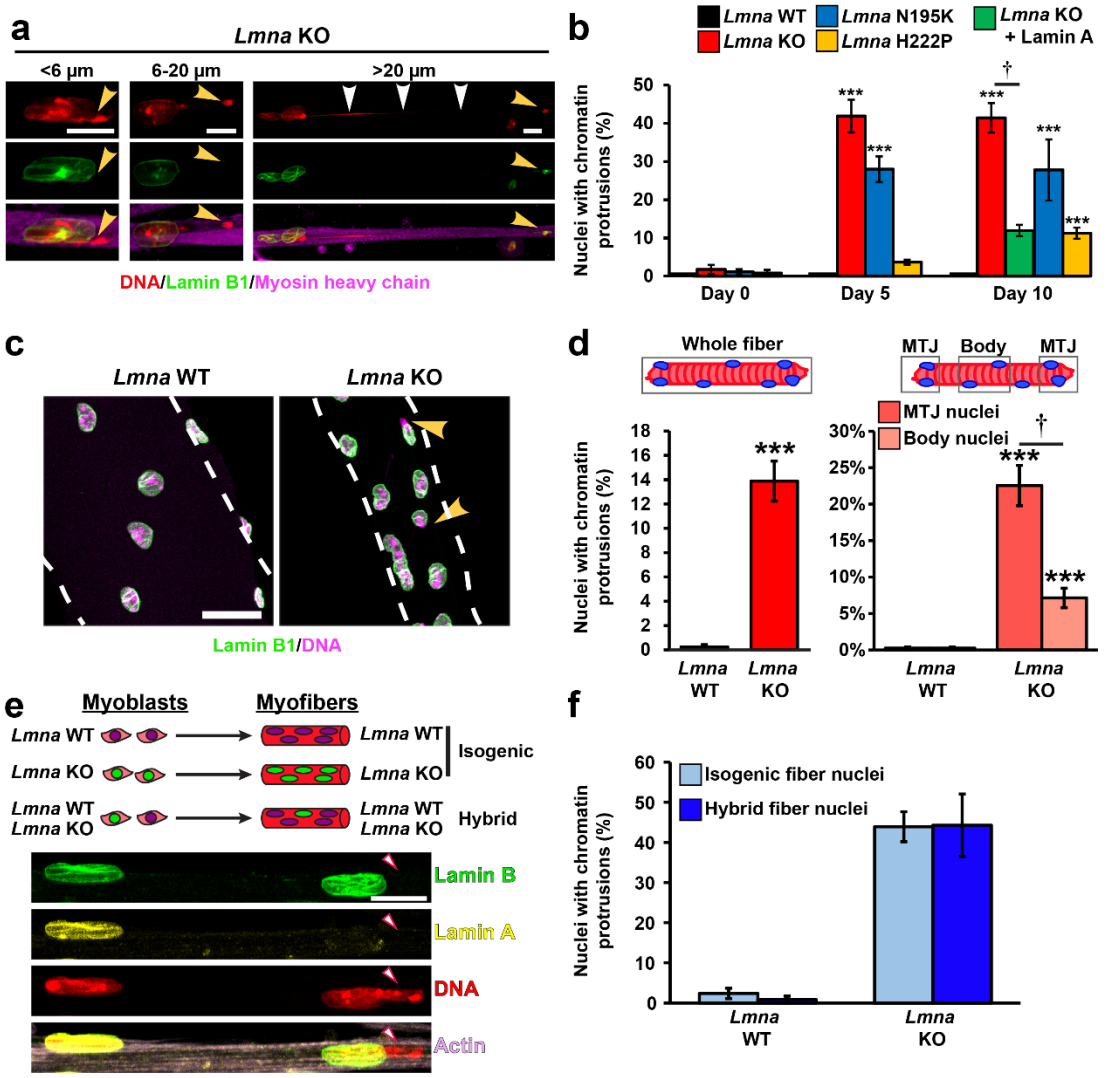

Figure 2.3. *Lmna* mutant myonuclei develop chromatin protrusions during differentiation. (**a**) Representative images of chromatin protrusions observed in *Lmna* KO myofibers after 10 days of differentiation. Yellow arrowheads indict the end of the protrusion; the white arrowheads indicate a thin chromatin tether protruding from the nucleus. Scale bar: 10 µm. (**b**) Quantification of the percentage of myonuclei containing chromatin protrusion at days 5 and 10 of differentiation in *Lmna* WT, *Lmna* KO, *Lmna* KO + Lamin A, *Lmna* N195K and *Lmna* H222P cell lines. Data from $n = 3$ independent experiments with 62-73 nuclei per genotype. ***, $p < 0.001$ *vs*. *Lmna* WT cells. †, $p < 0.01$ *vs*. *Lmna* KO. (**c**) Representative images of isolated single muscle fibers from *Lmna* WT and *Lmna* KO mice labeled for lamin B1 (green) and DNA (magenta). Arrowheads indicate the presence of chromatin protrusions in *Lmna* KO muscle fiber. Scale bar: 20 µm. (**d**) Quantification of the percentage of myonuclei with chromatin protrusion in isolated muscle fibers from *Lmna* WT and *Lmna* KO mice. Left, data based on analysis of total muscle fiber. Right, analysis for nuclei located at the MTJ compared to those within the body of the fiber. $n = 8$-11 mice per genotype, with 5 single fibers imaged per animal. ***, $p < 0.001$ *vs*. *Lmna* WT. †, $p < 0.01$ *vs*. nuclei in the muscle body. (**e**) Top, schematic of the generation of hybrid myofibers containing nuclei from both *Lmna* WT and *Lmna* KO cell lines. Bottom, corresponding representative images. Final hybrid fibers contained ~80% *Lmna* WT nuclei and 20% *Lmna* KO nuclei. Arrowheads denote *Lmna* KO nucleus with

a chromatin protrusion residing within the same myofiber as a *Lmna* WT nucleus. (**f**) Quantification of the number of chromatin protrusions from *Lmna* WT and *Lmna* KO contained within isogenic myofibers (control) or hybrid myofibers containing 80% *Lmna* WT and 20% *Lmna* KO nuclei. $n = 3$ independent experiments, in which 91-163 nuclei were quantified per experiment.

We quantified the number of nuclei with chromatin protrusions and compared genetically identical nuclei (e.g., wild-type or *Lmna* KO) from hybrid and isogenic control myofibers after ten days of differentiation (**Fig. 2.3f**).

Hybrid myofibers comprising ~80% wild-type nuclei and ~20% *Lmna* KO nuclei appeared healthy. Nonetheless, *Lmna* KO nuclei within the hybrid myofibers showed the same relative frequency of chromatin protrusions as nuclei from isogenic *Lmna* KO myofibers (**Fig. 2.3f**). Conversely, wild-type nuclei in hybrid fibers lacked chromatin protrusions and were thus not adversely affected by the presence of *Lmna* KO nuclei in the shared cytoplasm (**Fig. 2.3f**). These results indicate that the defects in nuclear structure are intrinsic to the *Lmna* mutant myonuclei and not due to impaired muscle fiber health, altered cytoplasmic signaling, or changes in the cytoplasmic architecture in *Lmna* mutant muscle fibers.

Lmna mutant myofibers exhibit extensive NE rupture *in vitro*

Physical compression by cytoskeletal forces can result in NE rupture, with depletion of lamins exacerbating the frequency of NE rupture[26, 30-34]. To examine whether the reduced nuclear stability seen in *Lmna* mutant muscle cells (**Fig. 2.2**) leads to NE rupture in *Lmna* mutant myofibers, we genetically modified primary myoblasts to co-express a fluorescent NE rupture reporter, consisting of a green fluorescent protein with

a nuclear localization signal (NLS-GFP)[26] and fluorescently labeled histone (H2B-tdTomato). NLS-GFP is normally localized to the nucleus, but rapidly spills into the cytoplasm upon loss of nuclear membrane integrity and is then gradually reimported into the nucleus after the nuclear membrane has been repaired[26]. *In vitro* differentiated *Lmna* KO myotubes frequently exhibited NE ruptures (**Fig. 2.4a**), which were absent in wild-type controls. To investigate NE rupture in more detail, we stably modified primary myoblasts with another fluorescent NE rupture reporter, cGAS-mCherry. Upon NE rupture, the cytoplasmic cGAS-mCherry reporter binds to the exposed genomic DNA and accumulates at the rupture site[26] (**Fig. 2.4b**). Unlike the transient cytoplasmic NLS-GFP signal, however, the cGAS-mCherry accumulation persists even after the NE has been repaired[26, 30]. Wild-type myotubes had no detectable accumulation of cGAS-mCherry (**Fig. 2.4c**). In contrast, *Lmna* KO myotubes displayed a progressive increase in the number of nuclear cGAS-mCherry foci during differentiation, starting around day two, which could be rescued by ectopic expression of wild-type lamin A (**Fig. 2.4c**). *Lmna* N195K showed intermediate levels of NE rupture (Suppl. Fig. S2.7A), whereas *Lmna* H222P myotubes had cGAS-mCherry accumulation comparable to wild-type controls (Suppl. Fig. S2.7b), consistent with the milder defects in nuclear stability in the *Lmna* H222P mutant cells (**Fig. 2.2b,c**; Supp. Fig. S2.4a).

Lamin A/C-deficient myofibers experience extensive NE rupture *in vivo*

To test whether NE rupture occurs within *Lmna* KO muscle *in vivo*, we generated transgenic mice that express a fluorescent cGAS-tdTomato nuclear rupture reporter and

crossed these mice into the *Lmna* mutant mouse models. Single hindlimb muscle fibers isolated from *Lmna* KO offspring expressing the cGAS-tdTomato reporter revealed a large fraction of myonuclei with cGAS-tdTomato foci, which were absent in both wild-type littermates expressing the cGAS-tdTomato reporter and in *Lmna* KO mice that were negative for the cGAS-tdTomato reporter (**Fig. 2.4d-f**).

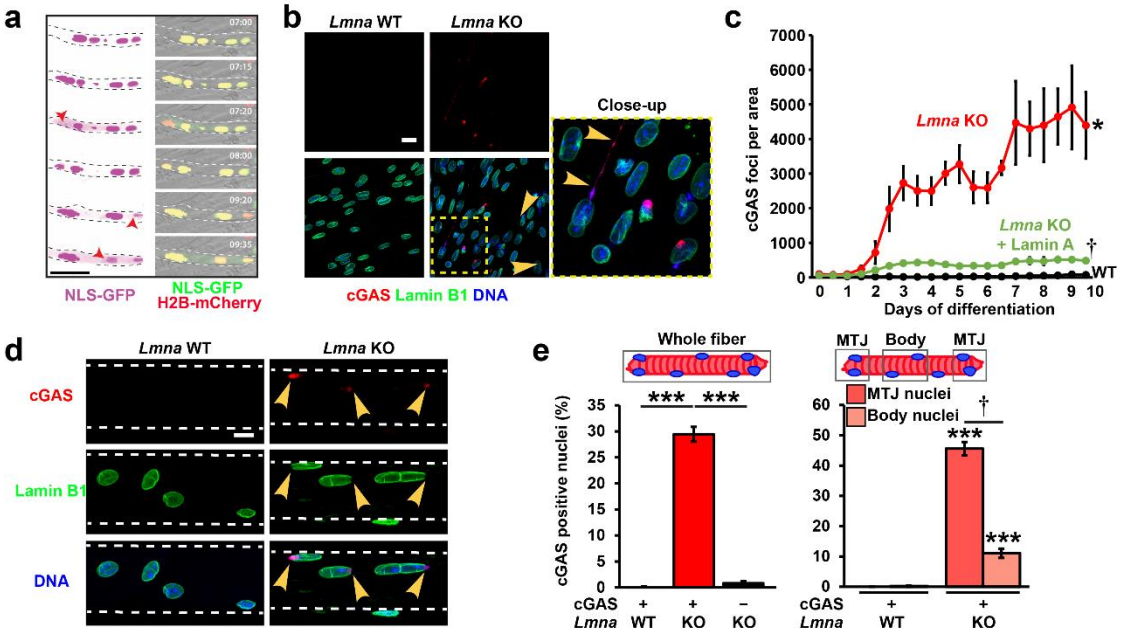

Figure 2.4. *Lmna* mutant myonuclei undergo NE rupture *in vitro* and *in vivo*. (**a**) Representative time-lapse image sequence of NE rupture in *Lmna* KO myonuclei. Red arrowheads mark two nuclei that undergo NE rupture, visibly by transient loss of NLS-GFP from the nucleus. Scale bar: 50 µm for all images. (**b**) Representative images of the accumulation of cGAS-mCherry at the sites of nuclear envelope rupture in *Lmna* KO myonuclei at day 5 of differentiation. Scale bar: 20 µm. (**c**) Quantification of cGAS-mCherry foci formation per field of view during myofiber differentiation in *Lmna* WT, *Lmna* KO, and *Lmna* KO cells expressing ectopic lamin A, expressed. $n = 3$ independent experiments. *, $p < 0.05$ vs. *Lmna* WT. †, $p < 0.01$ vs. *Lmna* KO. (**d**) Representative maximum intensity projection images of single muscle fibers from *Lmna* WT and *Lmna* KO mice expressing a cGAS-tdTomato NE rupture reporter, showing accumulation of cGAS-tdTomato at the site of nuclear NE in *Lmna* KO muscle fibers. Scale bar: 10 µm. **(e**) Quantification of the percentage of myonuclei positive for cGAS-tdTomato foci in isolated muscle fibers from *Lmna* WT and *Lmna* KO mice expressing the cGAS-tdTomato transgene (cGAS+) or non-expressing littermates (cGAS–). Analysis performed for whole fiber (left) and by classification of nuclei located at the MTJ or within the body of the fiber (right). $n = 5$-8 mice per genotype, with 5 fibers per animal. ***, $p < 0.001$ *vs*. *Lmna* WT. †, $p < 0.01$ *vs*. nuclei in the muscle body.

Within *Lmna* KO muscle fibers, the frequency of NE rupture was significantly higher at the MTJ than in the myofiber body nuclei (**Fig. 2.4e**; Suppl. Fig. S2.8), consistent with the increased frequency of chromatin protrusions in the MTJ myonuclei. The amount of cGAS-tdTomato accumulation scaled with disease severity such that *Lmna* KO fibers had the highest amount of cGAS-tdTomato foci, *Lmna* N195K fibers had an intermediate amount, and *Lmna* H222P fibers had no nuclear cGAS-tdTomato accumulation, closely matching the *in vitro* data (Suppl. Fig. S2.7). As an independent approach to detect loss of nuclear-cytoplasmic compartmentalization in muscle fibers, we analyzed the intracellular localization of endogenous heat shock protein 90 (Hsp90), which is typically excluded from the nucleus in healthy muscle fibers[35]. In our *in vitro* assays, Hsp90 was cytoplasmic in wild-type myofibers, whereas all three *Lmna* mutant models had increased nuclear Hsp90 levels during myoblast differentiation (Suppl. Fig. S2.9a,b). Similarly, muscle fibers isolated from *Lmna* KO mice, but not wild-type littermates, had a significant increase in nuclear Hsp90 (Suppl. Fig. S2.9c,d), confirming the occurrence of NE rupture *in vivo*. Taken together, these findings indicate widespread NE rupture in laminopathic skeletal muscle.

Lmna KO myonuclei have increased levels of DNA damage *in vitro* and *in vivo*

Recent studies found that nuclear deformation and NE rupture can cause DNA damage in migrating cells[26, 30, 36]. To investigate whether chromatin protrusions and NE rupture can similarly lead to DNA damage in muscle cells, we quantified DNA damage in differentiating primary myoblasts by staining for γH2AX, a marker for double stranded

DNA damage[37]. Both *Lmna* KO and wild-type myoblasts had elevated levels of DNA damage at the onset of differentiation (**Fig. 2.5a,b**), consistent with previous reports that show the transition from myoblasts to myotubes is associated with a transient increase in γH2AX levels[38, 39]. However, while γH2AX levels in wild-type myotubes subsequently decreased and then remained stable at low levels, the fraction of myonuclei with severe DNA damage in the *Lmna* KO cells continued to increase from day five to day ten post-differentiation, with nearly 20% of *Lmna* KO myonuclei exhibiting severe DNA damage at day ten (**Fig. 2.5b**). Consistent with the increased DNA damage, *Lmna* KO myotubes exhibited significantly increased activity of the DNA-dependent protein kinase, DNA-PK (**Fig. 2.5c**), one of the major DNA damage response pathways in post-mitotic cells[37]. Single muscle fibers isolated from *Lmna* KO mice similarly contained many myonuclei with severe γH2AX staining (**Fig. 2.5d,e**) and increased DNA-PK activity, especially at the MTJ (**Fig. 2.5f**), confirming the presence of extensive DNA damage in *Lmna* KO muscle fibers *in vivo*. The *Lmna* N195K and *Lmna* H222P single muscle fibers also showed increased DNA damage, but to a lesser extent than *Lmna* KO mice, consistent with disease severity and other phenotypic markers (**Fig. 2.5e**). In contrast, muscle fibers isolated from wild-type mice contained only low levels of DNA damage (**Fig. 2.5d,e**). Of the myonuclei with extensive γH2AX staining, 82% also had chromatin protrusions, signifying a link between physical damage to the nucleus and DNA damage (Suppl. Fig. S2.10).

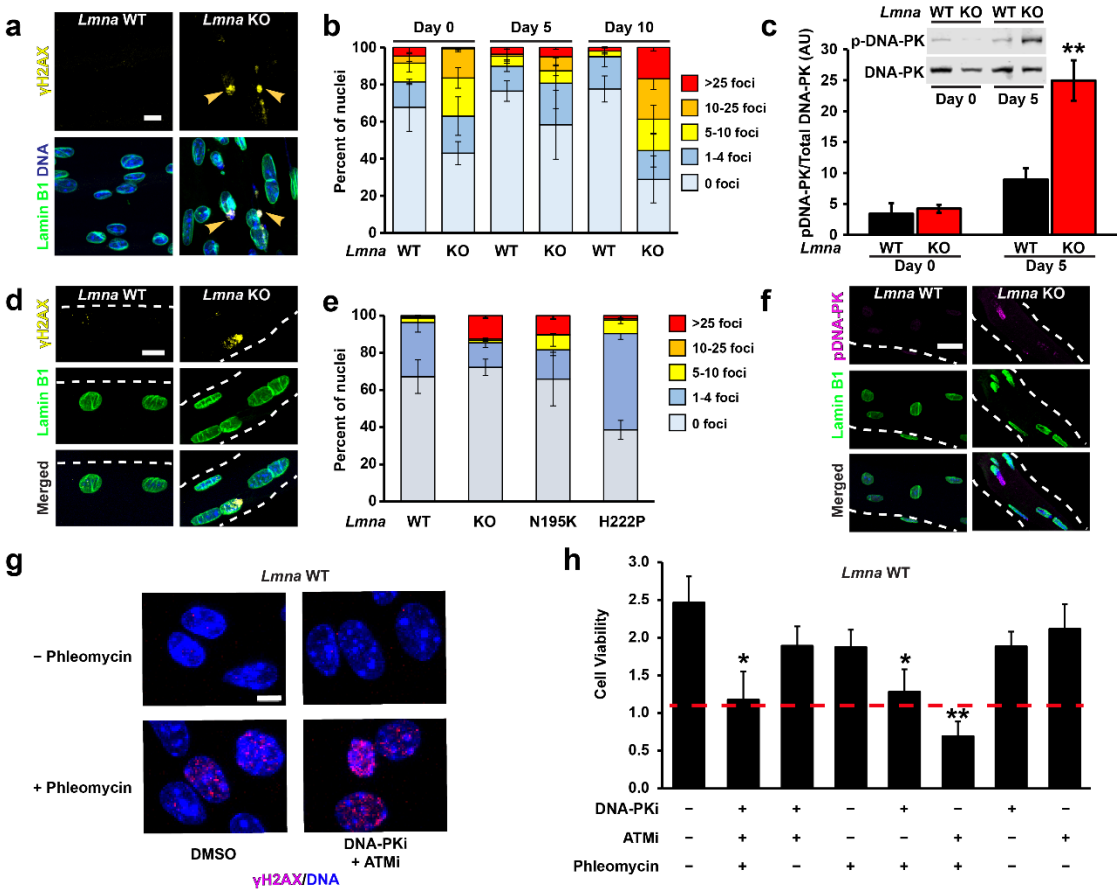

Figure 2.5. *Lmna* KO mice have increased DNA damage in myonuclei *in vitro* and *in vivo*. (**a**) Representative images of γH2AX foci, a marker of a double-stranded DNA break, in *Lmna* KO myonuclei. Arrowheads indicated γH2AX foci at the sites of chromatin protrusions. Scale bar: 10 μm. (**b**) Quantification of the extent of DNA damage based on the number of γH2AX foci per nucleus during myofiber differentiation. *Lmna* KO myonuclei show a progressive increase in the amount of severe DNA damage during myofiber differentiation. n = 3 independent cell lines per genotype. (**c**) Quantification of DNA-PK activity in *Lmna* WT and *Lmna* KO myotubes at day 5 of differentiation by probing for the phosphorylation of DNA-PK at S2053, an autophosphorylation specific site. n = 3 lysates from independent cell lines. **, $p < 0.01$ vs. *Lmna* WT. (**d**) Representative images of γH2AX foci in isolated single muscle fibers from *Lmna* WT and *Lmna* KO mice. Scale bar: 10 μm. (**e**) Quantification of the extent of DNA damage based on the number of γH2AX foci per nucleus in isolated single fibers. n = 3-5 mice per genotype in which 5 fibers are imaged per animal. (**f**) Representative image of p-DNA-PK (S2053) in isolated muscle fibers from *Lmna* WT and *Lmna* KO mice. Scale bar: 20 μm. (**g**) Representative image of γH2AX foci following treatment with phleomycin, with or without DNA-PK + ATM inhibition. Scale bar: 10 μm. (**h**) Quantification of cellular viability in *Lmna* WT myofibers using MTT assay following DNA damage induction with phleomycin, with and without concurrent treatment with DNA-PKi (NU7441) and/or ATMi (KU55933). n = 3 independent experiments per condition. **, $p < 0.01$ vs. untreated control; *, $p < 0.05$ vs. untreated control. Dashed red line indicates the corresponding quantity of the *Lmna* KO untreated control.

To determine whether the accumulation of DNA damage during *in vitro* differentiation of *Lmna* KO myoblasts was caused by progressive new nuclear damage or defects in DNA damage repair, which had been reported in several progeroid laminopathies[40-42], we subjected *Lmna* KO and wild-type myofibers to a pulse of gamma irradiation and monitored γH2AX levels at 3, 6, and 24 hours post-treatment. Consistent with previous studies[43], irradiation resulted in a rapid increase in the number of γH2AX foci at 3 hours that then gradually resolved and returned to baseline by 24 hours post irradiation (Suppl. Fig. S2.11). Notably, *Lmna* KO myofibers displayed a DNA damage profile nearly identical to wild-type controls, suggesting that their ability repair DNA damage is not significantly impaired.

Accumulation of DNA damage induces myofiber death

To test whether accumulation of DNA damage is sufficient to explain the progressive decline in myofiber viability in the *Lmna* KO cells, we subjected *Lmna* KO and wild-type myofibers to repeated treatments of phleomycin, a radiation mimetic agent, in conjuction with inhibition of DNA damage repair with NU7441, a DNA-PK-specific inhibitor, and/or KU55933, an ATM-specific inhibitor (**Fig. 2.5g**). Combined treatment with phleomycin and DNA damage repair inhibition (by one or both inhibitors in combination) caused loss of viability in wild-type myofibers comparable to that observed in untreated *Lmna* KO cells (**Fig. 2.5h**). In contrast, phleomycin, alone or in combination with DNA damage repair inhibition, did not further reduce viability in *Lmna* KO myofiber (Suppl. Fig S2.12), suggesting that the preexisting DNA damage in

these cells is already sufficient to drive myofiber decline. Taken together, these findings demonstrate the adverse effect of DNA damage on myofibers.

Nuclear damage in *Lmna* KO myofibers can be prevented by microtubule stabilization

We surmised that NE ruptures in *Lmna* mutant myofibers resulted from cytoskeletal forces acting on mechanically weak myonuclei, and that reducing mechanical stress on the nuclei would decrease nuclear damage. In striated muscle cells, the microtubule network remodels significantly upon differentiation to form a cage-like structure around the myonuclei[44] (Suppl. Fig. S2.13), in large part due to the redistribution of centrosomal proteins at the NE[45]. To test if stabilizing this microtubule network and thereby reinforcing myonuclei can reduce chromatin protrusions and NE rupture, we treated *in vitro* differentiated myoblasts with low doses of the microtubule stabilizing drug, paclitaxel. Here, we focused on the *Lmna* KO model, which showed the most severe nuclear defects. The microharpoon assay confirmed that microtubule stabilization reinforced *Lmna* KO nuclei in differentiated myofibers and significantly reduced nuclear deformation in response to cytoplasmic force application (**Fig. 2.6a,b**). Furthermore, paclitaxel treatment significantly reduced the percentage of nuclei with chromatin protrusions (**Fig. 2.6c**) and the incidence of NE rupture detected with the cGAS-mCherry reporter in the *Lmna* KO cells (**Fig. 2.6d**), suggesting that nuclear damage indeed arises from mechanical stress on the myonuclei and can be prevented by mechanically stabilizing the nuclei.

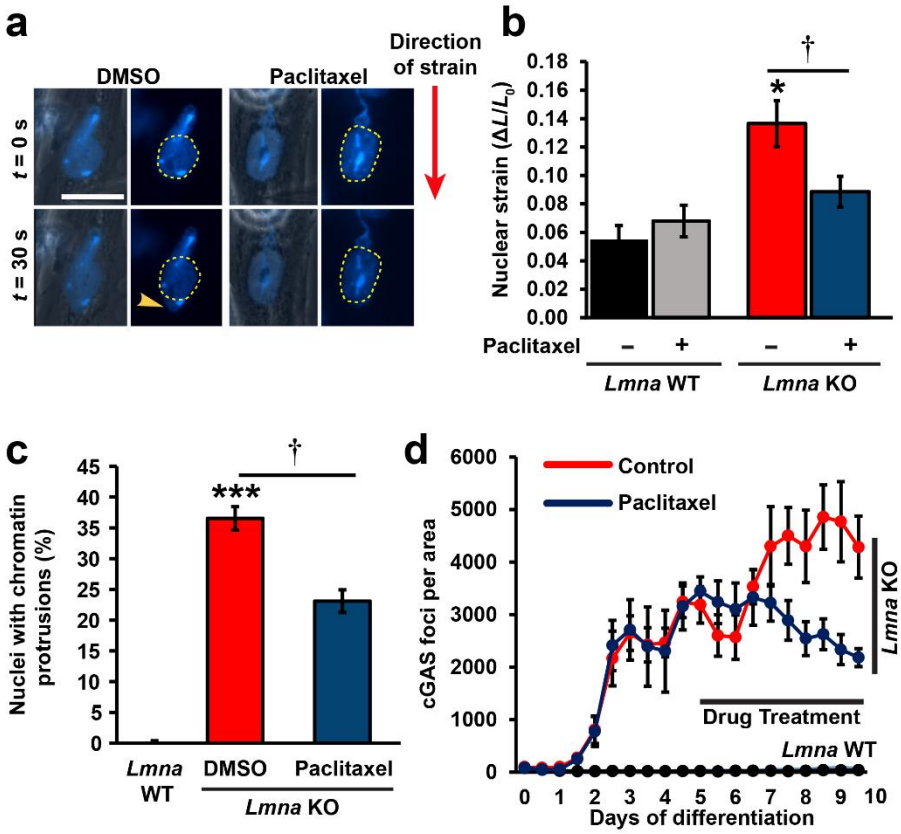

Figure 2.6. Mechanical reinforcement of *Lmna* KO myonuclei by microtubule stabilization reduces nuclear damage. (**a**) Representative image of nuclear deformation following microharpoon in *Lmna* KO myotubes at day five of differentiation. Myotubes were treated for 24 hours with either paclitaxel or DMSO control. Yellow dotted line denotes the perimeter of the nucleus prior to strain application. Scale bar: 20µm. (**b**) Quantification of nuclear strain in *Lmna* WT and *Lmna* KO myofibers using microharpoon assay following 24 hours of treatment with 50 nM paclitaxel or DMSO vehicle control. *, $p < 0.05$ *vs*. *Lmna* WT. †, $p < 0.05$ *vs*. vehicle control. (**c**) Quantification of chromatin protrusions at day 7 of differentiation following treatment with the paclitaxel (50 nM) or DMSO starting at day 4. $n = 3$ independent experiments. ***, $p < 0.001$ *vs*. *Lmna* WT. †, $p < 0.01$ *vs*. vehicle control. (**d**) Quantification of cGAS-mCherry foci formation during 10 myofiber differentiation following treatment with paclitaxel (10 nM) or DMSO control, starting at day 5 of differentiation. $n = 3$ independent experiments.

Kinesin-mediated nuclear movements are responsible for nuclear damage in *Lmna* KO myonuclei

The finding that nuclear damage occurred only during myoblast differentiation, when the cytoskeleton significantly remodels, and that microtubule stabilization significantly reduced the amount of nuclear damage in *Lmna* KO myofibers, suggest that the nuclear

defects result from cytoskeletal forces acting on the mechanically weaker *Lmna* mutant myonuclei. Physical stress may be imparted to myonuclei via (1) actomyosin-mediated contractile forces, and/or (2) forces due to nuclear movements at various stages of muscle development, including myoblast migration and fusion[46], microtubule-driven spacing[44, 47-54], shuttling to the periphery of myofibers[55-57], and anchoring at the fiber periphery and neuromuscular junctions[58]. To address whether NE damage is caused by actomyosin contractility, we treated *Lmna* KO and wild-type myotubes with nifedipine, a calcium channel blocker. Nifedipine treatment effectively abrogated myotube contraction, but did not reduce the frequency of chromatin protrusions and NE ruptures in *Lmna* KO myonuclei (Suppl. Fig. S2.14), indicating that actomyosin contractility is not required to induce NE damage. Therefore, we focused our attention to cytoskeletal forces exerted on the nucleus during nuclear migration in differentiating myotubes.

Based on the timing of the onset of NE rupture (**Fig. 2.4c**) and a progressive increase in the length of the chromatin tethers with differentiation (Suppl. Fig. S2.15), we examined the role of myonuclear spreading along microtubules during myotubes maturation[59, 60]. Time-lapse sequences of *Lmna* KO myoblasts expressing the NLS-GFP and/or cGAS-mCherry reporters revealed that NE rupture frequently occurred when myonuclei were moved along the length of myotubes by microtubule-associated motors (**Fig. 2.7a**). Thus, we reasoned that inhibiting nuclear movement should prevent nuclear damage in *Lmna* KO myofibers. Supporting this hypothesis, depletion of Kif5b, a subunit of kinesin-1 that is required for nuclear migration in myotubes [59-61], almost completely abolished chromatin protrusions (**Fig. 2.7b,c**; Suppl. Fig. S2.16), NE rupture (**Fig. 2.7d,e**), and DNA damage in the *Lmna* KO myotubes (**Fig. 2.7f,g**). These findings

indicate that nuclear movement by microtubule-mediated forces are sufficient to cause nuclear damage in *Lmna* mutant myofibers, and that mechanically induced NE damage, rather than disturbed cytoplasmic signaling or gene expression, is responsible for the increased DNA damage in these cells.

Skeletal muscle biopsies from patients with *LMNA*-associated muscular dystrophy show severe DNA damage

Finally, to corroborate the findings from the *in vitro* and *in vivo* mouse models of striated muscle laminopathies in a clinically relevant context, we examined skeletal muscle biopsy samples from patients with *LMNA*-related muscular dystrophies and age-matched controls (**Table 2.1**). Muscle tissues were immunofluorescently labeled for 53BP1, an established marker for DNA double strand breaks[62, 63], and myofiber nuclei were identified based on labeling for DNA, actin, and dystrophin (**Fig. 2.8a,b**, Suppl. Fig. S2.17). Intriguingly, tissues from individuals with the most severe forms of the muscular dystrophy, i.e., those with early childhood and juvenile onsets, had significantly increased DNA damage compared to age-matched controls (**Fig. 2.8c**), thus closely mirroring the findings in the most severe laminopathy mouse models **(Fig. 2.5e).** In summary, *LMNA* mutations result in increased DNA damage, which is detrimental to myofiber health both in laminopathy mouse models and human patients.

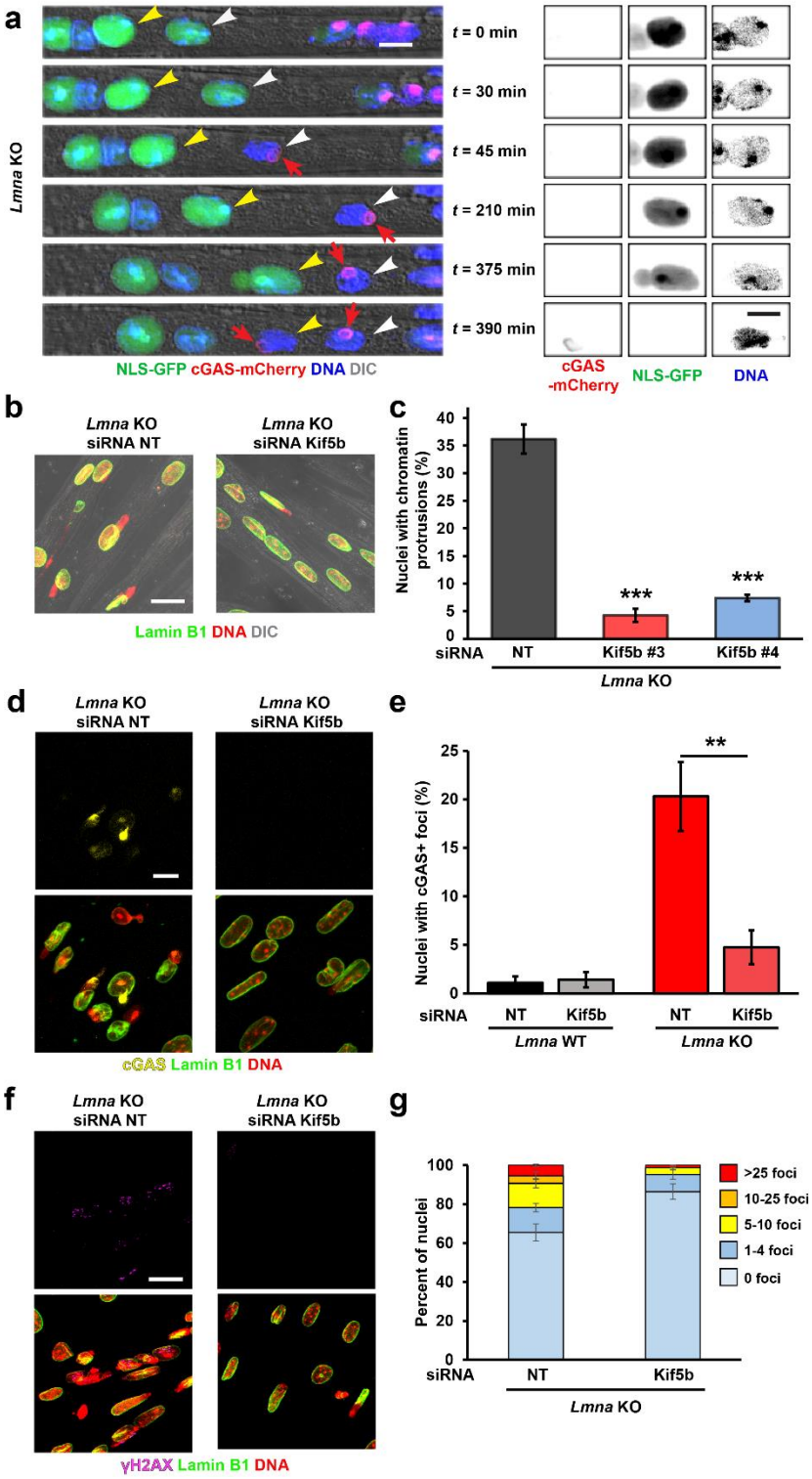

Figure 2.7. Myonuclear ruptures occur during nuclear migration in *Lmna* KO myotubes. (**a**) Representative time-lapse image sequence of NE rupture in *Lmna* KO myonuclei during nuclear migration at day five of differentiation. White and yellow arrowheads mark two individual nuclei that undergo NE rupture, visibly by transient loss of NLS-GFP from the

nucleus and stable accumulation of cGAS-mCherry at the site of rupture (red arrow). Images on the right show close-ups of the nucleus marked with a yellow arrowhead. Scale bar: 10µm for all images. (**b**) Representative images of *Lmna* KO myofiber at day 5 of differentiation treated with either a non-target control siRNA (siRNA NT) or siRNA against kinesin-1 (siRNA Kif5b) at day 0. Scale bar: 20 µm. (**c**) Quantification of the number of chromatin protrusions at day 5 of differentiation in *Lmna* KO cells treated with non-target (NT) siRNA or depleted for Kif5b using two independent siRNAs (Kif5b#3 and Kif5b#4). $n = 4$ independent experiments, with 155-270 nuclei counted per image. ***, $p < 0.001$ *vs*. NT control. (**d**) Representative images of cGAS-mCherry accumulation in *Lmna* KO cells treated with either non-target control siRNA (siRNA NT) or siRNA against Kif5b. Scale bar: 20 µm (**e**) Quantification of the number of *Lmna* KO myonuclei positive for cGAS-mCherry foci following treatment with either non-target siRNA (siRNA NT) or siRNA against Kif5b. $n = 3$ independent experiments, in which a total of 911-1383 nuclei per condition were quantified. **, $p < 0.01$ vs. NT. (**f**) Representative images of *Lmna* KO cells treated with either non-target (NT) siRNA or siRNA against Kif5b and immunofluorescently labeled for γH2AX, showing fewer chromatin protrusions and less DNA damage in the Kif5b depleted cells. Scale bar: 20 µm (**g**) Quantification of the number of γH2AX foci in *Lmna* KO myonuclei following treatment with either non-target siRNA or siRNA against Kif5b. $n = 3$ independent experiments in which 27-53 nuclei are counted per image.

Discussion

The mechanism by which many *LMNA* mutations result in predominately muscle-specific diseases, such as AD-EDMD and *LMNA*-CMD, has long puzzled researchers and clinicians, presenting a major hurdle in the development of effective treatment approaches. Here, we present comprehensive evidence in support of the 'mechanical stress' hypothesis. By using three mouse models of striated muscle laminopathies with varying onset and severity, we were able to systematically assess the frequency of nuclear damage, including chromatin protrusions, NE rupture, and DNA damage, in muscle fibers *in vitro* and *in vivo* in a uniform genetic background. Our studies revealed a striking correlation between the nuclear defects observed during *in vitro* myoblast differentiation, myonuclear defects in isolated muscle fibers, and disease onset and severity in the mouse model.

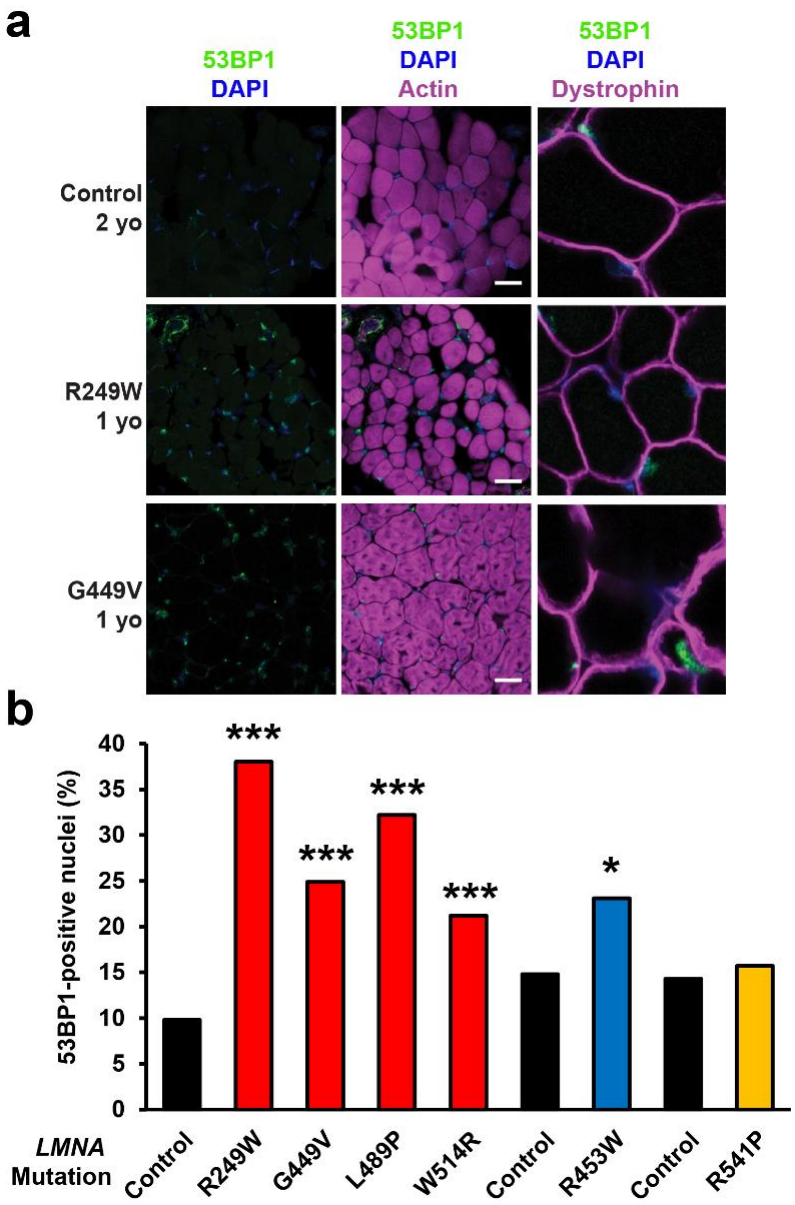

Figure 2.8. Human muscle biopsy tissue from individuals with *LMNA* muscular dystrophy showed increased 53BP1 staining. Cryopreserved human muscle biopsy tissue from individuals with *LMNA* muscular dystrophy and age-matched controls was sectioned and stained with antibodies to either (**a**) 53BP1, DAPI, and phalloidin or (**b**) 53BP1, DAPI, and dystrophin. Yellow arrowheads denote nuclei within muscle fibers, identified by dystrophin labeling of the muscle fiber membrane. Each muscular dystrophy patient possesses a *LMNA* mutation that results in a single amino acid substitution (**Table 2.1**). The *LMNA* mutations cause reduced fiber size, abnormally shaped fibers, and increased nuclear 53BP1 staining. (**c**) Quantification of the percentage of 53BP1-positive nuclei. ***, $p < 0.001$ *vs*. age-matched control; *, $p < 0.05$ *vs*. age-matched control. $n = 91$-363 nuclei per sample. Scale bar: 30 µm.

Table 2.1. Clinical information on patient muscle biopsy samples.

Nucleotide change	Amino acid substitution	Age on onset	Age of diagnosis (yo)	Age when muscle biopsy obtained (yo)	Tentative diagnosis/comments	Reference
745C>T	R249W	3 months	<1	2	Congenital MD, early onset with dropped head, unable to sit unassisted at 3 yo	unpublished
1346G>T	G449V	6 months	3	1	Congenital MD, non-ambulatory at 13 yo	72, 102
1466T>C	L489P	<2	7	2	Congenital MD , moderately severe at 2 yo	72, 102
1540T>C	W514R	2-3 yo	5	3	Mild to moderate myopathy at 14 yo	72, 102
1357C>T	R453W	n.a.	6	10	Mild myopathy at 5.5 yo	unpublished
1622G>C	R541P	n.a.	<52	52	n.a.	unpublished

Notably, analysis of biopsies from individuals with *LMNA*-related muscular dystrophies showed a similar trend, with samples corresponding to the most severe forms of muscular dystrophy having the largest fraction of myonuclei with DNA damage. The limited number of available human samples and inherent genomic heterogeneity, however, limits the conclusions that can be made. Our results are consistent with previous reports of NE damage and intrusion of cytoplasmic organelles into the nucleoplasm in skeletal muscle fibers of patients with EDMD[64-67], cardiac myocytes in *LMNA*-dilated cardiomyopathy patients[68, 69], lamin A/C-deficient mice[13, 70], and muscle and tendons of lamin-deficient fruit flies[71, 72]. Unlike those previous reports, however, we now provide detailed information on the extent, timing, and cause of the NE damage, revealing a striking correlation of NE rupture and disease severity.

Although increased DNA damage and altered DNA damage repair have been reported previously in *LMNA* mutant cells, those cases were linked to progeroid diseases, including Hutchinson-Gilford progeria syndrome (HGPS) and atypical Werner syndrome (AWS)[40-42, 73, 74]. Our findings demonstrate for the first time that cytoskeletal forces acting on myonuclei result in nuclear damage and DNA damage in skeletal muscle fibers *in vitro* and *in vivo*. The precise mechanisms by which NE damage and NE rupture cause DNA damage and cell death remains to be elucidated. The DNA damage could arise from exposure of genomic DNA to cytoplasmic nucleases following NE rupture, or nuclear exclusion and efflux of DNA repair factors, as previously discussed in the context of confined cell migration[75-77]. The close association of DNA damage with NE defects in our studies (Suppl. Fig. S2.10) suggests that the DNA damage is linked to mechanically induced NE defects, which is further supported by the

finding that depletion of kinesin-1 abolished both NE defects and DNA damage in *Lmna* KO cells (**Fig. 2.7b-f**).

Given the known association between lamin A/C and the DNA damage response protein 53BP1[78], loss of lamin A/C could also impair DNA damage repair efficiency, although this effect may be limited to proliferating cells and the associated replication stress[79-81]. In our experiments, post-mitotic *Lmna* KO myofibers exposed to DNA-damaging irradiation exhibited similar DNA damage repair dynamics as wild-type cells, indicating that the observed increase in DNA damage in *Lmna* KO myofibers is not caused by defective DNA damage repair. Nonetheless, it is possible that the efficiency of DNA damage repair decreases over the course of the differentiation, as the highest levels of DNA damage were found in myofibers at late stages of maturation. Such a decrease in DNA repair efficiency is consistent with work showing that satellite cells repair radiation-induced DNA double strand breaks more efficiently than their differentiated counterparts[82], and reduced DNA damage repair could amplify the progressive DNA damage in differentiating myoblasts. In wild-type myofibers, repeated exposure to DNA damaging agents, when combined with DNA damage inhibition, was sufficient to induce cell death to the same extent as observed in untreated *Lmna* KO cells (**Fig. 2.5g,h**), demonstrating that accumulating DNA damage is sufficient to induce cell death even in post-mitotic cells such as myofibers.

The role of DNA damage response signaling in post-mitotic muscle function is an area of increasing interest. DNA damage results in rapid activation of DNA damage response pathways, including DNA-PK and ATM, which results in stabilization of p53, one of the primary DNA damage response pathway that can induce cell cycle arrest,

senescence, and apoptosis.[83, 84] The consequences of increased DNA damage response signaling in postmitotic cells remain poorly characterized, but recent findings point to an intriguing role of DNA damage response pathways in skeletal and cardiac muscle. Increased activity of DNA-PK, one of the major DNA damage sensing pathways in interphase cells[37], was recently linked to the age-related decline of metabolic, mitochondrial, and physical fitness of skeletal muscle cells[35]. Furthermore, cardiac-specific expression of *Lmna* D300N results in increased DNA damage and activation of p53 in a laminopathy mouse model, and cardiac specific deletion of the *Trp53* gene encoding p53 significantly improved the cardiac defects, although only marginally improved overall survival[74]. Consistent with increased p53 signaling caused by accumulating DNA damage, we found evidence of caspase-3 activation and a progressive loss in viability in *Lmna* KO and N195K myofibers (**Fig. 2.1e,f**). While the mechanisms controlling apoptosis in a post-mitotic tissue such as skeletal muscle are not well understood and remain controversial[85], this type of cell death has been observed in myofibers during other muscle wasting conditions[86], in *Lmna* E82K mutant [87] and heterozygous *Lmna*$^{+/-}$ mouse hearts[88], and recently in a cardiac-specific *Lmna* D300N mouse model[74].

While we cannot exclude the possibility that altered cytoplasmic signaling and gene regulation pathways contribute to the increased NE and DNA damage in *Lmna* mutant muscle cells[74, 89], our data suggest that the damage is force-dependent and nuclear-intrinsic, as depletion of Kif5b almost completely prevented DNA damage in *Lmna* KO myofibers (**Figs. 2.3e,f, 2.4f,g, 2.7b-g**). Our findings support a model in which cytoskeletal forces cause chromatin protrusions and NE ruptures in mechanically

weakened *Lmna* mutant muscle cell nuclei, triggering DNA damage, which then leads to myofiber dysfunction and death in striated muscle laminopathies (**Fig. 2.9**). Given the diverse roles of lamins in cellular function, we acknowledge that additional mechanisms may contribute to the pathogenesis of laminopathies, and their specific contribution may depend on the particular cellular context.

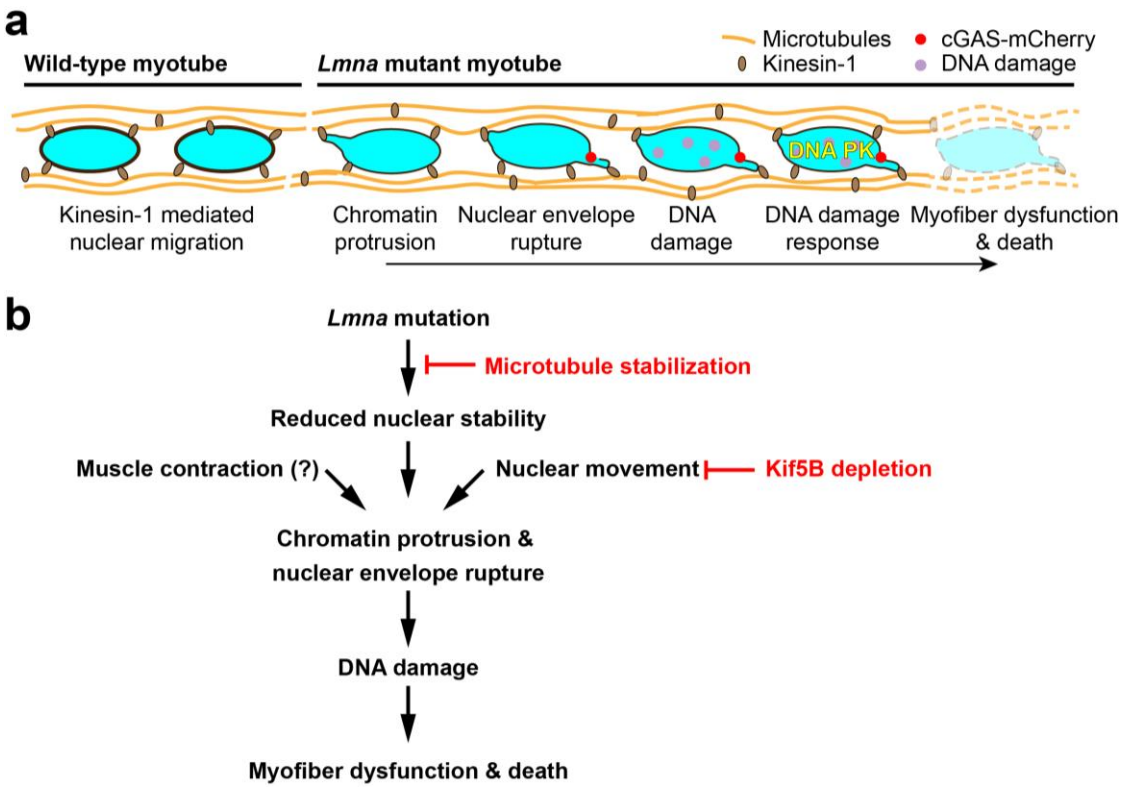

Figure 2.9. Proposed mechanism by which *Lmna* mutations result in myofiber dysfunction and death. (**a**) Kinesin-1 motor proteins spread myonuclei along the myotubes axis during differentiation. In *Lmna* mutant cells, which have mechanically weaker nuclei, the localized forces associated with nuclear migration cause chromatin protrusion and NE ruptures. This mechanically induced nuclear damage results in DNA damage, detected by H2AX foci, and activation of the DNA damage response pathways, which leads to decline in myofiber health and cell death. (**b**) Schematic flow chart delineating the steps described in panel A, along with interventions explored in this work. Stabilizing microtubules surrounding the myonuclei reinforces the *Lmna* mutant nuclei and prevents chromatin protrusions and NE ruptures. Inhibiting nuclear movement by Kif5b depletions similarly prevents nuclear damage. Muscle contractions may also contribute to nuclear damage *in vivo*.

Although *Lmna* mutant myoblasts have mechanically weaker nuclei than wild-type myoblasts, we found that NE damage only arose during myoblast differentiation, when cytoskeletal forces acting on the myonuclei increase. Surprisingly, nuclear damage during *in vitro* myofiber differentiation was associated with kinesin-1 mediated nuclear movements, independent of actomyosin contractions (**Fig. 2.7b-e,** Suppl. Fig. S2.14). Kinesin-1 applies localized point forces at the NE of skeletal myonuclei, either directly or through microtubules anchored at the NE, to ensure correct nuclear positioning[60]. These forces acting on the weakened NE are likely sufficient to induce NE rupture in the *Lmna* mutant myonuclei, based on recent studies on lamin A/C-depleted cells subjected to precisely controlled tensile forces[90]. Furthermore, mutations in genes encoding lamins A/C and other NE proteins linked to muscular dystrophies could disrupt perinuclear cytoskeletal organization, including that of desmins[70] and the perinuclear microtubule network, which helps to resist cytoplasmic strain and physically protect myonuclei, while also serving as the rails by which myonuclei are positioned[91], thereby further promoting nuclear damage in myofibers.

Our experimental data provides novel mechanistic insights into the cellular processes that contribute to the development of striated muscle laminopathies, thereby informing future research efforts to target. Microtubule stabilization is one approach to correct the perturbed force balance and should be further explored as a therapy for striated muscle laminopathies. Paclitaxel was recently reported to improve cardiac conduction defects in *Lmna* H222P mice by restoring proper connexin 43 localization[92]. Here, we highlight an additional mechanism by which microtubule stabilization may mitigate damaging forces in striated muscle laminopathies. In addition, our work indicates that DNA

damage is increased in mouse models of laminopathies, as well as human patients, and that targeting cell signaling pathways activated by DNA damage, such as DNA-PK[35] and p53[74] may provide a mechanism to ameliorate muscle wasting. Furthermore, our studies found that hybrid myofibers containing ~20% *Lmna* KO and ~80% wild-type nuclei were indistinguishable from their isogenic wild-type controls, suggesting that delivery of wild-type lamin A/C to a subset of myonuclei by gene delivery or stem cell therapy may be sufficient to rescue myofiber function. Further studies will need to identify the critical number of wild-type nuclei required to rescue cellular health in laminopathic tissue for therapeutic applications.

Beyond striated muscle laminopathies, insights gained from this work are highly relevant to other biological systems in which nuclei are exposed to physical stress from the cytoskeleton, such as in confined migration of cancer cells[93], or intracellular nuclear positioning of polarized epithelial, or neuronal cells[94]. For example, in neuronal cells lacking functional lamin A[95], defects in B-type lamins[96] or other NE proteins (e.g., nesprin-1) may make these cells more susceptible to kinesin-mediated nuclear damage leading to neurodevelopmental defects (e.g., cerebellar ataxia). Taken together, these findings highlight a novel mechanism by which weakened myonuclei experience microtubule-mediated NE damage, leading to DNA damage and muscle dysfunction, potentially explaining the phenotypes seen in striated muscle laminopathies and a spectrum of other diseases caused by NE defects.

Methods

Animals. *Lmna* KO ($Lmna^{-/-}$)[13], *Lmna* H222P ($Lmna^{H222P/H222P}$)[15], and *Lmna* N195K ($Lmna^{N195K/N195K}$)[14] have been described previously. $Lmna^{+/-}$, $Lmna^{H222P/+}$, and $Lmna^{N195K/+}$ mice were backcrossed at least seven generations into a C57-BL/6 line. For each mouse model, heterozygous mice were crossed to obtain homozygous mutants, heterozygous mice, and wild-type littermates. *Lmna* mutant mice were provided with gel diet (Nutri-Gel Diet, BioServe) supplement to improve hydration and metabolism upon onset of phenotypic decline. Dmd^{mdx} mice have been described previously[97]; mice were obtained from the Jackson Laboratory in a C57BL background and hemi- or homozygous animals were bred to produce all hemi- and homozygous offspring. All mice were bred, maintained and euthanized according to IACUC approved protocols. Data from wild-type littermate controls for *Lmna* KO, *Lmna* N195K and *Lmna* H222P showed no difference in any of the experimental outcomes between the different wild-type littermates, so wild-type data was combined into a single group unless otherwise specified. For both *in vivo* and *in vitro* studies, cells and or tissues were isolated from a single mouse and counted as a single replicate. All data are based on at least two independently derived primary cell lines for each genotype.

Nuclear envelope rupture reporter mouse (cGAS/MB21D1-tdTom transgenic mouse). To detect NE ruptures *in vivo*, we generated a transgenic mouse expressing FLAG tagged human $cGAS^{E225A/D227A}$ fused to a tdTomato fluorescent protein (cGAS-tdTomato) under the control of the commonly used constitutive active CMV promoter. The cGAS mutations are in the magnesium-binding domain, abolishing the enzymatic activity and downstream production of interferon, while still remaining the ability to

bind to genomic DNA. The mammalian expression cassette including promoter and terminator (CMV-3xFLAG-cGAS$^{E225A/D227A}$-tdTomato-SV40polyA) was released from the expression vector, removing the prokaryotic domains. The purified linear DNA was then injected into the pronucleus of fertilized embryos collected from super-ovulated C57BL/6 mice and transplanted into pseudo-pregnant recipients. The resulting transgenic mouse model was used to cross into the *Lmna* KO background to generate 3×FLAG-cGAS$^{E225A/D227A}$-tdTomato positive *Lmna* KO mice within two generations.

Myoblast isolation. Cells were harvested from *Lmna* KO, *Lmna* N195K, *Lmna* H222P, and wild-type littermates between 3-5 weeks for *Lmna* KO mice, 4-6 weeks for *Lmna* N195K, and 4-10 weeks for *Lmna* H222P mice using a protocol adapted from[13]. With the exception of the *Lmna* KO myoblasts, these time-points were prior to the onset of disease phenotypes. Myoblasts from wild-type littermates were harvested at the same time. Muscles of the lower hindlimb were isolated, cleaned of fat, nerve and excess fascia, and kept in HBSS on ice until all mice were harvested. The muscles were digested in 4 ml:1 g of tissue wet weight in a solution of 0.5% Collagenase II (Worthington Biochemicals), 1.2 U/ml Dispase (Worthington Biochemicals), 1.25 mM $CaCl_2$ (Sigma) in HBSS/25 mM HEPES buffer. Digestion was carried out in a 37˚C water bath for a total time of 60 minutes. At 20 minutes intervals, digestion cocktails were removed and triturated 40 times with a 5 ml pipet. In the case of difficult to digest tissues, an extra 25% of 1% Collagenase II was added to the digestion after 40 minutes.

When tissues were fully digested, the reaction was quenched using equal volumes of DMEM supplemented with 10% fetal bovine serum (FBS) and 1% P/S (D10 media, Gibco). The cell suspension was strained through 70 and 40 μm filters (Greiner

Bioscience) sequentially to remove undigested myotube fragments and tendon. The cell suspension was centrifuged at 800 × g for 5 minutes and washed with 8 ml of D10 media for a total of four times. Cells were then resuspended in primary myoblast growth media (PMGM; Hams F-10 (Gibco) supplemented with 20% horse serum and 1% penicillin/streptomycin and 1 µl/ml basic fibroblast growth factor (GoldBio)) and plated onto a 2% gelatin coated T25 flask. Cells were allowed to sit undisturbed for 72 hours. Capitalizing on the fact that myoblasts adhere much more weakly than fibroblasts, cells were passaged using PBS (calcium- and magnesium-free) instead of trypsin to purify the myoblasts. Cells were washed for 2-3 minutes at room temperature using a volume of PBS sufficient to coat the bottom of the flask and dislodged using manual agitation. When necessary, a 0.000625% trypsin solution was used to aid in the myoblast removal. Myoblasts were re-suspended in PMGM and re-plated onto gelatin coated flasks. This process was continued 3-4 times until pure myoblast cultures were achieved[98]. Cells were maintained in culture on gelatin coated flasks with media changes every other day. All experiments were carried out prior to passage 12. Each independent experiment was done on a different set of lamin mutant and wild-type littermates such that each independent experiment was sourced from a different animal to account for heterogeneity in phenotype.

Myoblast differentiation. Myoblasts were differentiated according to a protocol modified from[16]. Coverslips for differentiation were prepared by first coating with CellTak (Corning) according to the manufacturer's protocol and then coating with growth factor reduced Matrigel (Corning) diluted 1:100 with IMDM with Glutamax (Gibco). Pre-cooled pipette tips were used to avoid premature polymerization. Matrigel

was allowed to polymerize at 37˚C for 1 hour and the excess solution was aspirated. Primary myoblasts were seeded at a density of 55,000 cells/cm^2 in PMGM. Cells were allowed to attach for 24 hours before being switched to primary myoblast differentiation media (PMDM) composed of IMDM with Glutamax and 2% horse serum without antibiotics. This timepoint was considered day 0. One day after the onset of differentiation, a top coat of 1:3 Matrigel:IMDM was added to the cells and allowed to incubate for 1 hour at 37˚C. PMDM supplemented with 100 ng/ml agrin (R&D Systems) was added to the cells and henceforth replaced every second day. Cells were allowed to differentiate for a total of 0, 5, or 10 days.

Plasmids and generation of fluorescently labeled cell lines. Each of the mutant myoblast lines were stably modified with lentiviral vectors to express the nuclear rupture reporter NLS-GFP (pCDH-CMV-NLS-copGFP-EF1-blastiS) and cGAS-mCherry (pCDH-CMV-cGAS$^{E225A/D227A}$-mCherry2-EF1-blastiS). cGAS is a cytosolic DNA binding protein; we used a cGAS mutant (E225A/D227A) with abolished enzyme activity and interferon production, but that still binds DNA[99] and serve as a NE rupture reporter[26]. For rescue experiments, *Lmna* KO cells were modified with human lamin A (pCDH-CMV-preLamin A-IRES-GFP-puro).

Viral modification. Pseudoviral particles were produced as described previously[26]. In brief, 293-TN cells (System Biosciences, SBI) were co-transfected with the lentiviral-containing, packaging and envelope plasmids using PureFection (SBI), following manufactures protocol. Lentivirus-containing supernatants were collected at 48 hours and 72 hours after transfection, and filtered through a 0.45 μm filter. Cells to be transduced were seeded into 6-well plates so that they reached 50-60% confluency on

the day of infection and transduced at most 2 consecutive days with the viral supernatant using the TransDux Max system (SBI). The viral solution was replaced with fresh culture medium, and cells were cultured for 72 hours before selection with 1 μg/mL of puromycin or 2 μg/mL blasticidin S for 2-5 days. After selection, cells were subcultured and maintained in their recommended medium without the continued use of selection agents.

Extended imaging using incubator microscope. Long term imaging was performed using an Incucyte imaging system, which allows for incubator imaging to minimize the effects of humidity and CO_2 changes. The differentiating cells expressing combinations of NLS-GFP and cGAS-mCherry were imaged using the Incucyte dual color filter module from day 0 to day 10, every 30-60 minutes with a 20× objective. Resulting images were analyzed using the Incucyte software, which performs fluorescence background subtraction using a top hat method and then subsequent thresholding. cGAS-mCherry cells were thresholded and then analyzed for increase in fluorescent foci over time to track the rate of increase in NE rupture or damage. NLS-GFP cells were used to investigate the frequency and presence of NE rupture. To verify the results obtained from the Incucyte, cells were fixed and stained with appropriate antibodies to evaluate DNA damage and NE rupture.

Isolation of single muscle fibers. Single muscle fibers were harvested in a protocol adapted from Vogler et al.[100]. As previously described, fibers were isolated from the extensor digitorum longus (EDL) of male and female *Lmna* KO and wild-type litter mates at 5-6 weeks of age and *Lmna* H222P and wild-type litter mates were harvested at 6-8 weeks of age at 23-25 weeks of age in order to compare pre- and post-phenotype

onset tissue[13, 15, 101]. Briefly, the EDL (extensor digitorus longus) and plantaris were isolated from the mouse and placed directly into a 1 ml solution of F10 media with 4,000 U/ml of Collagenase I (Worthington Biochemicals). The tissue was digested for 15-40 minutes depending on muscle size in a 37˚C water bath with agitation by inversion every 10 minutes. The reaction was quenched by transferring the digestion mixture to 4 ml of PMGM. Single fibers were hand-picked from the digested tissue using fire polished glass Pasteur pipettes. When necessary, the tissue was further dissociated by manual pipetting with a large-bore glass pipet. Fibers were washed once in fresh media prior to fixation with 4% paraformaldehyde (PFA) for 15 minutes at room temperature and subsequent IF staining.

Pharmacological treatments. For preliminary experiments, myoblasts were differentiated using the standard protocol and treated with pharmacological treatments starting at day 5 of differentiation. For chromatin protrusion studies, paclitaxel was administered to differentiated myotubes in two 24 hours bursts at day 4 and day 6-post differentiation with a 24 hour recovery in between. Myotubes were then fixed in 4% PFA at day 7 and stained with anti-lamin B and DAPI in order to quantify the percentage of myonuclei with chromatin protrusions. For long term studies using the cGAS reporter, myotubes were treated with 10 nM of paclitaxel starting at day 5 and then media was refreshed every day. To inhibit myotube contraction, cells were treated with 5 μM nifedipine starting at day 5 and then media was refreshed every day. For DNA damage induction and inhibitor experiments, cells were treated with 20μg/ml of phleomycin for a two-hour pulse on Day 3,4, and 5 of differentiation. Concurrently, cells were treated with NU7441 (2 μM), KU55933 (2 μM) starting at day 2 of

differentiation through day 10 of differentiation.

Biophysical assays. To evaluate nuclear deformability in high throughput, we designed and fabricated a microfluidic, micropipette aspiration device. The mask and wafers were produced in the Cornell NanoScale Science and Technology Facility (CNF) using standard lithography techniques. PDMS molds of the devices were cast using Sylgard 184 (Dow Corning) and mounted on coverslips using a plasma cleaner as described previously[26]. Three port entrances were made using a 1.2 mm biopsy punch. Pressures at the inlet and outlet ports were set to 1.0 and 0.2 psi (relative to atmospheric pressure, P_{atm}), respectively, using compressed air regulated by a MCFS-EZ pressure controller (Fluigent) to drive single cells through the device. Myoblasts (~5×10^6 cells/mL suspended in 2 % bovine serum albumin (BSA), 0.2 % FBS and 10 μg/mL Hoechst 33342 DNA stain in PBS) were captured within an array of 18 pockets, and then forced to deform into 3 μm wide × 5 μm tall micropipettes. The selected pressures resulted in detectable nuclear deformations without causing significant damage to the cells (tested using propidium iodide staining). The remaining port was set to P_{atm} and outfitted with a handheld pipette to flush cells from the pockets at the start of each image acquisition sequence. Brightfield and fluorescence images were acquired every 5 seconds for a minimum of 60 seconds using an inverted microscope and 20×/NA 0.8 air objective. Nuclear protrusion length was calculated using a custom-written MATLAB program, made available upon request.

For the microharpoon studies, myoblasts were seeded in 35 mm glass bottom dishes and differentiated as previously described, except without the addition of a Matrigel top coat to allow microharpoon access. A Sutter P-97 micropipette puller was used to create

microharpoons from borosilicate glass rods (Sutter; OD: 1.0 mm, ID: 0.78, 10 cm length) with tip diameters of ≈1 μm. Day 4 myotubes (*Lmna* KO and wild-type) were treated for 24 hours with either 50 nM Paclitaxel or the corresponding 0.1% DMSO. The following day, the microharpoon assay was performed as previously described by our laboratory[22], with slight modifications to the pull parameters to accommodate myotubes. The microharpoon was inserted ≈5-7 μm from the edge of the nucleus and pulled 15 μm at a rate of 1 μm/s. Pull direction was always orthogonal to the long axis of the myofiber. Images were acquired at 40× (+1.6×) every 5 seconds. Nuclear strain and centroid displacement were calculated using a custom-written MATLAB program, made available upon request.

siRNA treatment. siRNAs used were as follows: Kif5b#3 (target sequence 5′-CAGCAAGAAGTAGACCGGATA-3′; Qiagen SI00176050), Kif5b#4 (target sequence 5′-CACGAGCTCACGGTTATGCAA-3′; Qiagen SI00176057), and non-target (NT) negative control (ON-TARGETplus non-targeting pool, Dharmachon, D-001810-10). Myoblasts were seeded at a density of ~15,000 cells per well in a 96-well glass bottomed dish containing a matrigel coating. Once adhered, the myoblasts were transfected twice, 48 hours apart, with siRNA for NT or Kif5b using Lipofectamine RNAiMAX at a concentration of 150 nM in PMGM. After 12 hours, the myoblasts were switched to PMDM and differentiated for 5 days.

Immunofluorescence staining of mouse cells and tissues. Cells were fixed in pre-warmed 4% PFA at the appropriate time point(s) and washed with PBS. Cells were blocked and permeabilized with a solution of 3% BSA, 0.1% Triton-X 100 and 0.1% Tween (Sigma) for 1 hour at room temperature. Cells were stained with primary

antibodies diluted in blocking solution according to Table 2 at 4˚C overnight. Samples were washed with PBS and incubated for 1 hour at room temperature with 1:250 dilution of AlexaFluor antibodies (Invitrogen) and 1:1000 DAPI (Sigma). Single muscle fibers were stained using the same procedure in Eppendorf tube baskets with an increase in blocking solution Triton-X concentration to 0.25%.

***Human patient biopsy staining*.** Cryopreserved human quadriceps muscle biopsy tissue from *LMNA* muscular dystrophy individuals and age-matched controls were used for immunostaining as described [102]. An anti-rabbit polyclonal 53BP1 antibody (Novus) and anti-dystrophin mouse monocolonal antibody (Mab7A10, U of Iowa Hospitals and Clinics Pathology Core) were used at 1:1000 and 1:20 dilutions, respectively. Texas Red labeled phalloidin (Invitrogen) was used at 1:400 dilution. Secondary antibodies were a goat anti-rabbit Ig Alexa 488 conjugate (Invitrogen) and a goat anti-mouse IgG rhodamine Red-X conjugated (Molecular Probes), both used at 1:500 dilution. Slides were imaged on a Zeiss 710 confocal microscope (University of Iowa Central Microscopy Facility). The intensity of nuclear anti-53BP1 staining was quantified using ImageJ. 53BP1 positive nuclei possessed intensity values greater than one standard deviation above the mean for age-matched controls. To determine statistical differences, the number of 53BP1 positive nuclei in the *LMNA* muscular dystrophy samples was compared to that of age-matched controls using Fisher's exact test. The analysis of the human muscle samples was performed in a double-blinded manner. A pathologist generated the cryo-sections and coded the samples. The coded samples were stained, imaged, and quantified prior to decoding by an independent person. Samples were collected and analyzed following protocols approved by the corresponding IRB, with

informed consent from all participants.

Western analysis. Cells were lysed in RIPA buffer containing protease (cOmplete EDTA-Free, Roche) and phosphatase (PhosSTOP, Roche) inhibitors. Protein was quantified using Bio-Rad Protein Assay Dye and 25-30 µg of protein lysate was separated using a 4-12% Bis-Tris polyacrylamide gel using standard a standard SDS-Page protocol. Protein was transferred to a polyvinylidene fluoride (PVDF) membrane overnight at 4˚C at a current of 40 mA. Membranes were blocked using 3% BSA in tris-buffered saline containing 0.1% Tween-20 and primary antibodies (Table S2.2) were diluted in the same blocking solution and incubated overnight at 4˚C. Protein bands were detected using either IRDye 680LT or IRDye 800CW (LI-COR) secondary antibodies, imaged on an Odyssey® CLx imaging system (LI-COR) and analyzed in Image Studio Lite (LI-COR)

Imaging acquisition. Cells on coverslips and mounted single muscle fibers were imaged with an inverted Zeiss LSM700 confocal microscope. Z-stack were collected using 20× air (NA = 0.8), 40× water-immersion (NA = 1.2) and 63× oil-immersion (NA = 1.4) objectives. Airy units for all images were set between 1 and 1.5. Epi-fluorescence images were collected on a motorized inverted Zeiss Observer Z1 microscope equipped with CCD cameras (Photometrics CoolSNAP EZ or Photometrics CoolSNAP KINO) or a sCMOS camera (Hamamatsu Flash 4.0). H&E histology images were collected on an inverted Zeiss Observer Z1 microscope equipped with a color CCD camera (Edmund Optics, EO-0312C).

Image analysis. Image sequences were analyzed using ZEN (Zeiss), ImageJ, or

MATLAB (Mathworks) using only linear adjustments uniformly applied to the entire image region. Region of interest intensities were extracted using ZEN or ImageJ. To quantify cleaved caspase-3 (i.e. active) area and myofiber health, maximum intensity protections were generated, which were then blinded to the observer. Cleaved caspase-3 area was calculated by thresholding of the caspase-3 and myosin heavy chain fluorescent signal and expressing the cleaved caspase-3 signal relative to the myosin heavy chain signal. Myofiber health and contractions were scored using a blinded analysis according to the scales provided in Suppl. Fig. S2.3. To count the number of DNA protrusions, and DNA damage foci, confocal image stacks were three-dimensionally reconstructed and displayed as maximum intensity projections. Protrusions lengths were both counted and measured by the presence of DAPI signal beyond the lamin B rim of the nucleus. Aspect ratio was quantified based on a thresholded lamin B rim to avoid the confounding factor of the DNA protrusions outside the body of the nucleus. Nuclear rupture was detected by an increase of the cytoplasmic NLS-GFP signal, or the localization of cGAS-mCherry to the nucleus. For better visualization of NLS-GFP cells many of the fluorescent single color image sequences were inverted. Graphs were generated in Excel (Microsoft), and figures were assembled in Illustrator (Adobe). DNA damage was determined by counting H2AX foci and then binned based on foci number. If damage was so severe that individual foci could not be counted, these nuclei were placed in the >25 foci category. For Hsp90 quantification, average nuclear Hsp90 fluorescence intensity was determined from a single mid-nucleus z-plane image and normalized to the cytoplasmic intensity at two points immediately adjacent to the nucleus.

MTT assay. Myoblasts, seeded in a 96-well plate and differentiated as previously described for 0, 5, or 10 days, were assayed for cell viability according to the manufacturer's instructions (Promega, CellTiter 96 Non-Radioactive Cell Proliferation Assay). Fresh differentiation media was added two hours prior to the addition of 15 μL MTT 3-(4,5-dimethylthiazol-2-yl)-2,5-diphenyltetrazolium bromide dye. After incubation for 3 hours in MTT dye, 100 uL of Stop Solution was added to solubilize the formazan product (appears purple). Following overnight incubation at 37°C and 5% CO_2, the absorbance of each well (measured at 590 nm) was analyzed using a microplate reader.

Gamma irradiation. A pulse of gamma-irradiation (5 Gy) was administered to myotubes differentiating (5 days) in a 96 well plate. Non-irradiated controls, along with treated cells following 3, 6, or 24 hours of recovery, were PFA-fixed and stained with anti-γH2AX, anti-lamin B and DAPI. A custom macro was used to quantify the mean integrated density of nuclear γH2AX signal from maximum intensity projections of confocal z-stacks.

Statistical analysis. Unless otherwise noted, all experimental results were taken from at least three independent experiments and *in vivo* data were taken from at least three animals. For data with normal distribution, we used either student's t-tests (comparing two groups) or one-way ANOVA (for experiments with more than two groups) with post-hoc tests. When multiple comparisons were made, we adjusted the significance level using Bonferroni corrections. All tests were performed using GraphPad Prism. Micropipette aspiration data were natural log-transformed (Suppl. Fig. S2.5A) and analyzed by linear regression of the log-log data. In addition, data was analyzed with a

multilevel model, in which the log-transformed protrusion length was the dependent variable in the model and the log-transformed time, genotype, and their interaction were treated as independent fixed effects. Variance from individual experiments and other effects were considered in the model as random effects. Post-hoc multiple comparisons test with Dunnett correction were performed to determine differences between *Lmna* mutant cells (*Lmna* KO, *Lmna* N195K, and *Lmna* H222P) and control cells (pooled wild-type). Analyses were carried out using JMP software. Unless otherwise noted, * denotes $p \leq 0.05$, ** denotes $p \leq 0.01$, and *** denotes $p \leq 0.001$. Unless otherwise indicated, error bars represent the standard error of the mean (SEM). The data that support the findings of this study are available from the corresponding author upon reasonable request.

Data and code availability. The data that support the findings of this study are available from the corresponding authors upon reasonable request. MATLAB codes used for the microharpoon assay and micropipette aspiration analysis is available upon request.

REFERENCES

1. de Leeuw, R., Gruenbaum, Y. & Medalia, O. Nuclear Lamins: Thin Filaments with Major Functions. *Trends Cell Biol* **28**, 34-45 (2018).
2. Worman, H.J. Cell signaling abnormalities in cardiomyopathy caused by lamin A/C gene mutations. *Biochem Soc Trans* **46**, 37-42 (2018).
3. Naetar, N., Ferraioli, S. & Foisner, R. Lamins in the nuclear interior - life outside the lamina. *J Cell Sci* **130**, 2087-2096 (2017).
4. Davidson, P.M. & Lammerding, J. Broken nuclei--lamins, nuclear mechanics, and disease. *Trends Cell Biol* **24**, 247-256 (2014).
5. Maggi, L., Carboni, N. & Bernasconi, P. Skeletal Muscle Laminopathies: A Review of Clinical and Molecular Features. *Cells* **5** (2016).
6. Emery, A.E. Emery-Dreifuss muscular dystrophy - a 40 year retrospective. *Neuromuscular disorders : NMD* **10**, 228-232 (2000).
7. Quijano-Roy, S. *et al.* De novo LMNA mutations cause a new form of congenital muscular dystrophy. *Annals of neurology* **64**, 177-186 (2008).
8. Muchir, A. *et al.* Identification of mutations in the gene encoding lamins A/C in autosomal dominant limb girdle muscular dystrophy with atrioventricular conduction disturbances (LGMD1B). *Human Molecular Genetics* **9**, 1453-1459 (2000).
9. Zwerger, M. *et al.* Myopathic lamin mutations impair nuclear stability in cells and tissue and disrupt nucleo-cytoskeletal coupling. *Hum Mol Genet* **22**, 2335-2349 (2013).
10. Gruenbaum, Y. & Foisner, R. Lamins: nuclear intermediate filament proteins with fundamental functions in nuclear mechanics and genome regulation. *Annual review of biochemistry* **84**, 131-164 (2015).
11. Pimentel, M.R., Falcone, S., Cadot, B. & Gomes, E.R. In Vitro Differentiation of Mature Myofibers for Live Imaging. *Journal of visualized experiments: JoVE* (2017).
12. Denais, C.M. *et al.* Nuclear envelope rupture and repair during cancer cell migration. *Science* **352**, 353-358 (2016).
13. Sullivan, T. *et al.* Loss of A-type lamin expression compromises nuclear envelope integrity leading to muscular dystrophy. *J Cell Biol* **147**, 913-920 (1999).
14. Mounkes, L.C., Kozlov, S.V., Rottman, J.N. & Stewart, C.L. Expression of an LMNA-N195K variant of A-type lamins results in cardiac conduction defects and death in mice. *Human Molecular Genetics* **14**, 2167-2180 (2005).
15. Arimura, T. *et al.* Mouse model carrying H222P-Lmna mutation develops muscular dystrophy and dilated cardiomyopathy similar to human striated muscle laminopathies. *Human molecular genetics* **14**, 155-169 (2004).
16. Pimentel, M.R., Falcone, S., Cadot, B. & Gomes, E.R. In Vitro Differentiation of Mature Myofibers for Live Imaging. *Journal of visualized experiments : JoVE* (2017).
17. Roman, W., Pimentel, M.R. & Gomes, E.R. An In Vitro System to Measure the Positioning, Stiffness, and Rupture of the Nucleus in Skeletal Muscle, in

The LINC Complex 283-293 (Springer, 2018).
18. Melcon, G. *et al.* Loss of emerin at the nuclear envelope disrupts the Rb1/E2F and MyoD pathways during muscle regeneration. *Human Molecular Genetics* **15**, 637-651 (2006).
19. Cohen, T.V. *et al.* Defective skeletal muscle growth in lamin A/C-deficient mice is rescued by loss of Lap2α. *Human molecular genetics* (2013).
20. Dahl, K.N., Engler, A.J., Pajerowski, J.D. & Discher, D.E. Power-law rheology of isolated nuclei with deformation mapping of nuclear substructures. *Biophysical journal* **89**, 2855-2864 (2005).
21. Discher, D.E., Boal, D.H. & Boey, S.K. Simulations of the erythrocyte cytoskeleton at large deformation. II. Micropipette aspiration. *Biophysical Journal* **75**, 1584-1597 (1998).
22. Fedorchak, G. & Lammerding, J. Cell Microharpooning to Study Nucleo-Cytoskeletal Coupling. *The Nuclear Envelope: Methods and Protocols*, 241-254 (2016).
23. Lombardi, M.L., Zwerger, M. & Lammerding, J. Biophysical assays to probe the mechanical properties of the interphase cell nucleus: substrate strain application and microneedle manipulation. *Journal of visualized experiments : JoVE* (2011).
24. Tan, D. *et al.* Phenotype-Genotype Analysis of Chinese Patients with Early-Onset LMNA-Related Muscular Dystrophy. *PLoS One* **10**, e0129699 (2015).
25. Le Berre, M., Aubertin, J. & Piel, M. Fine control of nuclear confinement identifies a threshold deformation leading to lamina rupture and induction of specific genes. *Integrative biology* **4**, 1406-1414 (2012).
26. Denais, C.M. *et al.* Nuclear envelope rupture and repair during cancer cell migration. *Science* **352**, 353-358 (2016).
27. Maciejowski, J., Li, Y., Bosco, N., Campbell, P.J. & de Lange, T. Chromothripsis and kataegis induced by telomere crisis. *Cell* **163**, 1641-1654 (2015).
28. Gnocchi, V.F. *et al.* Uncoordinated transcription and compromised muscle function in the lmna-null mouse model of Emery- Emery-Dreyfuss muscular dystrophy. *PLoS One* **6**, e16651 (2011).
29. Cutler, A.A., Jackson, J.B., Corbett, A.H. & Pavlath, G.K. Non-equivalence of nuclear import among nuclei in multinucleated skeletal muscle cells. *J Cell Sci* **131**, jcs207670 (2018).
30. Raab, M. *et al.* ESCRT III repairs nuclear envelope ruptures during cell migration to limit DNA damage and cell death. *Science* **352**, 359-362 (2016).
31. Robijns, J. *et al.* In silico synchronization reveals regulators of nuclear ruptures in lamin A/C deficient model cells. *Scientific reports* **6**, 30325 (2016).
32. De Vos, W.H. *et al.* Repetitive disruptions of the nuclear envelope invoke temporary loss of cellular compartmentalization in laminopathies. *Hum Mol Genet* **20**, 4175-4186 (2011).
33. Hatch, E.M. & Hetzer, M.W. Nuclear envelope rupture is induced by actin-based nucleus confinement. *J Cell Biol* **215**, 27-36 (2016).
34. Vargas, J.D., Hatch, E.M., Anderson, D.J. & Hetzer, M.W. Transient nuclear

envelope rupturing during interphase in human cancer cells. *Nucleus* **3**, 88-100 (2012).
35. Park, S.-J. *et al.* DNA-PK promotes the mitochondrial, metabolic, and physical decline that occurs during aging. *Cell metabolism* **25**, 1135-1146. e1137 (2017).
36. Irianto, J. *et al.* Nuclear constriction segregates mobile nuclear proteins away from chromatin. *Molecular biology of the cell* **27**, 4011-4020 (2016).
37. Blackford, A.N. & Jackson, S.P. ATM, ATR, and DNA-PK: The Trinity at the Heart of the DNA Damage Response. *Molecular Cell* **66**, 801-817 (2017).
38. Larsen, B.D. *et al.* Caspase 3/caspase-activated DNase promote cell differentiation by inducing DNA strand breaks. *Proceedings of the National Academy of Sciences* **107**, 4230-4235 (2010).
39. Connolly, P.F. & Fearnhead, H.O. DNA-PK activity is associated with caspase-dependent myogenic differentiation. *The FEBS journal* **283**, 3626-3636 (2016).
40. Burla, R., La Torre, M., Merigliano, C., Verni, F. & Saggio, I. Genomic instability and DNA replication defects in progeroid syndromes. *Nucleus* **9**, 368-379 (2018).
41. Larrieu, D., Britton, S., Demir, M., Rodriguez, R. & Jackson, S.P. Chemical inhibition of NAT10 corrects defects of laminopathic cells. *Science* **344**, 527-532 (2014).
42. Hutchison, C.J. The role of DNA damage in laminopathy progeroid syndromes. *Biochem Soc Trans* **39**, 1715-1718 (2011).
43. Polo, S.E. & Jackson, S.P. Dynamics of DNA damage response proteins at DNA breaks: a focus on protein modifications. *Genes Dev* **25**, 409-433 (2011).
44. Gimpel, P. *et al.* Nesprin-1α-dependent microtubule nucleation from the nuclear envelope via Akap450 is necessary for nuclear positioning in muscle cells. *Current Biology* **27**, 2999 (2017).
45. Starr, D.A. Muscle Development: Nucleating Microtubules at the Nuclear Envelope. *Current Biology* **27**, R1071-R1073 (2017).
46. Chang, W., Worman, H.J. & Gundersen, G.G. Accessorizing and anchoring the LINC complex for multifunctionality. *The Journal of cell biology* **208**, 11-22 (2015).
47. Elhanany-Tamir, H. *et al.* Organelle positioning in muscles requires cooperation between two KASH proteins and microtubules. *J Cell Biol* **198**, 833-846 (2012).
48. Espigat-Georger, A., Dyachuk, V., Chemin, C., Emorine, L. & Merdes, A. Nuclear alignment in myotubes requires centrosome proteins recruited by nesprin-1. *J Cell Sci* **129**, 4227-4237 (2016).
49. Folker, E.S., Schulman, V.K. & Baylies, M.K. Translocating myonuclei have distinct leading and lagging edges that require kinesin and dynein. *Development* **141**, 355-366 (2014).
50. Meinke, P. *et al.* Muscular Dystrophy-Associated SUN1 and SUN2 Variants Disrupt Nuclear-Cytoskeletal Connections and Myonuclear Organization. *PLoS genetics* **10**, 18 (2014).

51. Metzger, T. *et al.* MAP and kinesin-dependent nuclear positioning is required for skeletal muscle function. *Nature* **484**, 120-124 (2012).
52. Stroud, M.J. *et al.* Nesprin 1α2 is essential for mouse postnatal viability and nuclear positioning in skeletal muscle. *J Cell Biol*, jcb. 201612128 (2017).
53. Wilson, M.H. & Holzbaur, E.L. Opposing microtubule motors drive robust nuclear dynamics in developing muscle cells. *J Cell Sci* **125**, 4158-4169 (2012).
54. Wilson, M.H. & Holzbaur, E.L. Nesprins anchor kinesin-1 motors to the nucleus to drive nuclear distribution in muscle cells. *Development* **142**, 218-228 (2015).
55. Falcone, S. *et al.* N-WASP is required for Amphiphysin-2/BIN1-dependent nuclear positioning and triad organization in skeletal muscle and is involved in the pathophysiology of centronuclear myopathy. *EMBO molecular medicine* **6**, 1455-1475 (2014).
56. Roman, W. *et al.* Myofibril contraction and crosslinking drive nuclear movement to the periphery of skeletal muscle. *Nature Cell Biology* **19**, 1189-1201 (2017).
57. D'Alessandro, M. *et al.* Amphiphysin 2 orchestrates nucleus positioning and shape by linking the nuclear envelope to the actin and microtubule cytoskeleton. *Developmental cell* **35**, 186-198 (2015).
58. Bone, C.R. & Starr, D.A. Nuclear migration events throughout development. *J Cell Sci* **129**, 1951-1961 (2016).
59. Wilson, M.H. & Holzbaur, E.L. Nesprins anchor kinesin-1 motors to the nucleus to drive nuclear distribution in muscle cells. *Development* **142**, 218-228 (2015).
60. Roman, W. & Gomes, E.R. Nuclear positioning in skeletal muscle. *Seminars in cell & developmental biology* (2017).
61. Gache, V., Gomes, E.R. & Cadot, B. Microtubule motors involved in nuclear movement during skeletal muscle differentiation. *Mol Biol Cell* **28**, 865-874 (2017).
62. Bekker-Jensen, S., Lukas, C., Melander, F., Bartek, J. & Lukas, J. Dynamic assembly and sustained retention of 53BP1 at the sites of DNA damage are controlled by Mdc1/NFBD1. *The Journal of Cell Biology* **170**, 201-211 (2005).
63. Loewer, A., Karanam, K., Mock, C. & Lahav, G. The p53 response in single cells is linearly correlated to the number of DNA breaks without a distinct threshold. *BMC biology* **11**, 114 (2013).
64. Vigouroux, C. *et al.* Nuclear envelope disorganization in fibroblasts from lipodystrophic patients with heterozygous R482Q/W mutations in the lamin A/C gene. *J Cell Sci* **114**, 4459-4468 (2001).
65. Fidzianska, A. & Hausmanowa-Petrusewicz, I. Architectural abnormalities in muscle nuclei. Ultrastructural differences between X-linked and autosomal dominant forms of EDMD. *J Neurol Sci* **210**, 47-51 (2003).
66. Fidzianska, A., Toniolo, D. & Hausmanowa-Petrusewicz, I. Ultrastructural abnormality of sarcolemmal nuclei in Emery-Dreifuss muscular dystrophy (EDMD). *J Neurol Sci* **159**, 88-93 (1998).

67. Park, Y.E. *et al.* Nuclear changes in skeletal muscle extend to satellite cells in autosomal dominant Emery-Dreifuss muscular dystrophy/limb-girdle muscular dystrophy 1B. *Neuromuscular disorders : NMD* **19**, 29-36 (2009).
68. Gupta, P. *et al.* Genetic and ultrastructural studies in dilated cardiomyopathy patients: a large deletion in the lamin A/C gene is associated with cardiomyocyte nuclear envelope disruption. *Basic research in cardiology* **105**, 365-377 (2010).
69. Sylvius, N. *et al.* In vivo and in vitro examination of the functional significances of novel lamin gene mutations in heart failure patients. *Journal of Medical Genetics* **42**, 639-647 (2005).
70. Nikolova, V. *et al.* Defects in nuclear structure and function promote dilated cardiomyopathy in lamin A/C-deficient mice. *The Journal of clinical investigation* **113**, 357-369 (2004).
71. Uchino, R., Nonaka, Y.K., Horigome, T., Sugiyama, S. & Furukawa, K. Loss of Drosophila A-type lamin C initially causes tendon abnormality including disintegration of cytoskeleton and nuclear lamina in muscular defects. *Dev Biol* **373**, 216-227 (2013).
72. Dialynas, G. *et al.* LMNA variants cause cytoplasmic distribution of nuclear pore proteins in Drosophila and human muscle. *Hum Mol Genet* **21**, 1544-1556 (2012).
73. Graziano, S., Kreienkamp, R., Coll-Bonfill, N. & Gonzalo, S. Causes and consequences of genomic instability in laminopathies: Replication stress and interferon response. *Nucleus* **9**, 258-275 (2018).
74. Chen, S.N. *et al.* DNA Damage Response/TP53 Pathway Is Activated and Contributes to the Pathogenesis of Dilated Cardiomyopathy Associated with Lamin A/C Mutations. *Circ Res* (2019).
75. Hatch, E.M. Nuclear envelope rupture: little holes, big openings. *Curr Opin Cell Biol* **52**, 66-72 (2018).
76. Shah, P., Wolf, K. & Lammerding, J. Bursting the Bubble - Nuclear Envelope Rupture as a Path to Genomic Instability? *Trends in cell biology* **27**, 546-555 (2017).
77. Irianto, J. *et al.* DNA Damage Follows Repair Factor Depletion and Portends Genome Variation in Cancer Cells after Pore Migration. *Current biology : CB* **27**, 210-223 (2017).
78. Pozo, F.M. *et al.* Regulatory cross-talk determines the cellular levels of 53BP1 protein, a critical factor in DNA repair. *Journal of Biological Chemistry* **292**, 5992-6003 (2017).
79. Gibbs-Seymour, I., Markiewicz, E., Bekker-Jensen, S., Mailand, N. & Hutchison, C.J. Lamin A/C-dependent interaction with 53BP1 promotes cellular responses to DNA damage. *Aging Cell* **14**, 162-169 (2015).
80. Singh, M. *et al.* Lamin A/C Depletion Enhances DNA Damage-Induced Stalled Replication Fork Arrest. *Molecular and Cellular Biology* **33**, 1210-1222 (2013).
81. Redwood, A.B. *et al.* A dual role for A-type lamins in DNA double-strand break repair. *Cell Cycle* **10**, 2549-2560 (2011).

82. Ferdousi, L.V. *et al.* More efficient repair of DNA double-strand breaks in skeletal muscle stem cells compared to their committed progeny. *Stem Cell Research* **13**, 492-507 (2014).
83. Williams, A.B. & Schumacher, B. p53 in the DNA-damage-repair process. *Cold Spring Harbor perspectives in medicine* **6**, a026070 (2016).
84. Kruiswijk, F., Labuschagne, C.F. & Vousden, K.H. p53 in survival, death and metabolic health: a lifeguard with a licence to kill. *Nature reviews. Molecular cell biology* **16**, 393-405 (2015).
85. Schwartz, L.M. Skeletal Muscles Do Not Undergo Apoptosis During Either Atrophy or Programmed Cell Death-Revisiting the Myonuclear Domain Hypothesis. *Frontiers in Physiology* **9**, 1887 (2019).
86. Cheema, N., Herbst, A., McKenzie, D. & Aiken, J.M. Apoptosis and necrosis mediate skeletal muscle fiber loss in age-induced mitochondrial enzymatic abnormalities. *Aging Cell* **14**, 1085-1093 (2015).
87. Lu, D. *et al.* LMNA E82K mutation activates FAS and mitochondrial pathways of apoptosis in heart tissue specific transgenic mice. *PLoS One* **5**, e15167 (2010).
88. Wolf, C.M. *et al.* Lamin A/C haploinsufficiency causes dilated cardiomyopathy and apoptosis-triggered cardiac conduction system disease. *Journal of Molecular and Cellular Cardiology* **44**, 293-303 (2008).
89. Gonzalo, S. DNA damage and lamins. *Adv Exp Med Biol* **773**, 377-399 (2014).
90. Zhang, Q. *et al.* Local, transient tensile stress on the nuclear membrane causes membrane rupture. *Mol Biol Cell*, mbcE18090604 (2018).
91. Wang, S., Reuveny, A. & Volk, T. Nesprin provides elastic properties to muscle nuclei by cooperating with spectraplakin and EB1. *J Cell Biol* **209**, 529-538 (2015).
92. Macquart, C. *et al.* Microtubule cytoskeleton regulates connexin 43 localization and cardiac conduction in cardiomyopathy caused by mutation in A-type lamins gene. *Human Molecular Genetics* (2018).
93. McGregor, A.L., Hsia, C.R. & Lammerding, J. Squish and squeeze-the nucleus as a physical barrier during migration in confined environments. *Current opinion in cell biology* **40**, 32-40 (2016).
94. Gundersen, G.G. & Worman, H.J. Nuclear positioning. *Cell* **152**, 1376-1389 (2013).
95. Jung, H.J. *et al.* Regulation of prelamin A but not lamin C by miR-9, a brain-specific microRNA. *Proc Natl Acad Sci U S A* **109**, E423-431 (2012).
96. Coffinier, C. *et al.* Deficiencies in lamin B1 and lamin B2 cause neurodevelopmental defects and distinct nuclear shape abnormalities in neurons. *Mol Biol Cell* **22**, 4683-4693 (2011).
97. Bulfield, G., Siller, W.G., Wight, P.A. & Moore, K.J. X chromosome-linked muscular dystrophy (mdx) in the mouse. *Proc Natl Acad Sci U S A* **81**, 1189-1192 (1984).
98. Springer, M.L., Rando, T.A. & Blau, H.M. Gene delivery to muscle. *Current protocols in human genetics / editorial board, Jonathan L. Haines ... [et al.]* **Chapter 13**, Unit13.14-Unit13.14 (2002).

99. Civril, F. *et al.* Structural mechanism of cytosolic DNA sensing by cGAS. *Nature* **498**, 332-337 (2013).
100. Vogler, T.O., Gadek, K.E., Cadwallader, A.B., Elston, T.L. & Olwin, B.B. Isolation, Culture, Functional Assays, and Immunofluorescence of Myofiber-Associated Satellite Cells. *Methods in molecular biology* **1460**, 141-162 (2016).
101. Arimura, T. *et al.* Nuclear accumulation of androgen receptor in gender difference of dilated cardiomyopathy due to lamin A/C mutations. *Cardiovasc Res* **99**, 382-394 (2013).
102. Dialynas, G. *et al.* Myopathic lamin mutations cause reductive stress and activate the nrf2/keap-1 pathway. *PLoS Genet* **11**, e1005231 (2015).

CHAPTER 3

THE LMNA H222P MUTATION CAUSES SEVERE FIBER SIZE MISREGULATION IN RESPONSE TO INJURY BUT NORMAL MYOGENIC TRANSCRIPTION FACTOR SIGNALING[3]

The *Lmna* H222P mouse model is ideal for long term evaluation of myogenic differentiation and regeneration in EDMD due to the delayed phenotype onset, long life span, and direct relevance to human disease. Most skeletal muscle studies in laminopathy models of EDMD have focused on the *Lmna* null mouse model, which displays significant changes in early muscle-specific transcription factor expression; however, due to the early death of the animals at 4-8 weeks, this model is not suitable for long-term studies. A full picture of the long-term consequences of early signaling defects is necessary to identify potential treatment approaches. In this study, we evaluated both short term *in vitro* differentiation of *Lmna* H222P myoblasts and long term *in vivo* muscle regeneration to understand the relative contribution of early and late stages of myogenic differentiation to the disease progression. We found that Lmna H222P myoblasts only exhibit minor differences to wild-type (WT) littermates in terms of *in vitro* differentiation, based on cell proliferation, expression levels of MyoD, myogenin, and MyHC, and nuclear spacing. We also determined that satellite cell

[3] Chapter currently in progress for publication in Cells, Laminopathy Special Issue, end of July 2018. Earle A, Zheng H, Modi S, Mount R, Lammerding J.

AE contributed to design of all experiments, *in vivo* studies and analysis, proliferation studies, preliminary cell culture experiments, and statistical testing. HZ and SM carried out primary myoblast differentiation study and analysis, RM assisted with *in vivo* studies and analysis, and single muscle fiber isolations.

dynamics in *Lmna* H222P mice in response to cardiotoxin injurgy were not significantly different compared to WT at early (8 days post injury) or late (28 days post injury) time points. However, we detected a significant misregulation of fiber diameter in injured mice, even pre-phenotype onset, and the defect was exacerbated in injured post-phenotype mice. These results indicate that the later stages of growth and maturation of muscle fibers in the *Lmna* H222P mouse models may play an important role in the disease progression, and targeting the underlying mechanisms may present a potential treatment approach.

Introduction

Despite the large number of *Lmna* mutations leading to both cardiac and skeletal muscle defects, the majority of studies in the context of skeletal muscle have focused on evaluating the *Lmna* null mutation. Since cardiac defects are the primary contributing factor to mortality, this is not surprising, but the role of skeletal muscle in quality of life is non-trivial, and often being the earliest presentation of symptoms such as joint contractures and muscle wasting[1]. Due to the major role that Lamin A/C plays in transcription factor regulation and epigenetics, and the importance of these signaling processes in muscle differentiation, the primary focus of EDMD muscle research has focused on these areas[2]. Muscle differentiation is a tightly regulated process where muscle stem cells, also called satellite cells, switch from a quiescent to a proliferative phenotype (**Figure 3.1**)[3]. Expression of MyoD, the muscle commitment transcription factor, determines that the stem cell will exit the cell cycle and follow the muscle differentiation cascade to fuse into the either an existing or a *de novo* muscle fiber. This

early stage of muscle proliferation and commitment has been the focus of a significant body of research on *Lmna* null myoblasts.

Interestingly, many groups have come to different conclusions on where the primary defects lie. Some studies have found increased satellite cell and myoblasts proliferation[4-5] while other studies that found decreased proliferation[6, 7]. Similarly, most studies have found delayed differentiation linked back to insufficient in MyoD expression levels[4, 6, 8, 9] however there have also been studies that show premature differentiation[7] or normal differentiation[10]. One finding that has been consistent among all *in vitro* and *in vivo* studies in the *Lmna* null model is epigenetic misregulation, namely an increase in histone acetylation and an inefficient turnover of methylated genes during the differentiation process[11, 9, 8, 5, 12]. Some of the key pathways beyond the muscle differentiation cascade that have been shown to be misregulated by multiple groups are the Rb pathway[4, 5, 13, 9, 6,] SMAD signaling[7, 6] and HDAC signaling[10, 11, 9, 8, 12]. Interestingly, despite the large body of research pointing to defects in the early stages of muscle differentiation, *Lmna* null mice[14] are indistinguishable from WT littermates at birth in terms of size, muscle mass, and muscle function. Indeed, despite possibly delayed or less robust differentiation, all the studies mentioned above show that *Lmna* null myoblasts are capable of undergoing muscle differentiation and forming MyHC positive myofibers. Few studies have investigated possible changes in the later stages of differentiation, after fusion and the major muscle regulation genes have already done the work of creating a myofibers, although one study did show abrogated nuclear positioning at myonuclear junctions[11].

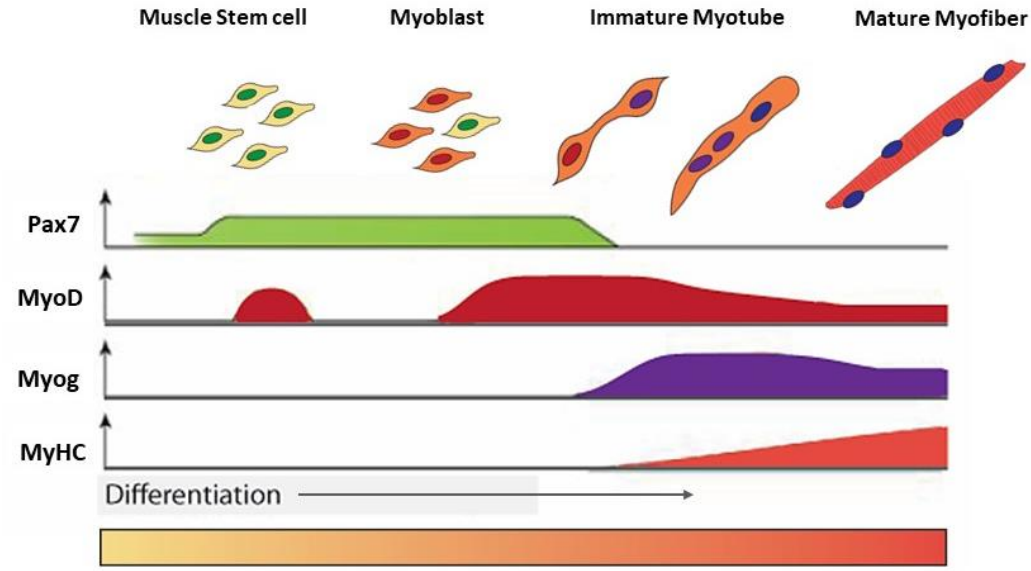

Figure 3.1 Overview of myogenic differentiation. Muscle stem cells, which express Pax7, cycle through proliferative and quiescent phenotypes based on the expression of MyoD. Myoblasts indicate commitment to differentiation by permanently upregulating MyoD. Myoblasts will fuse together to form myotubes and begin to expression additional myogenic factors, such as myogenin (Myog). Late stage differentiation is marked by myonuclei spreading along the fiber and expression of Myosin heavy chain (MyHC). Figure adapted from[15]

A major drawback to using the *Lmna* null mouse to model human disease is that deletion of the *LMNA* gene is lethal in humans[16]. The *Lmna* H222P mouse model was designed to be analogous to human mutations and shows fewer non-muscle specific effects than the *Lmna* null mouse[17]. Similarly to *Lmna* null mice, *Lmna* H222P mice are born apparently normal, but continue to show no phenotype until approximately 10 weeks of age[17]. At this point, the muscle function begins to decline and the mice eventually die around 24 weeks of age due to cardiac failure. The original description of the mouse by the Bonne group showed a substantial defect in Smad2/4 localization that was conserved in both cardiac and skeletal muscle[17]. The study also showed evidence of changes in chromatin regulation that were later confirmed as being directly caused by inefficient binding of Lamin A/C and LADs to heterochromatin[5]. In addition to these signaling changes, there have also been structural defects noted in myonuclear

positioning that are present prior to phenotype onset and get increasingly worse as the disease progresses[11].

Other work on the *Lmna* H222P mouse has focused specifically on cardiac defects where small molecular drugs inhibiting ERK1/2, MAPK 1/2, and c-Jun or activating WNT signaling have shown a preventative effect on dilated cardiomyopathy[18-20]. Of these compounds, only ERK1/2 inhibition was also tested in skeletal muscle, where it showed a positive impact muscle histopathology and grip strength[21]. Despite the large number of studies specifically focused on the efficacy of myogenic differentiation and regeneration in the *Lmna* null mouse model, there has yet to be a full characterization of the muscle differentiation process in the *Lmna* H222P mouse model.

This paper will focus on characterizing proliferation and differentiation of *Lmna* H222P myoblasts both *in vitro* and *in vivo*. We found that *Lmna* H222P myoblasts did not show significant changes in proliferation rate or expression of myogenic transcription factors at any time in differentiation. However, *Lmna* H222P cells did show minor nuclear spacing defects that arose at later stages of differentiation, corroborating previous studies. To test muscle stem cell proliferation efficacy *in vivo,* we injured both pre- and post- phenotype onset mice with a myotoxin to test satellite cell activation. In response to injury, initial satellite cell dynamics were not significantly different from WT mice. To evaluate later stages of differentiation, we evaluated centrally located nuclei, fibrosis, and fiber size, which are all markers of muscle regeneration, at both early and time point after injury. Of these three metrics, only fiber size regulation was severely disrupted in the *Lmna* H222P mouse, indicating defects in muscle maturation and

growth. Taken together, these data point to both a potential mechanism to that explains the wasting phenotype seen in the disease as well as a need for additional studies focusing of later stages of muscle differentiation and maturation.

Results

***Lmna* H222P myoblasts show similar proliferative behavior to WT myoblasts**

Lmna null, *Lmna* H222P and WT cells were grown at 15,000 cells/cm^2 and labeled with EdU to evaluate proliferation rates. None of the three genotypes showed any significant differences in proliferation rate for the first 48 hours after initial seeding (**Figure 3.2A, B**). To better understand the dynamics of the changes in proliferation and the impact of cell density, myoblasts from all three lines were imaged every hour over the course of two days after seeding at lower density (5,000 cells/cm^2) to allow for longer term imaging before high cell density would promote differentiation. The proliferation rates between WT and *Lmna* mutant myoblasts over three days were not significant at any time point (**Figure 3.2C)**. These data match the EdU proliferation rates and point to relatively normal proliferation behavior.

Cell confluence during differentiation was also imaged every hour from the onset of differentiation for five days. Under differentiation conditions, myoblasts should rapidly stop proliferating and begin to fuse and form myotubes. This assay, instead of evaluating proliferation, primarily indicates myotubes formation and growth due to an increase in cytoplasmic area during differentiation. WT and *Lmna* H222P cells showed a continuous increase in growth area until five days of differentiation when the area plateaus (**Figure 3.2D**). The *Lmna* null cells however, showed a stabilization of cell

area around two days of differentiation, and by five days are already declining in cell area. This loss of area was likely due to cell death because the cell width measure is constant (data not shown).

Lmna H222P myoblasts show similar myogenic transcription factor signaling to WT myoblasts

MyoD is the key muscle transcription factor that controls the switch from proliferating to terminally committed myoblasts[15]. Since previous studies have reported defects in MyoD induction in *Lmna* null cells[6, 9, 4] evaluated MyoD transcription factor expression in *Lmna* H222P cells as well. We assayed the fraction of MyoD positive nuclei at four and 24 hours after seeding and found similar levels in all three genotypes **(Figure 3.3A,D**). Evaluating later myogenic transcription factors also showed no significant differences between *Lmna* H222P and WT cells. Myogenin, a mid-differentiation transcription factor that helps to regulate myotube specific genes, showed no significant differences to WT in either *Lmna* mutant cell line, although both lines trended toward reduced levels at day five of differentiation compared to WT (**Figure 3.3B,E**)[15].

This trend could be due to inefficient epigenetic changes in the *Lmna* mutant cells that impacts the dynamics of muscle specific genes[5, 11], however, additional later time points will be necessary to validate the significance of this trend. Myosin heavy chain (MyHC), the terminal muscle differentiation marker that is responsible for sarcomere formation, showed nearly identical expression in *Lmna* H222P and WT cells.

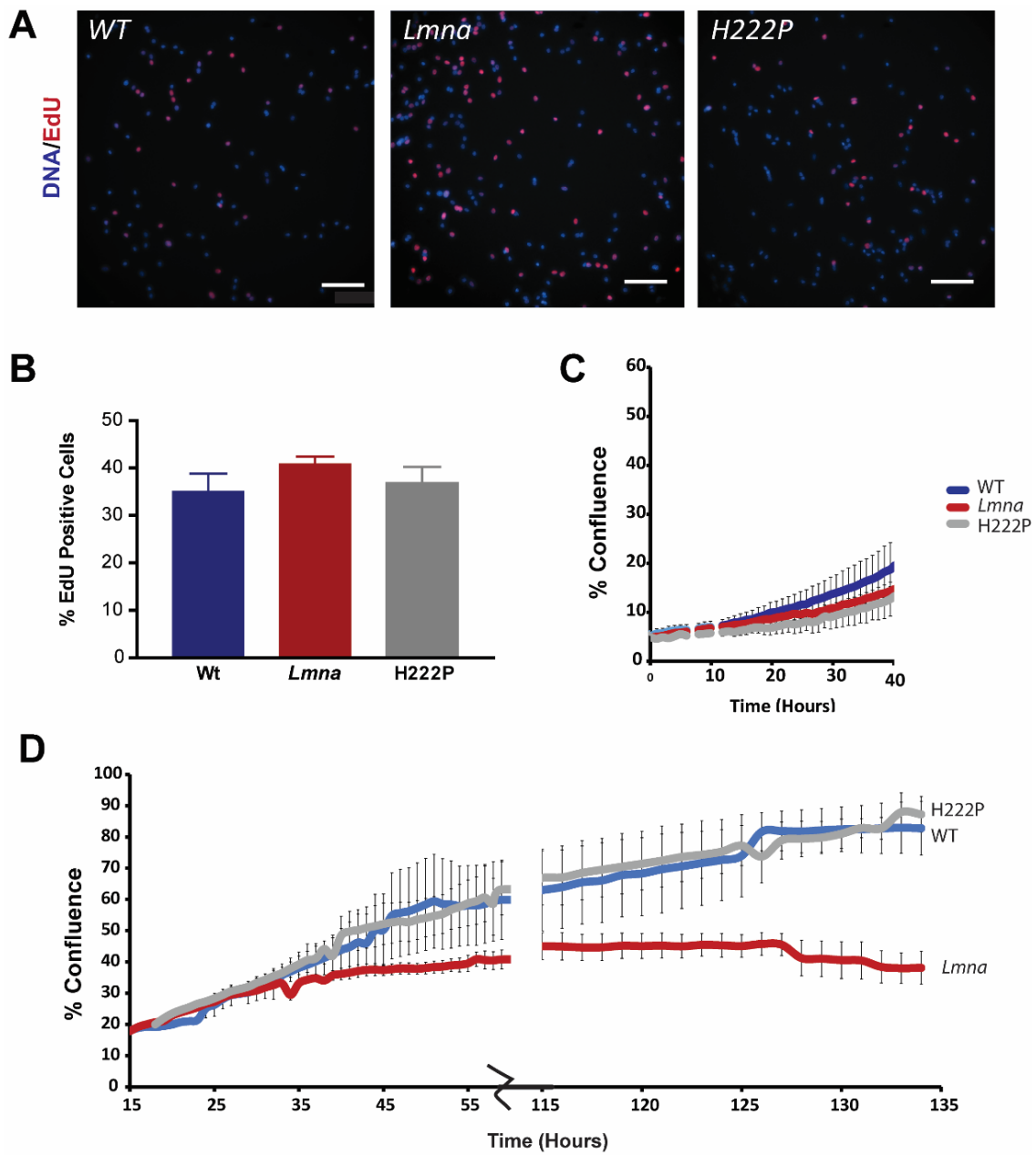

Figure 3.2. ***Lmna* mutant myoblasts show similar proliferative behavior to WT myoblasts** **A)** Representative images of *Lmna* mutant and WT myoblasts. Cells were labeled with EdU 24 hours after seeding with a four hour pulse. N = 3 independent experiments. Scale bar: 100 µm. **B)** Quantification of nuclei with active DNA replication based on positive EdU staining shows similar proliferation regardless of *Lmna* genotype. **C)** Automated cell confluence measurement from 40 hours of live-cell imaging of proliferating myoblasts again show no longer term changes in proliferation rate. N = 3 independent experiments. **D)** Automated cell confluence measurement over six days of cell differentiation shows an early plateau of cell area in *Lmna* null cells that preceded an early loss of cell area by day five of differentiation. N = 3 independent experiments.

Lmna null myofibers at both two and five days of differentiation compared to WT had slightly lower, although not significant levels of MyHC (**Figure 3.3C,F**). Taken together, these data indicate that the overall myogenic differentiation of *Lmna* H222P myoblasts is not impaired compared to WT cells.

Lmna H222P cells show only minor defects in nuclear spacing compared to *Lmna* null cells

As myofibers fuse, the nuclei all aggregate in the center of the fiber. As they mature, the nuclei need to first spread out longitudinally and then move to the periphery of the fiber so that the sarcomeres are not disrupted and the nuclei can interact at the neuromuscular junctions to control electrical signaling[11, 22]. Nuclear spacing along the myofiber axis and anchoring to the myofiber periphery are two of the last stages of muscle differentiation. We evaluated the fusion index, the number of nuclei per fiber, and distance between nuclei at both two and five days of differentiation for WT and both *Lmna* mutant cell lines.

Despite no significant differences in cell fusion at day two, there were many more highly multinucleated fibers (> 10 nuclei per fiber) present in the *Lmna* null cells at five days of differentiation compared to both WT ($p < 0.01$) and *Lmna* H222P ($p < 0.05$) myofibers (**Figure 3.4A, C, D**). Nuclear spacing and fusion in the *Lmna* H222P cells were comparable to WT controls. The increase in the number of nuclei per fiber in the *Lmna* null myotubes also led to an increase in the fraction of clustered nuclei, defined as at least two touching nuclei. However, this increase was not currently significant

(**Figure 3.4E**) based on N = 2 independent experiments for *Lmna* null cells and N = 3 for the other two cell types. Additional replicates are expected to make this significant at least at five days of differentiation because over 50% of *Lmna* null internuclear distance measurements are zero, while only 20% of WT internuclear distances are zero. Lending additional weight to this expectation, the average internuclear distance at five days of differentiation in *Lmna* null cells is significantly lower than WT (**Figure 3.4F**).

One major reason for this is preserved nuclear spreading in the WT cells, which can be seen by the significant increase in internuclear distance between day two and day five of differentiation. Regarding average internuclear distance, the *Lmna* H222P cells behave similarly to controls, although the spreading is not as pronounced as in WT cells. Additional experiments at later time points may shed light on whether the spacing is preserved or lost during continued differentiation. Similar trends in nuclear spacing defects are observed *in vivo*.

Interestingly, *Lmna* null isolated single fibers *in vivo* only show defects in nuclear spacing at the myotendinous junction (MTJ) while the muscle fiber body appeared generally normal (**Figure 3.4B**). *Lmna* H222P single muscle fibers show abnormal nuclear morphology, but there is an overt absence of nuclear clustering that is very similar to WT fibers. Quantification of *in vivo* nuclear spacing is still ongoing, but other groups have noted abnormal spacing that is more prominent at the MTJ in *Lmna* null fibers[12].

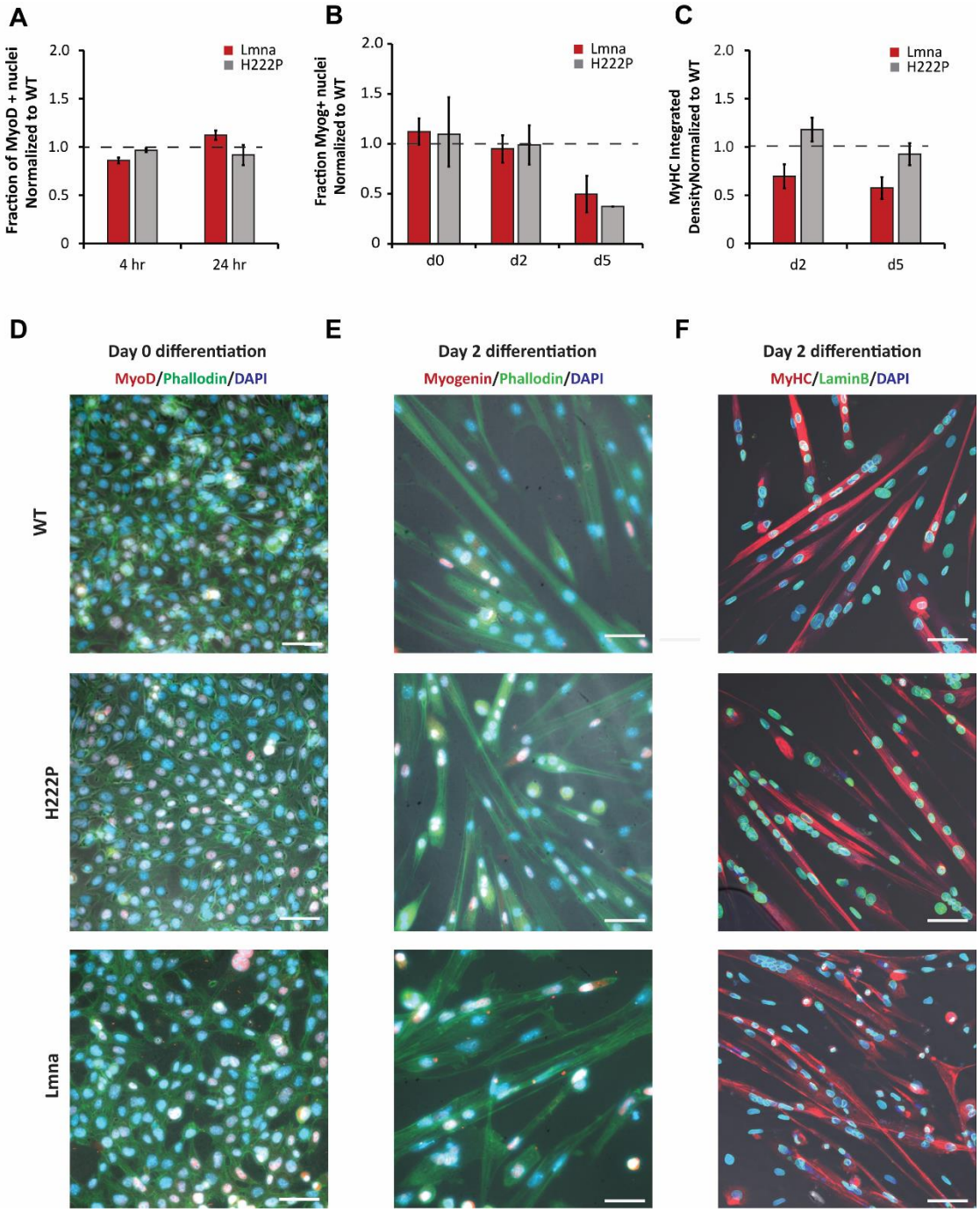

Figure 3.3. ***Lmna*** **mutant cells show no major defects in myogenic transcription factor regulation**. **A)** MyoD expression shows no defects at early time points, $p > 0.1$. N = 3 independent experiments. **B)** Myogenin expression is similar to WT. *Lmna* null cell $p = 0.21$. $Lmna^{H222P/H222P}$ $p = 0.025$. N= 3 independent experiments, except $Lmna^{H222P/H222P}$ 5d where N=2. **C)** *Lmna* null cells trend toward lower MyHC expression, but were not significantly different from WT. Two day differentiation $p = 0.06$, five day differentiation $p = 0.28$. $Lmna^{H222P/H222P}$ cells behave the same as WT with two day differentiation $p = 0.51$ and five day differentiation $p = 0.26$. N = 3 independent experiments. **D-F)** Representative images of MyoG, myogenin, and MyHC staining at day 0 or day 2 of differentiation. Scale bar 20 μm.

Given the prominence of the MTJ in disease progression[12, 23], it is noteworthy to see another major defect exacerbated in this region of the fiber. However, these defects in the *Lmna* H222P model do not seem sufficient to explain the muscle loss phenotype shown in the animal.

Lmna H222P mice show normal regenerative capacity but defects in fiber size distribution following myotoxin injury

Given the relatively normal proliferation and differentiation of *Lmna* H222P myoblasts *in vitro*, we wanted to further investigate this process in an *in vivo* regeneration model. *In vitro* differentiation assays take the myoblasts out of their native environment, where immune cells and fibroblasts help to modulate the differentiation cascade[24]. In addition to a providing a more complete system, *in vivo* models also allow for longer term evaluation. *In vitro* assays are limited in time duration to at most 14 days of differentiation and myofibers maturity level, even with advanced cell culture platforms[25]. Melcon et. al. had previously evaluated both the *Lmna* null and *EMD* mouse model for transcription factor signaling and found no defects in the *Lmna* null mouse regenerative capacity three days after cardiotoxin injury[10]. However, this study did not include the *Lmna* H222P mouse model and only looked at very early regeneration. Given our lack of significant findings at early stages of differentiation, we hypothesize that the later stages of differenation and muscle maturation may play a larger role in the disease phenotype.

The *Lmna* H222P mouse model has a longer life span and later phenotype onset than

the *Lmna* null mouse, making it better suited for longer term experiments when fibers are typically fully regenerated[26]. In order to evaluate both early and late stages of muscle regeneration, we evaluated mice at early time points post injection (8 dpi) and later times points (28 dpi) and also performed an added triple injected condition to determine whether the satellite cells were depleted during multiple rounds of regeneration (**Figure 3.5A**). The *Lmna* H222P mouse has the added benefit of a well-defined phenotype onset which occurs around 10 weeks of age[17]. This allowed us to inject mice pre- and post-phenotype onset to determine whether phenotypic disease progression contributed to changes in the regeneration process. Pre- phenotype onset mice were injected at 5-7 weeks of age and post-phenotype onset mice were injected at 15-17 weeks of age. These two groups of mice will be referred to as "young" and "old" respectively (**Figure 3.5B**). The number of Pax7+ satellite cells normalized to muscle area was used as the primary marker of regeneration efficiency (**Figure 3.5C**). Pre-phenotype onset "young" mice, show equivalent robust satellite cell proliferation to WT mice at eight days post injection (**Figure 3.5F**).

To determine whether *Lmna* H222P satellite cells show a self-renewal defect, we injected pre-phenotype onset mice with three rounds of cardiotoxin spaced 8 days apart to force satellite cells to constantly cycle in between injuries. The triple injected mice showed no significant change in satellite cell activation compared to WT at eight days post injection which indicates that there are no self-renewal defects (**Figure 3.5G).**

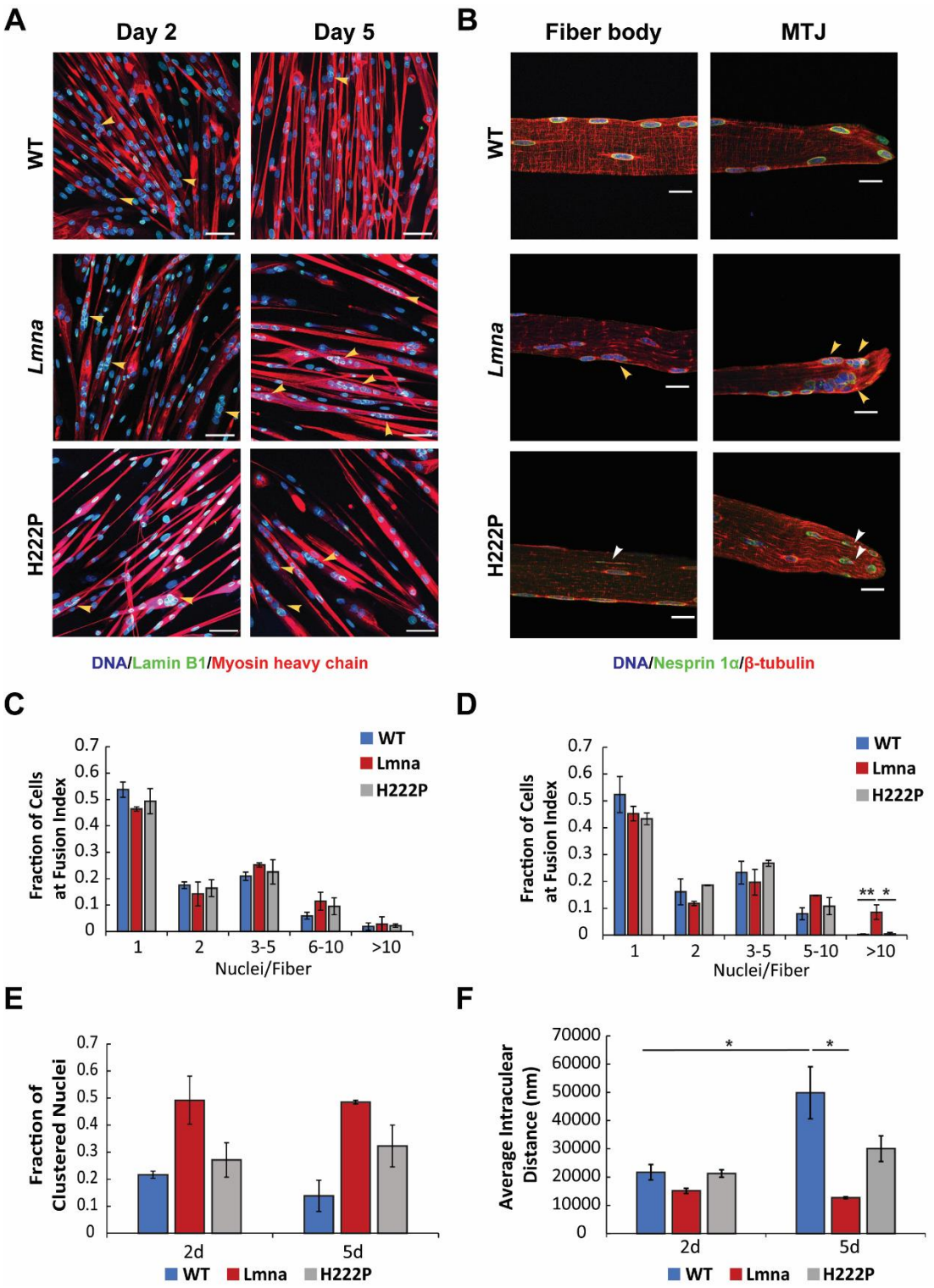

Figure 3.4. *Lmna* null, but not *Lmna* H222P myofibers show defects in nuclear spacing *in vitro* and *in vivo*. A) Representative images of two and five day myofibers stained for Lamin B and MyHC show increased nuclear clustering in the *Lmna* null fibers compared to WT as indicated by yellow arrows. Scale bar 50 μm. **B)** Representative images of isolated single muscle fibers show increased nuclear clustering at the MTJ of *Lmna* null fibers but not in the

fiber body. *Lmna* H222P fibers do not show clustering, but do show abnormal morphology at the MTJ. Scale bar 20 μm. **C)** and **D)** histograms of nuclei at different fusion index bins show a significant increase in *Lmna* null nuclei in highly multinucleated myotubes compared to both WT and *Lmna* H222P myotubes. *, $p < 0.05$, ** $p < 0.01$. N = 2 independent experiments for *Lmna* null cells and N = 3 independent experiments for WT and *Lmna* H222P cells at all time points. **E)** Fraction of clustered nuclei where at least two nuclei are touching. **F)** Average internuclear distance show significant loss of nuclear spacing in *Lmna* null cells compared to WT at day five of differentiation. *, $p < 0.05$.

In both WT and *Lmna* H222P triple injected mice, there was a decrease in the overall number of satellite cells in the cardiotoxin injured animals, although it was not quite significant to single injected animals ($p > 0.15$). To evaluate long term changes in satellite cell behavior, pre- and post- phenotype onset mice were evaluated after 28 days of regeneration when satellite cell numbers normally return to baseline[26].

Twenty-eight days post injection pre-phenotype onset mice show a significant reduction in satellite cell numbers from eight dpi, although there is still a roughly ~2-4 fold increase from baseline in both WT and *Lmna* H222P mice (**Figure 3.5C, D)**.Interestingly, "young" WT mice show a significant increase to *Lmna* H222P mice even at this late stage in regeneration. As these mice were not yet skeletally mature, it is possible that the increase in satellite cells in the WT mice was due to a stunted muscle development period in the *Lmna* H222P mice. Post-phenotype onset mice show a statistically similar response in satellite cells 28 dpi, although the cardiotoxin injected *Lmna* H222P mice show a significant increase over PBS injected *Lmna* H222P mice ($p < 0.01$) which could indicate a slight defect in return to quiescence (**Figure 3.5C, E**). Other markers of regeneration, such as centrally located nuclei and fibrosis, show no significant changes between *Lmna* H222P and WT mice (Supplemental Figure S3.1).

The most striking difference between WT and *Lmna* H222P mice was the change in fiber size, another indicator of regeneration. Fiber size during the early regeneration process is typically smaller as new cells fuse into the damaged muscle and then returns to baseline over time[24]. The "young" WT mice showed a small downward shift of approximately 10 μm at 8 days post injection (**Figure 3.6A, B, C**). *Lmna* H222P mice had both a higher starting average cell area, approximately one third higher than WT, and a larger downward shift of 40 μm at 8 dpi. The increase in fiber diameter at baseline was likely due to a predominance of Type II fibers, which are typically larger in diameter[27]. This observation matches patient and mouse data that showed a marked atrophy of Type I/IIA fibers (the small diameter group) and a preference for Type IIB/X fibers (the larger diameter group) in muscle biopsies and histology in EDMD patients[28, 29, 30, 31, 11].

The large downward shift could be indicative of signaling defects and other hypertrophy related genes that lead to smaller fibers for an extended time after injury[32]. Twenty-eight days after injection in "young" mice of both genotypes showed similar fiber size distributions (**Figure 3.6A, B, D**). The similarity of 28 days to eight days post injection in the "young group" could be due to the persistent growth and development of muscle that occurs prior to skeletal maturity, as discussed above[33]. The "old" group, corresponding to post-phenotype onset *Lmna* H222P mice, showed different trends than the "young" mice (**Figure 3.6A, B, E**).

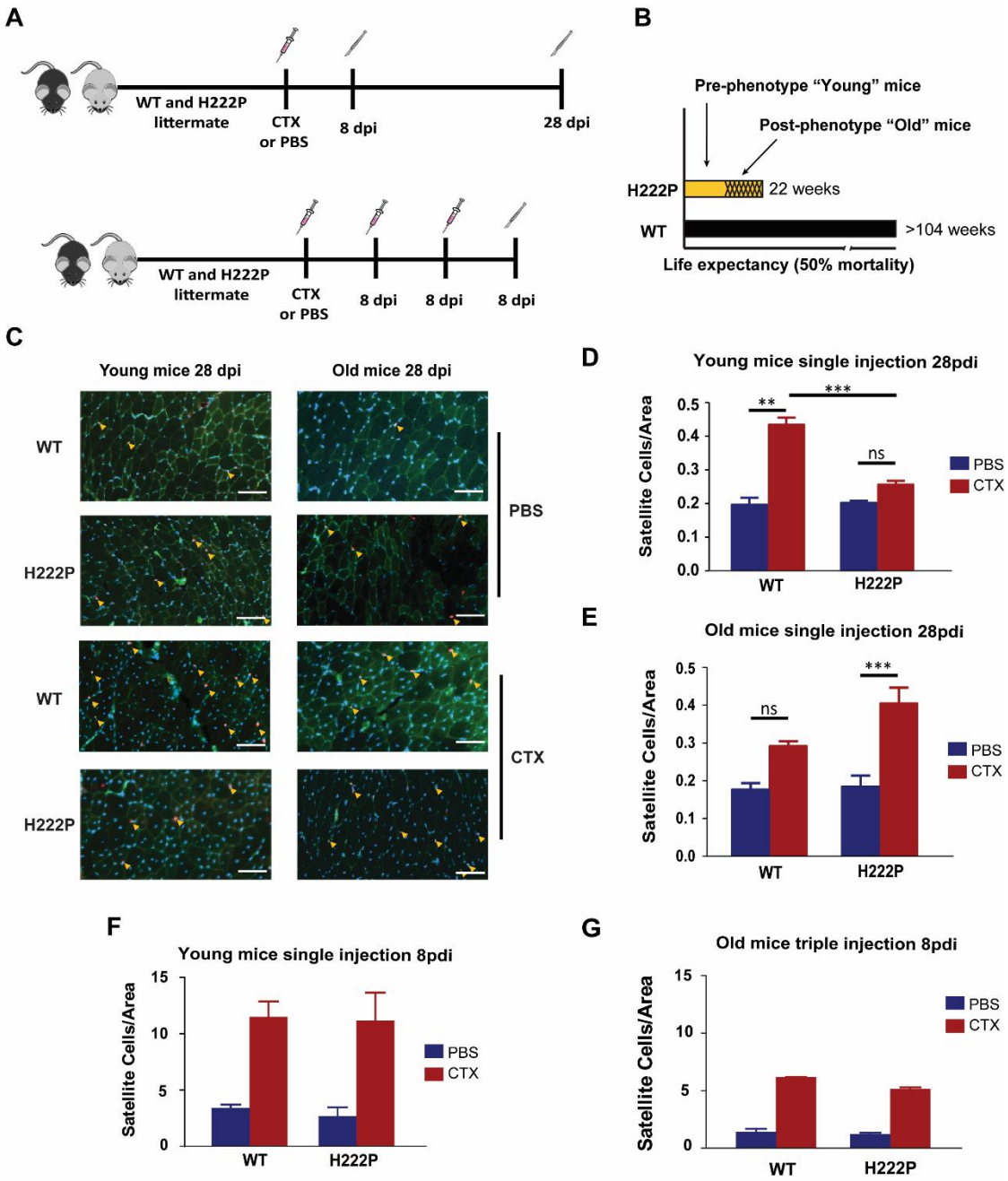

Figure 3.5. *Lmna* H222P mice show no major long-term defects in satellite cell dynamics in mice. A) Representative images of Pax7+ satellite cells in regenerating muscle indicated by yellow arrow heads. Scale bar 100 μm. **B)** Pre- phenotype onset, "young", mice show no changes in satellite cell activation between WT and *Lmna* H222P mice at 8 dpi. N ≥4 animals per genotype. **C)** Pre- phenotype onset, "young", WT mice show a persistent increase in satellite cell activation above *Lmna* H222P mice at 28 dpi that may be due to active muscle building processes in the WT mice that are absent in the *Lmna* H222P mice. ***, $p < 0.001$. N ≥ 2 animals per genotype. **D)** Triple injected "young" WT and *Lmna* H222P mice show no significant changes in satellite cell response indicating normal self-renewal processes in mutant mice. N ≥ 3 animals per genotype. **E)** Post-phenotype onset, "old", mice show no significant changes in

satellite cell numbers 28 days poste injection between WT and *Lmna* H222P mice. However, *Lmna* H222P CTX injected muscles do show significantly more satellite cells compared to control PBS muscles ** $p < 0.01$. $N \geq 2$ animals per genotype.

In WT animals, by 28 days post injection, the fiber size distribution returned to normal, which is indicative of complete regeneration of the stable fiber type and diameter profile that exists after mice reach skeletal maturity [33]. Post-phenotype *Lmna* H222P onset mice showed a major shift to smaller fiber diameters even in the PBS control (**Figure 3.6A, B, E**). Upon injury in the "old" *Lmna* H222P mice, the fiber size was further reduced, with a preferential loss of larger diameter fibers. This supports the delayed fiber hypertrophy model which is evidenced by the extended period of smaller fiber diameters in pre-phenotype mice as well. Additional data is needed to solidify this hypothesis, but as many of the pathways that are important for muscle fiber hypertrophy and size regulation such as MAPK, Akt-mTor, NFκB, and AMPK have been shown to be misregulated due to mutations in the *Lmna* gene, it is possible that this represents a major defect in the maturation of *Lmna* mutant muscle fibers [16, 34, 35, 36].

Additionally, many of these targets have been shown to be helpful in ameliorating cardiac defects, so they may also play a helpful role in preventing skeletal muscle decline[34, 37]. Since cardiotoxin injury exacerbates this phenotype even in pre-phenotype onset mice, injury models may be a helpful platform to further investigate these metabolic changes in the muscle of laminopathy models.

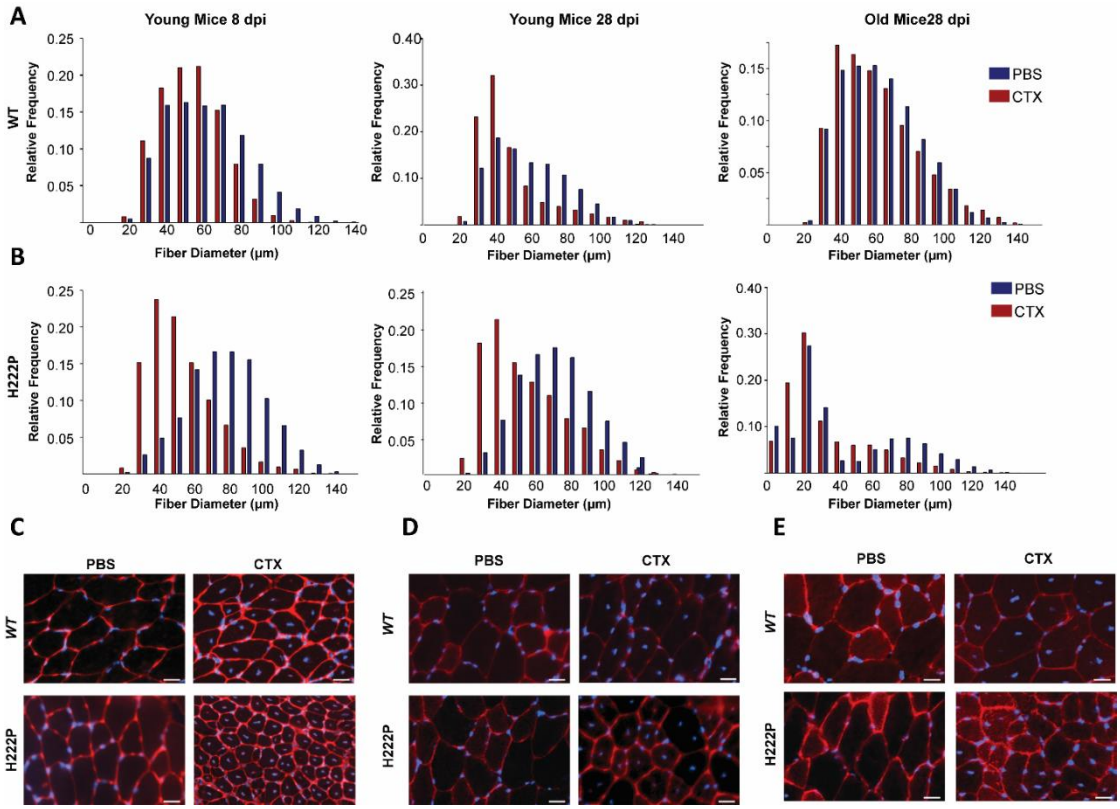

Figure 3.6. **Muscle fiber diameter is highly disrupted after cardiotoxin injury in *Lmna* H222P mice.** Histograms of fiber diameter distributions of the tibialis anterior (TA) in control and injured mice. **A)** WT mice show largely stable fiber diameters with only a small downward shift in cardiotoxin (CTX) injured young animals. **B)** *Lmna* H222P mice show significant loss of larger diameter fibers with both injury pre-phenotype. The larger shift in fiber diameters in the sustained out to 28 dpi in young mice. **, $p < 0.01$ *Lmna* H222P CTX vs WT CTX. In skeletally mature mice, WT mice show a full regeneration and return to standard fiber type distribution 28 dpi whereas post-phenotype onset $Lmna^{H222P/H222P}$ mice show the appearance of a bimodal distribution indicative of a fiber type shift in the PBS control. Injured mice show a loss of the larger diameters which along with the pre-phenotype onset data supports a defect in fiber maturation and hypertrophy. ***, $p < 0.001$ *Lmna* H222P CTX vs WT CTX. **C-E)** Representative images of fiber diameter. Scale bar 25 μm.

Discussion

We preformed quantification and clarification on the role of the *Lmna* H222P mutation on muscle differentiation and *in vitro* and *in vivo*. Despite only minimal defects and changes in early differentiation based on proliferation rates, myogenic signaling, and nuclear spacing, we found evidence of major defects *in vivo*. Satellite cell dynamics are generally normal but we identified major changes in fiber size regulation after

regeneration that points to severe defects in fiber growth and hypertrophy signaling cascades. In addition, the presence of a fiber size phenotype even in advanced phenotype animals in the absence of injury points to the significant contribution of fiber size misregulation to the disease pathology.

Although previous studies on *Lmna* null myoblast differentiation have generally pointed to key misreuglation of myogenic transcription factor signaling, we did not see any evidence of significant misregulation in the *Lmna* null or H222P model in our studies. This may in part be due to the high density (75,000 cells/cm^2) at which we carried out these experiments. In additional experiments done in our lab, we carried out primary myoblast differentiation at a two thirds (50,000 cells/cm^2) and one third (25,000 cells/cm^2) of the density used in the experiments and saw remerge of the myogenic transcription factor delays previous published that were significantly decreased at the high density used in this study (data not shown)[4, 6, 7]. As another study has pointed to the likely contribution of cell density of the function of *Lmna* null cells[6], it will be important to investigate the myogenic signaling in *Lmna* H222P myoblasts at lower densities as well. However, given the fact that the *Lmna* H222P mice are indistinguishable from their WT littermates for over two months, it would not be surprising if there were no major issues in myogenic signaling, at least in young *Lmna* H222P mice.

Previous work has focused on early stages of regeneration on the *Lmna* null model. Within the *Lmna* null mouse model, multiple reports found decreased Pax7+ satellite

cells compared to WT and *in vitro* culture of fiber associated Pax7+ cells and a decrease in differentiation potential of MyoD compared to WT [6, 12]. However, cardiotoxin injury done on *Lmna* null mice has revealed no overt regeneration defects, but only a delay in Rb expression in the *Lmna* null mice compared to WT controls [10]. These data largely support our findings that there were no major defects in myogenic signaling and differentiation potential of *Lmna* null myoblasts. However, the major limitation of the *Lmna* null mouse model is its short lifespan, precluding that model from evaluation of the impacts of the loss of Lamin A/C on the later stages of muscle development and maturation.

Our *in vivo* regeneration experiments done in the *Lmna* H222P mouse model are the first to evaluate long term consequences of myotoxin injury in a laminopathy model. Due to the longer life span and pre-phentoypic period, this model provides a system to look at correlative effects of long term impacts of injury and regeneration and phenotype progression. In line with the phenotype, our *in vivo* experiments showed a slow progression of fiber atrophy that was exacerbated by injury, which matches the phenotypic progression of the model. We showed that the effective early stage differentiation, which was observed in our *in vitro* experiments, was also seen in the mouse following cardiotoxin injury in the $Lmna^{H222P/H222P}$ model. This was shown by overall normal Pax7+ dynamics, appropriate formation and resolution of regenerating fibers as marked by centrally located nuclei, and no overt changes in fibrosis. In addition, there were no self-renewal defects based on sufficient satellite cell activation in the *Lmna* H222P mouse, even after multiple rounds of injury, providing an answer,

at least in this model, to a long held hypothesis that inefficient stem cell response could contribute to disease progression in laminopathies. The most striking finding was a major shift in fiber diameter in pre-phenotype onset mice, indicative of a switch in fiber type in the muscle. This phenotype has been identified in the absence of centrally located nuclei in multiple patient and mouse samples, pointing to an overall wasting phenotype in the muscle [11, 4]. Given that the *Lmna* H222P mice are capable of full muscle regeneration, further study of the wasting phenotype is important. Since our data suggest that injury can exacerbate the muscle wasting phenotype prior to the natural phenotype onset in the *Lmna* H222P mouse, injury models may prove to be a useful tool to study the metabolic and other changes occurring in the muscle that produce this fiber diameter shift.

To further investigate the misregulation of muscle growth, we plan to carry out experiments to examine altered protein and mRNA levels of MAPK, Akt-mTor, NFκB, and AMPK. Given previous studies that found a positive impact of ERK1/2 inhibition on both cardiac and skeletal muscle, other key pathways evaluated in cardiac tissues may play a role in skeletal muscle as well[18, 19, 38]. Metabolically, the *Lmna* null mouse has major defects in the Akt pathway that are rescuable by treatment with rapamycin[34, 39]. Although the *Lmna* H222P model is less severe, it would not be surprising to find a more muscle targeted metabolic defect that contributes to muscle wasting. One major complication in interpreting the results of our current data is that muscle injury invokes a large inflammatory response, which may impact other elements of muscle development due to prolonged signaling by both expanding fibroblast and immune cell

pools[26]. To confirm our results, we are currently carrying out experiments to induce hypertrophy in the *Lmna* H222P model in the absence of an inflammatory response. A synergist ablation model, which disables the gastrocnemius to induce excessive force on the plantaris, has been previously shown to induce a robust hypertrophy and induction of satellite cell proliferation and differentiation in the absence of injury[40]. This model has the additional benefit of inducing a mechanical overload that may alter the mechanical load on the nucleus, leading to an abrogated mechanotransduction response, a long held hypothesis for laminopathy disease mechanism[16]. Additional data from these experiments will help us to understand if and how force and inflammation plays a role in the maintenance of cellular size and satellite cell dynamics, and if this process is altered in laminopathies.

Methods

Animals. *Lmna* KO ($Lmna^{-/-}$)[41] and *Lmna* H222P ($Lmna^{H222P/H222P}$)[17] have been described previously. $Lmna^{+/-}$ and $Lmna^{H222P/+}$ mice were backcrossed at least seven generations into a C57-BL/6 line. For each mouse model, heterozygous mice were crossed to obtain homozygous mutants, heterozygous mice, and wild-type littermates. *Lmna* mutant mice were provided with gel diet (Nutri-Gel Diet, BioServe) supplement to improve hydration and metabolism upon onset of phenotypic decline. All mice were bred, maintained and euthanized according to IACUC approved protocols. Data from *Lmna* KO and *Lmna* H222P were normalized to their own littermate controls. For both *in vivo* and *in vitro* studies, cells and or tissues were isolated from a single mouse and counted as a single replicate. All data are based on at least two independently derived

primary cell lines for each genotype.

Myoblast isolation. Cells were harvested from *Lmna* KO, *Lmna* H222P, and wild-type littermates between 3-5 weeks for *Lmna* KO mice and 4-10 weeks for *Lmna* H222P mice using a protocol adapted from[41]. With the exception of the *Lmna* KO myoblasts, these time-points were prior to the onset of disease phenotypes. Myoblasts from wild-type littermates were harvested at the same time. Muscles of the lower hindlimb were isolated, cleaned of fat, nerve and excess fascia, and kept in HBSS on ice until all mice were harvested. The muscles were digested in 4 ml:1 g of tissue wet weight in a solution of 0.5% Collagenase II (Worthington Biochemicals), 1.2 U/ml Dispase (Worthington Biochemicals), 1.25 mM $CaCl_2$ (Sigma) in HBSS/25 mM HEPES buffer. Digestion was carried out in a 37˚C water bath for a total time of 60 minutes. At 20 minutes intervals, digestion cocktails were removed and triturated 40 times with a 5 ml pipet. In the case of difficult to digest tissues, an extra 25% of 1% Collagenase II was added to the digestion after 40 minutes.

When tissues were fully digested, the reaction was quenched using equal volumes of DMEM supplemented with 10% fetal bovine serum (FBS) and 1% P/S (D10 media, Gibco). The cell suspension was strained through 40 and 70 μm filters (Greiner Bioscience) sequentially to remove undigested myotube fragments and tendon. The cell suspension was centrifuged at 800 × g for 5 minutes and washed with 8 ml of D10 media for a total of four times. Cells were then resuspended in primary myoblast growth media (PMGM; Hams F-10 (Gibco) supplemented with 20% horse serum and 1%

penicillin/streptomycin and 1 µl/ml basic fibroblast growth factor (GoldBio)) and plated onto a 2 % gelatin coated T25 flask. Cells were allowed to sit undisturbed for 72 hours. Capitalizing on the fact that myoblasts adhere much more weakly than fibroblasts, cells were passaged using PBS (calcium- and magnesium-free) instead of trypsin to purify the myoblasts. Cells were washed for 2-3 minutes at room temperature using a volume of PBS sufficient to coat the bottom of the flask and dislodged using manual agitation. When necessary, a 0.000625% trypsin solution was used to aid in the myoblast removal. Myoblasts were re-suspended in PMGM and re-plated onto gelatin coated flasks. This process was continued 3-4 times until pure myoblast cultures were achieved[42]. Cells were maintained in culture on gelatin coated flasks with media changes every other day. All experiments were carried out prior to passage 15. Each independent experiment was done on a different set of lamin mutant and wild-type littermates such that each independent experiment was sourced from a different animal to account for heterogeneity in phenotype.

Myoblast differentiation. Coverslips for differentiation were pre-coated with crosslinking gelatin. Briefly coverslips were coated using 2% gelatin for 1 hour, then the gelatin was aspirated and the coating was fixed with 1% glutaraldehyde (Sigma) for 30 minutes at room temperature and incubated with 1 M ethanolamine (Sigma) for 30 minutes at room temperature. Coverslips were washed extensively to remove additional chemicals and stored at 4°C for up to a month prior to use. Pre-treated cover slips were coated with growth factor reduced Matrigel (Corning) diluted 1:100 with IMDM with Glutamax (Gibco) immediately prior to use. Pre-cooled pipette tips were used to avoid

premature polymerization. Matrigel was allowed to polymerize at 37˚C for 1 hour and the excess solution was aspirated. Primary myoblasts were seeded at a density of 75,000 cells/cm^2 in IMDM + 20% HS + 1% P/S + 1% Chick Embryo Extract[25]. Cells were allowed to attach for 24 hours before being switched to primary myoblast differentiation media (PMDM) composed of IMDM with Glutamax and 2% horse serum. PMDM supplemented with 100 ng/ml agrin (R&D Systems) was added to the cells and henceforth replaced every second day. Cells were allowed to differentiate for a total of 0, 2, or 5 days.

Extended imaging using incubator microscope. Long term imaging was performed using an Incucyte imaging system, which allows for incubator imaging to minimize the effects of humidity and CO_2 changes. The proliferating or differentiating cells were imaged for 2 or 5 days every 30-60 minutes with a 20× objective. Resulting images were analyzed using the Incucyte software, which performs a thresholding algorithm to detect cells imaged with phase contrast and calculates the percent area coverage of cells.

Isolation of single muscle fibers. Single muscle fibers were harvested in a protocol adapted from Vogler et al.[43]. As previously described, fibers were isolated from male and female *Lmna* KO and wild-type litter mates at 5-6 weeks of age and *Lmna* H222P and wild-type litter mates were harvested at 6-8 weeks of age at 23-25 weeks of age in order to compare pre- and post-phenotype onset tissue [17, 41, 44]. While *Lmna* H222P male and female mice show differences in cardiac defects, they do not exhibit differences in progression of skeletal muscle defects [17, 44], so both male and female mice were used for

analysis. Briefly, the EDL (extensor digitorus longus) and plantaris were isolated from the mouse and placed directly into a 1 ml solution of F10 media with 4,000 U/ml of Collagenase I (Worthington Biochemicals). The tissue was digested for 15-40 minutes depending on muscle size in a 37˚C water bath with agitation by inversion every 10 minutes. The reaction was quenched by transferring the digestion mixture to 4 ml of PMGM. Single fibers were hand-picked from the digested tissue using fire polished glass Pasteur pipettes. When necessary, the tissue was further dissociated by manual pipetting with a glass pipet. Fibers were washed once in fresh media prior to fixation with 4% paraformaldehyde (PFA) for 15 minutes at room temperature and subsequent IF staining.

Muscle Injury. To induce regeneration, the Tibialis Anterior (TA) was injected with 0.03 mg/ml cardiotoxin (or control PBS injections) at weight scaled injection volumes to avoid volume overload. The injection volume was determined by first injecting muscle with bromophenol blue followed by euthanasia and qualitatively assessment of the muscle dye coverage and amount of dye in the surrounding tissue. These qualitative observations were correlated with TA and body weight to develop a linear regression model for injection volume vs body weight. *Lmna* H222P mice were injected pre-phenotype onset (5-7 weeks of age), or post-phenotype onset (15-17 weeks of age). These groups were labeled “young” and “old” for reporting purposes. To test for the ability of the stem cells to self-renew, young mice were injected every 8 days for a total of three injections, then harvested 8 days after final injection. Mice were blinded and randomly assigned into a PBS or CTX group and both TAs were injected with the same

solution under isoflurane anesthesia. Analgesic and wet food on the cage floor was provided until three days post injection. Tissue were preserved for histology and immunoflourescene in isopentane cooled in liquid nitrogen and stored in -80°C. Tissues were cryosectioned on a Leica 3050 S cryostat at 7μm and stored at -20°C prior staining.

Immunofluorescence staining. Cells were fixed in pre-warmed 4% PFA at the appropriate time point(s) and washed with PBS. Cells were blocked and permeabilized with a solution of 3% BSA, 0.1% Triton-X 100 and 0.1% Tween (Sigma) for 1 hour at room temperature. Cells or tissues from all conditions were stained for either Pax7 (DHSB, 1:200), laminin (Novus Biologicals, 1:100), phalloidin (Invitrogen, 1:50), Texas Red Conguated Wheat Germ Agglutinin (Sigma, 1:100), β-tubulin (Sigma, 1:500), Myog F5D (DSHB, 1:100), MyHC A4.1025 (DSHB, 1:100), or MyoD (Santa Cruz, 1:75) and counterstained with DAPI (Thermoscientific, 1:1000) diluted in blocking solution according to at 4˚C overnight. Samples were washed with PBS and incubated for 1 hour at room temperature with 1:250 dilution of AlexaFluor antibodies (Invitrogen) and 1:1000 DAPI (Sigma). Single muscle fibers were stained using the same procedure in Eppendorf tube baskets with an increase in blocking solution Triton-X concentration to 0.25%. Cryopreserved TA muscle from injured and control mice were stained as described[40].

Imaging acquisition. Cells on coverslips and mounted single muscle fibers were imaged with an inverted Zeiss LSM700 confocal microscope. Z-stack were collected using 20× air (NA = 0.8), 40× water-immersion (NA = 1.2) objectives. Airy units for

all images were set between 1 and 1.5. Epi-fluorescence images were collected on a motorized inverted Zeiss Observer Z1 microscope equipped with CCD cameras (Photometrics CoolSNAP EZ or Photometrics CoolSNAP KINO) or a sCMOS camera (Hamamatsu Flash 4.0). Hematoxylin and eosin histology images were collected on an inverted Zeiss Observer Z1 microscope equipped with a color CCD camera (Edmund Optics, EO-0312C).

Image analysis. Image sequences were analyzed using ZEN (Zeiss), ImageJ, or MATLAB (Mathworks) using only linear adjustments uniformly applied to the entire image region. Region of interest intensities were extracted using ZEN or ImageJ. To quantify cell area and myofiber health, maximum intensity protections were generated, which were then blinded to the observer for analysis. Average fiber size, as well as percentage of centrally located nuclei was analyzed semi-automatically using the "SMASH", (Semi-Automatic Muscle Analysis using Segmentation of Histology) Matlab App. Wheat Germ Agglutinin (WGA) stained sections were used to determine fibrosis using ImageJ intensity measurements [45]. To verify the fibrosis data, Pico Sirius red staining was analyzed using the autoflourescent properties of the collagen allowing for the total stained area to be quantified [46].

Statistical Analysis. Unless otherwise noted, all experimental results were taken from at least three independent experiments and *in vivo* data were taken from at least three animals. For data with normal distribution, we used either student's t-tests (comparing two groups) or one-way ANOVA (for experiments with more than two groups) with

post-hoc tests. When multiple comparisons were made, we adjusted the significance level using Tukey corrections. All tests were performed using GraphPad Prism. Unless otherwise noted, * denotes $p \leq 0.05$, ** denotes $p \leq 0.01$, and *** denotes $p \leq 0.001$. Unless otherwise indicated, error bars represent the standard error of the mean (SEM).

REFERENCES

1. Maggi, L., Carboni, N. & Bernasconi, P. Skeletal Muscle Laminopathies: A Review of Clinical and Molecular Features. *Cells* **5**, 14 (2016).
2. Kaminski, A., Fedorchak, G.R. & Lammerding, J. The Cellular Mastermind(?) - Mechanotransduction and the Nucleus, in *Mechanotransduction*, Vol. 126. (eds. A.J. Engler & S. Kumar) 157-203 (2014).
3. Bentzinger, C.F., Wang, Y.X., Dumont, N.A. & Rudnicki, M.A. Cellular dynamics in the muscle satellite cell niche. *EMBO reports* **14**, 1062-1072 (2013).
4. Frock, R.L. *et al.* Lamin A/C and emerin are critical for skeletal muscle satellite cell differentiation. *Genes & Development* **20**, 486-500 (2006).
5. Perovanovic, J. *et al.* Laminopathies disrupt epigenomic developmental programs and cell fate. *Science Translational Medicine* **8**, 14 (2016).
6. Cohen, T.V. *et al.* Defective skeletal muscle growth in lamin A/C-deficient mice is rescued by loss of Lap2. *Human Molecular Genetics* **22**, 2852-2869 (2013).
7. Janin, A. *et al.* SMAD6 overexpression leads to accelerated myogenic differentiation of LMNA mutated cells. *Scientific Reports* **8**, 15 (2018).
8. Solovei, I. *et al.* LBR and Lamin A/C Sequentially Tether Peripheral Heterochromatin and Inversely Regulate Differentiation. *Cell* **152**, 584-598 (2013).
9. Bakay, M. *et al.* Nuclear envelope dystrophies show a transcriptional fingerprint suggesting disruption of Rb-MyoD pathways in muscle regeneration. *Brain* **129**, 996-1013 (2006).
10. Melcon, G. *et al.* Loss of emerin at the nuclear envelope disrupts the Rb1/E2F and MyoD pathways during muscle regeneration. *Human Molecular Genetics* **15**, 637-651 (2006).
11. Mejat, A. *et al.* Lamin A/C-mediated neuromuscular junction defects in Emery-Dreifuss muscular dystrophy. *Journal of Cell Biology* **184**, 31-44 (2009).
12. Gnocchi, V.F. *et al.* Uncoordinated Transcription and Compromised Muscle Function in the Lmna-Null Mouse Model of Emery-Dreifuss Muscular Dystrophy. *Plos One* **6** (2011).
13. Somech, R. *et al.* The nuclear-envelope protein and transcriptional repressor LAP2 beta interacts with HDAC3 at the nuclear periphery, and induces histone H4 deacetylation. *Journal of Cell Science* **118**, 4017-4025 (2005).
14. Sullivan, T. *et al.* Loss of A-type lamin expression compromises nuclear envelope integrity leading to muscular dystrophy. *Journal of Cell Biology* **147**, 913-919 (1999).
15. Bentzinger, C.F., Wang, Y.X. & Rudnicki, M.A. Building Muscle: Molecular Regulation of Myogenesis. *Cold Spring Harbor Perspectives in Biology* **4**, 16 (2012).

16. Fedorchak, G.R., Kaminski, A. & Lammerding, J. Cellular mechanosensing: Getting to the nucleus of it all. *Progress in biophysics and molecular biology* **115**, 76-92 (2014).
17. Arimura, T. *et al.* Mouse model carrying H222P-Lmna mutation develops muscular dystrophy and dilated cardiomyopathy similar to human striated muscle laminopathies. *Human molecular genetics* **14**, 155-169 (2004).
18. Choi, J.C. *et al.* Elevated dual specificity protein phosphatase 4 in cardiomyopathy caused by lamin A/C gene mutation is primarily ERK1/2-dependent and its depletion improves cardiac function and survival. *Human Molecular Genetics* **27**, 2290-2305 (2018).
19. Le Dour, C. *et al.* Decreased WNT/beta-catenin signalling contributes to the pathogenesis of dilated cardiomyopathy caused by mutations in the lamin a/C gene. *Human Molecular Genetics* **26**, 333-343 (2017).
20. Wu, W., Shan, J.A., Bonne, G., Worman, H.J. & Muchir, A. Pharmacological inhibition of c-Jun N-terminal kinase signaling prevents cardiomyopathy caused by mutation in LMNA gene. *Biochimica Et Biophysica Acta-Molecular Basis of Disease* **1802**, 632-638 (2010).
21. Muchir, A. *et al.* Inhibition of extracellular signal-regulated kinase 1/2 signaling has beneficial effects on skeletal muscle in a mouse model of Emery-Dreifuss muscular dystrophy caused by lamin A/C gene mutation. *Skeletal Muscle* **3**, 10 (2013).
22. Roman, W. *et al.* Myofibril contraction and crosslinking drive nuclear movement to the periphery of skeletal muscle. *Nature Cell Biology* **19**, 1189-1201 (2017).
23. Mittelbronn, M., Sullivan, T., Stewart, C.L. & Bornemann, A. Myonuclear degeneration in LMNA null mice. *Brain Pathology* **18**, 338-343 (2008).
24. Dumont, N.A., Bentzinger, C.F., Sincennes, M.-C. & Rudnicki, M.A. Satellite Cells and Skeletal Muscle Regeneration. *Comprehensive Physiology* **5**, 1027-1059 (2015).
25. Pimentel, M.R., Falcone, S., Cadot, B. & Gomes, E.R. In Vitro Differentiation of Mature Myofibers for Live Imaging. *Journal of visualized experiments: JoVE* (2017).
26. Hardy, D. *et al.* Comparative Study of Injury Models for Studying Muscle Regeneration in Mice. *Plos One* **11**, 24 (2016).
27. van Wessel, T., de Haan, A., van der Laarse, W.J. & Jaspers, R.T. The muscle fiber type-fiber size paradox: hypertrophy or oxidative metabolism? *European Journal of Applied Physiology* **110**, 665-694 (2010).
28. Hong, J.S. *et al.* Cardiac dysrhythmias, cardiomyopathy and muscular dystrophy in patients with emery-dreifuss muscular dystrophy and limb-girdle muscular dystrophy type 1B. *Journal of Korean Medical Science* **20**, 283-290 (2005).
29. Mittelbronn, M. *et al.* Myofiber degeneration in autosomal dominant Emery-Dreifuss muscular dystrophy (AD-EDMD) (LGMD1B). *Brain Pathology* **16**, 266-272 (2006).

30. Barateau, A. *et al.* Distinct Fiber Type Signature in Mouse Muscles Expressing a Mutant Lamin A Responsible for Congenital Muscular Dystrophy in a Patient. *Cells* **6**, 14 (2017).
31. Ruggiero, L. *et al.* MUSCLE FIBER TYPE DISPROPORTION (FTD) IN A FAMILY WITH MUTATIONS IN THE LMNA GENE. *Muscle & Nerve* **51**, 604-608 (2015).
32. Dayanidhi, S. & Lieber, R.L. SKELETAL MUSCLE SATELLITE CELLS: MEDIATORS OF MUSCLE GROWTH DURING DEVELOPMENT AND IMPLICATIONS FOR DEVELOPMENTAL DISORDERS. *Muscle & Nerve* **50**, 723-732 (2014).
33. Schiaffino, S. & Reggiani, C. FIBER TYPES IN MAMMALIAN SKELETAL MUSCLES. *Physiological Reviews* **91**, 1447-1531 (2011).
34. Liao, C.Y. *et al.* Rapamycin Reverses Metabolic Deficits in Lamin A/C-Deficient Mice. *Cell Reports* **17**, 2542-2552 (2016).
35. Lammerding, J. *et al.* Lamin A/C deficiency causes defective nuclear mechanics and mechanotransduction. *Journal of Clinical Investigation* **113**, 370-378 (2004).
36. Chandran, S. *et al.* Suppression of myopathic lamin mutations by muscle-specific activation of AMPK and modulation of downstream signaling. *Human Molecular Genetics* (2018).
37. Muchir, A. *et al.* Activation of MAPK pathways links LMNA mutations to cardiomyopathy in Emery-Dreifuss muscular dystrophy. *Journal of Clinical Investigation* **117**, 1282-1293 (2007).
38. Wu, W., Muchir, A., Shan, J.A., Bonne, G. & Worman, H.J. Mitogen-Activated Protein Kinase Inhibitors Improve Heart Function and Prevent Fibrosis in Cardiomyopathy Caused by Mutation in Lamin A/C Gene. *Circulation* **123**, 53-61 (2011).
39. Pallafacchina, G., Calabria, E., Serrano, A.L., Kalhovde, J.M. & Schiaffino, S. A protein kinase B-dependent and rapamycin-sensitive pathway controls skeletal muscle growth but not fiber type specification. *Proceedings of the National Academy of Sciences of the United States of America* **99**, 9213-9218 (2002).
40. Kirby, T.J., McCarthy, J.J., Peterson, C.A. & Fry, C.S. Synergist Ablation as a Rodent Model to Study Satellite Cell Dynamics in Adult Skeletal Muscle, in *Skeletal Muscle Regeneration in the Mouse: Methods and Protocols*, Vol. 1460. (ed. M. Kyba) 43-52 (Humana Press Inc, Totowa; 2016).
41. Sullivan, T. *et al.* Loss of A-type lamin expression compromises nuclear envelope integrity leading to muscular dystrophy. *J Cell Biol* **147**, 913-920 (1999).
42. Springer, M.L., Rando, T.A. & Blau, H.M. Gene delivery to muscle. *Current protocols in human genetics / editorial board, Jonathan L. Haines ... [et al.]* **Chapter 13**, Unit13.14-Unit13.14 (2002).
43. Vogler, T.O., Gadek, K.E., Cadwallader, A.B., Elston, T.L. & Olwin, B.B. Isolation, Culture, Functional Assays, and Immunofluorescence of Myofiber-

Associated Satellite Cells. *Methods in molecular biology* **1460**, 141-162 (2016).
44. Arimura, T. *et al.* Nuclear accumulation of androgen receptor in gender difference of dilated cardiomyopathy due to lamin A/C mutations. *Cardiovasc Res* **99**, 382-394 (2013).
45. Smith, L.R. & Barton, E.R. SMASH - semi-automatic muscle analysis using segmentation of histology: a MATLAB application. *Skeletal Muscle* **4** (2014).
46. Vogel, B., Siebert, H., Hofmann, U. & Frantz, S. Determination of collagen content within picrosirius red stained paraffin-embedded tissue sections using fluorescence microscopy. *MethodsX* **2**, 124-134 (2015).

CHAPTER 4

INVESTIGATING THE ROLE OF EXTRACELLULAR MATRIX ON DISEASE PRGRESSION IN EMERY DREIFUSS MUSCULAR DYSTROPHY[4]

The extracellular matrix is a key component of a cell's microenvironment. Unlike many other environmental factors which are either chemical or mechanical in nature, the extracellular matrix (ECM) generates both mechanical and chemical stimuli[1]. It has already been shown that *LMNA* knockout cells have defective mechanosensing of substrate stiffness *in vitro*[2], and clinically, myopathies caused by *LMNA* mutations present with increased muscle tissue stiffness and progressive degeneration and fibrosis that increases with age[3]. Other studies have evaluated the effect of *LMNA* deletion on collagen (the primary molecule present in fibrosis) synthesis in fibroblasts and found no specific change *in vitro*[4]. To elucidate the potential mechanisms leading to muscle cell degeneration, the microenvironment of muscle should be characterized due to the role it plays not only in mechanotransduction, but also in the storage and release of growth

[4] This represents preliminary work that will be published in the form of a methods paper Summer, 2019. Portions of this chapter were taken from Felicia Sadikin, an undergraduate student supervised and mentored by Ashley, and her 2017 honors thesis entitled "*Evaluating The Role Of The Extracellular Matrix In Emery- Dreifuss Muscular Dystrophy Using Solubilized Native Muscle Matrix And Decellularized Tissue Scaffolds*."

Earle A, Zheng H†, Modi S†, Sadikin F†, Spektor R, Soloway P, Lammerding J. Extracellular Matrix Derived from Mice with Lamin A/C mutations causing Muscular Dystrophy lead to Alterations in Muscle Differentiation and Maturation. ASCB National Conference, San Diego CA, December 2018. (Poster)

Sadikin F†, **Kaminski-Earle A**, Lammerding J. Analysis of Extracellular Matrix in Mice with Muscular Dystrophy and its Effect on Myoblast Function, BMES National Meeting, Minneapolis, MN, October 2016. (Poster)

factors and other chemical signals. Interestingly, another laminopathy, Hutchinson-Guilford Progeria Syndrome (HGPS), which manifests in a premature aging phenotype, shows that ECM misregulation causes a major cause of disease progression[5]. Culturing HGPS cells on wild-type (WT) tissue derived ECM from blood vessels, one of the tissues that is clinically involved in the disease, rescued the signaling and morphology defects present when the HGPS cells were cultured on their own matrix[5]. The key factor that leads to altered ECM in HGPS blood vessels is β-catenin accumulation in the nucleus[5]. Previous studies have also found that mutations in lamin A/C lead to defects in cell proliferation, collagen production, and satellite cell differentiation due to impaired TGF- β signaling[6]. Given these studies, we hypothesize that muscle ECM is similarly misregulated during normal disease progression in Emery Dreifuss muscular dystrophy (EDMD).

The ECM is a highly dynamic structure that is constantly remodeled as different components are deposited, degraded, or modified. Fibroblasts are the primary cell type that build and maintain the ECM. They secrete soluble and insoluble ECM proteins, which are then remolded by a variety of mechanical and protease factors coming from fibroblasts and other cell types[7]. This leads to a distinct ECM for each tissue type that provides the structural, chemical and mechanical cues that pattern a particular tissue. This balance of secreting new protein and the breakdown of existing protein is a tightly controlled process in both normal homeostasis, and regeneration, that is necessary to maintain functional tissue[8]. In the event of tissue damage, fibroblasts will transiently increase ECM secretion to maintain tissue shape, allowing time for tissue specific cells to proliferate and immune cells to clear out debris[9]. After the major cell populations

have recovered, the excess ECM is degraded. When this rise and fall of ECM is chronically disrupted, homeostasis is permanently distorted, leading to and contributing to, multiple diseases such as cancer, and cellular processes such as angiogenesis, morphogenesis and development, maintenance of stem cell niches, and wound repair[8, 10].

The molecular composition, topography and mechanical properties of the ECM are closely tied to mechanotransduction and cell signaling[11, 12]. ECM-cytoskeletal coupling has been well established. The role of integrins as well as extracellular and intracellular integrin associated proteins, such as fibronectin and vinculin, respectively, have highlighted the importance of the ECM in cell adhesion, proliferation, and migration[13]. More recently, the LINC complex (linker of nucleus and cytoskeleton) and the nuclear lamina have provided some of the missing structures in mechanotransduction pathways. Laminopathic cells have multiple disrupted mechanotransduction pathways, possibly leading to incorrect sensing and responding to ECM signals, as discussed in detail in Chapter 1[14].

For the muscle laminopathies, fibrosis, at minimum, is an important consequence of the disease. Muscle fibrosis often occurs due to altered use (hypertrophy due to exercise or hormones, and atrophy due to aging, denervation and regeneration) and is usually transient[15]. It results in increased collagen content, stiffness, and variability of muscle fiber size. In disease states, however, fibrosis is unresolvable, chronic, and interferes with normal muscle function. Muscle ECM provides the greatest resistance to mechanical strain, making it the main contributor to the mechanical properties of

muscle[15]. Skeletal muscle ECM is primarily composed of type I and III collagen, although specific regions also have more specific compositions. For instance, the perimysium has a greater abundance of the proteoglycan (PG) decorin, whereas the endomysium and epimysium have more chondroitin sulfate, collagen XVIII, perlecan and agrin[16]. The composition of these PGs are important because they play a role in the storage and release of growth factors such as TGF-beta, IL-1, and IGF and others. Given the increased chronic fibrosis in muscular dystrophy, along with impaired mechano-sensing due to lack of functional lamins, this may impact the course of muscle degeneration in AD-EDMD.

Tissue decellularization as a means of characterizing the ECM

Decellularization, the process of removing cellular components of a tissue while leaving behind a structurally and compositionally similar native ECM, entered the scientific stage as a potential method of tissue engineering many years ago[17]. Not only does it provide a useful scaffold to evaluate cellular phenotype in *vitro* but it also performs the task of removing the much more abundant cellular proteins to allow for cleaner evaluation of ECM proteins. Many labs have worked on developing methods that maximize cellular protein removal while minimizing losses to the ECM. Multiple classes of methods have been evaluated such as physical, detergent, biological, and hypo/hypertonic shock based protocols[18]. Physical methods, such as mechanical force and agitation, lyse cells and release material contained in membranes, but are ineffective in removing cellular content. Detergents, such as sodium dodecyl sulfate (SDS) and Triton X-100, are common chemicals used to disrupt membranes by interacting with

hydrophobic residues, interfering with lipid and protein interactions, and solubilizing and removing cellular components[19].

These detergent methods, however, are more prone to damaging ECM because detergents are non-discriminatory in their solubilization. Trypsin has been used to decellularize tissue by cleaving peptide bonds and digesting proteins[20] and Latrunculin B has been used to disrupt actin structure and solubilize cellular proteins[16]. Enzymes are harsher on GAGs than detergents and are not recommended when these proteins need to be evaluated[20]. Lastly, and most gently, hypotonic or hypertonic salt solutions can aid in decellularization by inducing osmotic shock, causing the release of cellular components. The effectiveness of this approach for larger tissue segments is limited due to large diffusion lengths[21]. Taken together, the method of decellularization used should depend on the downstream assays. My primary goal is to perform whole tissue decellularization for use in cell culture, proteomics, and imaging applications, requiring my final ECM scaffolds to be both fully decellularized and optically clear. The decellularization of whole tissues is highly diffusion limited compared to purely compositional studies which typically use minced tissues.

The method that we followed most closely was that of De Castro Bras et al., which generated three fractions of the original tissue: soluble components, cellular components, and the remaining insoluble ECM fraction using different buffers[19]. Being from Texas, they named the procedure the Texas 3-Step method. Minced muscles are first incubated in a 0.5 mM salt buffer that interrupts ionic interactions between proteins to remove soluble proteins. Second, the remaining tissue is incubated in SDS to remove

cytoplasmic and nuclear proteins. After complete decellularization in SDS, the ECM is deglycosylated, treated with DNAase, and solubilized for downstream proteomic analysis.

Despite the downsides and potential ECM damage associated with decellularization, multiple studies have shown enhanced differentiation of muscle progenitors on solubilized ECM coating compared to single component substrates based on MyHC staining, fiber width, and nuclear fusion index[22],[23]. It is possible that a major reason for this enhancement is laminin, an important muscle basement membrane protein. Studies evaluating difference in muscle differentiation between single ECM components showed that laminin supported the formation of larger C2C12 myotubes, higher fusion index and greater alignment compared to collagen and fibronectin[24]. In addition, another study showed that myotube formation is noticeably impaired in the absence of laminin[25]. Growth of C2C12 cells on 2D coatings and 3D scaffolds of decellulaized muscle ECM showed enhanced adhesion, proliferation, migration, and alignment compared to control substrates[26]. One major limitation of these studies is that they used the C2C12 mouse myoblasts, an immortalized cell line, which can behave differently from primary skeletal muscle myoblasts. Additionally, these studies focused on healthy matrix, rather than addressing the role of ECM changes in disease states.

Assessing the Role of ECM in EDMD: Project Overview

This study has three aims: 1) to characterize the ECM composition in EDMD and healthy control mice, 2) to characterize the structure of the muscle matrix in EDMD and

healthy controls and 3) to characterize the cellular response to muscle-derived mutant and wild-type ECM substrates compared to control matrices (e.g. gelatin, fibronectin, and Matrigel) (**Figure 4.1)**. I focused on the tibialis anterior (TA) muscle because it is impacted severely by EDMD pathology[27]. To accomplish these aims, I adapted the Texas 3-Step decellularization protocol to work for whole, intact tissues to allow for whole muscle multi-photon microscopy imaging and solubilization for mass-spectrometry analysis. To evaluate the biological impact of the protein composition, I differentiated primary myoblasts from EDMD mice and healthy WT controls on tissue derived matrices and control substrates.

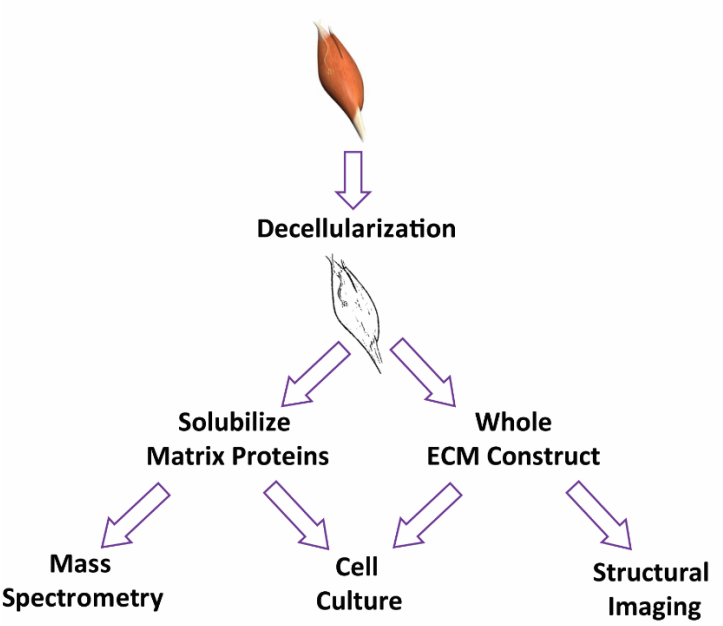

Figure 4.1. Decellularization project overview. TA muscle was decellularized as whole tissue and then either solubilization for proteomics and 2D cell culture coating or maintained as whole tissues for 3D cell culture and structural imaging.

Results

Optimized decellularization protocol preserves ECM components and removes cellular proteins

Initial rounds of decellularization included Latrunculin B and other physical methods (Supplemental Figure S4.1). We found that these methods were not capable of sufficiently removing cellular material in whole muscle, so we switched to detergent based methods for the rest of the optimization. Buffer 1, a hypertonic solution, and Triton X were incapable of fully decellularizing the tissue, regardless of the time in solution. Alternatively, using only SDS resulted in obvious loss of tissue even detectable by eye. A combination of hypo/hypertonic solutions and detergents showed the best decellularization by visual inspection. For the final optimization and validation of ECM integrity, we focused on a modified Texas 3-step method (**Figure 4.2A,B)**.

Solubilized protein concentration in the three buffers used in our so-called Cornell 3-Step protocol were measured and indicated that both short (4 hour) and long (8 hour) incubations in Triton-X incubation removed a similar amount of protein (**Figure 4.2C**). The eight hour incubation likely results in additional proteins being more easily solubilized and washed out of the tissue during the SDS incubation. A crude measurement of protein concentration in the solubilization buffers did not provide information on the specific components of the matrix, so we used more targeted, quantitative assays to evaluate hydroxyproline content, as a measurement of collagen[28], and DNA.

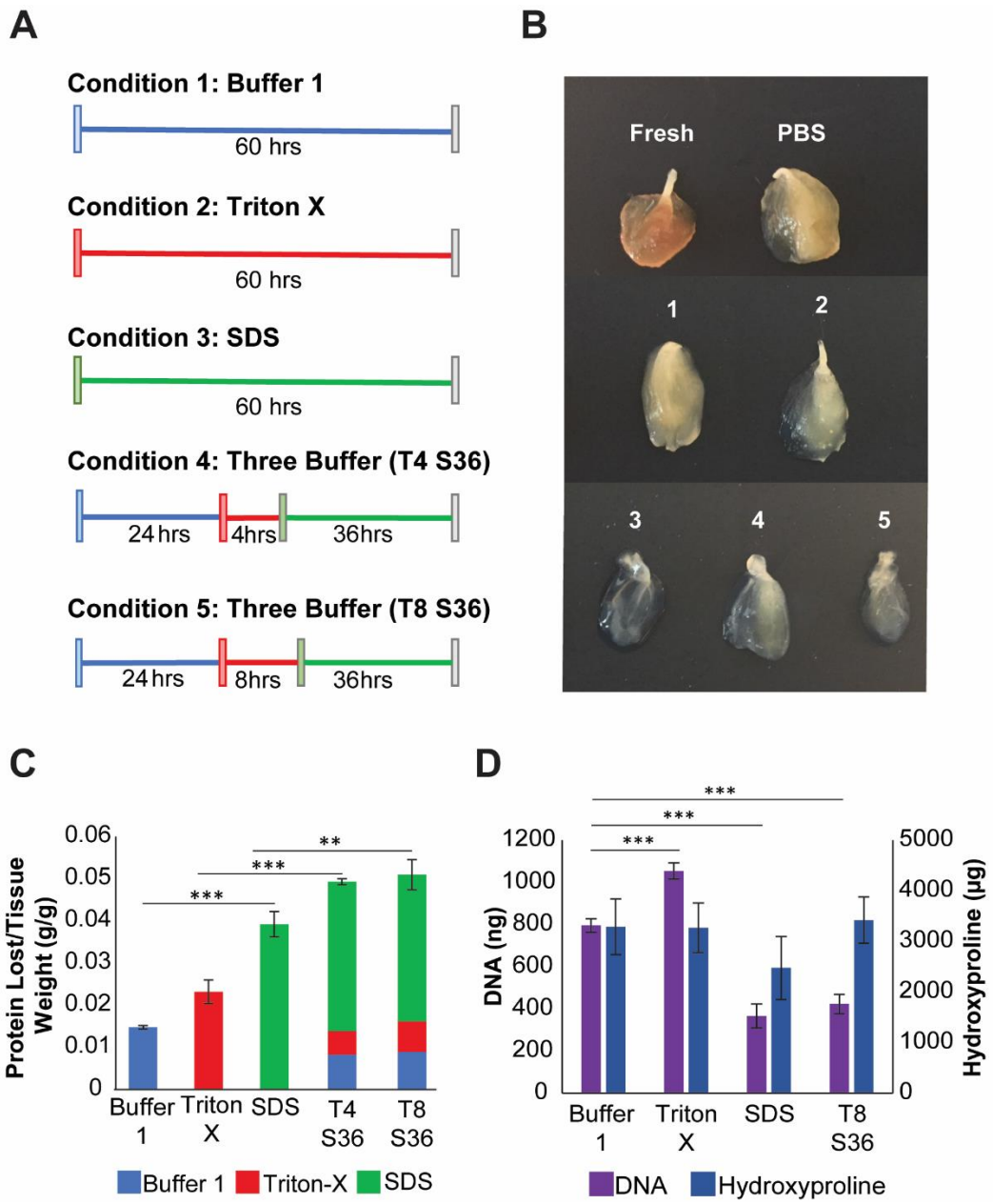

Figure 4.2. A combination of detergents and hypertonic solutions removes cellular components while maintaining ECM. A) Schematic of various decellularization protocols used to optimize the Cornell 3-Step method. **B)** Visual comparison of decellularization conditions presented in A) and also non-treated controls. Condition 4 has visible yellow tinted cellular area proximal to the tendon. **C)** Quantification of proteins solubilized in the decellularization buffer indicated significantly more protein removed using SDS compared to either Triton-X or hypertonic Buffer 1. $N = 3$ independent experiments. **D)** Biochemical assessment of DNA and hydrxyproline as a marker of collagen content indicated that T8 S36 removed DNA, but preserved hydroxyproline content compared to the most gentle decellularization condition. $N > 2$ independent experiments. ***, $P < 0.001$; **, $P < 0.01$.

There were no significant differences in collagen concentration between the control and the Cornell 3-Step protocol; however, incubation in SDS alone caused a significant drop in collagen retention. (**Figure 4.2D**). Regarding DNA, SDS was the only component that was capable of significantly reducing the DNA content below control levels, but worked as effectively in combination with other surfactants as it did alone. From these assays, we concluded that the combining incubation with Buffer 1 with eight hour Triton-X and 36 hours SDS incubation (T8 S36) condition removed the most protein and DNA, and was also able to preserve collagen as there was no significant loss of collagen compared to the least harsh condition (Buffer 1) (**Figure 4.2B-D**). Our results are not surprising given past studies that also found that the hydroxyproline content remained constant between untreated and decellularized muscles[21].

In order to further validate our protocol, we stained sections of decellularized tissues with antibodies against the ECM, actin, and DNA. Evaluating the structural elements of the cell, intracellular protein actin, as stained by phalloidin significantly decreased with increasing SDS incubation 1 to 5 (**Figure 4.3C**). All conditions with SDS (SDS, T4 S36, and T8 S36) removed all cellular components, but also led to a loss of clear polygonal fiber outlines present in the PBS condition. Despite preservation of total collagen based on the hydroxyproline assay, the long incubation in SDS seems to reduce some of the structural integrity and likely disrupts the protein epitopes (**Figure 4.3A, D)**. Fibronection showed a loss of staining intensity and structure (**Figure 4.3B, D**). Perniconi et al. also found fibronectin staining to be diffuse, despite high retention quantified via Western blot[29], so our results may again point to a loss of structural

epitopes for antibody recognition despite general high retention of the proteins. Laminin was well-preserved through decellularization and had comparable stained area in the optimized condition, T8 S36, as in the PBS control, as well as preserved a polygonal structure. These are similar results to previous studies that have also found the preservation of laminin following decellularization[26,29].

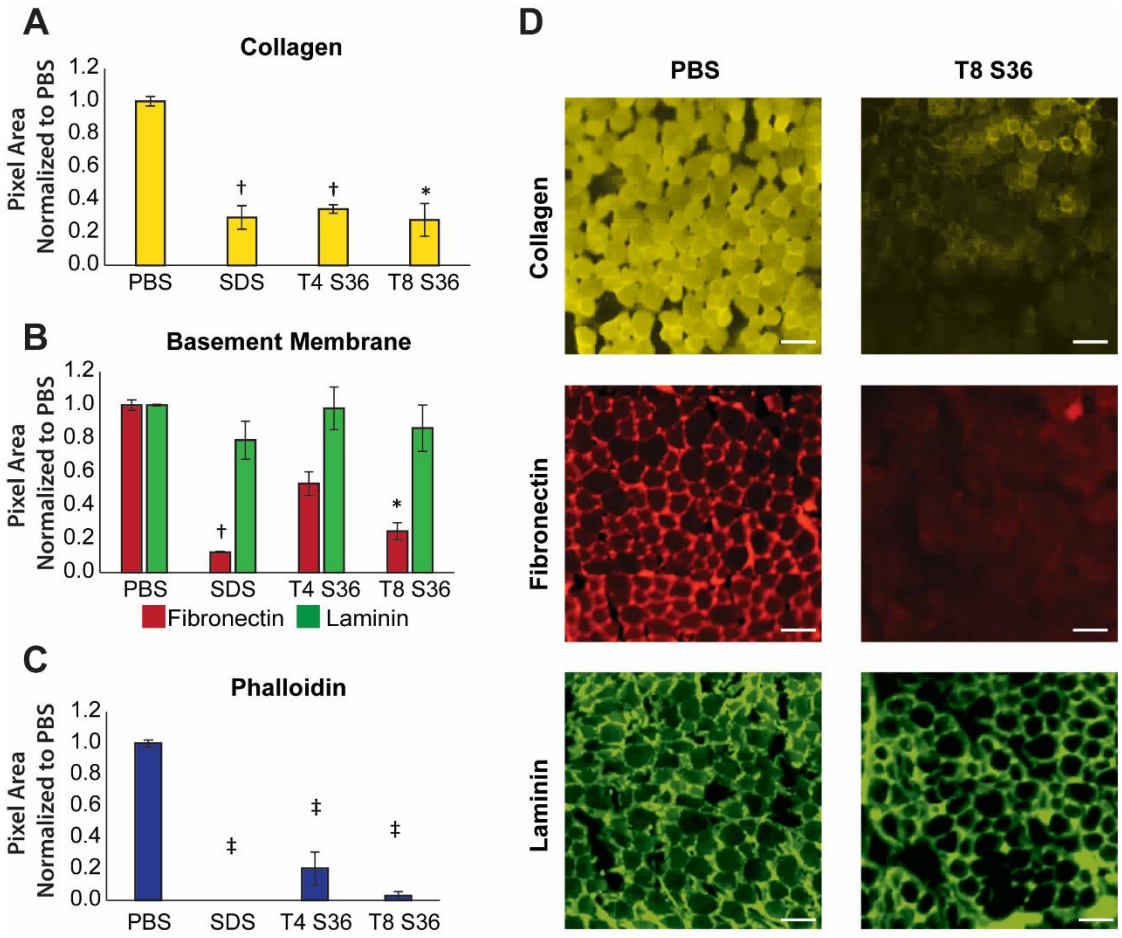

Figure 4.3. Immunofluorescent quantification of ECM indicates some loss of structural integrity. A-C) Quantification of stained area (# of pixels) normalized to PBS controls of collagen II, fibronectin, laminin, and phalloidin as a proxy for cellular protein content. Long incubations with SDS resulted in a significant loss of collagen II and cellular protein staining, but showed no difference in laminin staining. **D)** Representative images of ECM protein staining. ‡, $P < 0.001$; †, $P < 0.01$; *, $P < 0.05$ significance to PBS control. Scale bar = 75 µm.

Of the three ECM proteins that we evaluated, laminin is especially important to retain for the *in vitro* experiments as it is crucial for several processes involved in myogenesis

and enhances myoblast proliferation, migration, and alignment preceding the fusion[25]. Taken together, these data support some loss of structural integrity but overall maintenance of ECM composition.

Structural analysis shows no change in ECM between *Lmna* null and WT muscles, but proteomics data shows protein upregulation in *Lmna* null

Initial efforts in characterizing matrix structure and proteome was focused on analysis of the *Lmna* null mouse due to the more severe phenotype in this model. We also collected data for the *Lmna* H222P tissues, with analysis currently ongoing. Analysis of fibril density using a custom written Matlab code for thresholding and pixel counting of multi-photon images of WT and *Lmna* null decellularized muscles showed no overt difference in fibril density (**Figure 4.4A, B**). However, there was more variance in fibril density in the *Lmna* null samples (p=0.007) likely due to variations in disease severity and progression at the time of muscle isolation (**Figure 4.4C**).

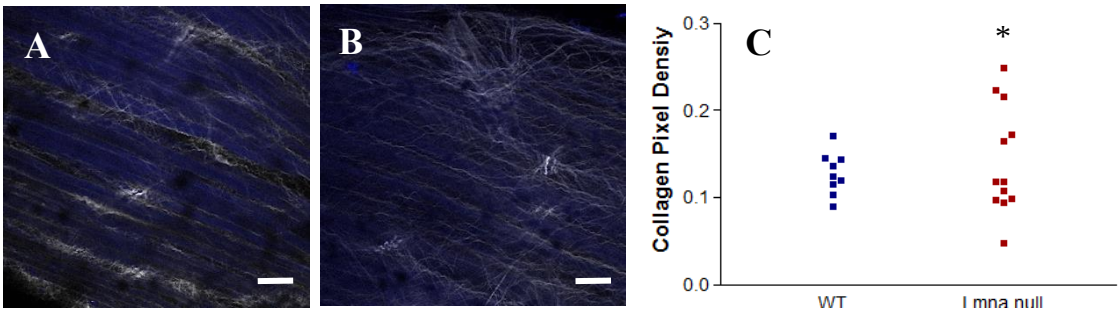

Figure 4.4. ***Lmna* null and WT mice show similar fibril densities. A)** WT and **B)** *Lmna* null decellularized muscle tissue collagen fibril density. **C)** *Lmna* null tissues show a significantly larger degree of variation between tissues. $N = \geq 3$ mice per group with ≥ 4 tissue regions imaged per tissue. , $P < 0.05$. Scale bar = 100 µm.

Mass spectroscopy indicated that ECM proteins are upregulated in the *Lmna* null tissue compared to WT. The primary proteins were structural, mostly collagen I isoforms, but laminin, a basement membrane protein, was also upregulated. Interestingly, these

changes were distinct from gene expression data from primary fibroblasts performed by a collaborator, which showed primarily changes in collagen IV isoforms and fibronectin (Soloway lab, data not shown) potentially suggesting a role for post-transcriptional changes in ECM production or in ECM remodeling in the animal. *Lmna* H222P muscles were evaluated using proteomics analysis.

Table 4.1. Key basement membrane and structural proteins are upregulated in KO vs WT mice based on TMT mass spectroscopy. *N* = 3 mice per genotype.

Protein	**Fold Change (KO v WT)**
Laminin subunit beta-2	*1.569*
Collagen alpha-1(III) chain	*1.603*
Collagen alpha-2(I) chain	*1.675*
Collagen alpha-1(I) chain	*1.681*
Collagen alpha-1(II) chain	*1.887*

C2C12 proliferation and differentiation indicate normal cellular behaviors on solubilized tissue derived ECM

Before testing primary myoblasts, we wanted to first validate that the solubilized ECM was effective as a growth substrate for C2C12 myoblasts, which are more tolerant and faster growing. C2C12 myoblasts were seeded on wild-type and *Lmna* H222P solubilized ECM, with gelatin and fibronectin serving as controls. Proliferation was monitored by imaging every hour for two days after seeding in growth media in an in-incubator imaging system. After 48 hours, the cells were more evenly spaced out on the gelatin and fibronectin and more clustered on the solubilized ECM (**Figure 4.5A**). Cells grown on gelatin had the highest growth rate in the first 48 hours and grew significantly faster than cells seeded on fibronectin, wild-type ECM, and mutant ECM, which all had similar growth rates (**Figure 4.5B**). The solubilized tissue-derived ECM from both

genotypes maintained a proliferation rate consistent with pure fibronectin and had no cytotoxic effect.

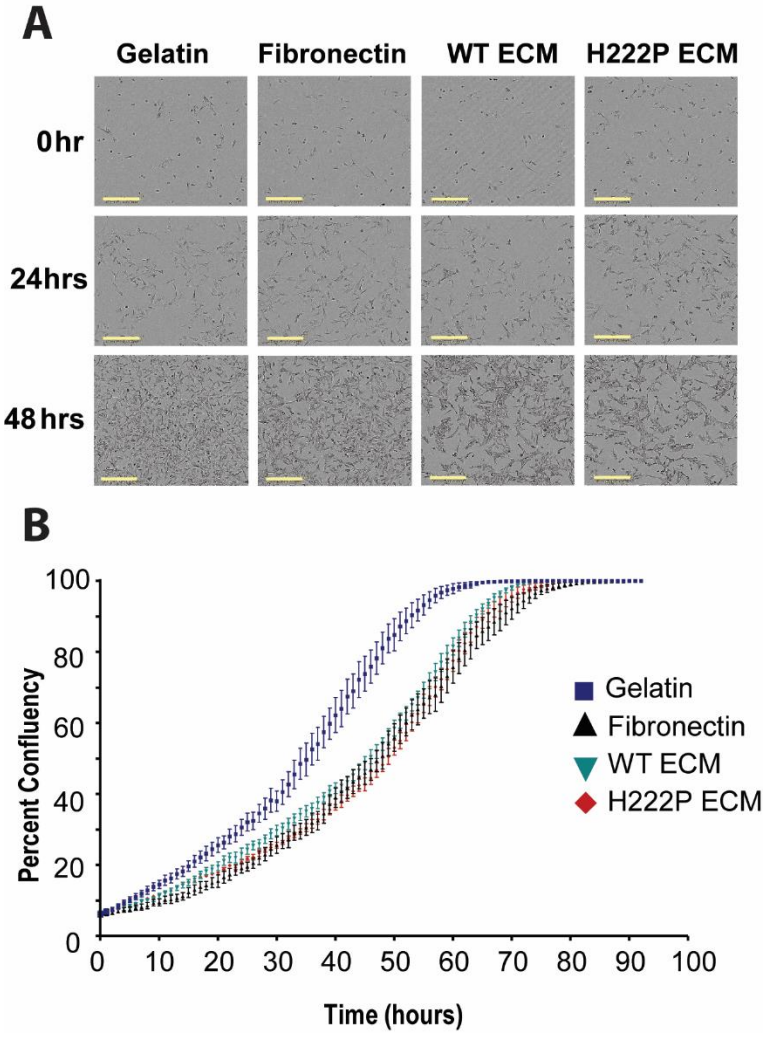

Figure 4.5. Solubilized ECM promotes similar proliferation to FN. None of the matrices had a cytotoxic effect on the cells although the cells were more clustered on the cell derived matrix. **A)** Phase contrast images of C2C12 proliferation over the first 48 hours taken by an in-incubator imaging system. Scale bar = 50 μm. **B)** Growth on gelatin was increased compared to fibronectin, wild-type ECM, and mutant ECM, $P < 0.001$, $P < 0.05$, and $P < 0.01$, respectively. $N = 3$ independent experiments.

For differentiation studies, we evaluated both high and low cell density to separate the effect of cell-cell signaling and the effect of the protein coating. We allowed the cells to differentiate for two or five days before evaluating myogenic transcription factors myogenin and myosin heavy chain (MyHC) (**Figure 4.6A)** as well as morphological factors such a fusion and elongation. Neither myogenin nor MyHC expression was significantly different on any ECM substrate (data not shown).

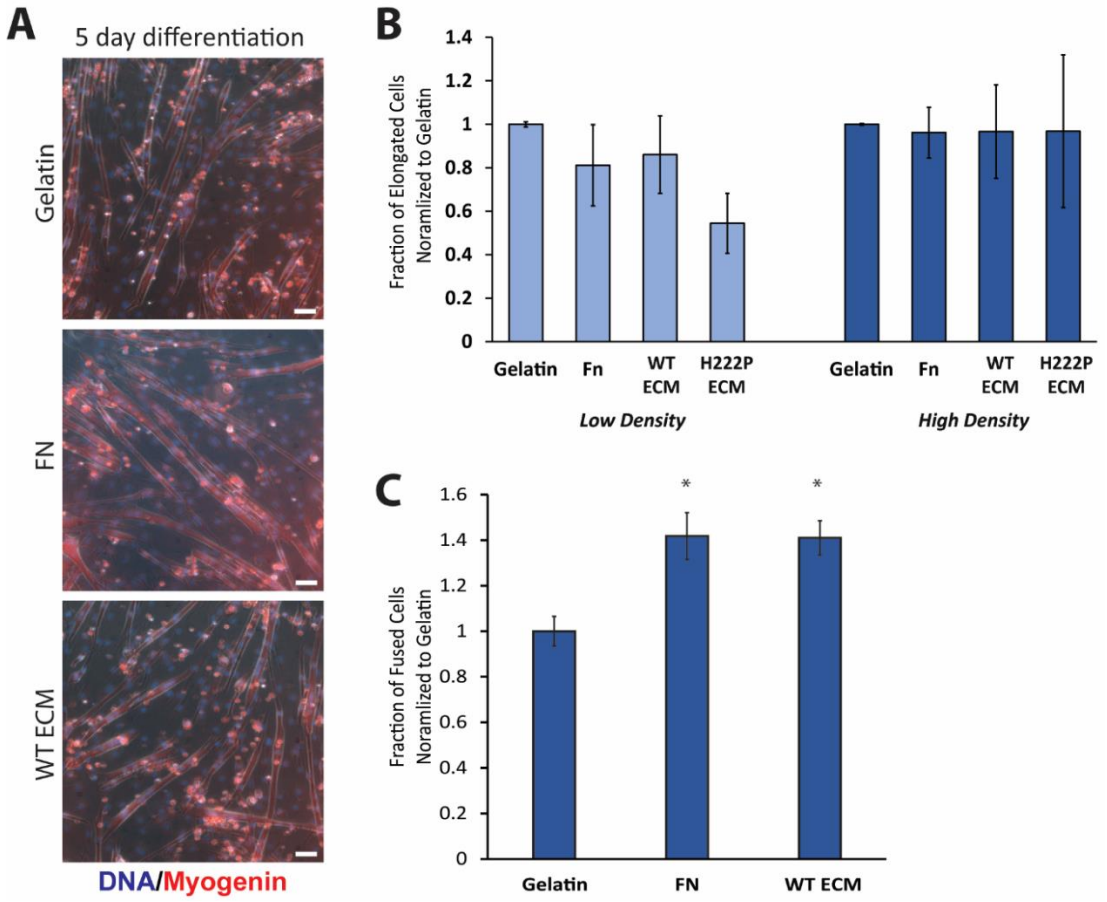

Figure 4.6. Solubilized ECM promotes similar differentiation of C2C12 cells compared to control substrates. A) C2C12 cells stained for myogenin show diffuse cyoplastmic expression at five days of differentiation and a large fraction of fused cells. Scale bar = 20 µm. **B)** Elongated (aspect ratio greater than two or multi-nucleated) C2C12 cells on gelatin, fibronectin, WT ECM, and *Lmna* H222P ECM substrates in low density and high density conditions after 2 days of differentiation show that low cell density leads to larger ECM effects to the *Lmna* H222P ECM. The fraction of elongated cells in each condition was normalized to the gelatin control in its experiment, $N > 2$ experiments. **C)** Fraction of fused cell noramiled to gelatin controls shows improved fusion of FN and solubilized WT ECM compared to gelatin control. $N > 2$ independent experiments.

Cell spreading is influenced by cell-matrix interactions, so elongation, which we defined as cells that had an aspect ratio greater than two or were multi-nucleated, allowed us to include all cells to qualitatively evaluate cell adhesion (**Figure 4.6B**). Since there were many cells that were unfused, we used this metric primarily at two days of differentiation. Although none of the values were significant, there was a larger impact

of the coating substrate on lower density experiments compared to high density experiments, with the *Lmna* H222P ECM producing the least elongated cells. Interestingly, gelatin produced very similar elongation on all experiments as indicated by the low error bars, whereas the other coatings were significantly more variable. Of the four coatings, only gelatin is a hydrogel that polymerizes, while the other three coatings merely adsorb to glass. At five days, we quantified fusion index as a morphological measure of muscle differentiation (**Figure 4.6C**). We found no difference in fusion index between FN and WT ECM, which both showed significantly higher fusion than C2C12 cell s grown on gelatin.

Primary myoblast differentiation shows nuclear spacing defects but not myogenic transcription factor changes

For the primary myoblast studies, we focused on *Lmna* null cells and matrix because of the more severe phenotype seen in these mice. We also added an additional control matrix, Matrigel, because of its similar properties to the tissue derived matrix, having been derived from mouse tumors. All the data presented in this section represents $N \geq 2$ per independent experiment per genotype. The analysis of the *Lmna* H222P data are in progress and not presented here. Expression of MyoD, the muscle commitment factor, and myogenin, a middle stage muscle transcription factor, revealed no significant contribution of ECM substrate on differentiation for either factor at any time point (data not shown). However, the *Lmna* null cells on all substrates had significantly less nuclear myogenin compared to WT cells based on a two-way ANOVA at two days of differentiation ($P = 0.03$), but were no longer significant at five days of differentiation

(Supplemental Figure S4.2).

To best understand the impact of both matrix composition and cell phenotype, a two-way ANOVA was used to asses whether there were significant interactions between cells and matrix on myosin heavy chain (MyHC) staining. Testing revealed significant interactions between both cells and the *Lmna* null matrix, such that there was an increase in MyHC staining when WT cells were grown on *Lmna* null matrix but a decrease in MyHC cells when *Lmna* null cells were grown on *Lmna* null matrix. At two days of differentiation, both cells and matrices show significant effects with *Lmna* null cells showing consistently less MyHC intensity and *Lmna* null matrix producing opposite effects depending on cell type as described above (P_{cells} = 0.0004 and P_{matrix} = 0.0265) (**Figure 4.7A**). At five days of differentiation, the matrix no longer had a significant effect but *Lmna* null cells again showed lower MyHC expression compared to WT cells (P_{cells} = 0.0085) (**Figure 4.7B**). This differing behavior based on cell type could indicate changes in specific cellular response to a unique protein in the *Lmna* null matrix, potentially through changes in integrin binding or actin signaling[2]. No other matrices showed significant effects on cell phenotype. Although a two-way ANOVA was deemed the most applicable statistical test to uncouple the cell-matrix interaction in these studies, the small absolute differences and the large error bars may indicate a limited biological relevance. Additional studies are needed to better understand the interactions and biological significance of these data, but cell intrinsic defects dominate the myogenic differentiation in *Lmna* null cells.

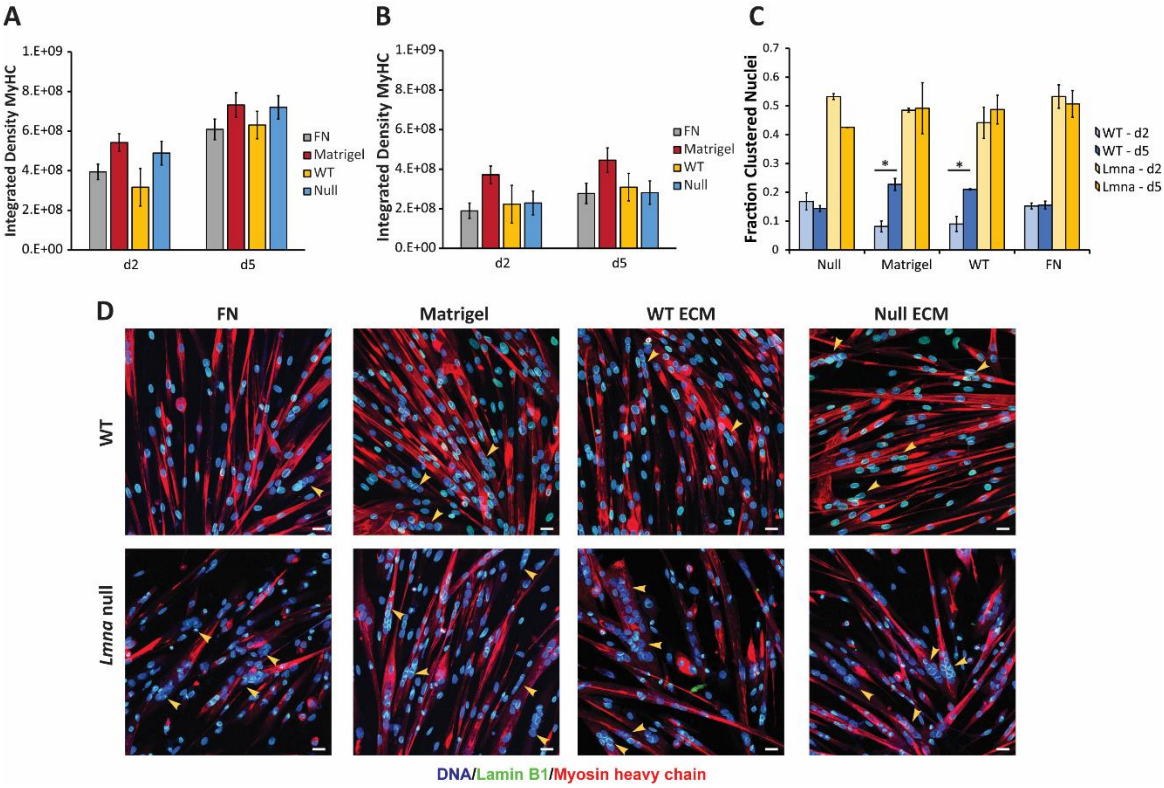

Figure 4.7. Changes in ECM composition lead to changes in myosin heavy chain expression and nuclear positioning. A) WT primary myoblasts showed high levels of MyHC expression on all substrates, with slightly lower expression on FN and WT matrices at day two of differentiation. However, *Lmna* null cells **B)** only had higher MyHC expression on Matrigel. The cell:matrix interaction for *Lmna* null ECM was significant at two days of differentiation due to the opposite effects in WT and *Lmna* null cells. *Lmna* null cells were significantly lower in MyHC expression on all matrices at both time points. **C)** Nuclear spacing defects in the *Lmna* null cells were not rescued on any of the matrices where clustered, or touching nuclei, occur more frequently in *Lmna* nulls cells than WT cells. However, Matrigel and WT matrix do significantly increase the amount of nuclear clustering seen in WT cells. *, $P < 0.05$. **D)** Representative images of WT and *Lmna* null myoblasts at two days of differentiation on each of the ECM substrates. Scale bar = 20 µm.

One of the most striking elements of the *Lmna* null cells was the presence of highly multi-nucleated myofibers and clustered nuclei as discussed in Chapter 3. There was an effect of matrix on WT nuclear spacing with Matrigel and WT matrix producing significantly more clustered nuclei than FN or *Lmna* null matrix at five days of

differentiation ($P < 0.05$) (**Figure 4.7C**). A recent paper showed the need for locally produced FN for proper nuclear positioning in muscle[38]. A similar role for cell adhesion proteins may change the dynamics of nuclear anchorage in the WT, but not the *Lmna* null, cells which have LINC complex defects[39].

3D Matrix is capable of supporting cellular differentiation for long culture times in vitro

To model *in vivo* environments more closely, primary myoblasts were seeded onto decellularized tissue scaffolds. The myoblasts spontaneously differentiated into myofibers only on the 3D scaffolds (**Figure 4.8**). The cells were seeded sparsely throughout the well, but over time migrated to the tissue at the center of the well and aligned with the directionality of the ECM, which is stained for laminin in the images as this protein was found to be best preserved through decellularization. This follows previous studies that found that the matrix provided cues to direct migration to specific locations and the fibers lined up longitudinally[26]. As seen in the middle image of the figure, myotubes preferred to grow along the laminin of the ECM, and not on the bare coverslip. Laminin is crucial for several processes involved in myogenesis, as it enhances myoblast proliferation, migration, and alignment preceding the fusion. Laminin is present in the samples both in the 3D decellularized tissue scaffold and also a thin layer around the cells, as myotubes secrete laminin that adjoin them[25].

Cells differentiated much slower in 3D than in 2D experiments. After five days of basic fibroblast growth factor and serum withdraw, few fibers had formed (data not shown).

Overall, our decellularized whole muscle 3D scaffolds were able to support myoblast adhesion, alignment, and growth. The 3D environment provided additional topographical cues that enhance myoblast growth and allowed the cells to also secrete their own matrix. Additional experiments are needed to evaluate the impact of 3D tissue derived matrix scaffolds in EDMD models of laminopathies.

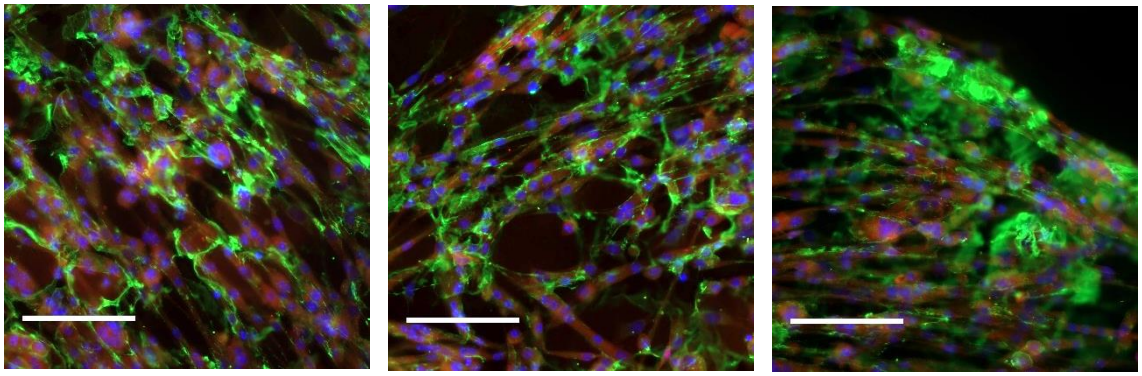

Figure 4.8. ECM scaffolds promote cellular differentiation. WT cells grown on decellularized ECM after 12 days in growth media stained for laminin (green), myogenin (red) and DAPI (blue. Scale bar = 100 μm.

Discussion

Here, we show optimization of a whole muscle tissue decellularization process that produces optically clear tissues for use as 3D constructs or solubilization for 2D cell culture coatings, as well as analysis via multiphoton microscopy and proteomics. Our Cornell 3-Step method maintains good ECM integrity, especially of the key muscle ECM protein, laminin, and does not elicit cytotoxic effects in cell culture. We showed limited changes in ECM architecture in *Lmna* null mice, but a few key compositional changes in laminin and collagen identified based on proteomics data. Results on *Lmna* H222P ECM are currently pending. *Lmna* null cells showed primarily cell intrinsic defects, despite small effects of matrix, especially for Matrigel which may be due to its

hydrogel properties compared to the other protein coatings. *Lmna* H222P ECM caused decreasing trends in C2C12 elongation and differentiation that were enhanced at lower seeding densities. Evaluation of *Lmna* H222P ECM on primary cells are currently in the process of quantification.

This project has seen multiple iterations of cell type, matrix, and quantification methods, and thus much of the data are still preliminary. The changes in C2C12 cell elongation may be due to the changes in cell adhesion factors mediating Rho/ROCK signaling through focal adhesion[2]. Staining for focal adhesion proteins and actin architecture, as well as following up with protein expression data is needed to confirm this hypothesis. This alone is an interesting finding and may indicate that there are differences between WT and *Lmna* H222P matrix. Additional work is needed to validate whether there are significant differences in *Lmna* H222P matrix, as well as whether the matrix changes occur prior to phenotype onset.

The studies on matrix structure and composition and primary myoblast culture were done using *Lmna* null cells and tissues, making it difficult to compare to the C2C12 data. The change in experimental set up was made due to the more severe phenotype of the *Lmna* null mouse model. The shortened life span of the animal means very fast changes to muscle function, potentially precluding significant changes in ECM which were not noted in the original publication[30]. The *Lmna* H222P mouse shows a disease progressing over months instead of days-weeks, leading to possibly more consistent changes in the matrix composition at has been documented to occur by 6 months of

age[31]. Overall, the effect of ECM appeared minimal, despite the statistical significance. WT ECM did not rescue defective differentiation, such as an increase in clustered nuclei in *Lmna* null cells, highlighting the prominence of cell-intrinsic defects as disease drivers. As discussed in the previous chapter, and shown in the C2C12 data, the high seeding density of the primary myoblasts may have decreased the effect of altered matrix structure or composition. Increased cell-cell contacts and signaling has been shown to decrease the role of matrix adhesion on cell phenotype[7]. As with the follow-up experiments done on Matrigel, these ECM experiments should be repeated at lower densities as already discussed in Chapter 3 to determine whether similar effects are with the primary myoblasts as the C2C12 cells. In addition, the statistics need to be closely evaluated to determine if there are biologically meaningful effects.

Another key aspect that has not been investigated yet is the effect of 2D versus 3D culture on *Lmna* mutant myoblasts. Multiple papers have shown defects in *Lmna* mutant cells ability to respond to mechanical stimuli such as substrate stiffness and cell patterning[12, 32, 33]. As the solubilized matrix only allows for the chemical signaling from the ECM, the 3D matrix could provide additional information on the role of combined mechanical and chemical signaling in this system.

In conclusion, this work has optimized a decellularization protocol that is useful for studying disease phenotypes and is amenable to imaging, proteomes, and cell culture. In studying *Lmna* null myoblasts, we have found that cell intrinsic changes dominate over ECM related changes.

Methods

Animals and Tissue Harvest. All animal procedures were conducted in accordance to the Cornell University Institutional Animal Care and Use Committee. Male and female mice with the *Lmna* H222P and *Lmna* null mutation were anesthesized with isofluorane and euthanized by cervical dislocation. "Young" *Lmna* H222P mice (5-7 weeks of age) and "Old" mice (at least 22 weeks of age) were used to analyze the mice before and after disease onset. All data presented here are based on the post-phenotype onset mice. All *Lmna* null mice and litter maters were harvested between 4 and 5 weeks of age. Wild-type C57BL/6 mice were used for decellularization optimization. Tibialis anterior (TA) muscles were harvested and placed in phosphate-buffered saline (PBS), snap frozen in liquid nitrogen, and stored at –80° C until needed. Muscles were completely thawed prior to decellularization at room temperature.

Tissue Decellularization. To account for different sizes of TAs, each muscle was weighed and decellularized in 20× volume/weight of solution rounded to 0.7, 1, or 1.3 mL. To limit the activity of the natural ECM proteases that are released during the decellularization process, protease inhibitors were added to all solutions in the room temperature steps to protect native ECM structure and composition.

The TAs muscles were first incubated in 500 mM NaCl, 10 mM Tris base, called Buffer 1, for 24 hours at 4° C with agitation. All further steps were performed rocking at room temperature in the presence of cOmplete Protease Inhibitor Cocktail (PI) (Sigma, 1 mM EDTA). Muscles were then transferred into 2% Triton X-100 and incubated for 8 hours

and then washed three times in Milli-Q for a total of 35 minutes. TA muscles were then incubated in 1% SDS for 36 hours or until visibly acellular, up to 48 hours. Finally, the tissues were washed three times and stored up to a week in MilliQ water with PI at 4°C until needed.

Muscles used for decellularization optimization and validation were incubated in phosphate buffered saline (PBS), Buffer 1, 2% Triton X, or 1% SDS for 60 hours with PI then washed three times in MilliQ water. Fresh muscles were thawed when the decellularization procedure was completed.

Biochemical Assays. The protein concentration of the Buffer 1, Triton X, and SDS solution fractions of each decellularization condition were determined using a Bradford Assay for Buffer 1 and Pierce Assay for Triton X and SDS fractions due to incompatibility with the Bradford reagent with high concentrations of detergent. Samples were mixed 1:50 with Bradford Reagent (Bio-Rad) or 1:15 with Pierce Reagent (Thermo Fisher), compared against BSA standards, and measured for absorbance at 595 nm and 660 nm, respectively.

For hydroxyproline and DNA assays, all tissues were frozen at –80° C, lyophilized, then digested in 1 mL papain digest solution for 16 hrs at 65° C before further processing. Hydroxyproline is almost exclusively found in collagen, therefore quantifying hydroxyproline content can indicate collagen content. The digested tissue was hydrolyzed by adding equal volumes of papain digest solution and 4.8 N HCl and incubated at 100° C for 3 hrs. The hydrolysate was dried and 450 µL of chloramine-T

reagent (0.056 M chloramine T, 50% n-propanol in acetate-citrate buffer) was added and left to oxidize for 25 min at room temperature. 500 µL of Ehrlich's aldehyde reagent (1M DMAB in n-propanol/perchloric acid (2:1 v/v)) was then added and the chromophore was developed by incubating at 65° C for 20 min. The samples were measured for absorbance at 550 nm and compared to hydroxyproline standards. Methods were adapted from Reddy & Enwemeka[28]. Double stranded DNA was quantified with Quant-iT PicoGreen dsDNA Assay Kit (Thermo Fisher). Equal amounts of TE solution and PicoGreen reagent were added to each sample and incubated for 5 minutes at room temperature. The samples were then read using 485 nm, 20 nm bandwidth excitation filter and a 528 nm, 25 nm bandwidth emission filter and compared to standards.

ECM Solubilization. ECM was solubilized for mass specectroscopy, tissues were first lysed using a TissueLyser (Qiagen) run for 2 minutes at 25 Hz. Protein was solubilized in 5% SDS supplemented with 1 mM DTT. Solution was heated at 95°C for 3 hours until protein was dissolved. Proteins were precipitated with a 1:1 mixture of acetone and ethanol on ice and centrifuged at 14,000g for 30 minutes to isolate pellet. Protein pellet was deglycosylated with PNGaseF (Thermo) and then resolubilized in 5% SDS.

To solubilize ECM for cell culture, we used a protocol modified from Chaturvedi et. al.[26]. Decellularized muscles were spin-vaporized for 3 hours and incubated in 1 M acetic acid/20 mM EDTA for 7 days, with agitation at 4° C[26]. The samples were filtered through a 70 µm filter to remove hair and large pieces of unsolubilized tissue and frozen

at -80° C. Samples were lyophilized, then reconstituted in 0.1M acetic acid in a 100x stock and sterile syringe filtered. Coverslips were prepared for the ECM coating by pretreating with 2% gelatin and crosslinking with glutaraldehyde. The reaction was quenched with ethanolamine and coverslips were washed 3-5 times until the solution pH was neutral[34]. Pre-coated coverslips were used immediately or stored at 4°C for up to 2 weeks. 500 µl of gelatin (2% w/v), fibronectin (3% stock solution), Matrigel (1:100) and wild-type and mutant solubilized ECM diluted in sterile PBS were added into the well, and incubated at 37° C for 1 hour, then the remaining protein was aspirated. Protein coating was validated by adding 9M urea, scraping the bottom of the well, and measuring protein concentration by Bradford Assay.

SDS-PAGE and Mass Spectrometry. Protein concentration of all decellularization solutions were quantified by Bradford or Pierce Assay to assess the amount of protein removed from the tissue. Solubilized decellularized protein fractions were run on a 4-12% Bis-Acrylimide gel and stained to Commassie Brilliant Blue. Multi-plex labeled TMT Mass Spectroscopy was done on only the extracellular fraction remaining at the end of decellularization. Sample concentration and preparation of mas spec was done by the Cornell Biotechnology Core Facility.

Cell Culture. All cells were cultured and differentiated in incubators at 37° C and 5% CO_2. C2C12 myoblasts were cultured and expanded in growth media (DMEM with 10% fetal bovine serum (FBS) and 1% penicillin-streptomycin (P/S)). For proliferation studies, cells were seeded at 5,000 cells/cm^2 and grown until they reached 100%

confluency in IncuCyte Zoom (Essen Biosciences) with images taken every 30 minutes. For differentiation studies, cells were seeded at 50,000 cells/cm^2 for low density conditions and 150,000 cells/cm^2 for high density conditions. Cells were left in growth media for 4 hours to adhere before growth media was replaced with differentiation media (DMEM with 2% FBS, 1% P/S). Cells were differentiated for 2 days and 5 days before fixing with 4% paraformaldehyde (PFA).

Primary myoblasts were isolated from the TAs of wild-type and mutant *Lmna*$^{H222P/H222P}$ and *Lmna*$^{-/-}$ mice at 4-8 weeks of age and expanded in primary myoblast growth media (F-10 with 20% horse serum (HS) and 2.5 ng/mL bFGF). For experiments, Gomes growth media (IMDM with 20% FBS, 1% P/S, 1% chick embryo extract) was used as cells adhered better in this formulation[35]. Prolieration experiemtns were seeded at 5,000 cells/cm^2 and for differentiation experiments, cells were seeded at 75,000 cells/cm^2, and left in growth media for 4 or 24 hours before fixing in 4% PFA. Cells for differentiation were seeded for 24 hours in growth media and then switched to differentiation media (IMDM with 2% HS) for two or five days. At two days of differentiation, media was added that included 50 ng/ml of agrin. After this, media was changed every two days until being fixed in 4% PFA.

Immunofluorescence Staining and Imaging. To quantify the level of decellularization and or muscle differentiation, cells or tissues from all conditions were stained for either collagen II (DHSB), laminin (Novus Biologicals), fibronectin (Invitrogen), or phalloidin (Invitrogen), Myog F5D (DSHB), MyHC A4.1025 (DSHB), or MyoD (Santa

Cruz) and counterstained with DAPI (Thermoscientific). Decellularized tissues were cryopreserved by coating in OCT and frozen in isopentane cooled in liquid nitrogen. Tissues were cryosectioned into 30 µm thick slices and fixed with 4% PFA. Fixed tissue samples were washed with PBS three times then permeabilized with 0.2% Triton X for 20 minutes. Samples were blocked with 1% bovine serum albumin (BSA) for 1 hour. Samples to be stained for collagen II had an additional 1 hour incubation with Mouse on Mouse Fab fragment blocking reagent (Vector Labs) to prevent cross reactivity with the primary mouse antibody. Samples were incubated overnight in 4°C in primary antibodies for collagen II (1:50, DHSB, CIIC1), fibronectin (1:200, Sigma), laminin (1:250, Novus Biologicals), phalloidin (1:200, Sigma), in 3% BSA with 0.25% Triton-X. Samples were then rinsed three times in PBS and incubated for 1 hour at room temperature in secondary antibody and 15 minutes in DAPI (1:10,000, Sigma). All samples were mounted with Mowiol Mounting Medium (Vogler et. al., 2016). Cell differentiation staining followed the same procedure with myosin heavy chain (1:200, DHSB A4.1025), myogenin (1:100, DSHB, F5D), and MyoD (1:75, Santa Cruz). Images were taken on Zeiss Epifluorescence microscope at 10x for tissues and 40x for cells.

Multi-Photon Microscopy. After decellularization, samples were transferred to 1% PBS with protease inhibitor and were stored at RT for no more than 6 hours before imaging. For imaging, samples were transferred to 200 nm NaCl enhance collagen second harmonic signal. Imaging was performed using a custom built 4 channel multiphoton microscope. Second harmonic generation and two photon autofluorescent signals were

generated by 840 nm, 140fs pulses (Ti:sapphire laser oscillator (Chameleon Vision) at 80MHz repetition rate. Fluorescent emission was filtered using 417/60nm (Semrock FF01-417/60-23.9-D) and 550/49nm bandpass (Semrock FF02-525/50-23.9D) filters separated with a 458 nm longpass (Semrock FF58-Di02-90x108) secondary dichroic. An Olympus 20x objected and 705 nm longpass (Semrock FF705-Di01-49x70) primary dichroic were used to separate excited and emitted light. Five distinct regions were imaged for at least three mice per group.

Image Analysis. All immunoflouresce analysis was done using ImageJ or Zen Decellularized tissue images were imported into ImageJ and separated into individual color channels. To analyze tissue staining, masks were created by tracing the outline of the tissue to analyze only the tissue area. Mean intensity of the masked region was measured for both red (collagen, fibronectin, laminin, or phalloidin) and blue (DAPI) channels. To quantify pixel percent area of each stain, each channel was filtered with Mexican Hat and Gaussian blur to remove background noise. Images were then thresholded and quantified with the 'analyze particles' feature to determine the tissues' area fraction that was stained.

To analyze differentiation markers in cells, the number of stained fibers were counted in each image and the number of nuclei in each fiber. A MATLAB program was used to count total nuclei (i.e. DAPI positive areas) in each image. The fraction of total cells that had differentiated into elongated cells was calculated for each protein coating. The number of nuclei that had fused to become part of multi-nucleated fiber, called fusion

index, was also calculated for each protein coating. In differentiation studies with primary myoblasts, the number of myogenin-positive nuclei was also counted. This was defined as the nuclei that had an accumulation of myogenin in the nuclei and had a brighter stain in the nuclei compared to the rest of the cell.

Analysis of SHG images was done in MATLAB. Fibril density was measured based on pixel density after thresholding with Otsu method thresholding. Otsu's method is used to automatically perform clustering-based image thresh holding[36]. The algorithm assumes that the image contains two classes of pixels or have bi-modal histogram (e.g. foreground and background) then calculates the optimum threshold separating those two classes so that their intra-class variance is minimal[37]. Thresholded images were converted to binary images, and then pixel density in 64 equal sized regions was calculated based on percentage of positive pixels per region. Regions at the top and bottom of the tissues that were empty sets due to tissue size and shape were manually removed. Pixel density per image was averaged over the whole tissue for >3 samples per group.

Statistical Analysis. To determine statistical significance between groups, one-way ANOVA test and Tukey post-test were used for decellularization validation and C2C12 2 day differentiation experiments. C2C12 5 day differentiation was measured with an unpaired t-test. Two-way ANOVA tests were used for fusion index and fraction of myogenin-positive nuclei in primary myoblasts on 2D solubilized ECM experiments. The threshold for significant was $P < 0.05$.

REFERENCES

1. Humphrey, J.D., Dufresne, E.R. & Schwartz, M.A. Mechanotransduction and extracellular matrix homeostasis. *Nature Reviews Molecular Cell Biology* **15**, 802-812 (2014).
2. Schwartz, C. *et al.* Lamins and nesprin-1 mediate inside-out mechanical coupling in muscle cell precursors through FHOD1. *Scientific Reports* **7**, 14 (2017).
3. Mittelbronn, M., Sullivan, T., Stewart, C.L. & Bornemann, A. Myonuclear degeneration in LMNA null mice. *Brain Pathology* **18**, 338-343 (2008).
4. Nguyen, D. *et al.* Collagen expression in fibroblasts with a novel LMNA mutation. *Biochemical and Biophysical Research Communications* **352**, 603-608 (2007).
5. Hernandez, L. *et al.* Functional Coupling between the Extracellular Matrix and Nuclear Lamina by Wnt Signaling in Progeria. *Developmental Cell* **19**, 413-425 (2010).
6. Van Berlo, J.H. *et al.* A-type lamins are essential for TGF-beta1 induced PP2A to dephosphorylate transcription factors. *Human Molecular Genetics* **14**, 2839-2849 (2005).
7. Humphrey, J.D., Dufresne, E.R. & Schwartz, M.A. Mechanotransduction and extracellular matrix homeostasis. *Nature* **15**, 802-812 (2014).
8. Bonnans, C., Chou, J. & Werb, Z. Remodelling the extracellular matrix in development and disease. *Nature* **15**, 786-801 (2014).
9. Swinehart, I. & Badylak, S. Extracellular matrix bioscaffolds in tissue remodeling and morphogensis. *Developmental Dynamics* **245**, 351-360 (2016).
10. Lu, P.F., Takai, K., Weaver, V.M. & Werb, Z. Extracellular Matrix Degradation and Remodeling in Development and Disease. *Cold Spring Harbor Perspectives in Biology* **3**, 24 (2011).
11. Juliano, R.L. & Haskill, S. SIGNAL TRANSDUCTION FROM THE EXTRACELLULAR-MATRIX. *Journal of Cell Biology* **120**, 577-585 (1993).
12. Swift, J. *et al.* Nuclear Lamin-A Scales with Tissue Stiffness and Enhances Matrix-Directed Differentiation. *Science* **341**, 16 (2013).
13. Geiger, B., Bershadsky, A., Pankov, R. & Yamada, K.M. Transmembrane extracellular matrix-cytoskeleton crosstalk. *Nature Reviews Molecular Cell Biology* **2**, 793-805 (2001).
14. Jaalouk, D.E. & Lammerding, J. Mechanotransduction gone awry. *Nat Rev Mol Cell Biol* **10**, 63-73 (2009).
15. Kjaer, M. Role of extracellular matrix in adaptation of tendon and skeletal muscle to mechanical loading. *Physiological Reviews* **84**, 649-698 (2004).
16. Gillies, A.R., Smith, L.R., Lieber, R.L. & Varghese, S. Method for Decellularizing Skeletal Muscle Without Detergents or Proteolytic Enzymes. *Tissue Engineering Part C-Methods* **17**, 383-389 (2011).
17. Badylak, S.F., Taylor, D. & Uygun, K. Whole-Organ Tissue Engineering:

Decellularization and Recellularization of Three-Dimensional Matrix Scaffolds, in *Annual Review of Biomedical Engineering, Vol 13*, Vol. 13. (eds. M.L. Yarmush, J.S. Duncan & M.L. Gray) 27-53 (Annual Reviews, Palo Alto; 2011).
18. Crapo, P.M., Gilbert, T.W. & Badylak, S.F. An overview of tissue and whole organ decellularization processes. *Biomaterials* **32**, 3233-3243 (2011).
19. de Castro Bras, L. *et al.* Texas 3-Step decellularization protocol: Looking at the cardiac extracellular matrix. *Journal of Proteomics* **86**, 43-52 (2013).
20. Gilbert, T.W., Sellaro, T.L. & Badylak, S.F. Decellularization of tissues and organs. *Biomaterials* **27**, 3675-3683 (2006).
21. Gillies, A.R., Smith, L.R., Lieber, R.L. & Varghese, S. Method of Decellularizing Skeletal Muscle Without Detergents or Proteolytic Enzymes. *Tissue Engineering* **17**, 383-389 (2011).
22. DeQuach, J.A. *et al.* Simple and High Yielding Method for Preparing Tissue Specific Extracellular Matrix Coatings for Cell Culture. *PLoSONE* **5** (2010).
23. Stern, M.M. *et al.* The influence of extracellular matrix derived from skeletal muscle tissue on the proliferation and differentiation of myogenic progenitor cells ex vivo. *Biomaterials* **30**, 2393-2399 (2009).
24. Duffy, R.M., Sun, Y. & Feinberg, A.W. Understanding the Role of ECM Protein Composition and Geometric Micropatterning for Engineering Human Skeletal Muscle. *Annals of Biomedical Engineering* **44**, 2076-2089 (2016).
25. Grzelkowska-Kowalczyk, K. The Importance of Extracellular Matrix in Skeletal Muscle Development and Function, in *Composition and Function of the Extracellular Matrix in the Human Body* (InTech, 2016).
26. Chaturvedi, V. *et al.* Interactions between Skeletal Muscle Myoblasts and their Extracellular Matrix Revealed by a Serum Free Culture System. *PLOS ONE* **10** (2015).
27. Maggi, L., Carboni, N. & Bernasconi, P. Skeletal Muscle Laminopathies: A Review of Clinical and Molecular Features. *Cells* **5**, 14 (2016).
28. Reddy, G.K. & Enwemeka, C.S. A simplified method for the analysis of hydroxyproline in biological tissues. *Clinical Biochemistry* **29**, 225-229 (1996).
29. Perniconi, B. *et al.* The pro-myogenic environment provided by whole organ scale acellular scaffolds from skeletal muscle. *Biomaterials* **32**, 7870-7882 (2011).
30. Sullivan, T. *et al.* Loss of A-type lamin expression compromises nuclear envelope integrity leading to muscular dystrophy. *Journal of Cell Biology* **147**, 913-919 (1999).
31. Arimura, T. *et al.* Mouse model carrying H222P-Lmna mutation develops muscular dystrophy and dilated cardiomyopathy similar to human striated muscle laminopathies. *Human molecular genetics* **14**, 155-169 (2004).
32. Aragona, M. *et al.* A Mechanical Checkpoint Controls Multicellular Growth through YAP/TAZ Regulation by Actin-Processing Factors. *Cell* **154**, 1047-1059 (2013).
33. Bertrand, A.T. *et al.* Cellular microenvironments reveal defective

mechanosensing responses and elevated YAP signaling in LMNA-mutated muscle precursors. *Journal of Cell Science* **127**, 2873-2884 (2014).
34. Beacham, D.A., Amatangelo, M.D. & Cukierman, E. Preparation of extracellular matrices produced by cultured and primary fibroblasts. *Current protocols in cell biology* **Chapter 10**, Unit 10.19 (2007).
35. Roman, W. *et al.* Myofibril contraction and crosslinking drive nuclear movement to the periphery of skeletal muscle. *Nature Cell Biology* **19**, 1189-1201 (2017).
36. Sezgin, M. & Sankur, B. Survey over image thresholding techniques and quantitative performance evaluation. *Journal of Electronic Imaging* **13**, 146-168 (2004).
37. Otsu, N. THRESHOLD SELECTION METHOD FROM GRAY-LEVEL HISTOGRAMS. *Ieee Transactions on Systems Man and Cybernetics* **9**, 62-66 (1979).
38. Roman, W., Martins, J.P. & Gomes, E.R. Local Arrangement of Fibronectin by Myofibroblasts Governs Peripheral Nuclear Positioning in Muscle Cells. *Developmental Cell* **46**, 102-+ (2018).
39. Lombardi, M.L. *et al.* The interaction between nesprins and sun proteins at the nuclear envelope is critical for force transmission between the nucleus and cytoskeleton. *Journal of Biological Chemistry* **286**, 26743-26753 (2011).

CHAPTER 5

EVALUATING STUDENT RESPONSE AND EFFICIACY OF A TWO-STAGE HOMEWORK SYSTEM USING A PAPER BASED AND ONLINE GRADING SYSTEM[5]

Engineering is often seen, especially by students, as synonymous to creative problem solving. Engineers are expected to find innovative solutions to problems with respect to constraints and changing variables (Jonassen, Strobel, & Lee, 2006). Developing these problem-solving skills and overall engineering competence and expertise builds upon learning foundational concepts (R. Streveler, Litzinger, Miller, & Steif, 2008). Within a problem, foundational concepts allow people to organize and define the overall framework, extract meaningful information and quantities, form and troubleshoot approaches logically, as well as to identify components of successful approaches to form novel procedures (Rittle-Johnson, Siegler, & Alibali, 2001). Knowing that a strong understanding of foundational concepts are a major key to student success, it is surprising that most homework structures do not emphasize learning these skills along with content.

[5] Chapter will serve as template for final article submission to be submitted to Journal of Engineering Education in Spring 2020 after collecting and analyzing another year of data from the BME 2110 class that is currently running.

Earle A, Holyoak D, Williams K. A two-stage homework system reinforces conceptual learning and can be effectively scaled up to larger class sizes with an on-line grading platform. ASCB National Conference, San Diego CA, December 2018. (Poster)

Within engineering, it is safe to say that homework is considered a necessary part of mastering almost all engineering competencies. As recently graduated engineering students, we have experienced and felt the effects of poorly executed, and poorly designed, homework. The engineering curriculum is quite demanding which often leads to students being forced to make choices on how they spend their time. Do you work out all the problems from scratch on your own, or do you google the question and see what help you can find? Do you work alone, with a group, or even take a divide and conquer approach to get your work done? Do you learn as you go or figure you will learn it in time for the exam? Do you receive feedback on your performance? If you do receive it, is it more than a grade? Do you get it while you still remember your thought process? Do you receive if before the exam on the material? Do you only focus on math, or do you also have homework focused on the concepts? Do your exams test both?

The list of questions could continue, but the gold-standard for engineering homework design is answerable. At most institutions, engineering homework is primarily math focused and feedback is limited, if existent, and is often given distally to the assignment. This distinctly goes against most of the recommendations that learning required frequent and fast feedback and also does not provide a good incentive to do more than just get the homework done (Martinez et. al., 2015). On the other side of the coin, students, often overwhelmed by their coursework, will do whatever it takes to get the work done and get the grade, and worry about fully unpacking the material when the exam comes. This needs no explanation, as "cramming" is well known to be an ineffective method of long term learning and leads to the persistence of misconceptions after the exam has passed. Although these experiences do not describe every engineering student or every

academic institution, these practices are prevalent enough to pose a major hindrance to students that often relegates homework from a true and deep learning experience to busywork.

This paper explores the role of homework in learning and specifically attempts to evaluate a novel method of homework design that aims to help students learn fundamental principles of problem solving by improving feedback, conceptual learning, correction of misunderstandings, and student anxiety over work load – four of the main issues that we believe are detrimental to the effectiveness of homework as a learning tool. Our method is called a two-stage homework system. In this system, students first submit an initial draft of the homework assignment in which they are assessed on their problem solving thought process and conceptual knowledge. After submission, students receive feedback on their conceptual draft and subsequently submit a second draft with their final conceptual and quantitative answers. This allows students to think through a concept, reflect upon their misconceptions, and correct their method of breaking own a problem with the guidance of the instructor's feedback. This tool will be evaluated in the context of a sophomore level Thermodynamics class, a subject that has traditionally been difficult for students to learn due to the large conceptual payload.

Introduction

Evolution of (and issues with) homework

Homework is broadly defined as "tasks assigned to students by school teachers to be carried out during non-school hours" (Cooper, 1989). The role of homework is

multifaceted and should provide students with a structure to tackle appropriate challenges, practice material discussed in class, get feedback on performance, and experience success in learning or mastering a concept (Wankat, 2001). This is extremely important as students will usually assume that they are correct until they see grade deductions for incorrect answers and the correct solutions posted. In theory, excellent homework performance should lead to excellent exam scores. However, studies show that homework grades are an inconsistent predictor of exam grade (Bas, 2017; Fernandez et al., 2006). These disparate results have fueled an age-old debate of whether homework actually helps student learning.

Homework is most useful when it closes the feedback loop and when students engage in it as intended (Nicol and Macfarlane-Dick, 2016) It must provide appropriate challenges, time to practice, regular feedback, and allow individual students to experience success, i.e. master the material, or the impact it has on students will vary based on how the individual student approaches homework. In a study based on social cognitive theory, it was found that self-efficacy, or the belief of an individual that he/she can perform at the required level, was the primary predictor of correlation between homework and final course grade (Bembenutty, 2012). In fact, self-efficacy, and not intrinsic motivation or help seeking behaviors, was the primary predictor of whether students were satisfied with their homework completion and what they learned from homework. Although this study did not correct for class size, homework type, or instructor differences, it provides a useful examination of the question, “Does homework help or hurt?”

If a student does not believe that they can perform at the appropriate level, how will that impact the way that they do homework under normal circumstances? It seems from the literature, and experience, that students will either value their grade and turn to cheating or decide they do not care and turn in poorly done assignments, or no assignment at all. What complicates this is that many engineering students do not view copying homework as cheating. Almost all students will say that copying someone else's work on an exam is cheating, but only 70% of students feel that it is cheating to copy from another student on a homework assignment, 50% that it is cheating to copy an assignment handed down from a more senior student, and only 20% that it is cheating to copy something directly from the textbook (Passow, 2006). These results, although not definite, represent the views of nearly 700 students at 11 different campuses. This general attitude explains how students working together in study groups would not consider it cheating to "work together" even if one or two people did most, if not all, of the work (Fernandez, 2006; Wankat, 2001). Interestingly, the number of students "cheating" on homework decreased from almost 30% during the second year down to almost 0% at the 4^{th} or 5^{th} years, when compared to their first year in college. It may be that these students realized that cheating on homework negatively impacted their learning and they changed their behavior (Williams, 2006).

Formative assessment and feedback

Formative versus summative assessment

Over the past few decades, teaching in higher education has gradually tried to incorporate formative assessment into classes that have traditionally used summative

assessment. (Nicol & Macfarlane-Dick, 2006). The purpose of formative assessment is to improve student learning by providing ideas and helpful information to enhance their ability to complete a task (Brown et al., 1997). Summative assessment focuses more heavily on ensuring students have sufficient knowledge in their program of study and is a more traditional approach to teaching and learning. While feedback is involved in both types of assessments, feedback is especially important in formative assessment where students typically submit drafts of assignments and obtain feedback from the instructor before they submit the final version of assignments. This gives students the opportunity to reflect on any mistakes they originally made and actively correct for their previous misconceptions. One potential drawback of implementing formative assessment in the classroom is the growing student population and greater amounts of workload required from instructors (Covic & Jones, 2008). This idea is especially critical because learning is not as effective if neither the teacher nor student is overwhelmed. Maintaining a manageable amount of work for both the teacher and student is a common goal for all courses (Attwood, 2009).

A brief summary of the history of feedback

High-quality feedback interventions are critical to achieving successful formative assessment in the classroom. However, how to supply effective feedback to students has been a subject of debate for many years. In a somewhat controversial review of the literature performed by Ammons (1956), he concluded that feedback interventions improve student learning and motivation regardless of feedback strategy. This review is now one of the most cited reviews in feedback literature. However, Kluger & DeNisi

(1996) pointed out that Ammons left out some key references that provided information that were inconsistent with his conclusions. Thus, one of the most influential reviews in the field ignored the high variability of feedback effectiveness. Kluger & DeNisi (1996) then sought to quantify the variability of feedback effectiveness with an extensive meta-analysis that analyzed 131 papers that led to 223,663 observations on feedback and performance. *They found that the effectiveness of feedback was highly variable, and that approximately one-third of feedback interventions reduced performance*! Based on these historical and seminal studies on feedback literature, a clear need exists in the present day to further investigate the types and timing of feedback that serve to improve performance rather than hinder it.

Categories and types of feedback

One of the main obstacles in delivering effective feedback strategies in the classroom is determining what types of feedback consistently improve student performance and understanding. Although many models of feedback are available in the literature, one of the most influential models was developed by Hattie & Temperley (2007). They suggest that feedback can be separated into four categories (or "levels"): *task feedback, processing feedback, self-regulation feedback, and self-feedback* (Hattie & Temperley, 2007). *Task feedback* informs the student whether something is correct or incorrect, or if the student needs to provide additional information or problem-solving steps to reach the correct answer. Although this type of feedback is generally effective, it is a very basic form of feedback that usually only applies to the problem at hand and thus does not lead to higher level skills. *Processing feedback* challenges students to think more

deeply about processes they are using to solve problems and try to relate processes to real-world scenarios. *Self-regulation feedback* helps students develop awareness of how to appropriately use their knowledge. This type of feedback can take the form of reminding students they already possess the skills necessary to accomplish a task, which encourages them to tackle problems with confidence. The last category of feedback is referred to as *self-feedback*, which is considered to be the least effective. Specifically, *self-feedback* simply informs students whether or not they did a "good job" on an assignment, and thus does not promote deeper thinking like processing feedback or self-regulation feedback. Although these four categories are all helpful in specific ways, keeping track of the types of feedback used in the classroom and emphasizing deeper levels of feedback such as processing and self-regulation is critical to maintain effective feedback practices.

The effects of positive versus negative feedback has also been an active research area for many years. In a recent review investigating the effects of feedback on the brain and neural networks (Dion & Restrepo, 2016), positive feedback was shown to have consistent beneficial effects from childhood through adulthood, whereas negative feedback was more beneficial after adolescence due to specific areas in the brain needing to mature (Grammer, Carraso, Gehring, & Morrison, 2014). Thus, in higher education, both positive and negative feedback are useful in student learning. Furthermore, Dion & Restrepo (2016) noted the difference between direct versus indirect feedback. When feedback is ambiguous or indirect, it can potentially hinder learning (Ernst & Steinhauser, 2015) and activate neural functions associated with

negative effects on learning (Sailer et al., 2007). Thus, feedback is most effective when it is “clear, explicit, and intelligible,” and teachers are thus responsible to ensure the feedback they provide is understood properly by students (Dion & Restrepo, 2016).

Feedback models

When effective feedback is successfully implemented in the classroom, students should be able to answer the following three questions according to a feedback model, also from Hattie & Temperley (2007). The questions are: "where am I going," "how am I going," and "where to next?" (Hattie & Temperley, 2007). The "where am I going" aspect of the model is focused on setting goals for students via specific cues and goal-oriented feedback. One objective in the classroom is to encourage students to commit to achieving a common goal. When this objective is accomplished, students are more likely to reach out for further feedback, which eventually results in self-regulation of their achievements (Locke & Latham, 1990). Thus, defining goals and supplying feedback to students related to those goals is a critical aspect of the "where am I going" part of the model. The second part of the model, "how am I going," involves a teacher, such as an instructor, peer, or the student themselves, supplying information related directly to performance on tasks and assessments. This part of the model is thought of as more traditional feedback, such as task or processing feedback. The last part of the model, "where to next," if used correctly with appropriate feedback, leads to enhanced challenges, developing strategies independently, and learning how to self-regulate tasks. Inappropriate use of this part of the model can lead to loading more work onto the students, which generally increases pressure and does not aid in learning. Importantly,

the questions in this model need to be accomplished with clear objective statements and consistent, effective feedback. When students are able to answer "where am I going," "how am I going," and "where to next," instructors have successfully implemented the model and students are capable of self-regulating their success. (Sadler, 1989).

Recent literature on formative assessment has expanded on the model from Hattie & Timperley (2007) and has made the goals of good feedback practice even clearer. Nicol & Macfarlane-Dick (2015) produced a seven-principle system that helps students become independent learners and improve self-regulation abilities through feedback. In summary, the seven principles are 1) clarify goals and expectations, 2) facilitate self-assessment and reflection, 3) deliver essential feedback information, 4) encourage dialogue between peers and teachers, 5) motivate and improve self-esteem, 6) provide opportunities to close the gap between current and desired performance, and 7) use student feedback to improve teaching. With these seven principals, students become aware of strategies they can use to regulate their own learning throughout college, and they can carry these strategies with them to remain life-long learners (Nicol & Macfarlane-Dick 2015).

Timing of feedback

Timing is an aspect of feedback that is not clearly understood, and studies have produced conflicting results (Anderson et al., 1995; Butler, Karpick, & Roediger III, 2007). Specifically, research studies have analyzed whether feedback should be provided immediately following a task or if feedback should be delayed. Findings

suggest that task feedback is most effective when it is given immediately (Clariana, Wagner, & Roher Murphy, 2000). This implies that students benefit most when they know whether or not they were successful at completing a task quickly after they attempted the task. This is especially true for the simpler tasks that do not require deep processing. For more complex problems, however, delayed feedback is preferred over immediate feedback (Clariana, Wagner, & Roher Murphy, 2000). By delaying feedback for complex tasks, students have the opportunity to process the problem and think independently for extended periods of time, which is more beneficial than intervening immediately. Timing of feedback is also dependent on the situation. For example, a meta-analysis determined immediate feedback is beneficial for classroom activities. For testing situations, however, delayed feedback is more effective (Kulik & Kulik, 1988). A more recent study compared how students performed on multiple-choice homework when given either immediate task feedback that indicated whether a question was correct or incorrect, or delayed feedback coupled with narrated solutions. Students who received delayed feedback far outperformed students who received immediate feedback (Gladding et al., 2015). In summary, many of these studies are conflicting, because testing situations more often require task feedback, and classroom activities are associated with processing feedback. Nevertheless, appropriate timing of feedback does have important consequences despite being context-dependent.

Misconceptions

In terms of teaching concepts, the need for the identification and engagement of student preconceptions and prior knowledge is widely recognized as an integral component of

effective teaching, including in the National Research Council's study on how people learn (Bransford, Brown, & Cocking, 2000). According to this study, the interaction of prior knowledge with new material can result in three outcomes contingent upon the consistency of the two entities. First, if prior knowledge is consistent with new material, then the new material will be learned with ease. Otherwise, contradictions within this interaction, or misconceptions, will lead to confusion. The appearance of these misconceptions results in the two other possible outcomes. Resolution of these misconceptions will facilitate greater understanding of the material, while a failure to identify and challenge foundational misconceptions can lead to deeper misunderstanding and detriments to long-term learning as well as retention in engineering (Boud & Falchikov, 2006; Brown, Hershock, Finelli, & O'Neal, 2009; McKeachie & Svinicki, 2013; Seymour & Hewitt, n.d.).

To address these misconceptions, a tremendous amount of research has been conducted on the instruction of conceptual knowledge, as exemplified by the eclectic 8,400 articles documented in Duit's bibliography, "Science Teachers' and Students' Conceptions and Science Education" (Duit, n.d.). Amongst these articles, the seminal work of Hestenes, Wells, and Swackhamer in developing the Force Concept Inventory has greatly impacted engineering education (Hestenes, Wells, & Swackhamer, 1992). Their work created a test to assess and measure students' conceptual learning on force and Newton's laws of motion and has since inspired similar concept inventories in numerous subjects, including thermodynamics (Evans et al., 2003; R. A. Streveler, Olds, Miller, & Nelson, 2003). Based on the scores of these concept inventories, Hake noticed that interactive

engagement of students as opposed to conventional lectures and homework assignments led to increased conceptual learning, as measured by the force concept inventory (Hake, 1998).

With this in mind, there has been a shift in strategies for teaching conceptual knowledge to more student-centered pedagogies that identify and correct misconceptions (Cakir, 2008; Longfield, 2009; Savion, 2009). Previous formal methods to identify misconceptions include the use of aforementioned concept inventories as method of assessment. However, the purpose and implementation of these concept inventories often determines the effect on student learning. For instance, if used at the end of a course, concept inventories can help instructors measure the effectiveness of their conceptual instruction to refine future iterations of the course, but these assessments would not directly affect the learning of the current students. If used at the beginning of the course, concept inventories can help measure students' grasp on prerequisite material and inform the foundational lectures of the course. Although these assessments are useful in highlighting more effective teaching methods, their impact on the student's ability to identify and engage their own misconceptions is more limited (R. Streveler et al., 2008).

In the shift to more student-centered pedagogies, frequent in-class assessments have gained prevalence (Mazur, 1999, 2013). In particular, immediate feedback assessment techniques, such as clickers and personal response systems, have gained widespread use for their amenability to large lecture-style classes (Sevian & Robinson, 2011). These

techniques can be employed prior to and following each conceptual unit to help students identify their own prior misconceptions and gaps in knowledge post explicit instruction. The results can also help the instructor modify the course to help students learn the necessary content (Cakir, 2008). These immediate feedback techniques have already shown improvements in the correction of misconceptions and retention of conceptual knowledge (Epstein, Lazarus, Calvano, Matthews, & others, 2002).

Similarly, "flipped" classroom approaches are becoming equally widespread. In these classrooms, students watch recorded lectures as homework and work on problem-based learning activities in class. In this way, instructors can see where misconceptions occur and immediately respond to correct these issues (Berrett, 2012). Both immediate feedback assessment techniques and flipped classroom approaches have made tremendous strides in empowering students as agents of their own learning and helping them identify and correct their own misconceptions. However, there is also merit in allotting students time to think through a concept and ensuring they reflect and act upon feedback to correct misconceptions. As of yet, few studies have evaluated homework interventions aimed at correcting misconceptions.

Interventions in thermodynamics

Regarding thermodynamics courses specifically, there have been multiple studies of the paradox of students that receive high homework grades and low exam grades. Thermodynamics is a difficult, abstract subject that requires significant time input on the part of the student to master the material (Sokrat, 2013). National averages of

passing rates for thermodynamics portion of the Fundamentals of Engineering professional licensing exam are between 40 and 65%, with minimal improvement in this area over the last ten years (Dukhan and Schumack, 2013). Some of the issues associated with poor performance on the exam stem from conceptual misunderstandings of the material. Many students can solve routine textbook problems yet provide incorrect answers to conceptual problems and are unable to sufficiently explain their answers (Dukhan, 2016). Some of these issues arise from historical misconceptions that lead to continued confusion in students today, while some stem from curricula that try to cover too much material in one semester (Sokrat, 2013).

Multiple studies have implemented online thermodynamics homework with rapid feedback or other more novel methods to try and combat these issues (Nasr and Ramadan, 2005; Taraban; 2005). Although these methods have met with some success the root issues still prevail. One educator who was implementing a homework system that focused on synthesis instead of memorization noticed that the students became frustrated when they were required to explain their answers (Nasr and Ramadan, 2005). After implementing homework that involves explanation and critical evaluation of problem solving and the resultant answer, another educator notes, "Most students respond favorably to this problem-solving approach… Of course, there still exists the typical student desire to have an example of every kind of problem that they will ever confront so that they can just change the numbers and crank out the answers" (Reardon, 2011). Even when students are given clear instructions to explain their answers they often avoid providing explanation and need to be repeatedly reminded to do so.

Although some of these behaviors could stem from students being overwhelmed by the curriculum (Sokrat, 2011), it is likely that many of the issues arise rather from the climate of many undergraduate engineering programs and prevailing attitudes about homework that students develop in high school.

Three studies focus on designing platforms to help students determine their misconceptions and synthesize course information in an engineering context. Armstrong (1995) implemented a novel "imperfect solutions" homework format in which students are provided answers to homework but some of them are secretly incorrect. The student needs to solve the problems and determine which solutions are incorrect and why. Although this particular study was a case study, it shows strong student support for the method with only three of 67 saying it was not at least "good" on a scale from Excellent, Good, Average, and Poor scale, and with only 2 of 67 saying that they would not like it to be used in other courses. In general, the students felt as if they were learning more while taking less time to complete the assignments.

Another homework method very similar to the one proposed in this chapter is Phase Arrayed Homework implemented by Godshall (2012). In this system, students prepare a problem before class, grade their own work in class as the answer is reviewed, and then can correct errors before the next class period to re-gain lost points. One time saving aspect of this homework system was student self-grading prior to submission of draft two, which could be implemented in this study if it is found that time is a major prohibitive factor. The Phase Arrayed Homework had multiple benefits, especially in

student perception. Two of the main benefits were decreased stress associated with assignments and increased confidence in problem solving. However, improvement over control classes on exam scores was varied over class years, from no improvement to moderate (5-10%) improvement. One major result of this study was that since re-submission was optional, as the semester progressed and students became more overwhelmed by their coursework, the number of people who took advantage of the extra attempt decreased, mirroring loss in gains on the exam.

Another helpful homework system evaluated a mastery learning approach which aimed to make homework more of a formative assessment than a summative assessment (Moore and Ranalli, 2015). This technique allowed students to resubmit homework indefinitely after receiving a grade of 2 (mastered), 1 (not mastered), or 0 (not attempted). There was no grade penalty given for a not mastered problem unless the corrections were never made. This limited the amount of grading needed which helped to reduce the grading burden. It was noted that students almost always resubmitted, unless other more pressing assignments starting piling up, up to three attempts. Student homework grades increased and students felt like they learned more from this homework method, however, no correlations between homework and exams were made in the scope of this study.

Hypothesis and scope of study

We believe that the incorporation of conceptual drafts and intermediate feedback will motivate students to not only think conceptually but also to reflect upon their misconceptions. We also think that removing the pressure of reaching the right quantitative answer on the conceptual homework will encourage students to engage and address their misconceptions instead of focusing on getting the correct answer. We also believe that this will help to decrease student work load/stress regarding their assignments and lead to enhanced learning.

Beyond this, our two-part homework system incorporates many beneficial features of formative and summative assessment, as well as effective feedback strategies that have been identified in past literature. We use a combination of formative assessment techniques (i.e. homework system) and summative assessment techniques (i.e. exams). The overarching goal is that students will gain strategic approaches that will lead to long-term benefits through formative assessment, and summative assessment will optimize short-term learning for students and provide feedback to the instructor to improve future performance of the students.

The primary questions that we will be investigating are:

1. Do students like the two-stage homework system?
2. Does feedback improve student understanding?
3. Does the two-stage homework result in long term gains in understanding as evidenced by the exam?

In addition to these main questions, we will also be evaluating the time spent by the instructors and students for this course and compare it to other courses to determine if a combination of formative and summative assessment leads to excessive workloads. This homework system was implemented in 2017 and 2018. The first year, all grading was done by a graduate teaching assistant and two undergraduate graders who primarily graded the lower level problems. In 2018, grading was done on Gradescope, an online homework submission and grading platform, due to an 80% increase in the number of students taking the course. In addition to the change in grading platform, all grading was now randomly distributed across a graduate teaching assistant, two undergraduate teaching assistants, and two undergraduate graders. A summary of changes in the course between 2017 and 2018, including adjustments made to other assignments and in class time, is given in **Figure 5.1**. The overall goal of the study is to determine ways to improve the student learning experience for the coming year.

Methods

The homework system was implemented in a sophomore level Biomolecular Thermodyanmics courses at Cornell University. The course was a mandatory course for all major students and was one of the first in-major courses that they took. In 2017 there were 34 (four male and 30 female) students and in 2018 there were 50 (10 male and 40

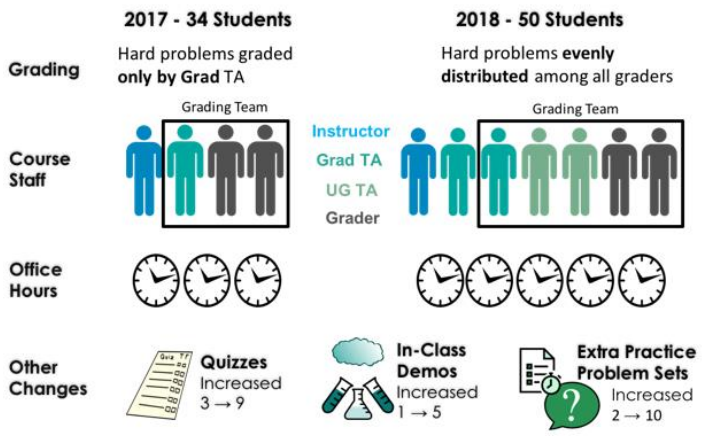

Figure 5.1. **Overview of changes made to the course between 2017 and 2018.** Although there were changes in the homework and grading format, additional office hour support, as well as practice problems, and other formative assessments were expanded. Student expereince in the class therefore did change considerably between the two years as a process of course development.

female) students enrolled. In 2017, the graduate TA and two undergraduate graders were all female, and the undergraduate graders had no involvement in the course. The graduate TA met with them weekly to discuss key points to be looking for in the grading. In 2018, there was roughly equal representation of males and females on the course staff. The graduate teaching assistant had not been involved in the course before, but all the undergraduate teaching assistants and graders had taken the course the previous year. Because there were already detailed homework solutions which also explained the concepts, the graduate TA did not meet with the undergraduate grading team each week.

Homework Design

For both years, the two-stage homework system, and the goal behind it, was explained on the first day of class. A written explanation posted online. Students were given a copy of the rubric (Supplemental File S5.1) and an example of full, partial, and no credit solutions to practice problems to use as a guide to help them understand that no math was needed or graded, and the correct answer was not expected full credit on the conceptual homework. An example of student homework and grading in 2018 is shown

in **Figure 5.2**.

Student Performance Analysis

To assess student performance on Homework 1 and Homework 2 of each homework assignment and each exam, the Earle gave a blinded numerical score between 0 and 2 that represented the student's understanding of the main concept of the problem. A score of 0 indicated that the student displayed no to minimal understanding of the concept being tested, a 1 meant that the student had a okay grasp of the concept, but was missing some key points, and a 2 represented complete conceptual understanding. With these numbers, we determined changes in understanding between Homework 1 and Homework 2 of the homework assignments, or relationships between understanding in homework and exams. Negative changes (i.e. "-2" and "-1") indicated a decline in conceptual understanding, or reversion to a previously held misconception. No change (i.e. "0") represented a student's understanding did not change between the two drafts. A positive change (i.e. "+1" and "+2") was indicative of an improvement in thoroughness of conceptual understanding.

Written Feedback Analysis

We analyzed the written feedback provided in homework assignments to determine if written feedback was effective in improving student performance and to determine which types of feedback were most effective. For the first three homework assignments of 2017 and the first five homework assignments of 2018. For 2017, we transcribed all feedback given on Homework 1 for a diverse group of students (n= 8-17 per

assignment). For 2018, all students (n= 48-50) were included because the homework and feedback were already electronic. We then categorized each instance of feedback into one of four categories: self, task, processing, or self-regulation. Next, we determined the change in student performance between Homework 1 and Homework 2 according to the scoring system previously mentioned. Relationships between feedback type and student performance were assessed.

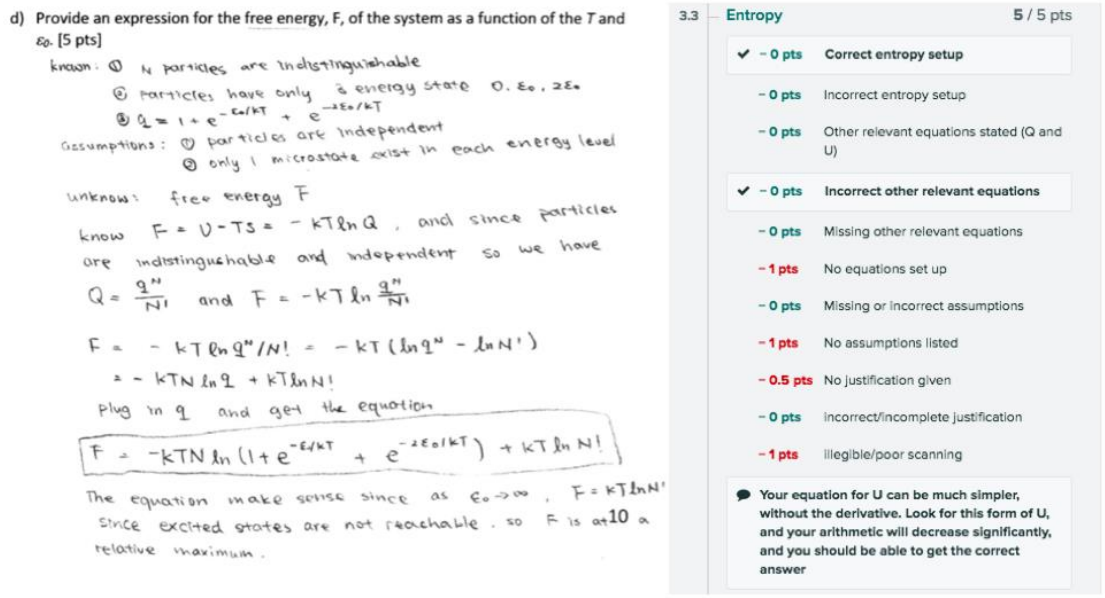

Figure 5.2 Example of conceptual homework and grading in Gradescope. Above is an examples of a conceptual homework and the feedback provided via Gradescope implemented in 2018. Students are asked to fully think through the homework problems based on assumptions, equations used, and estimated answer, and reasoning behind answer. Feedback online was given via both check boxes and written comments. In 2017, feedback was given via a rubric and written comments.

Surveys

Likert scale surveys were given early in the semester (early March) and at the end of the semester (early May) to evaluate student opinion of the two-stage homework system, self-efficacy, study habits, and collaboration habits (Supplemental File S5.2 and S5.3, respectively). The early semester survey was given after two homework assignments

were completed but prior to the first exam. The end of semester survey was given just prior to the final exam. It was combined with some general questions about the course as a whole. The self- efficacy questions were adapted from Bembenutty (2010) and Rowbautham and Schmidt (2013).

Focus Group

In 2017, we held a focus group to gain personal insight from students on their opinions of the two-part homework system, feedback in the course, and work habits. Four students out of 34 participated in the focus group. All four were women. The discussion was guided by a focus group question guide (Supplemental File S5.4) and led by two biomedical engineering graduate students who had no connections to the class. The session was recorded and transcribed. All responses remained anonymous to the instructors. In 2018, scheduling conflicts during the exam prep period precluded a focus group from being held.

Results

Students enjoy the homework system and generally feel learning gains

Overall, students had a positive experience with the two stage homework system, which was expected based on previous studies on formative assessment based homework strategies (Godshall, 2012; Armstrong, 1995; Moore and Ranalli, 2015). In the early parts of the course, many students pushed back against the need to "justify or contextualize" their answers. This was the largest component of the conceptual homework grade and many students felt that it was "way less relevant than it seems" or

felt that it was not necessary if they "already gave their assumptions." Seven out of the 34 students in the class specifically mentioned this key aspect of the homework assignment as something that they did not like. This was the highest level of Bloom's taxonomy that was on the homework and required the students to familiarize themselves with the course content beyond just plugging known values into the equations from class. Similar trends were noted in 2018. Like other studies, (Moore and Ranalli, 2015; Nasr and Ramadan, 2005) students needed to be reminded throughout the duration of the course to justify their answers and give a reason why their answers made sense in the context of the question and the class. However, more students found the system helpful than unhelpful early on, and the number of students who found it helpful increased as the semester progressed in 2017.

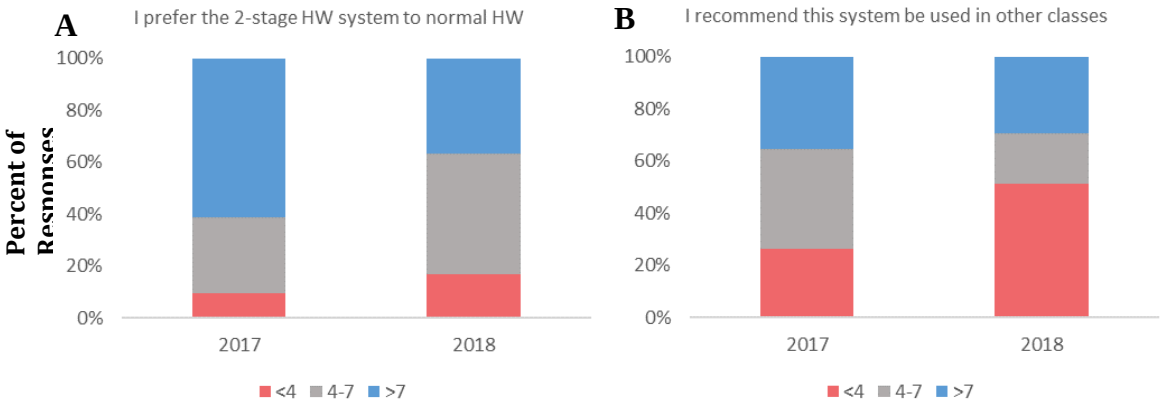

Figure 5.3. Student appreciation and recommendation of the homework system decreased in 2018. Graphs represent student responses to end of semester surveys with a likert scale ranging from 1 being strongly disagree and 10 being strongly agree. **A)** Students showed overall preference to neutral feelings toward the 2-stage system with very few students strongly not preferring it. **B)** Regarding recommendation to implement in other classes, 2017 more strongly recommended the system or were neutral whereas many students in 2018 strongly recommended against additional implementation.

This overall satisfaction and preference for this new homework in 2017 was most prominently shown in that 25 of 34 students recommended that this system would be

used in their other classes and 12 out of those 25 strongly recommended its use in other classes. In 2018, however, there was a drop in how many students would recommend this for another class. Only 20/41 students would recommend it, with 12/20 strongly recommending as shown in **Figure 5.3**. Although the survey responses were informative, many of the student quotes from the surveys highlight the impact that the homework had on at least a subset of students. Some students really appreciated the ability to make a mistake without it penalizing their grade.

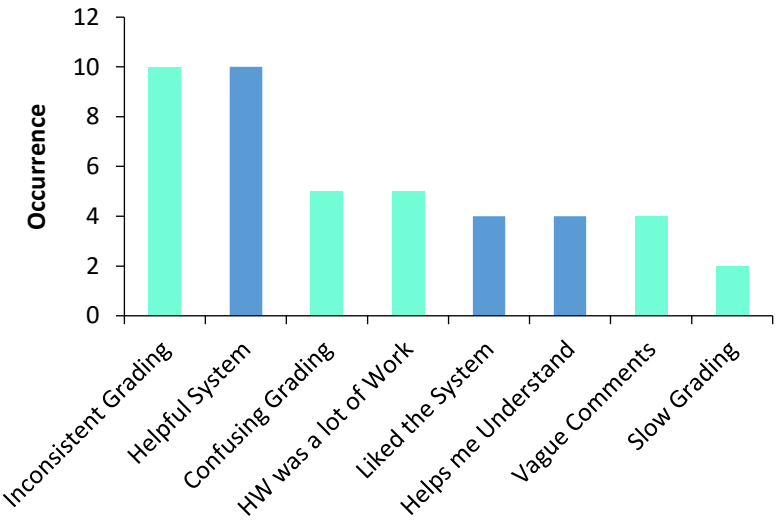

Figure 5.4. Grading was a major issue in 2018. Student written comments that mentioned homework from 2018 were coded into for content groups. Dark blue bars represent positive comments and teal bars represent negative comments. In general, multiple students commented on inconsistency, whereas very few mentioned that grading was slow (2-3 days maximum).

One student said, "[The homework system] makes me less afraid to make mistakes, so I don't mind answering questions wrong. Which is why I don't copy answers from online." And multiple students mentioned that reviewing their assignments specifically their mistakes helped them to learn, "the feedback points me in the right direction of thinking and helps a lot in my understanding of the homework," and "I think that the

two-stage homework set up is such a great idea. After the second homework is submitted, I understand the concepts so much better than I did the first time around," and more specifically, "It forces me to make corrections and review my mistakes."

Overall, these student quotes from both 2017 and 2018 highlighted the positive impact that the students felt that the system had on their ability to learn the material. It is likely that this homework system helps those who are in the middle and back of the pack more than at the forefront and that the students who more intuitively understand the material find it tedious and less helpful.

However, there was a new class of negative comments in 2018, beyond just disliking the need to explain and answer to a thought process students gave an increasing number of comments on the lack of clarity or helpfulness of the feedback. Content scoring of student homework feedback on the final course survey is shown in **Figure 5.4**. One student said, "it was a bit tedious, sometimes feedback was vague (like "conceptually correct"), but apparently, that doesn't mean it's actually correct." Other students commented on a lack of consistency, "The conceptual homework was great for feedback but grading was very inconsistent. Also, feedback was often vague or confusing," or, "homework was graded inconsistently, and feedback was confusing, sometimes misleading, and often unhelpful. Another student commented on how this was a persistent problem, "Inconsistent grading was another problem where two people would put similar or the same answer, yet one was marked wrong and the other correct; there were even times where I would have the same thing wrong as someone else yet I had

points taken off while they received full credit. The comments for the first 4 homeworks were also very unhelpful most of the time." These comments prompted us to evaluate grading consistency and style between graders in 2018, as inconsistent and indirect feedback has been previously linked with decreased student performance and increased stress levels (Ernst & Steinhauser, 2015).

One thing that was unanimous was that students were less overwhelmed by the workload in this course than others as shown in **Figure 5.5**. Based on the end of semester survey, students were overwhelmed by their cumulative coursework at a level of 8.7 and 8.5/10 for 2017 and 2018 respectively. In 2017, students were on average 4.2/10 points less overwhelmed by their work in thermodynamics. For this course in particular, no student rated their anxiety above an 8 (two students) and 17 out of 34 responded less than 5/10. These statements were further supported by the focus group. Student's discussed how the two stage system helps them to organize their time and spread their work load out. Student's also felt a confidence/grade boost from the system because the homework grades were high. However, in 2018, there was a slight loss in this gap, with students being on average 2.7/10 points less overwhelmed. There are likely a few reasons for this. Externally, in 2017, the largest source of student stress was in another biomedical engineering course that had a very heavy workload. The professor for that class changed the workload, making our class more comparable to others. Additionally, some course changes were made that may have increased student stress such as short notice 10 minute quizzes this semester, and the inconsistent grading mentioned by students. For next year, we will publish the quiz dates in the syllabus as well as develop additional interventions for grading

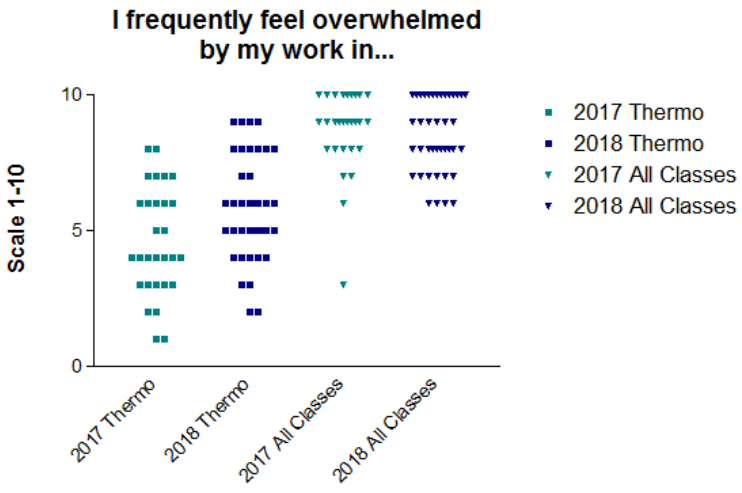

Figure 5.5. Students are more overwhelmed in 2018. Students self-reported feelings of being overwhelmed by their classwork in BME 2110 specifically and their overall course load. The mean response for our class was significantly lower than the total level of stress in students. However, from 2017 to 2018, there was an upward shift in stress levels in BME 2110 and a downward shift in stress levels in summative coursework.

.

In 2017, the focus group, which served as a more open ended way to get feedback, illuminated some key ideas about how the students perceived the two-stage homework verses its intention. It was originally stated that the first homework should have little to no math, however, almost none of the students actually treated the "conceptual" homework as conceptual. One student in the focus group said, ""I think after the first homework, we didn't take it for conceptual learning. We more thought of this as a first draft of the homework. So maybe if the directions for the first draft were different? Like instead of doing everything, don't do any math, don't solve anything. Write down bullets for what concepts it is bridging. Like actual words instead of math and stuff." What the student described as being more helpful, was the actual intention of the homework and what was described to the students both in class and in written documents. Despite continued reinforcement of this concept, it appears students struggle to adapt. Another student expanded on this, saying, "So even in the student's mind, that wasn't clear. Ashley called it a conceptual homework the first class, and then

we got our first homework, and we just thought of it as a practice round, we'll make stuff up if we don't know it, we'll put I don't know, we'll go to office hours Ashley, I promise. And then she'll check us off, and we'll be like, okay cool, and then we have a final draft. So I think it does increase understanding, but maybe not to the degree it wanted to." Further evaluating this statement, we evaluated student homework for statements such as "I don't understand what to do", or "I don't know how to solve the problem" and they were nearly entirely absent. Students at least discussed something that was related to the problems, or explained what they were confused about specifically. Despite the limited number of students participating in the focus group, the major take away was that the idea of the conceptual homework needs to be more fully described and reinforced in coming years.

There are diminishing returns on conceptual gains as the semester progresses

We evaluated the class average raw conceptual rating for each homework and saw overall retention of learning gains on the exams for at least four key concepts per exam, as shown in **Figure 5.6**. Exam 1 showed higher retention, with 95% and 91% maintenance of conceptual gains in 2017 and 2018, respectively. Exam 1 in 2017 shows even the retention of roughly one conceptual point gains, indicating overall efficacy of the system. Exam 2 showed a decrease in retention to 89% and 88%, while still generally showing a positive impact on performance. For comparison, concepts in 2018 that were quizzed but were not a prominent part of the homework showed only a 79% retention of correct answers from the quiz.

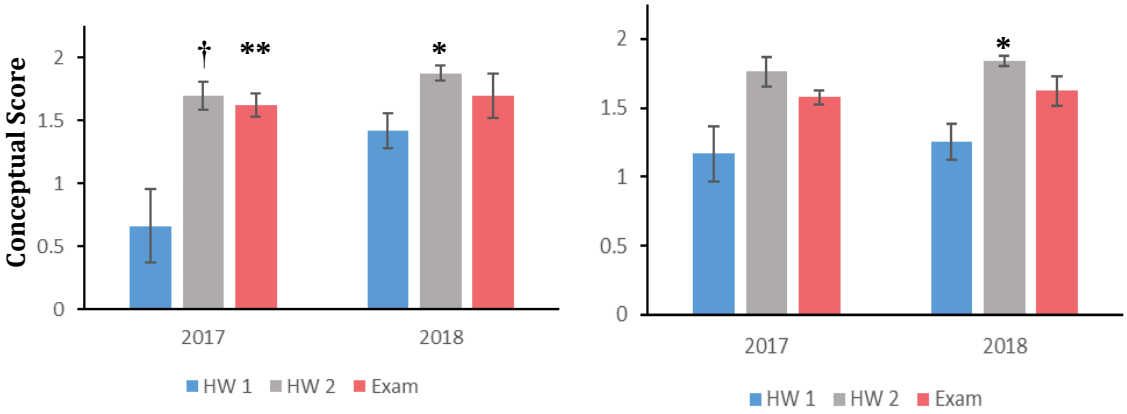

Figure 5.6. **Student retention is generally similar to HW2 on the Exam.** Effect of two-stage homework on conceptual understanding showed general improvement on the 0-2 conceptual scale. **A)** Student showed retention of gains on Exam 1 as well as significant improvements from HW1 to HW2 in 2017. **B)** Exam 2 conceptual scores showed diminishing returns on conceptual improvement from homework, but still statistically similar scores to HW 2. †, $P < 0.001$, **, $P < 0.01$, *, $P < 0.05$. All comparisons are made back to homework 1 within the same year.

To break this down and evaluate changes in individual students, we calculated differences in average conceptual score between homework submissions and the final homework and the exam. At least four concepts were averaged per student for all assignments. We called improvement a >10% positive change in average conceptual score and retention was a >10% negative change. Looking at changes in homework, all but one student in 2018 showed improvement or maintenance of conceptual understanding from Homework 1 to Homework 2, as shown in **Figure 5.7**. On the exams, we see a diminishing effect as the semester progresses with there being on average 1.5-3 fold more retained/improved scores on Exam 1 than Exam 2, for 2017 and 2018, respectively. The major losses in Exam 2 in 2018 largely came from one key concept, where we asked students to translate the idea of an average energy to an average length of a molecule. Most students were unable to do this problem, giving

them a score of 0 on the Exam compared to 2 on their homework.

With this concept removed, the distribution is similar to the 2017 Exam 2. Interestingly, students are approximately 5 times more likely to retain the conceptual gains that they made on homework than to show an improvement over the learning they already demonstrated through additional studying. This demonstrates the importance of gradual learning as opposing to last minute studying before an exam on actual student performance. With these factors in mind, we believe that the two-stage homework system had a lasting impact on students' conceptual understanding.

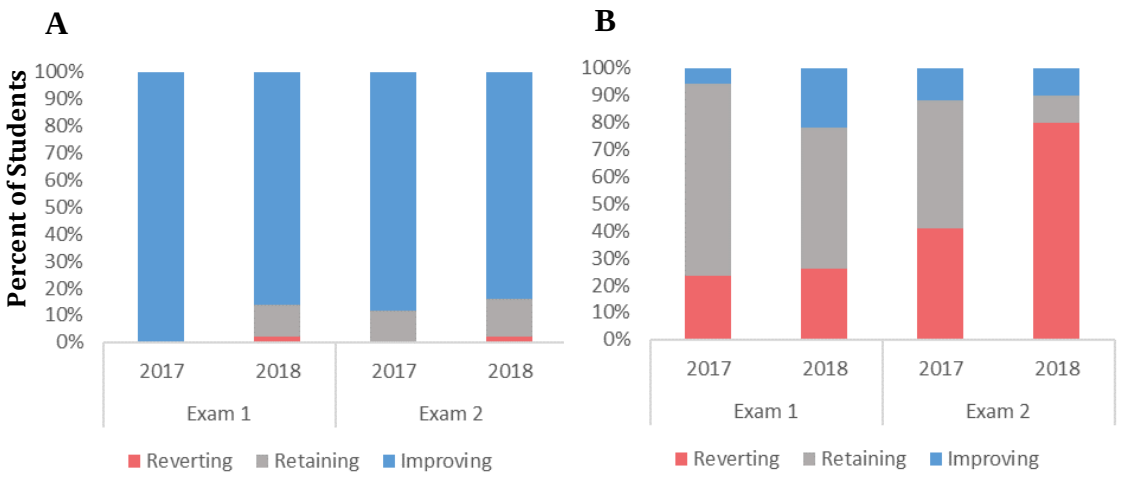

Figure 5.7. Students improve between homework submissions but do not always retain their improvement on the exam. The Two-Stage homework shows general helpfulness in **A)** increasing conceptual understanding from HW1 to HW2 on both exams. **B)** The homework shows retention of improvement of concepts tested on homework for ~80% of students for Exam 1. There is a drop in student retention in Exam 2 that is significantly worse during Exam 2018.

Written feedback improves student performance between submissions

We analyzed four types of feedback; self, task, processing and self-regulation, here ranked from lowest to highest cognitive level. In the representative set of homework problems analyzed, self- feedback by itself was given least in both 2017 and 2018, as

shown in **Figure 5.8.** The introduction of multiple graders, and more undergraduate graders, shifted the level of feedback to focus more on task feedback compared to self-regulation feedback. Three out of four undergraduate graders also only commented on questions where students were incorrect and did not take the time to re-inforce correct thinking. One important thing to discuss here is the presence of feedback even in the absence of the need to improve. In 2017, 37% of task, 18% of processing, and 30% of self-regulation feedback was given when there was no need for improvement. Previous studies have shown an important role for positive feedback on student performance, so this feedback to solidify the correct thought processes and approaches is likely integral to student success (Dion & Restrepo, 2016). The loss of reinforcement feedback on correct answers may have also lead to student frustration.

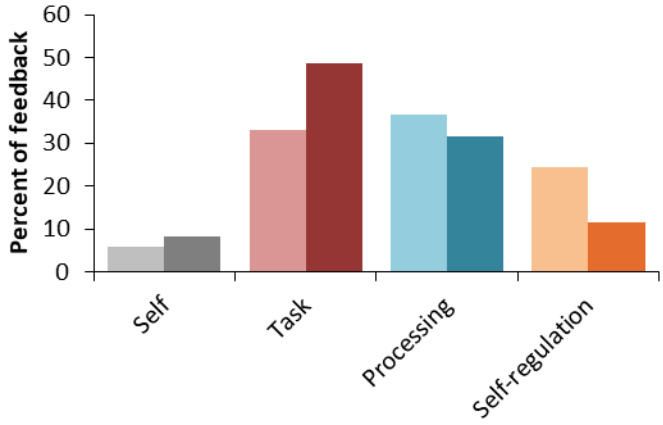

Figure 5.8. There is a decrease in self-regulation feedback with increasing undergraduate graders. Increasing the number of graders, specifically undergraduate graders, decreased the amount of Self-Regulation feedback and increased the amount of Task feedback.

To analyze the effectiveness of each type of feedback, we determined how student performance changed from Homework 1 to Homework 2 in 2017 and grouped these changes based on feedback category. Self-feedback was so rarely the only form of feedback given (two occurrences) that we cannot provide any meaningful results for this

category Task feedback improved student performance 19 out of 29 occurrences (66%) in 2017 and showed 90% improvement in 2018, however, fewer students improved to at a +2 level. This could be due to already higher performance on Homework 1 (**Figure 5.9A**). Processing feedback was similarly effective in 2018, showing roughly 80% improvement both years (**Figure 5.9B**). Self-regulation feedback, despite it being given fewer times, showed the greatest percentage of +2 improvement in 2018 (**Figure 5.9C)**. Overall improvement scores were roughly 80% again for both years. Interestingly, uncommented questions showed a ~90% improvement rate, with 50% of occurrences resulting in +2 score. This is likely due to these questions being brought up at office hours and more thoroughly address one-on-one or as a large group.

Multiple graders increases the variability of feedback

Switching to an online grading system in 2018 did not have a major effect on changes in conceptual learning. However, as mentioned above, there were more negative comments regarding grading consistency in 2018. Based on these student comments, we added additional questions into our end of semester survey, and added a grader survey to better understand how graders were approaching their task. Both graders and students found that Gradescope was a straightforward platform to work with, and graders felt that it improved their consistency as shown in **Table 5.1**. Contradicting many student opinions, graders felt that they were consistent in their grading at 8.3/10 and that they were good at give helpful comments at 7.5/10.

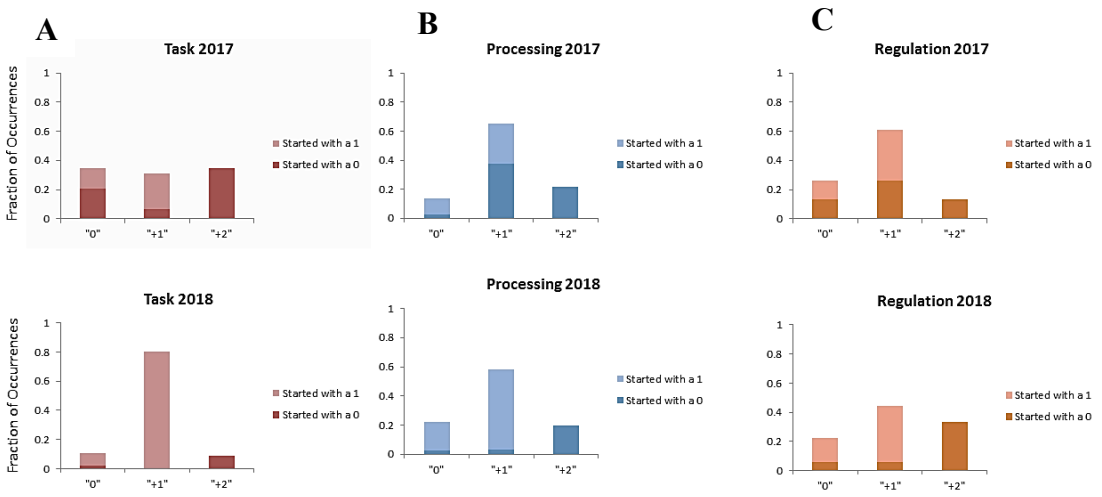

Figure 5.9. **High order feedback helps improve gains the most for worst performing students.** Effects of four feedback categories on student performance. **A)** Task feedback shows larger +1 gains in 2017 and larger +2 gains in 2017. **B)** Processing feedback also shows larger +1 gains in 2018, however equivalent +2 gains from a 0 score as 2017. **C)** Regulation feedback that was given in 2018 was highly effective for students starting with a 0 score despite being given less frequently than 2017.

Table 5.1. Grader and student responses to questions regarding homework showed overall satisfaction with the online grading system.

Response For End of Semester Survey (10 = Agree, 1 = Disagree)	***Agreement***
Grader: Gradescope is an easy platform to work with	8.2 ±1.5
Grader: Gradescope made grading faster and more efficient	8.6 ± 2.1
Student: Submitting HW on Gradescope is convenient and straight forward	7.7 ± 2.5
Student: Gradescope was useful for submitting and receiving feedback	7.2 ±2.5

To evaluate the types of comments that were given, we correlated the presence and type of feedback given by each grader. In general, almost none of the undergraduates provided as much self-regulation feedback as the graduate TAs (**Figure 5.10**). In addition, two of the undergraduates showed a high incidence of student's responses requiring correction/guidance that were left uncommented (**Figure 5.11**). Correlation for commenting on correct answer has not be done at this this time. During this analysis, it was also noted that some of the undergraduates left vague, unhelpful or confusing comments despite high commenting, such as undergraduate 2. These comments were

not clear or direct enough to determine the next step to take in correcting or solving the problem.

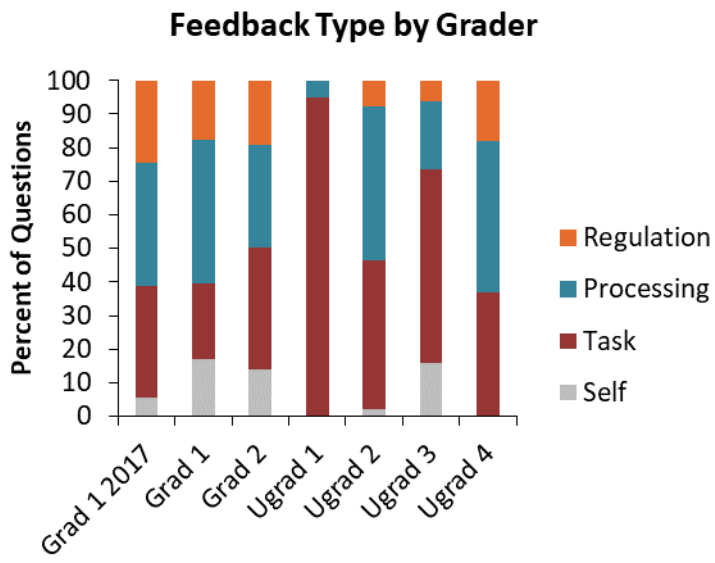

Figure 5.10. There is high variability in feedback type amongst graders. There is high person to person variability in grading styles. One undergraduate grader in particular gave almost no higher level feedback at all. This distribution in feedback sets the tone for what is important for a problem and likely exacerbated 2018 students' frustration with the inconsistency.

Discussion

Overall student response and efficacy were quite encouraging in response to the two-stage homework system as it shows general =improvement of student understanding that is maintained on the exams. However, there were some key limitations that bear discussion and some which will be the start of new interventions next year.

Student perception and limitations of the two-stage system

One major issue in comparison between the two years is the number of course changes that took place between year one and year two. Beyond this, as the course is still in development, determining how much time is needed to sufficiently cover concepts is still being determined. In 2017, there were additional hurdles in misunderstandings of students' prior knowledge, especially with regard to chemistry background as well as

some mistakes made during lecture due to unfamiliarity with the material that did not help the homework to reach its full potential. Despite improvements in this area in 2018, one major thing that needs to be further addressed for the next year of teaching is more time spent talking about how to make an assumption, or evaluate the validity of that assumption, or a ball park answer in class. These steps will be implemented next year to try and make the course self-consistent in its message.

Adding a recitation section that will implement "think alouds," a strategy in which the instructor models the thought process needed to break down a problem into component parts. Beyond this, the whole major curriculum is also in its infancy stages with communication between faculty regarding coordinating course work and exams lacking. One major element of engineering is learning foundational principles. Most of the professors know that they want to teach their students more foundational skills than simply content specific knowledge. However in a new department where classes are being rapidly developed, the communication of foundational principles is easy to lose in favor of heavier workloads and more content specific focus.

In the 2017 end of the semester survey, 21/34 students reported being very overwhelmed (9 out of 10 scale) by their coursework. This no doubt negatively contributed to their performance as pressing, or more overwhelming deadlines in certain classes will take precedence over classes deemed as less overwhelming. One student even described it this way, "It's reached the point where we are asking our other professors if we can have extensions because we can't finish our work for Class A. It feels really guilty because we shouldn't prioritize one class over another. It feels wrong to ask another professor

for an extension on things they don't control. It's not their fault. Every minute I'm not doing homework in one class; I'm doing work for Class A. So yeah this class doesn't really take up that much time." These results are corroborated by Sokrat (2013) and Godshall (2012). The department moving forward would benefit from coming up with a vision based on foundational principles that they can communicate to students in all their classes. This unified front of the need to understand problem solving, and then to be able to apply these skills in multiple specific areas, will help to focus faculty and students on the most essential and important skills. I believe that these overarching changes will help both faculty and students to be less stressed by their teaching which will lead to an improvement in learning outcomes (Atwood et.al., 2009).

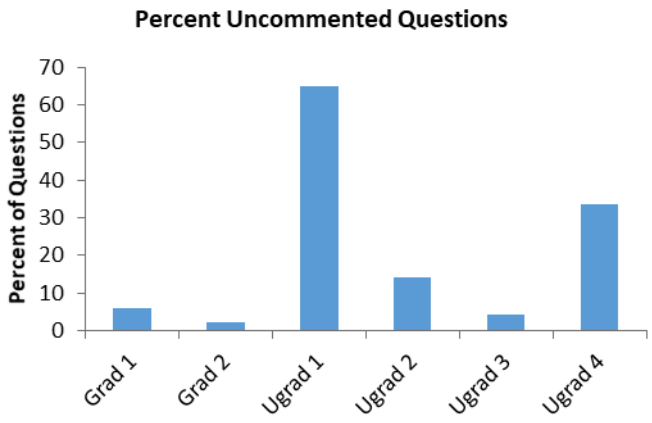

Figure 5.11. Quantification of students who did not show full conceptual understanding but did not receive a written comment directing them specifically on ow to improve their understanding showed high variability between undergraduate graders. The grader who showed almost 60% uncommented issues frequently finished his/her grader at the last minute and likely was rushing under time pressure.

Beyond this, a larger issue that was alluded to above was that of cultural change. This class was a distinct cultural change from their other classes, at a time when they are already transitioning from lower to upper level course work. Sophomore year is when material typically becomes more conceptual and simply being able to plug and chug

does not get you an A. The students are already in a cultural shock of their own as they start taking the classes that one day they will use for their jobs. This class, with the heavy conceptual focus of the homework and content, brought out a lot of that tension in the students as it forced this change into the light, and made them interact with it as part of their assignments. Like Watkins and Stevens (2013) found, the overall culture and expectation really matters. At a university like Cornell, students are generally competitive and grade focused. The homework system still seemed to have some impact, if not the intended one. As one student said, "I think it is helpful to have two drafts to any problem set. I think at this point with problem sets, people are just trying to get it done. You worry about understanding it the night before the prelim. That's the way it works here. So if you have two weeks of it, it forces you try to understand it maybe. So I do think you get more than the average understanding." Based on this feedback, I think the implementation of this thought process more tangibly into the classroom would help students to better assimilate the foundational problem solving skills that are being taught in this set-up. A major, and less discussed part, of the reasons students' liked the system may be simply due to the fact that they felt like it boosted their grade. This may have influenced their self-reporting on learning because the demand for high grades is so prominent. Other researchers also found that the high homework grade was a factor in their student's enjoyment of the intervention (Godshall, 2012; Moore and Ranalli, 2005).

Another major point of discussion, although not significant in the feedback from the two surveys was student collaboration. In 2017, many students made extensive use of

an online group chat, solutions manuals, and other supports. One student said in the focus group that, “The morning homework is due, it’s frantic with people texting each other.” Another student said, “Someone will say, “I went to office hours for ten minutes, and I got this,” so they’ll post that, and everyone else will be like “okay, great” and jumps on.” This sharing of information, while it can be good for building cohesion in the class, could also negatively affect some students understanding of the material. This is very difficult, if not impossible to control, but it is important to keep in mind with regard to what the actual purpose of the homework is. In 2018, based on our end of semester survey, there was a five-fold decrease in group chat participation. Whether or not this learning community was important for reducing stress levels will need to be evaluated in further years to determine if creating small learning community within the class will be majorly beneficial.

Limitations of Feedback Analysis

Our feedback analysis indicated that written feedback, in general, was effective in improving student performance. Furthermore, processing feedback was the most effective category of feedback compared to task and self-regulation, and self feedback occurred too rarely to include in our analysis. Indeed, this is in agreement with previous literature (Hattie & Timperley, 2007) that deeper levels of feedback that requires students to process problems are more effective in improving performance. However, we must note that the written feedback analyzed was not the only form of feedback provided to students for these homework sets. First, attending office hours was most likely a major factor in predicting student performance on Homework 2. Second, the

fact that the student had a second attempt at solving the same problem may have also played a role in the changes in scores between the two homework drafts. These two ideas correlate directly with our qualitative data from our focus group discussion with the students in 2017. Nonetheless, our analysis provides evidence that student performance improved with written feedback, and processing feedback was the most effective category of written feedback in improving scores between homework.

Limitations of Effectiveness Measures

We, as others, saw that homework is not a perfect predictor of exam performance, but similar to Bembenutty (2012), is modulated by other student specific factors such as self-efficacy, study habits, and collaboration with other students. A more in depth analysis of these factors was done in 2017 and can be found in Supplemental S5.5.

Beyond this, we have analyzed our data distinctly from other papers that have been published in evaluating homework and exam correlation. Instead of looking at exam grade versus homework grade, we concept scored both homework and exams and only evaluated the concepts that were directly linked back to specific homework problems. You could argue that this is removing the far-reaching effects that homework is supposed to have, but it also eliminates much of the noise in our data. It is possible, and noted for some students in our study, that they do very well on the concepts from homework, but show a drop off in understanding from problems that were focused on in class. We have not done any further correlation on conceptual understanding versus the overall course grade or even numerical exam grade. This may be an important factor

to look into in the future.

Implementation Limitations

Increasing course staff and transitioning to an online grading platform (https://gradescope.com/) made this homework system feasible for increasing class numbers. Although students felt that Gradescope helped them to be more consistent, student surveys and our analysis show that is not the case. For 2019, we will hold a half day grading training session to familiarize students with grading literature and teach them practically how to develop a grading rubric and grade based on conceptual understanding and not on math. Undergraduate TAs seem to be focused more on task feedback, and transitioning them to processing and self-regulation feedback will be one of the key elements of the training session. In addition, one advantage of the homework system is the ability to meet students exactly where they are regarding comments. Therefore, higher achieving students can be pushed to even deeper understanding while lower achieving students can be brought up to the standard. Having a clear rubric where the standard is clearly described, as well as pre-determined areas of growth, will assist in the consistency and accuracy of grading. Another inherent limitation is the fact that only one person scored the understanding of the students on the 0-1-2 scale. In the future, we could have multiple people scoring the homework and exams to get a more objective idea of student understanding of concepts.

Students seem to be positively affected by the two-stage homework. For the most part, students perceived that their learning was improved, and in an ideal world this would

translate to enhanced interest in the subject matter. Beyond this, looking at the performance outcomes, students almost always showed increased understanding because of feedback between the conceptual and final drafts of the homework. This, for the most part, resulted in sustained understanding on the exams. This is particularly interesting considering correcting misconceptions and long term learning. Although there were some limitations with the course, and lack of non-intervention control, we believe that the two-stage homework is worth pursuing to set the stage for a more concept focused engineering or STEM curriculum.

REFERENCES

1. Ammons, R. B. 1956. “Effects of Knowledge of Performance: A Survey and Tentative Theoretical Formulation.” *The Journal of General Psychology* 54 (2). Taylor & Francis Group : 279–99. doi:10.1080/00221309.1956.9920284.
2. Anderson, John R., Albert T. Corbett, Kenneth R. Koedinger, and Ray. Pelletier. 1995. “Cognitive Tutors: Lessons Learned.” *Journal of the Learning Sciences* 4 (2). Lawrence Erlbaum Associates, Inc. : 167–207. doi:10.1207/s15327809jls0402_2.
3. Armstrong, B. 1995. “The Imperfect Solutions Homework Format.” *IEEE Transactions on Education*.
4. Attwood, R. 2009. “Well, What Do You Know?” *Times Higher Education*.
5. Bas, G, C Senturk, and FM Cigerci. 2017. “Homework and Academic Achievement: A Meta-Analytic Review of Research.” *Issues in Educational Research*.
6. Bembenutty, H, and MC White. 2013. “Academic Performance and Satisfaction with Homework Completion among College Students.” *Learning and Individual Differences*.
7. Berrett, Dan. 2012. “How’flipping’the Classroom Can Improve the Traditional Lecture.” *The Education Digest* 78 (1). Prakken Publications, Inc.: 36.
8. Boud, David, and Nancy Falchikov. 2006. “Aligning Assessment with Long-Term Learning.” *Assessment & Evaluation in Higher Education* 31 (4). Taylor & Francis: 399–413.
9. Brown, G, J Bull, and M Pendleberry. 1997. “Assessing Student Learning in Higher Education Routledge.”
10. Brown, Marie Kendall, Chad Hershock, Cynthia J Finelli, and Chris O’Neal. 2009. “Teaching for Retention in Science, Engineering, and Math Disciplines: A Guide for Faculty.” *Occasional Paper* 25.
11. Butler, Andrew C., Jeffrey D. Karpicke, and Henry L. Roediger. 2007. “The Effect of Type and Timing of Feedback on Learning from Multiple-Choice Tests.” *Journal of Experimental Psychology: Applied* 13 (4): 273–81. doi:10.1037/1076-898X.13.4.273.
12. Cakir, Mustafa. 2008. “Constructivist Approaches to Learning in Science and Their Implications for Science Pedagogy: A Literature Review.” *International Journal of Environmental & Science Education* 3 (4): 193–206.
13. Clariana, Roy B, Daren Wagner, and Lucia C Roher Murphy. 2000. “Applying a Connectionist Description of Feedback Timing.” *Educational Technology Research and Development* 48 (3): 5–22. doi:10.1007/BF02319855.
14. Clark, R, and J Andrews. 2014. “Relationships, Variety & Synergy: The Vital Ingredients for Scholarship in Engineering Education? A Case Study.” *European Journal of Engineering Education*.
15. Covic, Tanya, and Mairwen K. Jones. 2008. “Is the Essay Resubmission Option a Formative or a Summative Assessment and Does It Matter as Long as the Grades Improve?” *Assessment & Evaluation in Higher Education* 33 (1). Routledge : 75–85. doi:10.1080/02602930601122928.

16. Dion, Jan Sedbastien, and Girardo Restrepo. 2016. “A Systematic Review of the Literature Linking Neural Correlates of Feedback Processing to Learning.” *Zeitschrift Fur Psychologie / Journal of Psychology* 224 (4): 247–56. doi:10.1027/2151-2604/a000260.
17. Dukhan, N, and M Schumack. 2013. “Understanding the Continued Poor Performance in Thermodynamics as a First Step toward an Instructional Strategy.” *ASEE Annual Conference*.
18. Epstein, Michael L, Amber D Lazarus, Tammy B Calvano, Kelly A Matthews, and others. 2002. “Immediate Feedback Assessment Technique Promotes Learning and Corrects Inaccurate First Responses.” *The Psychological Record* 52 (2). Association for Behavior Analysis International: 187.
19. Ernst, Benjamin, and Marco Steinhauser. 2015. “Effects of Invalid Feedback on Learning and Feedback-Related Brain Activity in Decision-Making.” *Brain and Cognition* 99: 78–86. doi:10.1016/j.bandc.2015.07.006.
20. Evans, D L, Gary L Gray, Stephen Krause, Jay Martin, Clark Midkiff, Branislav M Notaros, Michael Pavelich, et al. 2003. “Progress on Concept Inventory Assessment Tools.” In *Frontiers in Education, 2003. FIE 2003 33rd Annual*, 1:T4G--1.
21. Fernandez, A. 2006. “2006-67: HOMEWORK AS AN OUTCOME ASSESSMENT: RELATIONSHIPS BETWEEN HOMEWORK AND TEST PERFORMANCE.” *Age*.
22. Fleischmann, C, E Nakagawa, and T Kelley. 2016. “Redesigning the Student Learning Approach through Personality Types and Pedagogies, A Case Study in an Undergraduate Engineering Course.” *Universal Journal of Educational*. http://eric.ed.gov/?id=EJ1089682.
23. Froyd, Jeffrey E., Phillip C. Wankat, and Karl A. Smith. 2012. “Five Major Shifts in 100 Years of Engineering Education.” *Proceedings of the IEEE* 100 (SPL CONTENT): 1344–60. doi:10.1109/JPROC.2012.2190167.
24. Gladding, Gary, Brianne Gutmann, Noah Schroeder, and Timothy Stelzer. 2015. “Clinical Study of Student Learning Using Mastery Style versus Immediate Feedback Online Activities.” *Physical Review Special Topics - Physics Education Research* 11 (1): 1–8. doi:10.1103/PhysRevSTPER.11.010114.
25. Godshall, S. 2017. “Phased-Array Homework: Used to Shape and Steer Student Understanding.” *Usma.edu*. Accessed June 6. http://www.usma.edu/cfe/Literature/Godshall_11.pdf.
26. Grammer, Jennie K., Melisa Carrasco, William J. Gehring, and Frederick J. Morrison. 2014. “Age-Related Changes in Error Processing in Young Children: A School-Based Investigation.” *Developmental Cognitive Neuroscience* 9: 93–105. doi:10.1016/j.dcn.2014.02.001.
27. Hake, Richard R. 1998. “Interactive-Engagement versus Traditional Methods: A Six-Thousand-Student Survey of Mechanics Test Data for Introductory Physics Courses.” *American Journal of Physics* 66 (1). AAPT: 64–74.
28. Hattie, John, and Helen Timperley. 2007. “The Power of Feedback. [References].” *Review of Educational Research* .77 (1): 16–17. doi:10.3102/003465430298487.

29. Hestenes, David, Malcolm Wells, and Gregg Swackhamer. 1992. “Force Concept Inventory.” *The Physics Teacher* 30 (3). AAPT: 141–58.
30. Jenkins, James O. 2010. “A Multi-faceted Formative Assessment Approach: Better Recognising the Learning Needs of Students.” *Assessment & Evaluation in Higher Education* 35 (5): 565–76. doi:10.1080/02602930903243059.
31. Jonassen, D, J Strobel, CB Lee, Learning Technologies, Educational Technology Programme, Learning Sciences, and Technologies Academic Group. 2006. “Everyday Problem Solving in Engineering :” *Journal of Engineering Education* 9 (2): 139–51. doi:10.1002/j.2168-9830.2006.tb00885.x.
32. Kluger, Avraham N., and Angelo DeNisi. 1996. “The Effects of Feedback Interventions on Performance: A Historical Review, a Meta-Analysis, and a Preliminary Feedback Intervention Theory.” *Psychological Bulletin* 119 (2): 254–84. doi:10.1037/0033-2909.119.2.254.
33. Korpela, A, T Tarhasaari, and L Kettunen. 2016. “Structural Development of Substance in Engineering Education: Method of Cornerstones.” *International Conference*. http://link.springer.com/chapter/10.1007/978-3-319-50337-0_54.
34. Kulik, J. A., and C.-L. C. Kulik. 1988. “Timing of Feedback and Verbal Learning.” *Review of Educational Research* 58 (1). Sage PublicationsSage CA: Thousand Oaks, CA: 79–97. doi:10.3102/00346543058001079.
35. Lafuente Martínez, Marc, Ibis M. Álvarez Valdivia, and Ana Remesal Ortiz. 2015. “Making Learning More Visible through E-Assessment: Implications for Feedback.” *Journal of Computing in Higher Education* 27 (1): 10–27. doi:10.1007/s12528-015-9091-8.
36. Litzinger, Thomas, Lisa R Lattuca, Roger Hadgraft, and Wendy Newstetter. 2011. “Engineering Education and.” *Journal of Engineering Education* 100 (1): 123–50. doi:10.1002/j.2168-9830.2011.tb00006.x.
37. Locke, Edwin A., and Gary P. Latham. 1990. “Work Motivation and Satisfaction: Light at the End of the Tunnel.” *Psychological Science* 1 (4). SAGE PublicationsSage CA: Los Angeles, CA: 240–46. doi:10.1111/j.1467-9280.1990.tb00207.x.
38. Longfield, Judith. 2009. “Discrepant Teaching Events: Using an Inquiry Stance to Address Students’ Misconceptions.” *International Journal of Teaching and Learning in Higher Education* 21 (2): 266.
39. Mazur, Eric. 1999. “Peer Instruction: A User’s Manual.” AAPT.
40. Mazur, Eric. 2013. “Peer Instruction.”
41. McKeachie, Wilbert, and Marilla Svinicki. 2013. *McKeachie’s Teaching Tips*. Cengage Learning.
42. Moore, J, and J Ranalli. 2015. “A Mastery Learning Approach to Engineering Homework Assignments.” *122nd ASEE Annual Conference, Seattle, WA*. http://www.personal.psu.edu/jpm46/pubs/ASEE_2015a.pdf.
43. Nasr, KJ, and B Ramadan. 2005. “Implementation of Problem–Based Learning into Engineering Thermodynamics.” *Age*. https://peer.asee.org/implementation-of-problem-based-learning-into-engineering-thermodynamics.pdf.

44. Nicol, David J., and Debra Macfarlane-Dick. 2006. “Formative Assessment and Self-regulated Learning: A Model and Seven Principles of Good Feedback Practice.” *Studies in Higher Education* 31 (2): 199–218. doi:10.1080/03075070600572090.
45. Olds, B M, R A Streveler, and R L Miller. 2004. “Preliminary Results from the Development of a Concept Inventory in Thermal and Transport Science.” *Proceedings of the 2004 American Society for Engineering Education Annual Conference & Exposition*, no. 703..
46. Reardon, FH. 2001. “Developing Problem-Solving Skills in Thermodynamics Courses.” *Age*.
47. Rittle-Johnson, Bethany, and Robert S. Siegler. 2001. “Developing Conceptual Understanding and Procedural Skill in Mathematics: An Iterative Process.” *Journal of Educational Psychology* 93 (2): 346–62.
48. Rowbotham, M, and GS Schmitz. 2013. “Development and Validation of a Student Self-Efficacy Scale.” *J. Nurs. Care*.

49. Sadler, D. Royce. 1989. “Formative Assessment and the Design of Instructional Systems.” *Instructional Science* 18 (2). Kluwer Academic Publishers: 119–44. doi:10.1007/BF00117714.
50. Sadler, D. Royce. 1998. “Formative Assessment: Revisiting the Territory.” *Assessment in Education: Principles, Policy & Practice* 5 (1). Taylor & Francis Group : 77–84. doi:10.1080/0969595980050104.
51. Sailer, Uta, Simon Robinson, Florian Ph.S. Fischmeister, Ewald Moser, Ilse Kryspin-Exner, and Herbert Bauer. 2007. “Imaging the Changing Role of Feedback during Learning in Decision-Making.” *NeuroImage* 37 (4): 1474–86. doi:10.1016/j.neuroimage.2007.07.012.
52. Savion, Leah. 2009. “Clinging to Discredited Beliefs: The Larger Cognitive Story.” *Journal of the Scholarship of Teaching and Learning* 9 (1). ERIC: 81–92.
53. Sevian, Hannah, and William E Robinson. 2011. “Clickers Promote Learning in All Kinds of Classes-Small and Large, Graduate and Undergraduate, Lecture and Lab.” *Journal of College Science Teaching* 40 (3). National Science Teachers Association: 14.
54. Seymour, Elaine, and Nancy M Hewitt. 1997. “Talking about Leaving: Why Undergraduates Leave the Sciences, 1997.” *Boulder, CO: Westview*.
55. Sokrat, H, S Tamani, M Moutaabbid, and M Radid. 2014. “Difficulties of Students from the Faculty of Science with Regard to Understanding the Concepts of Chemical Thermodynamics.” *Procedia-Social and*.
56. Streveler, Ruth A., Thomas A. Litzinger, Ronald L. Miller, and Paul S. Steif. 2008. “Learning Conceptual Knowledge in the Engineering Sciences: Overview and Future Research Directions.” *Journal of Engineering Education* 97 (3): 279–94. doi:10.1002/j.2168-9830.2008.tb00979.x.

57. Streveler, Ruth A, Barbara M Olds, Ronald L Miller, and Mary A Nelson. 2003. “Using a Delphi Study to Identify the Most Difficult Concepts for Students to Master in Thermal and Transport Science.” In *Proceedings of the Annual*

Conference of the American Society for Engineering Education.
58. Taraban, R, EE Anderson, and MW Hayes. 2005. "Developing On-line Homework for Introductory Thermodynamics." *Journal of*. http://onlinelibrary.wiley.com/doi/10.1002/j.2168-9830.2005.tb00859.x/full.
59. Wankat, PC. 2001. "The Role of Homework." *Age*. https://peer.asee.org/9753.pdf.
60. Watkins, PJ, and DW Stevens. 2013. "The Goldilocks Dilemma: Homework Policy Creating a Culture Where Simply Good Is Just Not Good Enough." *The Clearing House:*. http://www.tandfonline.com/doi/abs/10.1080/00098655.2012.748642.

CHAPTER 6

A HOW TO GUIDE AND TEMPLATE FOR DESIGNING A PUZZLE BASED ESCAPE ROOM GAME[6]

Educational games are one active and effective way of engaging students with material while also providing additional motivation to tackle challenging concepts. A particularly popular game concept is the escape room, where students need to work in groups to solve a series of puzzles to prevent disaster from occurring in an imaginary universe, all within a specified amount of time. This paper presents a general guide to constructing an escape room for undergraduate classrooms. Unlike many recently published educational escape rooms, this template does not use any laboratory-based components, making it widely applicable to any class and any level, although it will be most easily adapted to classes that do include analytical components. The puzzles in the game escalate from remembering and understanding concepts to applying and evaluating techniques and data. Unlike many other games and puzzles, an escape room does not reveal the final answers until the allocated time is up, which forces students to work through challenging questions and find solutions within their group to advance in the game. The game provides students many instances for formative assessment, and encourages helpful discussions surrounding misconceptions and core course content while they escalate through the challenges.

[6] Manuscript accepted for publication at CourseSource April, 2019. AE sole author.

Introduction

Active learning techniques are proven to improve student learning outcomes[1]. Educational games have additional benefits beyond those common to active learning such as enhancing problem solving, communication, and cooperation skills[2]. Games also help to motivate students struggling to learn abstract concepts by making content more tangible and providing a fun way to interact with them. A newer game format is an escape room. Escape rooms create a scenario where players need to work together to solve a series of increasingly complex puzzles within a specified amount of time[3]. The number of publications on escape rooms at both the high school and university levels have dramatically increased in recent years and have shown that this game format successfully promotes understanding of key learning outcomes and positive student experiences[4,5,6,7].

However, designing a valuable educational game takes extensive time and planning[8] and few resources exist to help with the fundamental layout of an educational escape room. Most of the published escape room articles apply to physics or chemistry and involve primarily experimental challenges. Many courses, however, do not have laboratory components, or have extensive material to teach beyond a lab setting. This template is based on question sets and clues where one solution leads students to find the next challenge. Although the question format in this template is most easily translated to a course that involves some mathematical or graphical analysis (genetics, ecology, etc.), the template is adaptable to any class or material.

Purpose of the escape room challenge

I implemented this game in a sophomore level Biomolecular Thermodynamics class that comes at a hinge point between general science requirements and higher level coursework. I noticed that many of my students struggled to begin solving a problem that they did not immediately understand. During class or office hours, students would get as far as they could before guessing or waiting for the solution to be revealed. Having an openly revealed answer allowed students to avoid thoughtfully engaging in problem solving. When I was selecting a game format, I wanted to push my students to find the final answer as a team, even when they were not sure how to start, or if they got stuck in the middle. I wanted to teach them valuable skills in problem solving, increase their confidence and to help them self-correct their misconceptions. I used the escape room exactly described here as an out-of-class review session. The game could also be used as an in-class review broken over multiple days or modified to include mini lectures to adapt to a problem based learning environment.

Game set up and logistics

Escape rooms are typically based on a mystery or problem that must be solved in a time sensitive manner. My escape room was based on a 'zombie apocalypse'. The students were charged with finding the antidote to the zombie virus before it spreads beyond the city borders and destroyed human life as we know it. To do this, they needed to complete four Challenge Rounds to find and determine which antidotes can cure the virus. These Challenge Rounds escalate trough Bloom's Taxonomy, a framework for categorizing educational goals from less cognitively demanding (remembering and understanding)

to more demanding (applying, evaluating, and creating)[9].

The template described here is for a 2-2.5 hour escape room with 10 groups of five students. All of the questions as part of the template in the Supporting Files relate to chemical, phase, and mixture equilibrium from a unit in Biomolecular Thermodynamics. Some of the questions provided may be directly applicable in a chemistry, biochemistry, physical chemistry, or molecular biology course but primarily will serve as a template for question ideas. Before beginning to design your own game content, you need to first determine a few key game parameters: time limit, group size, and area of play. Each of these items will be important for determining how large your question banks need to be, how many distinct sets of clues you will need, how many rounds of challenges you will need to create, and how many/what type of hiding spots you will be able to use for solutions.

Time Limit

How much time you want to spend playing the game will determine how many questions you should make per Challenge Round. The earlier Challenge Rounds focus on the lower levels of Bloom's taxonomy (remember, understand) and the later challenges focus on the higher levels (apply, analyze, and evaluate). If you need to decrease the amount of time, it is best that you shorten individual rounds so that students are presented with questions of varying difficulty.

Group Size

You should aim to have no more than five students per group to enhance student collaboration, but fewer is likely better for more cohesive group dynamics. I randomly assigned groups so students would meet and work with new people to get exposed to new ways of approaching problems. Another reason for random groups was to increase the problems that normal study groups in the class saw so that they could compare notes while preparing for the exam. Because multiple teams are completing similar tasks in the same physical space (e.g., a classroom), each group needs to receive their own distinct set of questions per Challenge Round. You should create a question bank for each round that you can draw from to create a distinct set of questions for each group. A recommended number of questions for each Challenge Round will be discussed in detail later.

Area of Game Play

Once you have selected your overall room or building area, make a list of places you could hide your clues such as stairs, windows, tables, chairs, rooms, etc. If you are in a single room, you could have players tell you a code to get their next clue without having them find it or set up a matrix of envelopes where a solution will indicate which envelope provides the next set of questions (here used for Challenge Round 2 with a template provided in Supporting File S6.4: Escape Room Design – Challenge Round 2: Color Barcode Envelope Map.ppt). The answers for Challenge Round 1 assume a whole building area and would need to be modified if you had a smaller area.

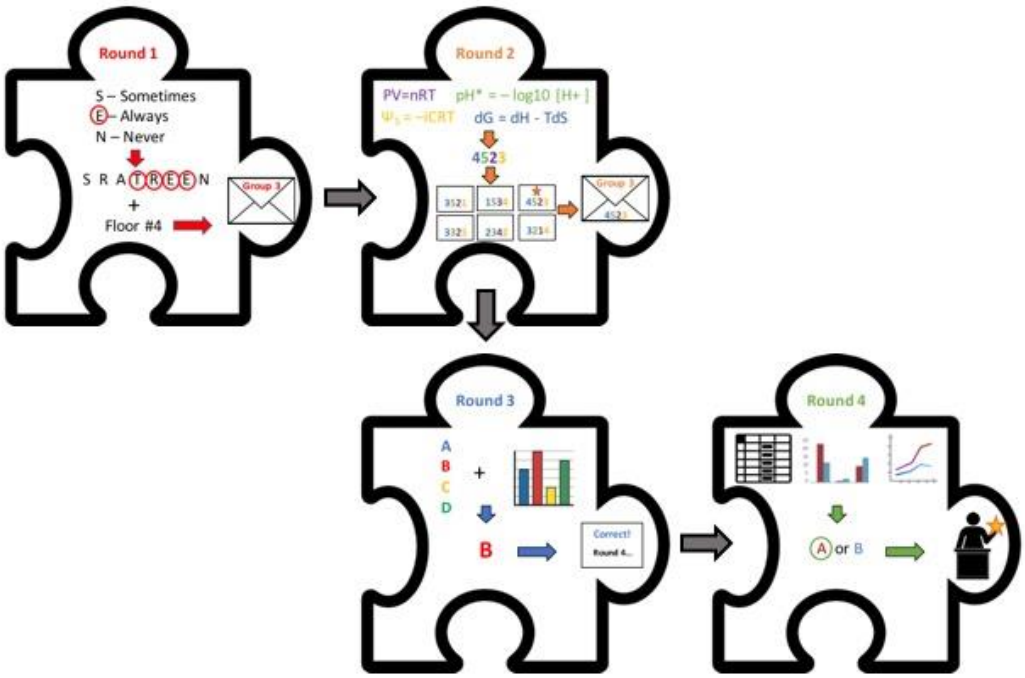

Figure 6.1. Escape Room overview and puzzle flow. This escape room follows a linear design where each Challenge Round provides vital information for the next. The solution to each Challenge Round will provide a clue or cypher that indiates where the next set of questions can be found. When students have solved all four rounds, they present their solutions to the instructor to save the day.

Game design and play

Once you have determined the length and space for your game, you can dive into creating content! For clarity, an overview of game play is shown in Figure 6.1. The solution to each Challenge Round will provide students with the information leading them to the hidden location of question(s) for the next round. To begin the game, you should divide students into groups and then explain the virtual game universe (zombie apocalypse), their challenge (find an antidote), how they will get there (solving the challenges), and how much time they have to finish (time limit). Once you have explained the game, you will provide each group the description of the game universe and the final answer template (Supporting File S6.1: Escape Room Design – Description

of Universe and Final Answer Sheet.docx) as well as the two parts that make up Challenge Round 1 (Supporting File S6.2: Escape Room Design – Challenge Round 1: ASN and Find the Floor.docx) and start the timer!

Challenge Round 1: Always, Sometimes, Never (ASN) and Find the Floor

Challenge Round 1 is the only round designed with two parts:

1. Always, Sometimes, Never (ASN)– Remember and Understand
    a. Students are given eight statements and must determine and explain if the statement is always, sometimes, or never true
        i. The correct answers spell out the location/item (stairs, chair, etc.) where the next clue is hidden on/near.
2. Find the Floor – Apply
    a. Students are given a math based problem.
        i. The correct answer is a positive integer that indicates which floor the next clue is hidden on.

ASN Questions

The ASN questions, originally developed by Swan and Ridgway[10], enhance a traditional true/false question by including an intermediate "sometimes" option. The ASN questions are often most effective when they address common mistakes or key misconceptions. The American Association for the Advancement of Science has published a list of misconceptions in life science, physical science, earth science and the nature of science that may be helpful in generating question ideas[11].

An example ASN question is:

Mutations are changes in the DNA sequence that affect phenotype.

A - Always

L - Sometimes

E - Never

Answer: Sometimes, because there are multiple DNA base pair sequences that encode the same amino acid. It is possible that a change in the base pairs, or a mutation, would result in the same amino acid sequence, and therefore a fully functional protein that would not illicit a phenotype. These mutations are called silent mutations.

For use in the game, each answer is associated with a letter, similar to a multiple-choice question. When the letters corresponding to the correct answers from each question are written out in order, they spell out a location hint for the next set of questions. To make sure students cannot simply guess the correct answers, multiple words should be embedded in the answer options such that a wrong set of answers could still produce a non-applicable word (such as oven). In my experience, most groups initially arrive at incorrect answers, but since their answers lead to a non-sense or unhelpful word they go back and recheck their answers. The template provided (Supporting File S6.2: Escape Room Design – Challenge Round 1: ASN and Find the Floor.docx) has the question layout for eight questions for 10 teams with location clues such as bench, chair, etc. You should create a question bank ~2-3 times larger than the number of groups participating

in the Escape Room so that you can mix and match questions to create a unique set of eight questions per group. For instance, for 10 teams my question bank consisted of 26 questions. If you are planning a shorter game, you should use fewer questions per team.

Find the Floor

The second half of Challenge Round 1 will tell groups more information about where to find their next set of questions. Students are given a math question with an integer answer that matches the floor the location clue (chair, bench, plant, etc) is on. Based on the math question you are having them solve, you may need to be clever and have them select the digit in the 10's or 1's place if you want to use floors, or you could design the problem to provide a specific room number, etc. You only need the number of questions as you have floors or rooms accessible to you. For instance, I made four questions because my building had four floors to hide clues on. Having their location and floor clue, students can search for their hidden envelope containing Challenge Round 2 questions. To ensure the teams know they found the right envelope, each envelope should be labeled with the correct team number.

Challenge Round 2: Color Coded Matching

Inside their hidden envelope students will find three items: 1) a map/matrix for envelopes set up on the board in the main classroom for the game (Supporting File S6.4: Escape Room Design – Challenge Round 2: Color Barcode Envelope Map.ppt), 2) a color-coded equation sheet (Supporting File S6.5: Escape Room Design – Challenge Round 2: Color Coded Equation Sheet.pdf), and 3) the second set of challenge questions

(Supporting File S6.3: Escape Room Design – Challenge Round 2: Color Coded Equation Questions.docx).

1. Color Coded Matching – Analyze
    a. Students are given eight problems/questions and an equation sheet that is color coded to equation type (i.e., general, chemical reactions, phase changes, etc.) and are asked to determine which equations are needed to solve each problem.
        i. The correct answers will produce a list of equations used from each equation color category. Listing in order the total number of red, green, blue etc. equations used for the solution creates a number bar code that indicates the correct envelope for their team on the envelope map.

The question sheets should indicate how many total equations/relationships were needed to solve the problem. An example would be:

You have a reaction with a ΔG^o = 5.8 kJ/mol at 298 K.

a. Is this reaction favorable or unfavorable?

b. What is the K_{eq} for this reaction.

c. You want to couple the reaction with ATP hydrolysis, for which ΔG^o = –30.5 kJ/mol. What is the new equilibrium constant for the reaction when it is coupled with ATP assuming that ATP, ADP and Pi have a concentration of 5 mM, 6 mM, and 2 mM respectively. [2 equations needed]

Again, you will need a question bank ~2-3 times larger than the number of groups to create different question sets and barcodes per group. Once the students determine how many of each colored equation/principle they need to solve the problem, the envelope map instructs them to alphabetize the colors, and then write the number of equations of each color type in order. For instance, the students may have used yellow equations six times, blue equations two times, pink equations four times, and green equations one time. The bar code generated would be "2146", corresponding to blue – green - pink - yellow. The students then find this barcode on the map to determine which envelope on the board belongs to them. To prevent the students from guessing as envelopes are removed from the matrix, extra envelopes are placed included as decoys. When a group selects an envelope, they'll know they are correct if their group number is written on the back. If a group picked a decoy envelope, or another group's envelope, they would need to return the envelope to the board, check their answers, and try to determine where they made a mistake to fix their barcode. Groups can continue to attempt a solution until they find the correct envelope.

Challenge Round 3: Rank the Options

Inside the correct envelope, students will find a single piece of paper with their third challenge question (Supporting File S6.6: Escape Room Design – Challenge Round 3: Rank the Options Question.docx).

1. Rank the Options - Evaluate
    a. Given a set of four possible antidotes (or reagents, temperatures, etc.) and their properties, students need to determine which ones will be effective based on scientific concepts covered in class.
        i. The correct answer leads to a specific container which holds the last clue

For this challenge, you will need approximately as many "antidotes" or conditions as groups to allow for enough variation between groups. I provided each group two antidotes that would be effective, and two antidotes that would be ineffective. To ensure students go through the calculations and digest the results, I asked for the second most effective option as the final answer. An example questions would be:

Rank from best to worst, which of the four chemicals listed below would be able to remove the zombie plasmid from the water at 37˚C based on the enthalpy and entropy of mixing the plasmid with water (a model for blood) and mixing the plasmid with your chemical.

Chemical	**$h_W - h_C$**	**$s_W - s_C$**	**$\mu_w - \mu_c$**
B	-340	-5	
D	-50	75	
G	100	25	
F	250	-15	

When designing your own "antidotes" and rankings, make sure you have only a few correct answers (I had 3/10 correct antidotes) and some answers that are incorrect for all the groups as further described in the supporting files (Supporting File S6.6: Escape

Room Design – Challenge Round 3: Rank the Options Question.docx). Each second best chemical letter corresponds to a labeled bowl or container with the chemical letter label facing a wall so that student cannot see the options ahead of time. Once students find an answer, they can go to the containers and see if the answer they found has a corresponding container. If they do not find the chemical letter, they know they have to re-asses their work. If they picked one of the incorrect answer bins, they would find a piece of paper telling them their answers was wrong and they needed to try again. Selection of the correct bin would provide them with the question for the final challenge.

Challenge Round 4: Find the Antidote

The final challenge question asked students to determine which of two antidotes would cure the zombie virus based on experimental, numerical, or graphical data provided to them. This question lends itself well to identification of laboratory techniques, interpretation of data or designing a sequence of experiments to solve a problem. I had students determine which of two enzymes would work better based on given reaction rates (Supporting File S6.7: Escape Room Design – Challenge Round 4: Find the Antidote.docx). They were provided data for each set and had to perform calculations based on two different types of approaches to compute chemical rate constants, i.e., Arrhenius and Transition State Theory. I placed this last challenge at the 'evaluate' level of Bloom's Taxonomy, but asking for an experimental procedure would put it at the 'create' level.

Once students have determined the answer to the final puzzle, they inform the instructor

of their proposed solution and turn in their final answer sheets (Supporting File S6.1: Escape Room Design – Description of Universe and Final Answer Sheet.docx), along with their ASN explanations. If they are correct, they have completed the Zombie Apocalypse Rescue Mission, saved the day, and successfully escaped certain death! If they did not obtain the correct answer and there is still time remaining, the instructor can provide them with feedback and give them another chance.

Scientific Teaching Themes

Active Learning

This activity puts students in groups and has them collaboratively engage in problem solving. It also provides a memorable and somewhat emotional experience around which to organize information and shifts in understanding. Previous studies have shown that emotional triggers improve memory[12]. To further enhance the learning objectives, students should be asked to reflect on their teamwork, which content mistakes surprised them, and which of their strategies to solve the problems did or did not work[13]. To reduce stress of the game and enhance the quality of the reflection, this should be done once the team has finished the challenge or time is up.

Assessment

The escape room primarily functions as a means of self-assessment for the students because they receive informal feedback on their success after each round. Instructors also obtain informal feedback on student understanding based on how quickly the students move through the challenges and how many times they arrive at incorrect

answers before succeeding.

Inclusive Teaching

As this activity is based on group work, it helps to foster a learning community within each group and promotes the exchange of ideas and collaboration. Using randomized groups also helps students to hear perspectives that they may not usually hear.

Implementation Tips

If you are using this activity outside of class, you could offer extra credit or small gift cards for campus venues or coffee to boost participation. We provided a small amount of extra credit points for the team that finished first (5 pts), second (4 points), third (3 points), and every team that completed the challenge (2 pts). In our case, we initially set a time limit of three hours, but all teams finished within 2.5 hours, and the fastest group completed the task in 2 hours.

I found that groups wanted to check their answers before going to find their hidden clues in Challenge Round 1. I allowed this because it gave me the opportunity to provide them with feedback. However, limited availability of instructors can cause stress in a time sensitive game. For 8 groups, two instructors is the minimum to keep up with questions. If you do not want to allow answer checking, the game has enough built-in checks that the students should be able to receive feedback from the game directly. Make sure to tell the students that the game will give them feedback based on group number labeling so they know that they don't need you to confirm their answers.

A major potential issue is non-inclusive groups. This can lead to confusion for students who are struggling with the material. Keeping groups small, preferably 5 or fewer students, should help to encourage participation. If this is still an issue, you may need to implement checkpoints where a randomly selected student per group needs to explain one question from the previous round. If the student is unable to explain the question, you could assign a 15 minute penalty to their time.

From the instructor point of view, the most important thing to do is to make sure your answer keys are correct and that you have an accurate layout of all the clues. Creating a full layout of materials and locations before beginning is imperative. For each instructor present for the game, you should make a copy of the solutions so that all instructors are able to help answer questions or re-direct students who made minor mistakes. A full list of supplies and when to provide them are given in Supporting File S6.1 (Escape Room Design – Description of Universe and Final Answer Sheet.docx). Sample answer keys and timing tips are found throughout the supporting files for each Challenge Round.

Instructor and Student Reaction

Students were excited to try the escape room. Discussion started immediately and remained focused throughout. Students engaged deeply in conversation with each other when they realized their answers were incorrect, and they used both logic as well as information from the class to arrive at a solution. Challenge Round 1 and 2 (ASN Questions and Color Coded Equations) was especially effective at promoting theoretical

conversation between group members.

Students felt encouraged by the game. One student commented that the game was reassuring, “having to focus on completing the task helped me not to overthink problems and I realized I know the material better than I thought I did!” Another student commented on her engagement level, “Usually I end up checking out at review sessions, but this was really helpful because we covered so much material and I stayed focused the whole time.” Many students commented on how much fun it was to play, and how it helped them to study without getting stressed about the exam but rather to keep trying to get the right answer instead of giving up.

REFERENCES

1. Freeman S, Eddy SL, Mcdonough M, Smith MK, Okoroafor N, Jordt H, Wenderoth MP. 2014. Active learning increases student performance in science, engineering, and mathematics. Proceedings of the National Academy of Sciences 111:8410–8415.
2. Kumar R, Lightner R. 2007. Games as an Interactive Classroom Technique: Perceptions of Corporate Trainers, College Instructors and Students . International Journal of Teaching and Learning in Higher Education 19:53–63.
3. Weimker M, Elumir E, Clare A. Escape Room Games: "Can you transform an unpleasant situation into a pleasant one?". *In* Game Based Learning - English Dialog Orientation & playful learning analog and digital (translated from German). essay.
4. Dietrich N. 2018. Escape Classroom: The Leblanc Process—An Educational “Escape Game.” Journal of Chemical Education 95:996–999.
5. Vörös AIV, Sárközi Z. 2017. Physics escape room as an educational tool. AIP Conference Proceedings 1916.
6. Eukel HN, Frenzel JE, Dan Cernusca. 2017. Educational Gaming for Pharmacy Students - Design and Evaluation of a Diabetes Themed Escape Room . American Journal of Pharmaceutical Education.
7. Glavas A, Stascik A. 2017. Enhancing positive attitude towards mathematics through introducing Escape Room games. MATHEMATICS EDUCATION AS A SCIENCE AND A PROFESSION 281–293.
8. Kapp K. 2017. Games, Gamification, and the Quest for Learner Engagement. Main. Association for Talent Development.
9. Crowe A, Dirks C, Wenderoth MP. 2008. Biology in Bloom: Implementing Blooms Taxonomy to Enhance Student Learning in Biology. CBE—Life Sciences Education 7:368–381.
10. Swan M, Ridgway J. CL-1: Field-tested Learning Assessment Guide (FLAG): CATs: Mathematical Thinking. The Role of Principals in Successful Schools.
11. AAAS Science Assessment. AAAS Science Assessment ~ Ideas ~ When substances interact to form new substances, the atoms that make up the molecules of the original substances rearrange into new molecules. American Association for the Advancement of Science.

12. Nielson KA, Yee D, Erickson KI. 2005. Memory enhancement by a semantically unrelated emotional arousal source induced after learning. Neurobiology of Learning and Memory 84:49–56.
13. Fink D. 2003. A Self-Directed Guide to Designing Courses for Significant Learning.

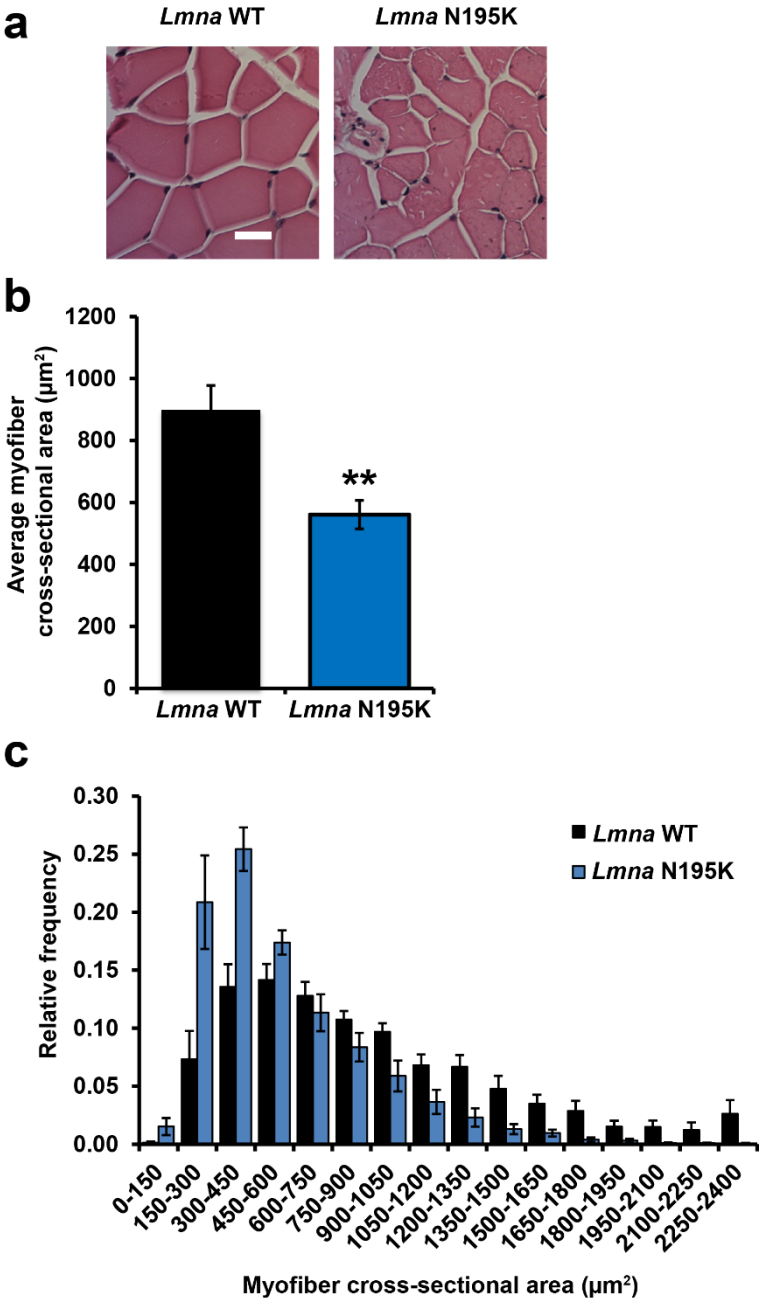

Supplemental Figure S2.1. ***Lmna*** **N195K mice develop muscular dystrophy**. (**a**) Representative H & E images of skeletal muscle from *Lmna* WT and *Lmna* N195K animal. Scale bar: 20 µm. (**b**) Quantification of the average myofiber cross-sectional area of *Lmna* WT and *Lmna* N195K mice. (**c**) Relative frequency of myofiber cross-sectional area in *Lmna* WT and *Lmna* N195K mice. *n* = 11-12 animals per genotype.

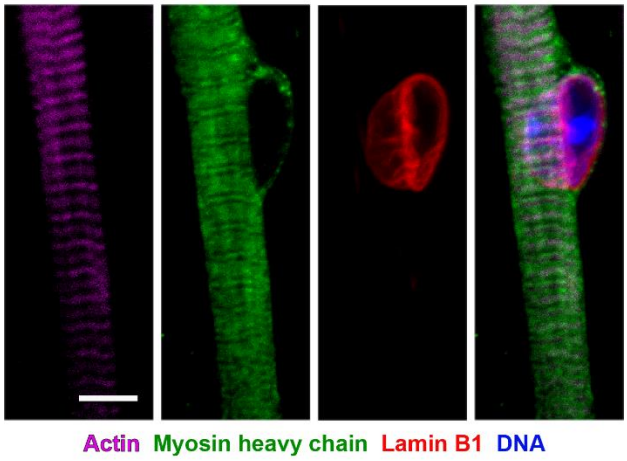

Supplemental Figure S2.2. ***In vitro*** **differentiation results in mature myofibers**. Representative image of a striated myofiber containing a peripheral nucleus at day 10 of differentiation. Scale bar: 5 µm.

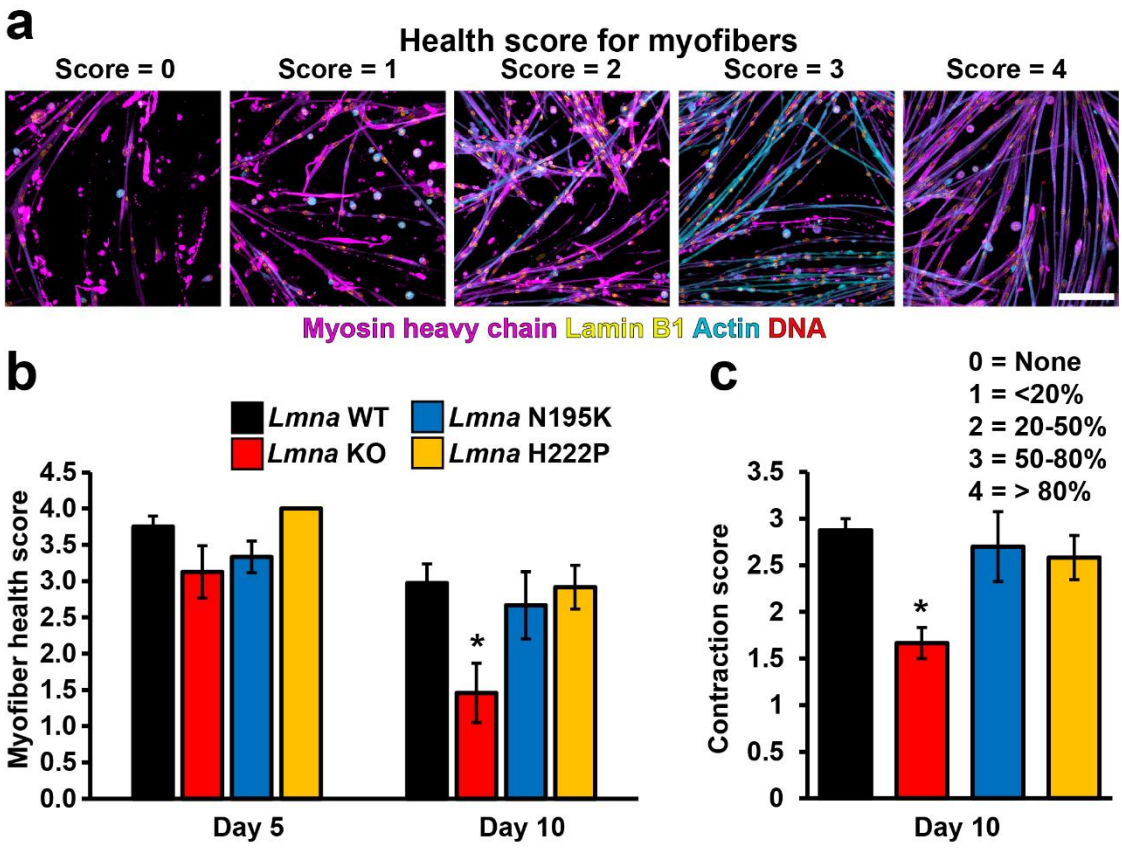

Supplemental Figure S2.3. Myofiber health scores. (**a**) Panel of representative images for different myofiber health scores used for quantification of myofiber health. Scale bar: 50 µm. (**b**) Quantification of myofiber health at days 5 and 10 of differentiation. Fibers were assigned health scores from 0 (worst) to 4 (best) based on their visual appearance; n = 3-5 independent cell lines for each genotype. *, $p < 0.05$ vs. *Lmna* WT. (**c**) Quantification of myofiber contraction at day 10 of differentiation. Fibers were assigned contraction scores from 0 (worst) to 4 (best) based on the percentage of cells that were visually contracting. *, $p < 0.05$ vs. *Lmna* WT; n = 3-5 independent cell lines for each genotype.

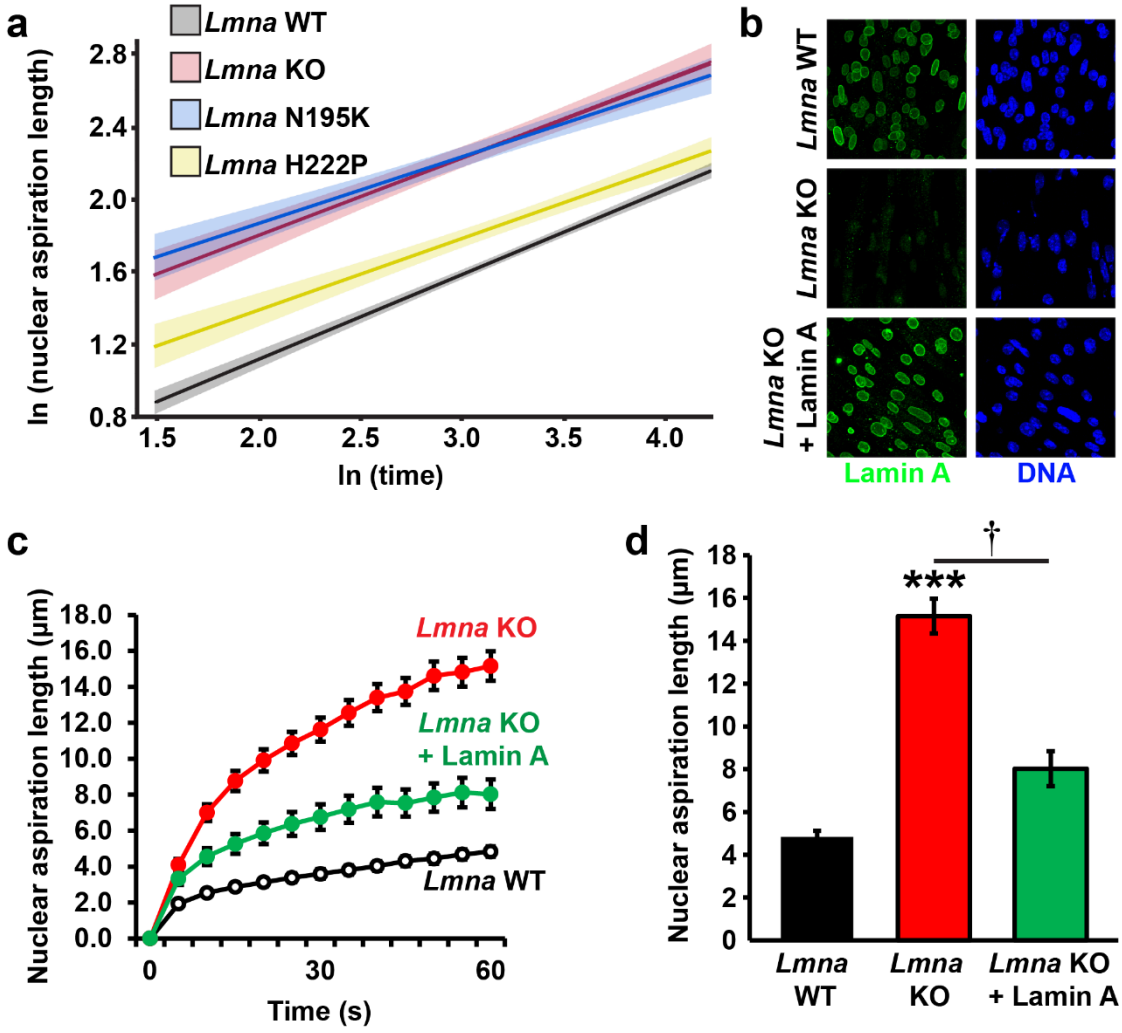

Supplemental Figure S2.4. **Micropipette aspiration analysis of *Lmna* mutant myoblasts and *Lmna* KO myoblasts ectopically expressing lamin A**. (**a**) Natural log transformation and plot of the micropipette aspiration data shown in Fig. 2b. The log-log data fits a linear regression model, in which all three *Lmna* mutants were significantly different ($p < 0.001$) from the wild-type controls. The slopes of the log-log data were not significantly different between the samples. A multilevel model including day-to-day variability confirmed that all three *Lmna* mutants were significantly different from the wild-type controls ($p < 0.0001$ for *Lmna* KO and *Lmna* N195K; $p < 0.001$ for *Lmna* H222P), although the statistical significance for the *Lmna* H222P myoblasts was lost when including additional variance components. (**b**) Representative immunofluorescence images of lamin A expression in *Lmna* WT, *Lmna* KO and *Lmna* KO cells ectopically expressing lamin A (*Lmna* KO + lamin A). (**c**) Measurement for nuclear deformation at 5 second intervals for *Lmna* WT, *Lmna* KO, and *Lmna* KO + Lamin A myoblasts during 60 seconds of aspiration. (**d**) Quantification of the nuclear deformation after 60 seconds of aspiration, showing that ectopic expression of lamin A significantly improves nuclear stiffness in *Lmna* KO myoblasts. $n = 41$-67 nuclei per genotype from 3 independent experiments. $n = 62$-73 nuclei per genotype from 3 independent experiments. ***, $p < 0.001$ *vs* *Lmna* WT cells. †, $p < 0.01$ *vs*. *Lmna* KO cells.

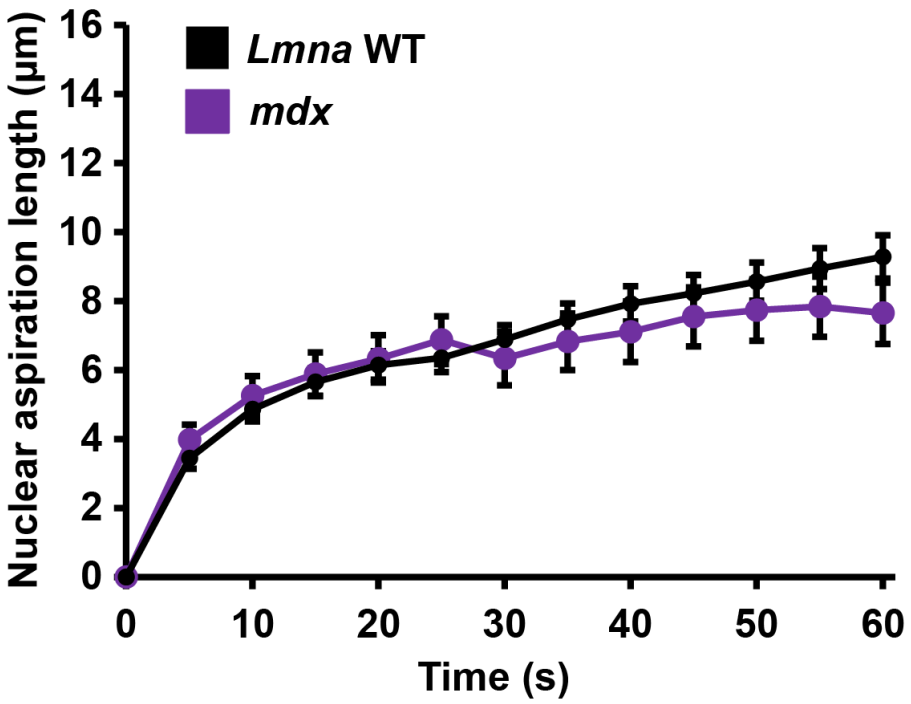

Supplemental Figure S2.5. *Mdx* myoblasts have normal nuclear stiffness. Measurement for nuclear deformation at 5 second intervals for *Lmna* WT and *mdx* myoblasts during 60 seconds of aspiration. *n* = 35-67 cells per condition.

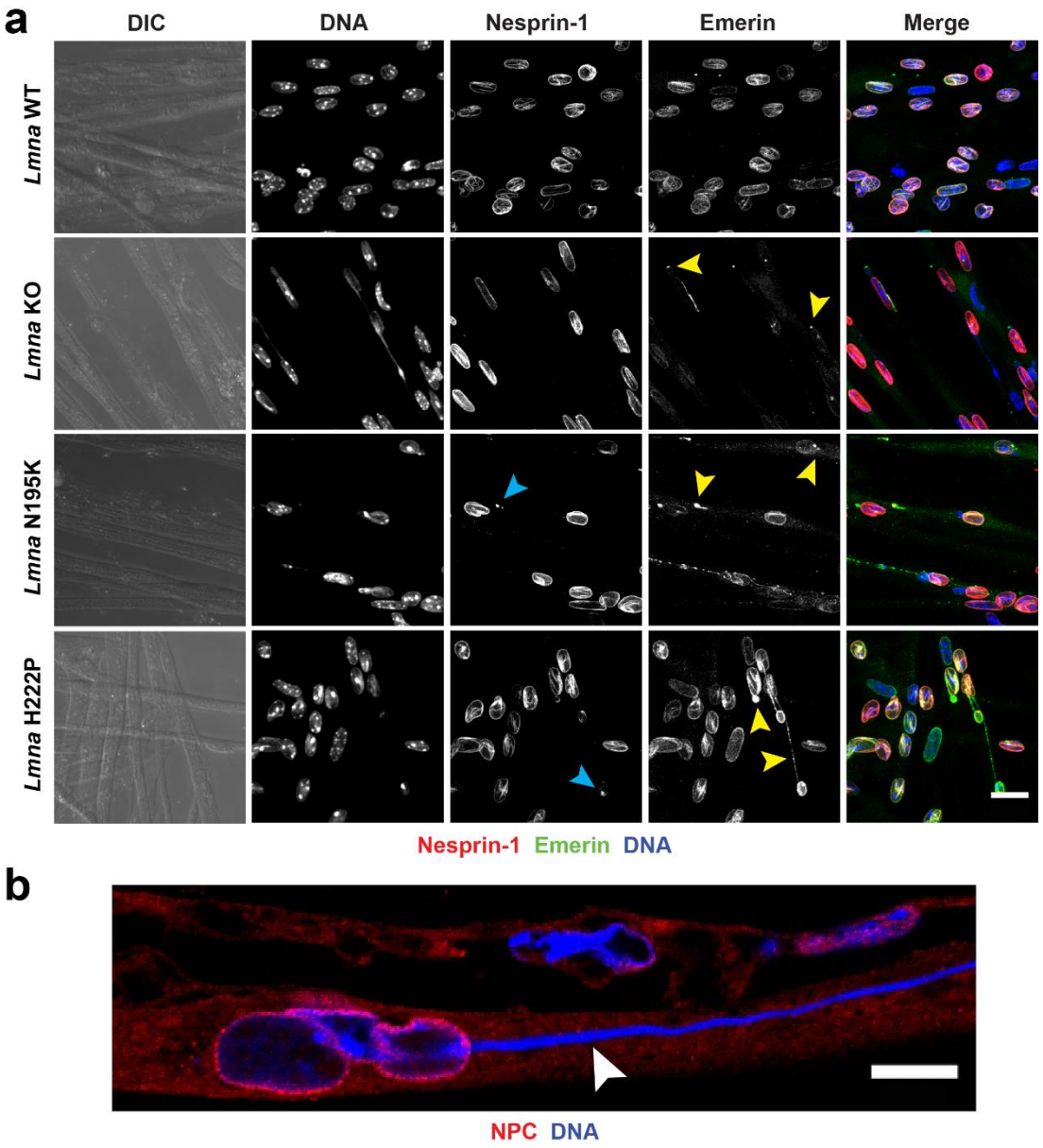

Supplemental Figure S2.6. Chromatin protrusions are surrounded by nuclear membranes containing emerin, with disturbed localization of nesprin-1 and nuclear pores. (**a**) Representative immunofluorescence images for nesprin-1 and emerin in *Lmna* WT, *Lmna* KO, *Lmna* N195K and *Lmna* H222P myofibers at day 5 of differentiation. Blue and yellow arrows denote chromatin protrusions that are enriched with nesprin-1 and emerin, respectively. Scale bar: 20 µm. (**b**) Representative image of immunofluorescence detection of nuclear pore complexes (NPC) in *Lmna* KO myofibers at day 10 of differentiation. Scale bar: 10 µm.

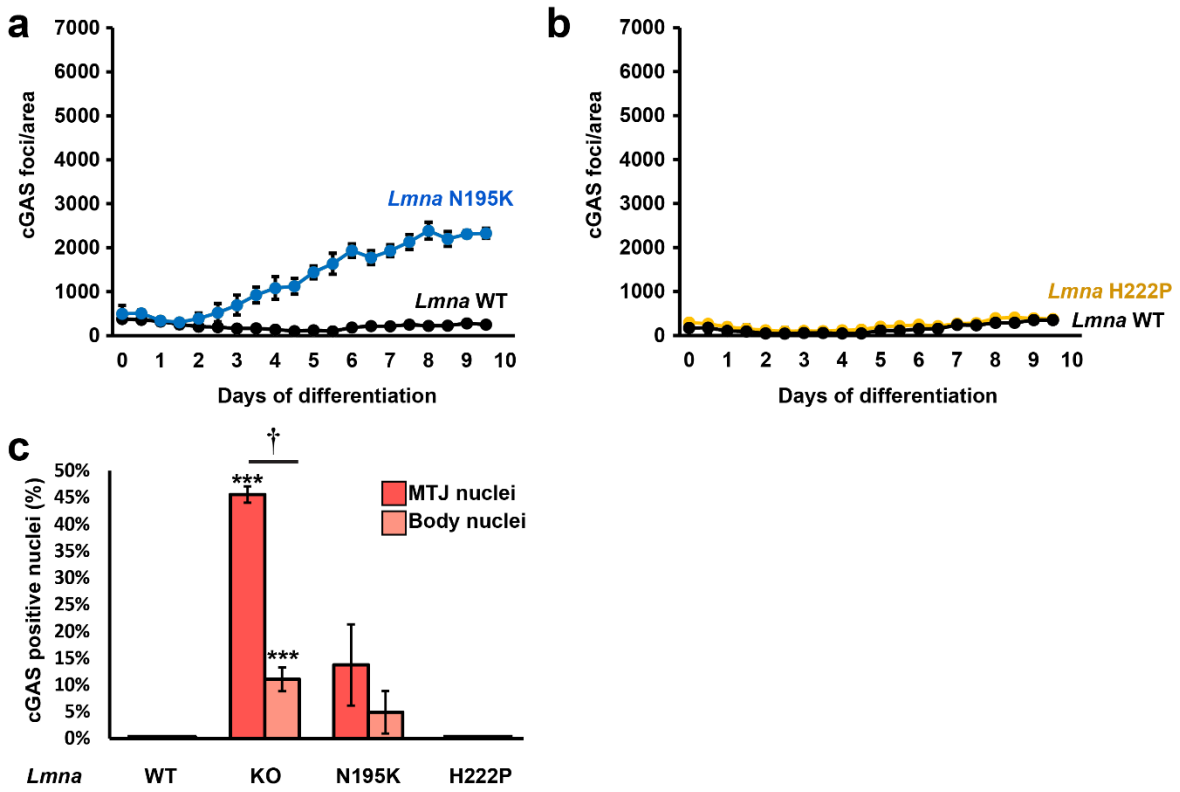

Supplemental Figure S2.7. Nuclear envelope rupture is increased in *Lmna* N195K myofibers *in vitro* and *in vivo*. Quantification of cGAS-mCherry nuclear envelope rupture reporter foci formation during 10 myofiber differentiation in *Lmna* N195K (**a**), *Lmna* H222P (**b**), and *Lmna* WT cells. (**c**) Quantification of the percentage of myonuclei positive for cGAS-tdTomato foci in isolated muscle fibers from *Lmna* WT, *Lmna* KO, *Lmna* N195K and *Lmna* H222P mice expressing the cGAS-tdTomato transgene (cGAS+) or non-expressing littermates (cGAS–). Analysis performed for whole fiber (left) and by classification of nuclei located at the MTJ or within the body of the fiber (right). Data for *Lmna* WT and *Lmna* KO reproduced from Fig. 4E for comparison. n = 5-8 mice per genotype, with 2-5 fibers per animal. ***, $p < 0.001$ *vs*. *Lmna* WT; *, $p < 0.05$ *vs*. *Lmna* WT; †, $p < 0.01$ *vs*. nuclei in the muscle body.

Supplemental Figure S2.8. Nuclear envelope rupture in *Lmna* KO muscle fibers is increased at myotendinous junctions. Representative image of a single isolated muscle fiber demonstrating the enrichment of cGAS+ nuclei at the myotendinous junctions. Scale bar: 200 μm.

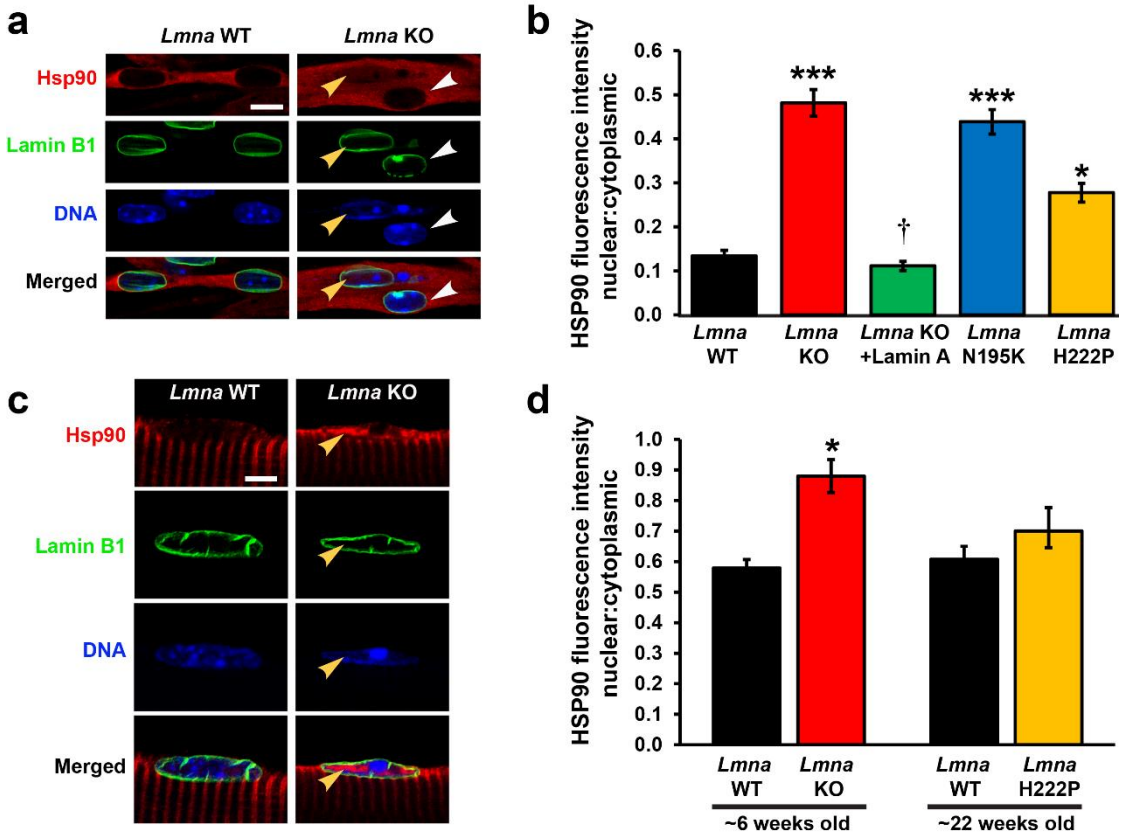

Supplemental Figure S2.9. *Lmna* mutant myonuclei have increased presence of Hsp90 *in vitro* and *in vivo*. (**a**) Representative image of nuclear localization of a large cytosolic protein, Hsp90, inside *Lmna* KO nuclei in myofiber differentiated for 10 days. White arrow indicates a nucleus with no observable chromatin defect and little Hsp90 nuclear accumulation, while the yellow arrow marks a nucleus with a chromatin protrusion and increased nuclear Hsp90 accumulation. Scale bar: 10 µm. (**b**) Quantification of the fluorescence intensity of nuclear Hsp90 levels for *Lmna* WT, *Lmna* KO, *Lmna* KO + Lamin A, *Lmna* N195K and *Lmna* H222P myofibers *in vitro*. For each nucleus, the nuclear fluorescence intensity was normalized to the cytosolic intensity immediately adjacent to each nucleus. n = 25-56 nuclei per genotype from 3 independent experiments. ***, $p < 0.001$ *vs*. *Lmna* WT ($p < 0.001$). (**c**) Representative image of Hsp90 nuclear localization in myonuclei from *Lmna* WT and *Lmna* KO mice. Scale bar: 10 µm. (**d**) Quantification of the fluorescence intensity of nuclear HSP90 levels for *Lmna* WT, *Lmna* KO, and *Lmna* H222P isolated single fibers. For each nucleus, the nuclear fluorescence intensity was normalized to the cytosolic intensity immediately beside each nucleus n = 25-56 nuclei per genotype from 3 independent experiments. ***, $p < 0.001$ *vs*. *Lmna* WT.

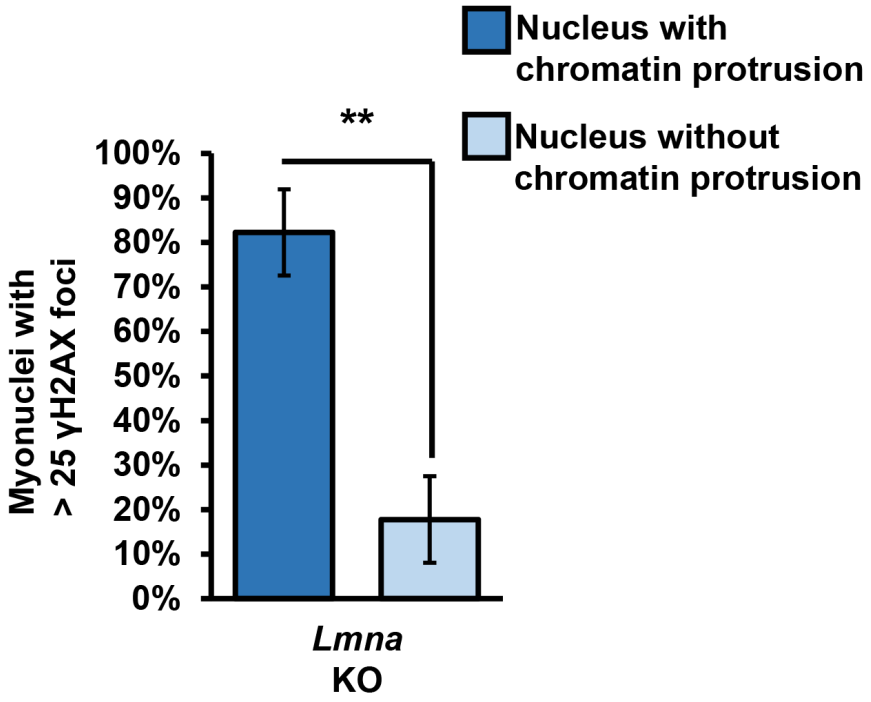

Supplemental Figure S2.10. The *Lmna* KO myonuclei with the highest amount of γH2AX foci frequently display chromatin protrusions. Analysis of DNA damage, assessed by γH2AX staining, in *Lmna* KO nuclei, comparing nuclei with chromatin protrusions to those without protrusions. Chromatin protrusions were assessed based on the presence of chromatin extending beyond the nuclear envelope, marked by lamin B-staining. n = 3 animals per genotype. **, $p < 0.01$ *vs*. no protrusion.

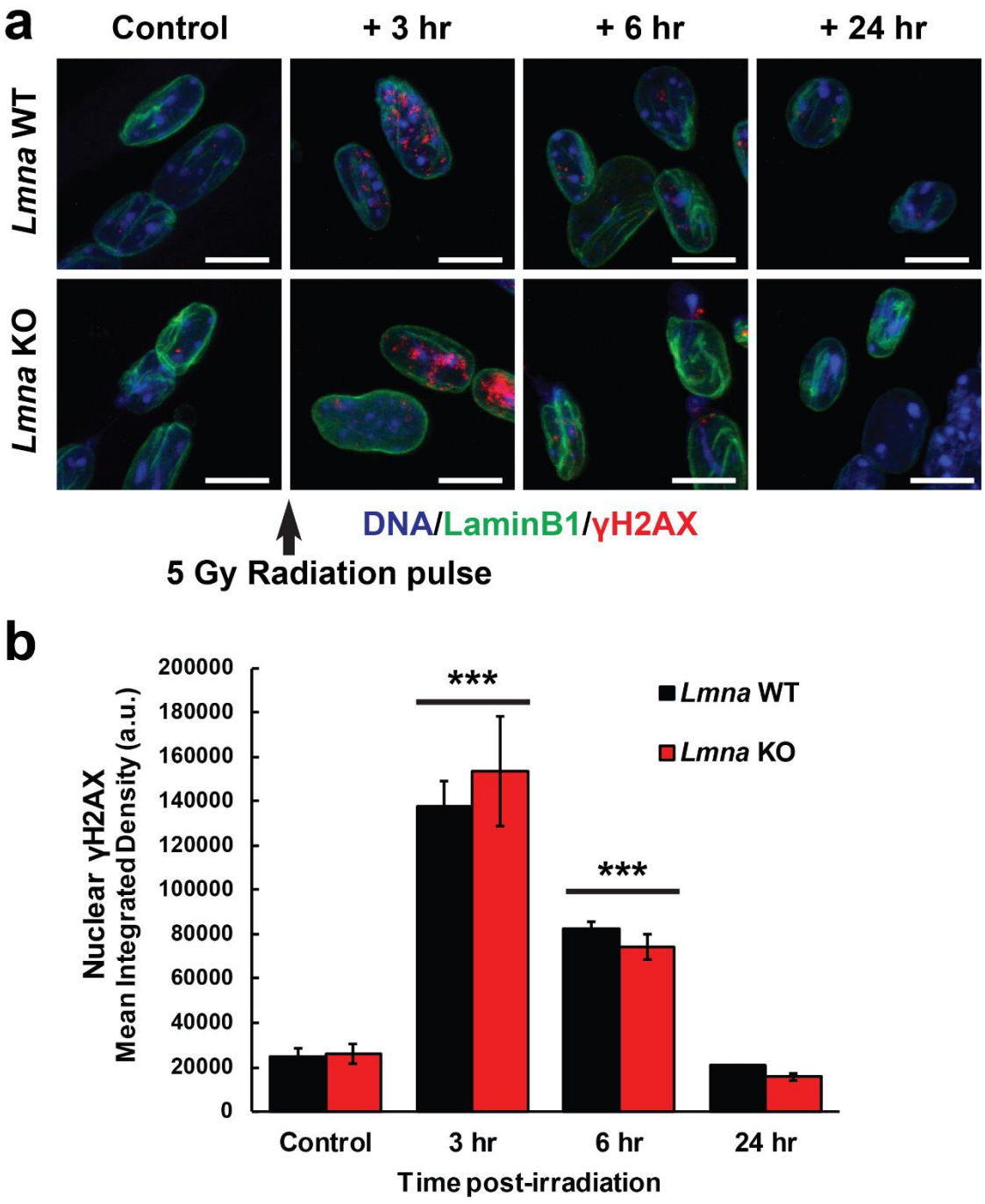

Supplemental Figure S2.11. *Lmna* KO myotubes have no defects in DNA damage repair. (**a**) Representative images of γH2AX foci in *Lmna* WT and *Lmna* KO myotubes at 3, 6 and 24 hours following a 5 Gy dose with radiation or no irradiation control. (**b**) Quantification of γH2AX after 3, 6 and 24 hours post-irradiation or no irradiation control. $n = 3$ independent cell lines. ***, $p < 0.01$ *vs*. control.

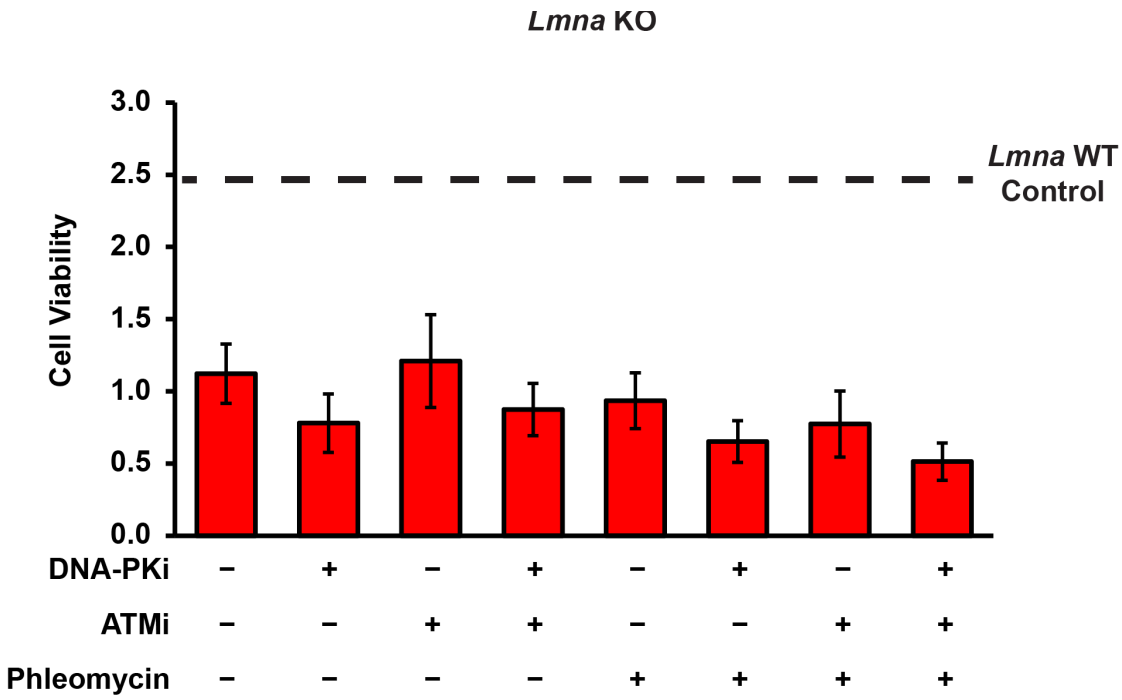

Supplemental Figure S2.12. Inducing DNA damage or inhibiting DNA repair does not promote additional cells death in Lmna KO myofibers. Quantification of cellular viability in Lmna KO myofibers using MTT assay following DNA damage induction with phleomycin, with and without concurrent treatment with DNA-PKi (NU7441) and/or ATMi (KU55933). n = 3 independent experiments per condition.

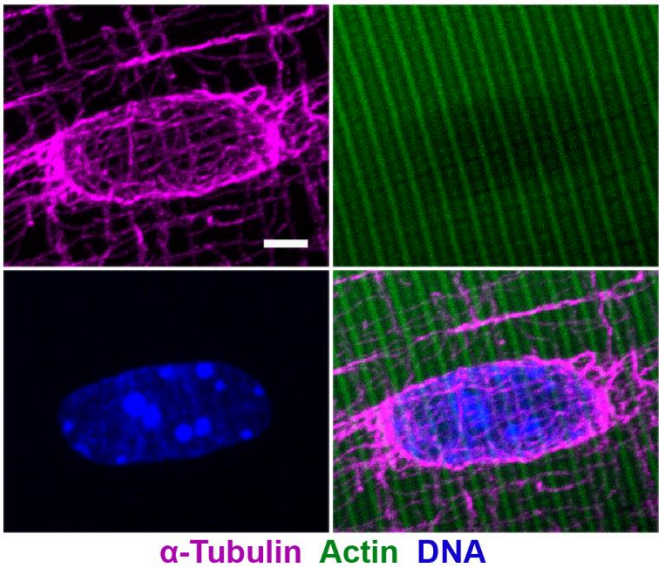

Supplemental Figure S2.13. Microtubules form cage-like structures around myonuclei. Representative immunofluorescence image of an isolated *Lmna* WT muscle fiber stained for tubulin (magenta), F-actin (green), and DNA (blue), showing characteristic 'microtubule cage' around myonucleus. Scale bar: 5 µm.

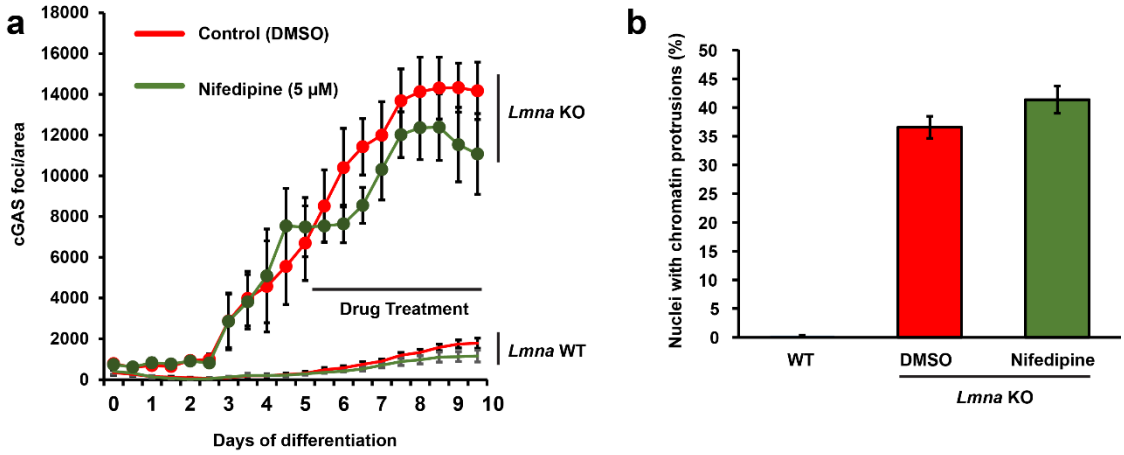

Supplemental Figure S2.14. Inhibiting myofiber contractility does not prevent nuclear envelope rupture in *Lmna* KO myofibers. (**a**) Quantification of cGAS-mCherry foci formation during 10 day myofiber differentiation follow treatment with nifedipine (5 µM), which inhibits contractility, or DMSO vehicle control, starting at day 5 of differentiation. $N = 3$ independent experiments. (**b**) Quantification of chromatin protrusions at day 7 of differentiation following treatment with nifedipine (5 µM) or DMSO, starting at day 4. Data generated from $n = 3$ independent experiments in which 27-53 nuclei were analyzed per genotype.

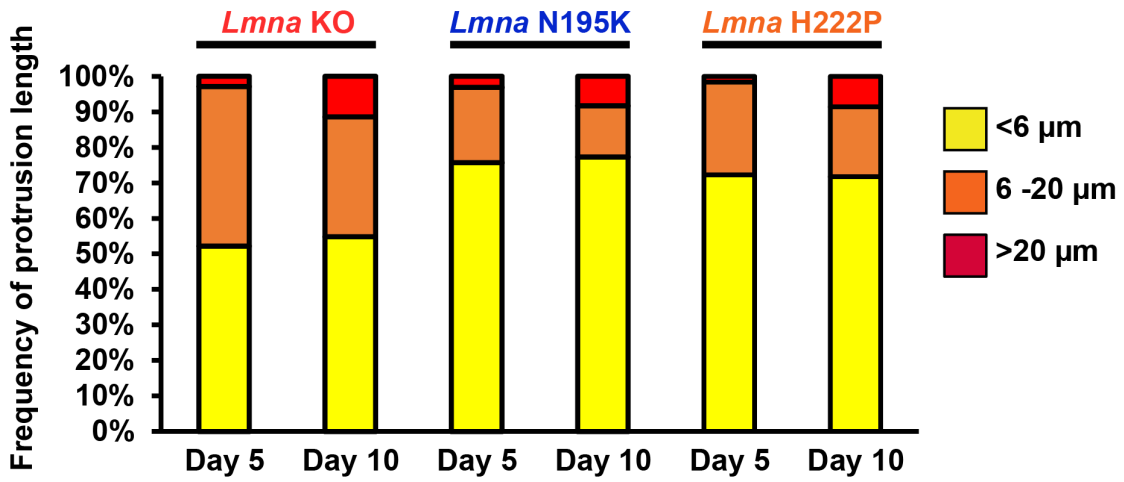

Supplemental Figure S2.15. Fraction of nuclei with severe chromatin protrusions increased over time in *Lmna* mutant myofibers. Quantification of the relative distribution of chromatin protrusion lengths in *Lmna* KO, *Lmna* N195K and *Lmna* H222P muscle cells at day 5 and day 10 of *in vitro* differentiation.

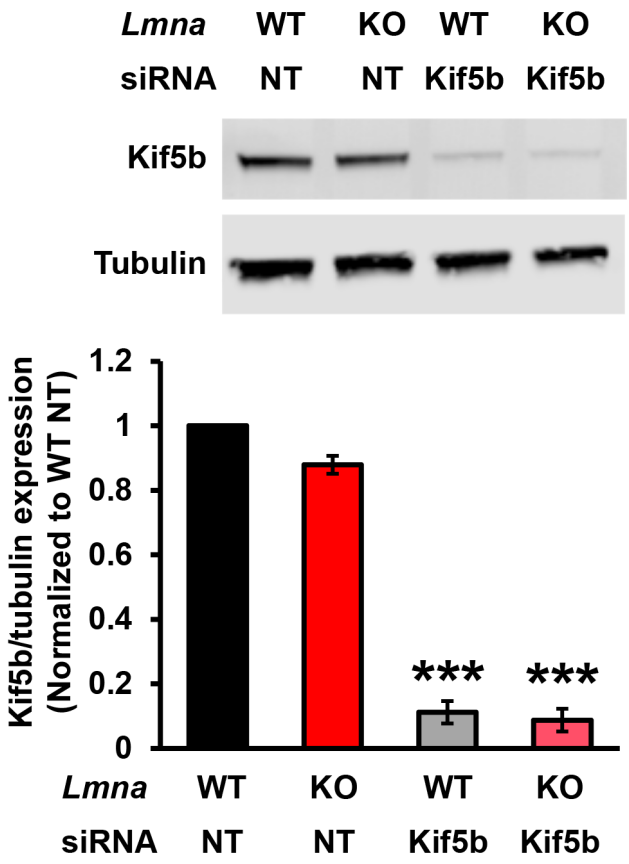

Supplemental Figure S2.16. Quantification of Kif5b depletion in myotubes following siRNA treatment. (**Top**) Western blot for Kif5b in myoblasts treated with a non-target control siRNA (siRNA NT) or siRNA against Kif5b. n = 3 independent experiments. (**Bottom**) Corresponding quantification. ***, $p < 0.001$ *vs*. respective genotype siRNA NT control.

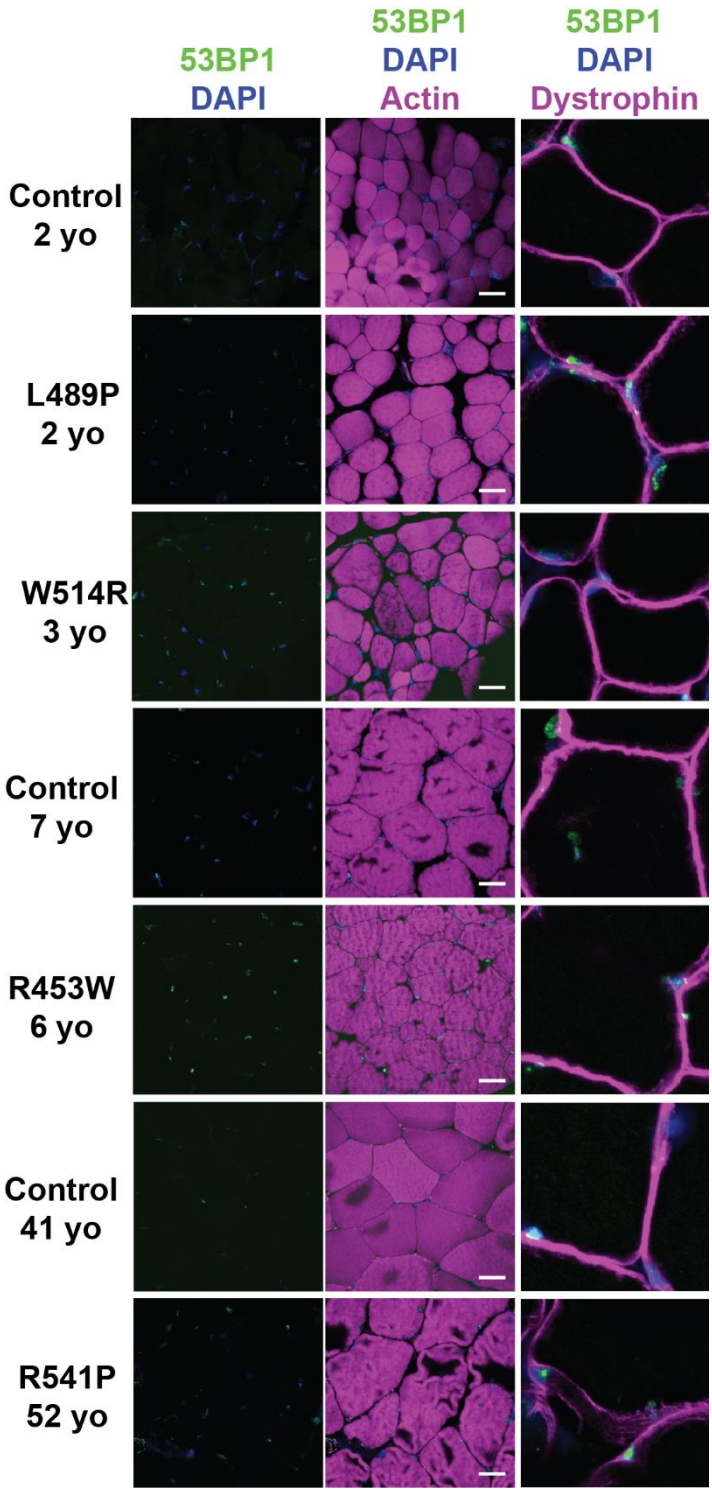

Supplemental Figure S2.17. Representative images of cryopreserved human muscle biopsy tissue from individuals with *LMNA* muscular dystrophy and age-matched controls stained with antibodies to (**a**) 53BP1, DAPI, and phalloidin or (**b**) 53BP1, DAPI, dystrophin.

Antibody	Cat#	Vendor	Dilution
MyHC	A4.1025	DSHB	1:100
MyHC	MAB4470-SP	Novus Biologicals	1:500
Lamin B (M-20)	sc-6217	Santa Cruz	1:200
Lamin B1 (B-10)	sc-374015	Santa Cruz	1:200
Lamin A (H-102)	sc-20680	Santa Cruz	1:200
Lamin A/C (E1)	sc-376248	Santa Cruz	1:200
Gamma-H2AX (Ser139)	80312	Cell Signaling	1:200
Gamma-H2AX (Ser139)	9718	Cell Signaling	1:200
HSP90 α/β (F-8)	sc-13119	Santa Cruz	1:200
Nesprin1-E	MANNES1E	Glen Morris	1:500
Nesprin-1-A	MANNES1A	Glen Morris	1:500
alpha-tubulin	T9026	Sigma	1:500(IF) 1:5000(WB)
NPC (414)	Ab50008	Abcam	1:500
Emerin	NCL-EMERIN	Leica	1:200
DNA-PKcs (S2056)	ab18192	Abcam	1:1000
DNA-PKcs	sc-390849	Santa Cruz	1:750
Cleaved Caspase-3	9661	Cell Signaling	1:500
53BP1	NB100-304	Novus Biologicals	1:1000
Dystrophin	Mab7A10	University of Iowa Hospitals and Clinics Pathology Core	1:20

Supplemental Table S2.1. Antibodies and corresponding dilutions. Primary antibodies for immunofluorescence staining and western blotting.

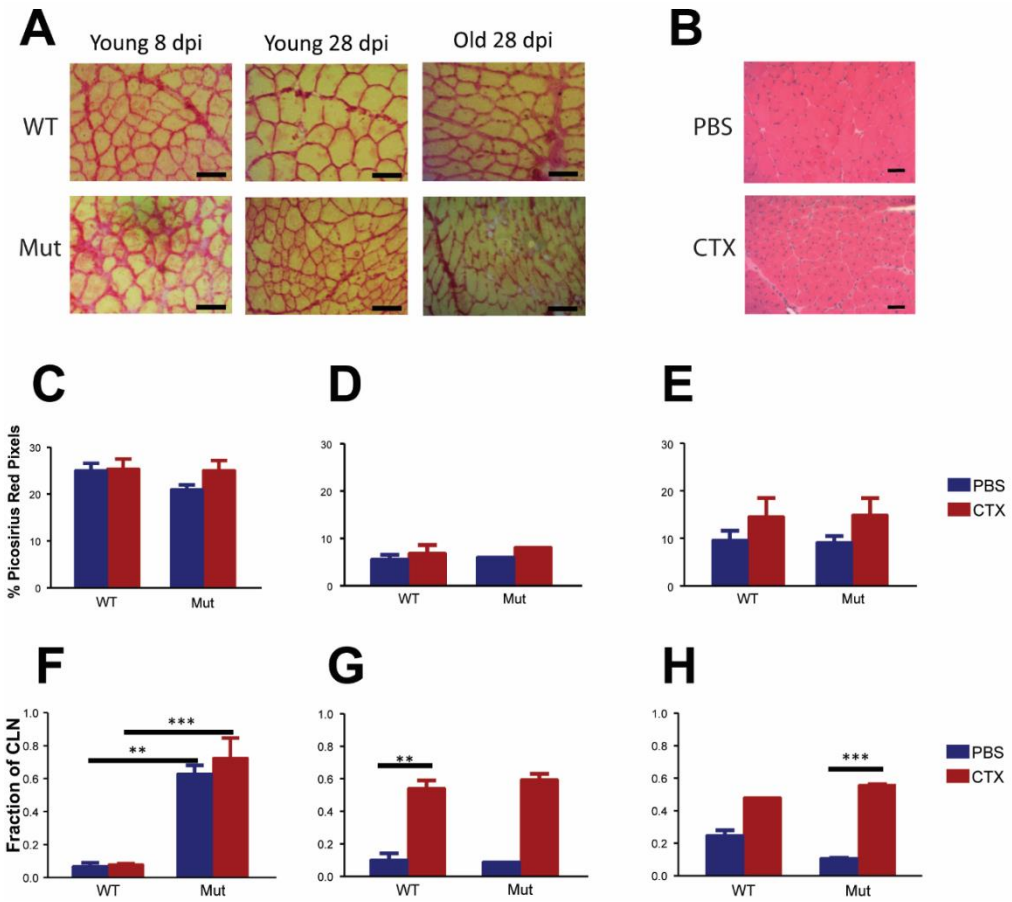

Figure S3.1. Regeneration in *Lmna* H222P mice is similar to WT in morphological metrics. There are no major defects in fibrosis or cenrally located nuclei in the *Lmna* H222P mouse model. **A)** Representative images of Pico Sirius red staining for collagen deposition. Scale bar 20μm. **B)** Representative images of H&E staining of centrally located nuclei 5 days after injection. Scale bar 20μm. **C-E)** There are no differnces in the amount of fibrosis at C, eight dpi in young animals, D, 28 dpi in young animals, and E, 28 dpi in old animals. **F-G)** There are limited changes in centrally located nuclei between WT and *Lmna* H222P mice. **F)** Eight days post injection in young animals showed a shockingly low amount of CLN in the WT animals. This data set should be expanded and checked. G, 28 dpi young animals and H, 28 dpi old animals show no major differences.

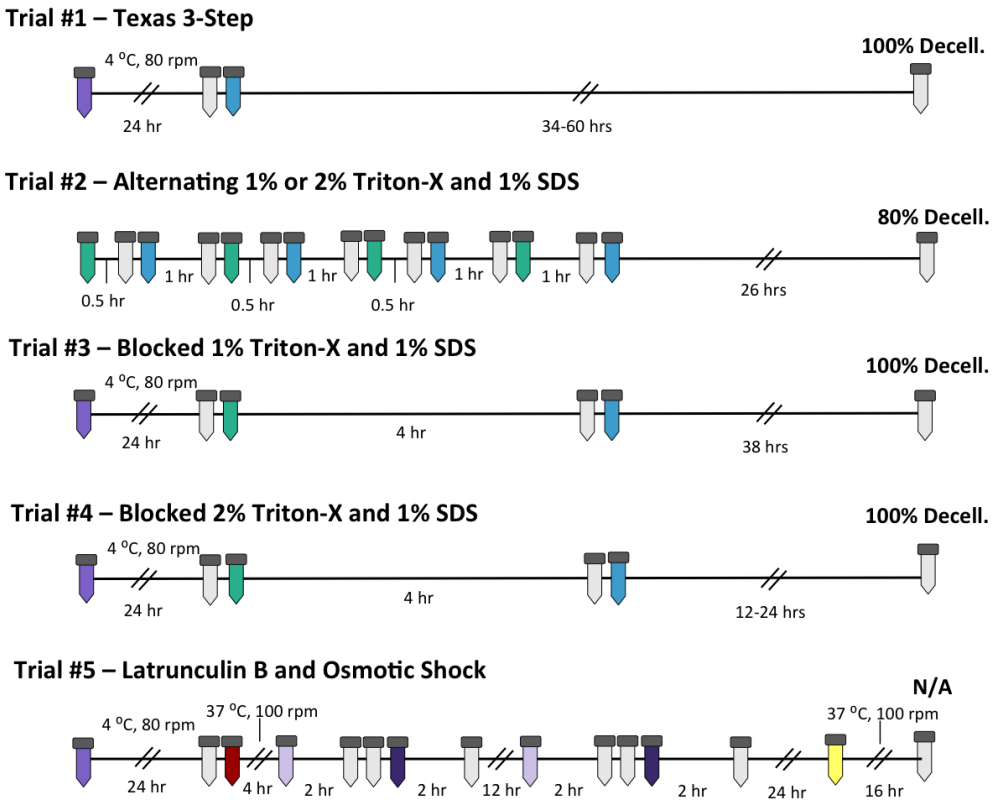

Figure S4.1. **Schematic of original decellularization methods testing during optimization of whole muscle decellularization protocol.** The methods attempted can be found in Figure 4S.1 were based on various methods I found in previous work [294-296]. So far, I have mostly focused on the TA and heart because those are thicker, harder to decellularize tissues. Once those are optimized, I will work on the diaphragm with may be sufficiently decellularized with a salt buffer. To prevent random tissue degradation, protease inhibitor is included in all buffers and refreshed daily when incubations last longer than 24 hours. All buffer volumes are adjusted to 20x of tissue weight to ensure sufficient solubilizing power. Blue represents SDS, green represents Triton-X, Purple represents different salt solutions, yellow represents DNAse I and red represents Latrunculin B.

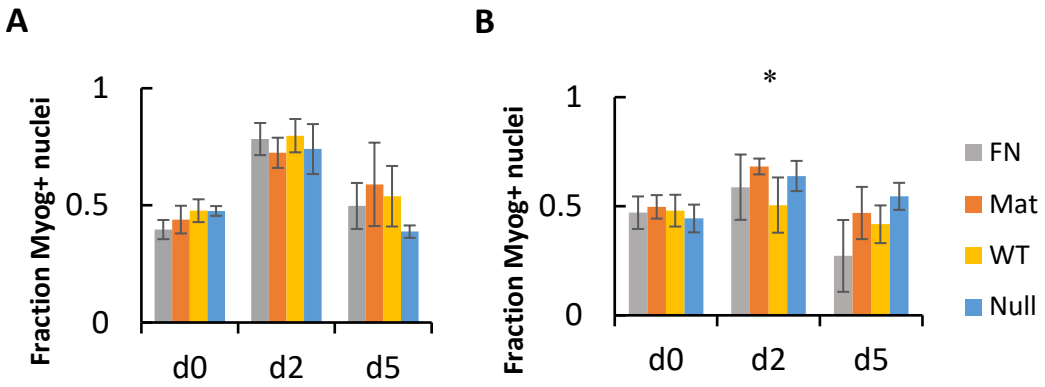

Figure S4.2 WT, A), and *Lmna* null B), cells show similar trends in Myogenin nuclear staining. Cell type was a significant factor at day two of differentiation ($p = 0.03$), showing lower expression on all substrates compared to WT cells.

Supplemental File S5.1: Grading Rubric for Conceptual Homework

Criteria	Mastering	Developing	Emerging
Problem Set Up	All known information is listed, a diagram is appropriately drawn and labeled and units are converted (when necessary). Unknown clearly specified.	All known information is listed, but either unit conversions are missing or diagram and labeling is missing or incorrect. Unknowns may be incorrectly determined.	Only some known information is listing with limited/no unit conversions or diagram with labeling
Assumptions and Problem Logic	All assumptions are listed and correct leading to identification of the appropriate equation.	Incorrect assumptions lead to incorrect equation.	Assumptions, and therefore problem logic, are missing. No way to determine conceptual grasp of problem.
Problem Solving Strategy and Skills	Student is able to link multiple concepts and multiple equations together to arrive at answer.	Student is able to partially develop a problem solving strategy, but at least one key concept is missing that prevents the student from completing the problem.	Multiple key concepts and/or relationships are missing such that the student is only able to begin the problem.
Organization and Neatness	Problem is written in a logical, step wise fashion that is easy to read and follow.	All problem components are present, but are disorganized, cramped, or otherwise difficult to read.	Problem is entirely disorganized, or illegible such that even if present, the other categories are impossible to score.
Critical Thinking	Student has provided a sound written and conceptual logic for feasibility or infeasibility of answer (or approach if problem was incomplete).	Student was able to determine whether an answer was feasible or not, but logic as to why is missing (or approach if problem was incomplete).	Student has not demonstrated that they evaluated the feasibility of their answer (or approach if problem was incomplete).

Supplemental File S5.2: Early Semester Survey for Two-Stage Homework System

Questions to be answered on a 1-5 scale.

- Pace of lectures. Do you find the pace of the lectures too slow (1), too fast (5), or about adequate (3)?

- Lecture organization. The lectures are well organized, and easy to follow. Completely agree (5); completely disagree (1).

- Lecture style. Is the balance of PowerPoint slides to work on the blackboard adequate (3), or too board heavy (5), or to PowerPoint heavy (1)?

- Lecture outcome. Do you feel like you understand the "take home point" of the lectures, and achieve the learning outcomes? Fully understand (5); completely confused (1).

- Friday Recitations. The Friday "recitation" style lectures are helpful. Complete agree (5), not helpful at all (1).

- Homework Feedback. The homework feedback helps me learn and reinforce the material. Completely agree (5), completely disagree (1).

- Homework Design. The two-stage homework helps me realize and correct my misconceptions. Completely agree (5), completely disagree (1).

Open-ended questions (free text response):

- What is something you would like to keep the same in the course moving forward?

- What is something you would like to change in the course moving forward?

- What is something you would like to keep the same about the homework moving forward?

- What is something you would like to change about the homework moving forward?

- Do you have any other comments or suggestions for the course?

Supplemental File S5.3: Early Semester Survey for Two-Stage Homework System

How well do the following do the statements describe you 1 being not at all and 10 being very well:

Homework Habits

1. I never work with other students on homework.

2. I disable notifications and avoid going on social media while I'm working.

3. When I don't know how to do a problem, I usually google the question to try and get help.

4. When I get stuck, I go on our class group chat to see what other students are doing.

5. I frequently *answer* peers questions on our group chat.

6. I like to do homework in a distraction free environment.

7. When I encounter new material I am confident that I can learn it.

8. I usually have facebook and other social media sites open while I'm working and take frequent breaks.

9. When I struggle to understand a concept, I find reading the textbook helpful.

10. I believe I can stay motivated, even when problems are difficult

11. Do you have any specific homework habits that you find particularly helpful in learning from homework?

Homework Process

1. I feel like I make slow progress and then all of a sudden how to do the question "clicks"

2. I usually know how to do the problems when after I sit down and look through my notes.
3. When I find a new idea or application in the homework, I am usually able to connect it back to what I already know from this or other classes

Response to Homework

1. I frequently feel overwhelmed by homework in *this class*

2. I frequently feel overwhelmed by the collective work that I have to do for *all of my classes*.

3. I spend much more time working on this class than I do my other classes.

4. I prefer the 2-stage homework system to normal homework.

5. I would recommend that other classes implement a similar homework system.

6. I feel like the 2-stage homework helps me learn

7. I believe that I can learn even the most difficult material if I try hard enough.

Do you have any other particular comments on how the 2-stage homework impacts your learning?

Supplemental File S5.4: Focus group questions for Two-Stage Homework System

Questions were modified from Bembenutty et. al. 2012

Background
1. Have you enjoyed the course?
2. How much do you feel you learned in the course?

Two-part homework system
1. What are your opinions of the two-part homework system?
2. Tell me about your positive experiences with the system.
3. Explain how your experiences differed from courses with a more traditional HW system (e.g. learning, course grade, time spent, etc.).
4. How could the instructors make the need to justify answers more clear?

Feedback
1. Were you more or less likely to pay attention to feedback on assignments?
2, Overall, how much do you like getting written feedback?
3. Would you have preferred a checkmark grade for the attempt of the first homework, and a numerical grade for the second homework?

Collaborations and resources
Did you use the solutions manual or other online sources for help on homework assignments?
How often did you collaborate on homework assignments?
How often did you use the online chat group?

Closing Remarks
If you were teaching the course, what would you change about the homework system?

Supplemental File S5.5: Additional analysis on factors contributing to conceptual understanding done in 2017 only

We also sought to evaluate other confounding factors outside of the two-stage homework system that could affect students' conceptual understanding. We used an end-of-semester Likert-scale based survey (**see Appendix 5C: End of Semester Survey**) with several questions graded on a scale from 1 – 10 to study students' self-efficacy and study habits.

We first focused on self-efficacy, or belief in one-self, as it has been reported to be the main factor linking homework grade to exam grade. We primarily focused on student responses to the questions focused on their reaction to new material, their persistence, and their self-confidence. We then used these responses to create categories of students' self-efficacy, as summarized in Table 1. We then found the average difference from homework Homework 2 to the exam across several concepts for each student self-efficacy category.

As expected, students with a high self-efficacy had the highest increase in conceptual understanding. Interestingly, persistence, regardless of confidence level, also led to an increase in conceptual understanding (see categories O, F, and P).

However, confident students spanned a large spectrum (n=11) and did not rank as highly as expected (rank 5 of 6). We therefore further analyzed the study habits of these confident students (**Table 5.S2**) by using the same end-of-semester Likert-scale based survey (**see Appendix 5C: End of Semester Survey**) based on questions related to

distractions. We primarily focused on whether they had a preference for no distractions, how frequently they took breaks, and how successful they were in creating a distraction free environment. We found that confident students with good study habits (**Category A in Table 5.S2**) showed the greatest improvement in conceptual understanding from home Homework 2 to the exam.

Table S5. 1 – Categories of student's efficacy ranked in difference in conceptual understanding from homework Homework 2 to the exam.

Categories	**Definition**	**n**	**Ranked difference from HW 2 to Exam**
V: Very Confident	Average > 8	6	1
C: Confident	Average > 6.67	11	5
O: Overall Confident but Not Persistent	Believe > 7, Persistent < 5	2	6
F: Overall Confident but Bad First Impressions	Believe > 7, New Material < 5	5	4
P: Persistent but Not Confident	Believe < 5, Persistent > 7	2	2
N: Not Confident	Average < 6	6	3

Table S5. 2– Categories of confident students' study habits associated with difference in conceptual understanding from homework to the exam.

Categories	**Definition**	**HW 2 to Exam**
A: Prefers no distractions and succeeds	Creation > 7, Breaks < 3	0.083
B: Prefers no distraction and fails	Distractions > 7, Breaks > 4	-0.306
C: No Preference / Likes Distractions	Preference < 6	-0.333

Supplemental File S6.1: Description of universe and final answer sheet

Below you will find the game scenario which includes the final answer sheet for the students to turn in when they solve all the rounds. You should make a table, like the one below that includes all the final answers per group so you can quickly check the final answer sheets.

Group	**Round 1**		**Round 2**	**Round 3**	**Round 4**
	Floor	*Object*	*Envelope Letter*	*Solvent Letter*	*Antidote Name*
1	3	Chair	I	B	Zombie Slayer
2	1	Flowers	H	H	Brain Food
3	2	Bench	D	B	Zombie Slayer
4	1	Chair	B	H	Brain Food
5	4	Stairs	J	B	Zombie Slayer
6	2	Chair	E	F	Drink Me
7	1	Tree	G	B	Zombie Slayer
8	2	Cubby	L	H	Brain Food
9	1	Stairs	K	F	Drink Me
10	4	Chair	A	B	Zombie Slayer

Supplies

- Challenge Round papers (printed either double or single sided as indicated below per round)
- Tape
- Scissors
- Envelopes (# of groups + 2) x (2 challenge solutions, Round 1 and Round 2)
- ≥4 containers for the final challenge

Location and Order of Round Presentation to Students

Provided to students at the beginning:

- Game/universe explanation (S1) – printed single-sided
- ASN Questions (S2) – printed double-sided w/Find the Floor
- Find the Floor Questions (S2) – printed double-sided w/ASN

Hidden throughout the building/floor (must be completed prior to the start of the game)

- Envelope labeled on the front with group number and filled with Color Coded Matching Questions (S3 – printed double sided), Envelope Map (S4 – printed single sided) and Color Coded Equation Sheet (S5 – printed single sided)

In Room

On Board/Wall (can be hung during Round 1)

- Envelopes labeled with Envelope Map Letters on the front and group numbers on the back that are filled with the Rank the Option Questions (S6 – printed single-sided)
- Bowls/Containers labeled (away from the students) with letter answers from rank the option questions that hold slips of paper indicating correct answers and the Find the Antidote Question (S7 – print single-sided) or notice of incorrect answer

It's almost the end of the semester, and all this rain is bringing more than soggy shoes and an almost insurmountable desire to lay around and binge watch Netflix. A top secret plant nearby was working on a zombie antidote for the upcoming zombie apocalypse, but all the rain followed by freezing temperatures caused their tank of zombie virus to burst! The scientists were the first to succumb as they tried to prevent the spill from reaching catastrophic levels….they failed. The virus spilled into the Lake of Shining Waters and all of the people living in downtown Awesome Town were transformed into zombies first thing in the morning when they drank their coffee. Greatest University on the Planet is still safe, because our water comes from a higher elevation and hasn't yet been contaminated, but all the Townies are starting to find the hill a mighty attractive place to feed their bloodlust.

A worker who had taken the day off was able to bring you the latest batch of solutions made as possible antidotes, but they didn't use waterproof markers to label them and all the labels washed off in the rain! You have only a very small amount of each sample, but this is the best chance you have to find a cure. Thankfully you've been studying for thermodynamics, and feel confident you can figure out what properties of the virus to attack, and how to determine which antidote will successfully bind with the virus in the cells!

Hurry though, you don't have much time to find the best antidote! In 150 minutes the zombies will be at your door <u>As you go, fill in the solutions to each round to turn in at the end of the game as proof that you found the correct antidote.</u>

Group Number: _____

Challenge Round One **Challenge Round Two**

Floor: _____ Envelope Letter: _____

Object: _____

Challenge Round Three **Challenge Round Four**

Solvent Letter: _____ Antidote Name: _____

Supporting File S6.2: Challenge Round One – ASN and find the floor

Below you will find the question sets and pairings that I used for Challenge Round 1 (ASN Questions and Find the Floor). When setting up this challenge, it is important to keep track of both the floor and hiding locations for each team. I suggest making both a question by question answer key as well as a table like the one below that summarizes the final answers for the challenge for each team. Each instructor present should be given a copy of both.

Group	Hidden Clue	Floor
1	Chair	3
2	Flowers	1
3	Bench	2
4	Chair	1
5	Stairs	4
6	Chair	2
7	Tree	1
8	Cubby	2
9	Stairs	1
10	Chair	4

ASN Questions: The correct answers for the ASN questions are shown in bold, while the answers that directly contribute to the clues are highlighted in yellow. If you shorten this section of the game, use the questions with yellow highlighted answers. The incorrect answers will result in decoy words to prevent students from guessing/searching for a word.

You can modify these codes for your own questions. Once you make up your questions and answers you can switch the letters so that the correct code letter matches the correct answer. Or, you can modify the yellow highlighted answers to make your own locations that work for your building/room. This will save you time in fully creating codes and hidden places.

Find the Floor: The answers are provided in the above table. If you change this question, make sure your answer is an integer value, or that you specify which digit (10s, 1s, 100s) of the question your students will use as their answer.

For the students: Before giving these questions to students, highlight all the text and remove the bold and highlighted answers. I recommend printing at least 2-3 copies per group so that everyone can read the questions. These sheets should be printed double sided.

Before the game: Take the print outs of Challenge Round 1 to the classroom, you'll hand them to the students. For the hidden clues, label an envelope for each group with the group number. Stuff the envelope with the three papers needed or Challenge Round 2: 1) color coded equation guide, 2) an envelope map with bar codes and instructions, and 3) a *question sheet specific for the group!*

Once all the envelopes are stuffed, use your table to hide all the clues. This needs to be done well in advance of students arriving so they don't accidently see you.

Examples are provided for the first three groups.

Group 1

1. When the atmospheric pressure = the vapor pressure, a liquid will boil
   B - Sometimes
   G - Always
   F - Never
2. When the experimentally determined change of free energy of mixing is less than 0, the two solutions will prefer to mix
   A - Sometimes
   O - Always
   E - Never
3. When Chi, the mixing parameter, is greater than 0, two solutions will not mix
   C - Sometimes
   N - Always
   S - Never
4. When the equilibrium constant for a reaction decreases with increasing temperature, the reaction is exothermic
   C - Sometimes
   H - Always
   T - Never
5. The real mixing entropy is greater than our calculated translational mixing entropy
   A - Sometimes
   U - Always
   H - Never
6. Adding a solute at x = 0.25 has no effect on the boiling temperature of a liquid
   P - Sometimes
   B - Always
   I - Never
7. The theoretical (based off our calculations) change in free energy of mixing the an accurate predictor of whether a solution will mix because it takes into account the entropy and enthalpy changes in mixing
   R - Sometimes
   O - Always
   B - Never
8. The equilibrium constant for mixing (K_{mix}) takes entropy into account
   Y - Sometimes
   T - Always
   S – Never

Find the location of your clue by writing the letters from the correct answers in order!
(Your clue word may be less than 8 letters long)

Group 1

The Zombie Virus is a circular plasmid that can have τ right handed or left handed turns as shown below.

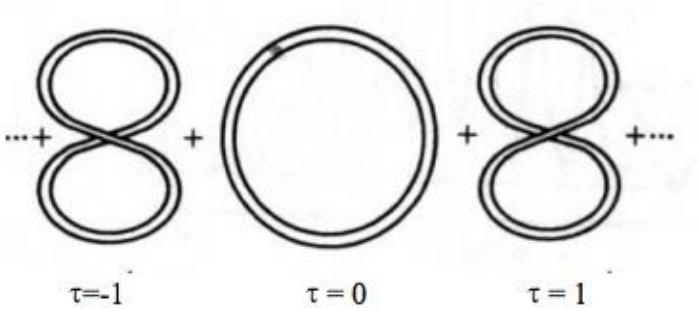

The energy in which is has τ turns is:

$$\varepsilon = \tau^2 B$$

Where B is a constant

If T = B/k, how many energy levels are populated, (i.e. have a probability rounding to 1%)?

The number of energy levels is the floor where your clue will be found!

Group 2

1. The experimentally determined change in free energy of mixing the most accurate predictor of whether a solution will mix because it takes into account the entropy and enthalpy changes in mixing
   B - Sometimes
   F - Always
   O - Never
2. When very similar chemical substances mix (pentane and octane for instance) we can assume that there is no change in the internal energy upon mixing
   W - Sometimes
   L - Always
   A - Never
3. We call what is mentioned above "real" mixing
   R - Sometimes
   I - Always
   O - Never
4. To use the partitioning equations, you will have three separate components for A, B, and S
   W - Sometimes
   N - Always
   D - Never
5. Adding a solute at x = 0.25 has no effect on the boiling temperature of a liquid
   D - Sometimes
   R - Always
   E - Never
6. The change in entropy of mixing an ideal solution is negative
   A - Sometimes
   O - Always
   R - Never
7. When the theoretical (based on calculations) change of free energy of mixing is less than 0, the two solutions will prefer to mix
   S - Sometimes
   W - Always
   O - Never
8. When the atmospheric pressure = the vapor pressure, a solid will sublimate
   X - Sometimes
   Q - Always
   R - Never

Find the location of your clue by writing the letters from the correct answers in order! (Your clue word may be less than 8 letters long)

Group 2

The Zombie Virus is a circular plasmid that can have τ right handed or left handed turns as shown below.

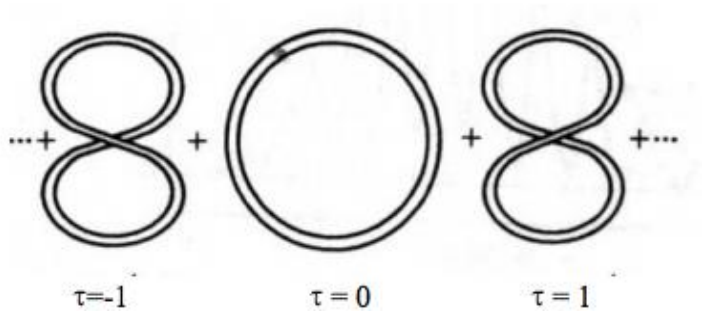

The energy in which is has τ turns is:

$$\varepsilon = (3\tau^2 + 3)B$$

Where B is a constant

If T = B/k, how many energy levels are populated, (i.e. have a probability rounding to 1%)?

The number of energy levels is the floor where your clue will be found!

Group 3

1. When the atmospheric pressure = the vapor pressure, a liquid will boil
   F - Sometimes
   L - Always
   T - Never
2. When the theoretical (based on calculations) change of free energy of mixing is greater than 0, the two solutions will prefer to mix
   B - Sometimes
   R - Always
   I - Never
3. When the equilibrium constant for a reaction increases with increasing temperature, the reaction is endothermic
   G - Sometimes
   E - Always
   A - Never
4. The change in entropy of mixing an ideal solution is positive
   S - Sometimes
   N - Always
   B - Never
5. The real mixing entropy is greater than our calculated translational mixing entropy
   C - Sometimes
   O - Always
   H - Never
6. Adding a solute at x = 0.25 has no effect on the boiling temperature of a liquid
   A - Sometimes
   O - Always
   H - Never
7. The equilibrium constant for mixing (K_{mix}) takes entropy into account
   K - Sometimes
   R - Always
   J - Never
8. Partial molar properties provide direct information on the properties of a single component of the system
   S - Sometimes
   T - Always
   D - Never

Find the location of your clue by writing the letters from the correct answers in order!
(Your clue word may be less than 8 letters long)

Group 3

The Zombie Virus is a circular plasmid that can have τ right handed or left handed turns as shown below.

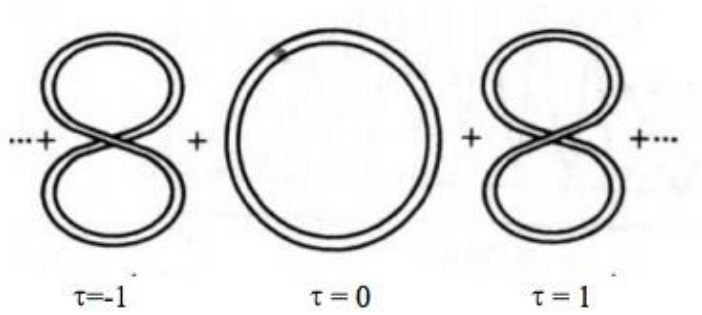

The energy in which is has τ turns is:

$$\varepsilon = (2\tau^2 + 2)B$$

Where B is a constant

If T = B/k, how many energy levels are populated, (i.e. have a probability rounding to 1%)?

The number of energy levels is the floor where your clue will be found!

Supporting File S6.3: Challenge Round Two – Color-coded equation sheets

Below are the components for Challenge Round 2 – color-coded equations. Each group will find three papers 1) the color coded equation sheet, 2) the bar coded envelope map, and 3) the specific question sheet per group in their envelope at the end of Challenge Round 1. The color-coded equation sheet is color coded by sub-topic (i.e. blue is general thermodynamics, green is reaction equilibrium, orange is general relationships that may apply to many different subtypes of equilibrium and etc.) You should create logical color groups out of your own equations. If you already have a set of review questions, you could write out the answers and create your equation bank from that.

I recommend having a list of each individual question and the solution, as well as the color code answers for each group for each instructor, such as the table below.

Question	**Equations Needed**
1. Ethalpic vs entropic contributions	2 purple, 2 orange
2. Salt needed to melt road ice	1 black, 1 blue
3. Real Housewives of Greece	2 yellow
4. ΔG and K_{eq} for aA + bB -> cC reaction	2 green, 2 orange
5. Solute S partitioning between A and B	1 purple, 1 orange, 2 pink, 1 blue
6. Determine sing of ΔG without calculations	3 orange, 1 green, 1 blue
7. Pooh Bear and ΔH_{mix}	2 purple, 2 orange
8. Plague antibiotic partitioning	3 orange, 2 pink
9. Liquid helium balloons	1 yellow
10. Salt vs glucose ice melting	1 black, 1 blue
11. ATP coupled reaction	1 green, 1 orange
12. Powerpuff girls ΔS	1 purple, 2 blue
13. Blood brain barrier tumor drug	1 blue, 1 orange, 2 pink
14. CO_2 vs O_2 transport and partitioning	1 orange, 1 green
15. Mixing 2 liquids based on Chi	1 orange, 1 purple

The bar codes are based on alphabetizing the number of each equation color. For instance, in this case, the alphabetized colors are black, blue, green, orange, pink, purple, yellow. You may choose different colors, which would change the bar code.

Group	**Barcode**	**Solution Envelope Letter**
1	**1337232**	**I**
2	**12310221**	**H**
3	**1423211**	**D**
4	**1337212**	**B**
5	**1138222**	**J**
6	**1327232**	**E**
7	**1434221**	**G**
8	**1228211**	**L**
9	**1326222**	**K**
10	**1338221**	**A**

Samples of the envelope map with instructions and a color-coded equation sheet are shown below. Both of these documents can be found in S4 and S5, respectively.

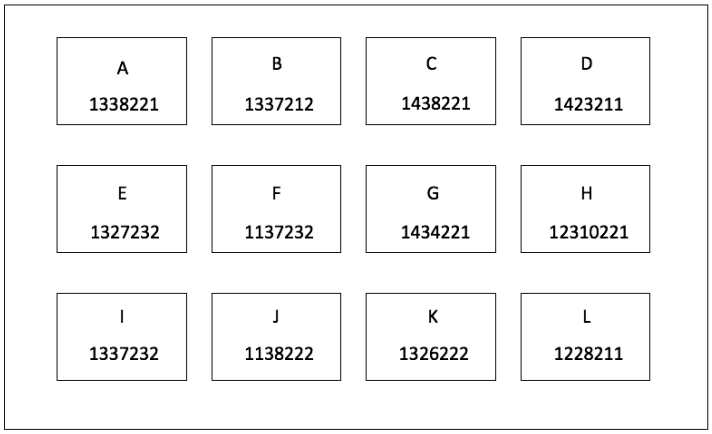

A 1338221	B 1337212	C 1438221	D 1423211
E 1327232	F 1137232	G 1434221	H 12310221
I 1337232	J 1138222	K 1326222	L 1228211

Envelope Map

1. *Determine the total number of each color equation you need to solve your problem set*
2. *Alphabetize the color names (i.e. blue, purple, yellow)*
3. *Write the number of equations for each color in order to make a barcode*
4. *Find your envelope!*

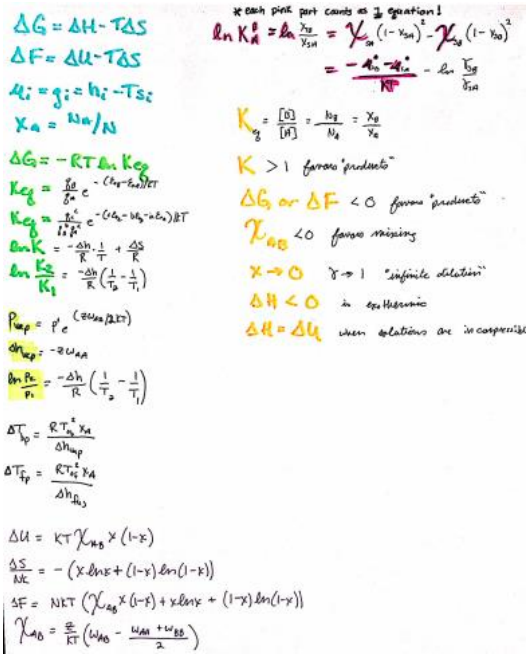

Before the Game: Before stuffing the Round 1 envelopes with these materials, you'll need to make sure to remove all answers that you've added for your benefit while creating barcodes and maps. The question sheets provided here should be printed double sided in duplicate so everyone in the group can see the questions. The equation sheet and envelope map should be printed single sided. *Take care that you stuff the envelopes with the correct team problems.*

You'll also need to also prepare the materials for Challenge Round 3 (Rank the Options) and have the envelopes lettered and stuffed by group according to the envelope map. You should write the group number on the back of the envelope so that the students have a check for their solution. You should then tape the envelopes on the board or wall for the students to be able to find.

Group 1

1. What is the equation for the change in free energy of mixing we derived in class?
    a. What are the signs of the enthalpic and entropic components of this equation?
    b. Comment on the how the signs of the enthalpic and entropic component determine the change in free energy of the system, and what drives the minimization of free energy.
    c. Why is it mathematically difficult to compute the real change in free energy of mixing based on our derivation of ΔS, consider the case of mixing of CO_2 and blood for your discussion? [3]

    2 purple, 1 orange

2. The weather this year is, shall we say, drunk. It's April and it's still snowing. Ithaca has hired you to determine an estimate of the additional salt needed to handle the continued presence of winter. The temperature outside is 20^o F and as a sample to start scale up, you assume you have 100 ml of ice. How much NaCl will you need to melt the ice in moles? T_{fus} = 32 F, ΔH_{fus} = 11,443.7 J/mol, MW water = 18.02 g/mol [2]

    1 black, 1 blue

3. Last time on "Real Housewives of Greece," we saw Aphrodite and Artemis get into a heated argument. Zeus demanded that both of them make a trip to the Cave of Wonders for meditation which is a secret escape of the God's below sea level. After a long trek down Mt. Olympus which is at 0.2 atm up in the clouds, to the depths of the cave, at p = 2.34 atm, Aphrodite decides to settle in and cook her favorite meal…spaghetti! She starts a fire and sets the pot of water, but after waiting until it reaches 80 C, she starts to get impatient because it hasn't boiled yet. Water has always boiled at 80 C when she makes it on Mt Olympus!
    a. Why won't the water boil?
    b. Calculate the new boiling temperature of water if the Δh = 40.66 kJ/mol.
    c. What is the bond energy of water in this equation? Assume z = 4. [2]

    2 yellow

4. You are evaluating the chemical equilibrium of a reaction aA + bB -> cC. You know that $q_A = 0.02$, $q_B = 0.06$ and $q_C = 0.09$. The cumulative difference in ground states between the products and reactants is – 50 J/mol. You can assume that this is a simple addition reaction and all stoichiometric coefficients equal 1. Determine i) the equilibrium constant for this reaction, ii) the Gibbs free energy of this reaction and iii) explain the relationship between Gibb's Free Energy and the K_{eq}. [4]

2 green, 2 orange

5. Given a solution of 2 immiscible solvents A and B with a solute S.
    a. Calculate the χ_{SA} and χ_{SB} at 295 K assuming that z =4 if $w_{ss} = -25$, $w_{AA} = -95$, $w_{BB} = -5$, $w_{SA} = -2$, and $w_{SB} = -96$. All interaction energies are in J/mol. What phase would you predict the solute to be in based off of these values?

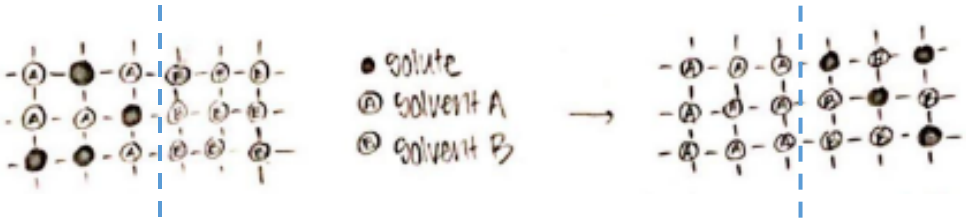

    b. The below pictures shows A, B, and S, before and after they reach equilibrium. Assuming each dot is a mole, calculate K_A^B for this equilibrium. [5]

1 purple, 1 orange, 2 pink, 1 blue

6. The equilibrium constant for the reaction 2A + B -> C + 2D is $K_1 = 1000$ at $T_1 = 50$ C.
    a. **Without doing any calculations**, what will the magnitude (small, large) and sign of ΔG be for this reaction?
    b. **Without doing any calculations,** given that $K_2 = 600$ at $T_2 = 60$ C, is this reaction endothermic or exothermic? What will the sign of ΔH be?
    c. Determine at which temperature the reaction will switch from being enthalpically to entropically driven. Comment on your answer. [5]

3 orange, 1 green, 1 blue

Group 2

1. Pooh bear wants to make some honey-water on a hot day to cool off. Pooh bear really likes honey, so he wants his drink to be 50:50 honey and water.
    a. Will honey and water mix at room temperature, 298 K, based on the exchange parameter? Assume that ΔH_{mix} = 2 J/mol and z = 6.
    b. Calculate the ΔF_{mix} and discuss whether enthalpy or entropy is driving the mixing. [3]

    2 purple, 2 orange

2. You want to travel back in time to 1665 to cure the world of the plague. You bring with you an antibiotic called chloramphenicol, C, which when injected into a vein, can be used to treat the plague.
    a. In order to fight the plague, we must get a chloramphenicol concentration of 0.0019 M in the cerebral spinal fluid which requires a blood concentration of 0.005, an easily achievable value in the blood. Find partition coefficient that is necessary for treatment? Please comment on your answer and which phase the drug prefers to be in.
    b. Given that one of the symptoms of plague is a 40.5 C fever, and knowing that $\Delta\mu^o$ of transferring the drug from the blood to the cerebral spinal fluid equals 2500 J/mol, how will the effectiveness of the drug be impacted by the temperature? [5]

    3 orange, 2 pink

3. You are at a birthday party with your friend who wants to make liquid helium from the gas inside a balloon at room temp (298 K).

    a. Using the phase diagram, determine the required temperature to change gaseous helium to liquid at 2 MPa. Will your friend be able to get liquid Helium, why or why not?
    b. Using the phase diagram to estimate two points, calculate a rough value for ΔH_{vap}. [1]

    1 yellow

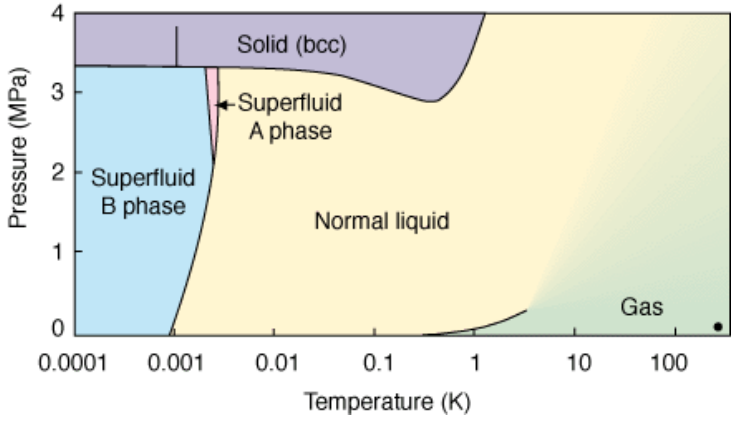

4. Explain why salt decreases the freezing point of water more than glucose if they are added into water at the same mole fraction.
    a. What mole fraction of salt would be necessary to add to water to decrease the freezing point by 5 ^{o}C given that Δh_{fus} = 6000 J/mol and T_{fp}^{o} = 273 K. [2]

    1 black, 1 blue

5. You are evaluating the chemical equilibrium of a reaction aA + bB -> cC. You know that q_A = 0.02, q_B = 0.06 and q_C = 0.09. The cumulative difference in ground states between the products and reactants is – 50 J/mol. You can assume that this is a simple addition reaction and all stoichiometric coefficients equal 1. Determine i) the equilibrium constant for this reaction, ii) the Gibbs free energy of this reaction and iii) explain the relationship between Gibb's Free Energy and the K_{eq}. [4]

    2 green, 2 orange

7. The equilibrium constant for the reaction 2A + B -> C + 2D is K_1= 1000 at T_1 = 50 C.
    a. **Without doing any calculations**, what will the magnitude (small, large) and sign of ΔG be for this reaction?
    b. **Without doing any calculations,** given that K_2 = 600 at T_2 = 60 C, is this reaction endothermic or exothermic? What will the sign of ΔH be?
    c. Determine at which temperature the reaction will switch from being enthalpically to entropically driven. Comment on your answer. [5]

    3 orange, 1 green, 1 blue

Group 3

1. You have a reaction with a ΔG^o = 5.8 kJ/mol at 298 K.
    a. Is this reaction favorable or unfavorable?
    b. What is the K_{eq} for this reaction.
    c. You want to couple the reaction with ATP which has a ΔG^o = -30.5 kJ/mol, what is the new equilibrium constant for the reaction when it is coupled with ATP assuming that ATP, ADP and P_i have a concentration of 5mM, 6mM, and 2 mM respectively. [2]

    1 green, 1 orange

2. The weather this year is, shall we say, drunk. It's April and it's still snowing. Ithaca has hired you to determine an estimate of the additional salt needed to handle the continued presence of winter. The temperature outside is 20° F and as a sample to start scale up, you assume you have 100 ml of ice. How much NaCl will you need to melt the ice in moles? T_{fus} = 32 F, ΔH_{fus} = 11,443.7 J/mol, MW water = 18.02 g/mol [2]

    1 black, 1 blue

3. You are at a birthday party with your friend who wants to make liquid helium from the gas inside a balloon at room temp (298 K).

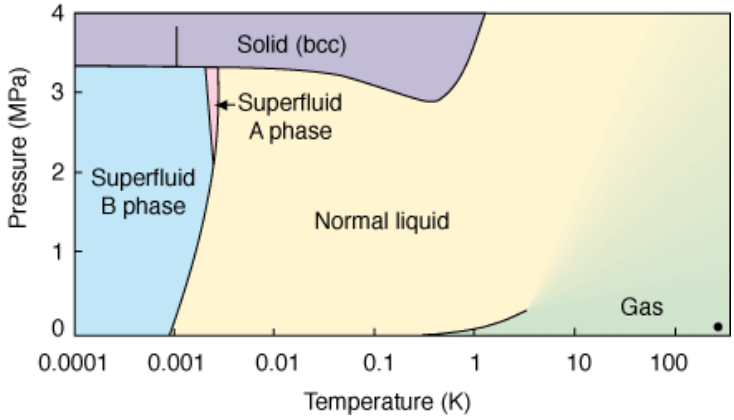

    a. Using the phase diagram, determine the required temperature to change gaseous helium to liquid at 2 MPa. Will your friend be able to get liquid Helium, why or why not?
    b. Using the phase diagram to estimate two points, calculate a rough value for ΔH_{vap}. [1]

    1 yellow

4. Sugar, spice, and everything nice. These are the ingredients chosen to create the perfect little girl, but Professor Utonium accidentally added an extra ingredient to the concoction: CHEMICAL X. Assume 1 mole of CHEMICAL X is added to 4 moles of the concoction.
    a. Calculate ΔS for mixing the concoction with Chemical X
    b. Given that $\Delta U = 41562$ J, calculate the temperature at which the concoction and CHEMICAL X becomes spontaneous, and thus the Powerpuff Girls are born! [3]

1 purple, 2 blue

5. The blood brain barrier prevents access of polar molecules to the brain. You are designing a drug that targets a brain tumor and must pass through the barrier. You know that $g_{D\text{-}Bl} = 4$ kcal/mol and $g_{D\text{-}Br} = 8$ kcal/mol, where Bl represents blood, and Br represents brain, at body temperature, 37 C.
    a. Find the equilibrium constant of the drug transferring from the blood to the brain.
    b. Assuming that you need a higher concentration in the brain than the blood, will this drug be effective? [4]

1 blue, 1 orange, 1 pink

6. CO_2 and O_2 are able to dissolve in the blood to transport waste or nutrients from the lungs to the tissues and vice versa.
    a. Given that O_2 has a $x_O = 0.003$ and CO_2 has a $x_C = 0.06$ in the blood, determine which gas is more likely to transfer into the blood from a pure gaseous phase at 37 C.
    b. If a patient has a fever of 39 C, how will the equilibrium constant be effected given that $\Delta H = 66.34$ kJ/mol [2]

1 orange, 1 green

Supporting File S6.4: Challenge Round Two – Color-coded bar code envelope map

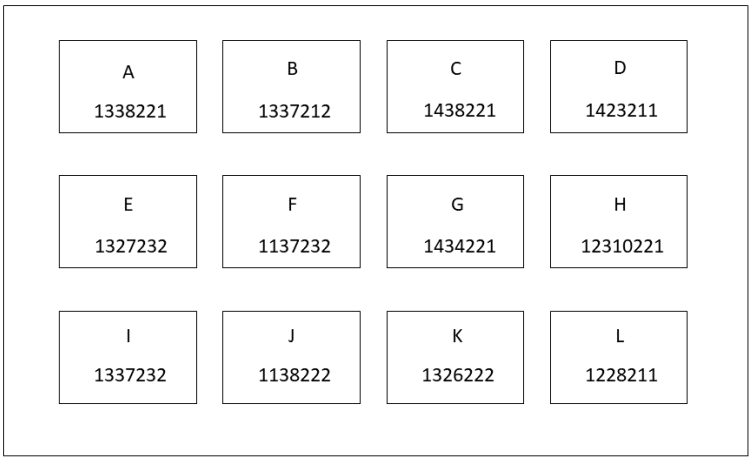

Envelope Map

1. *Determine the total number of each color equation you need to solve your problem set*
2. *Alphabetize the color names (i.e. blue, purple, yellow)*
3. *Write the number of equations for each color in order to make a barcode*
4. *Find your envelope!*

Supporting File S6.5: Color-coded equation sheet

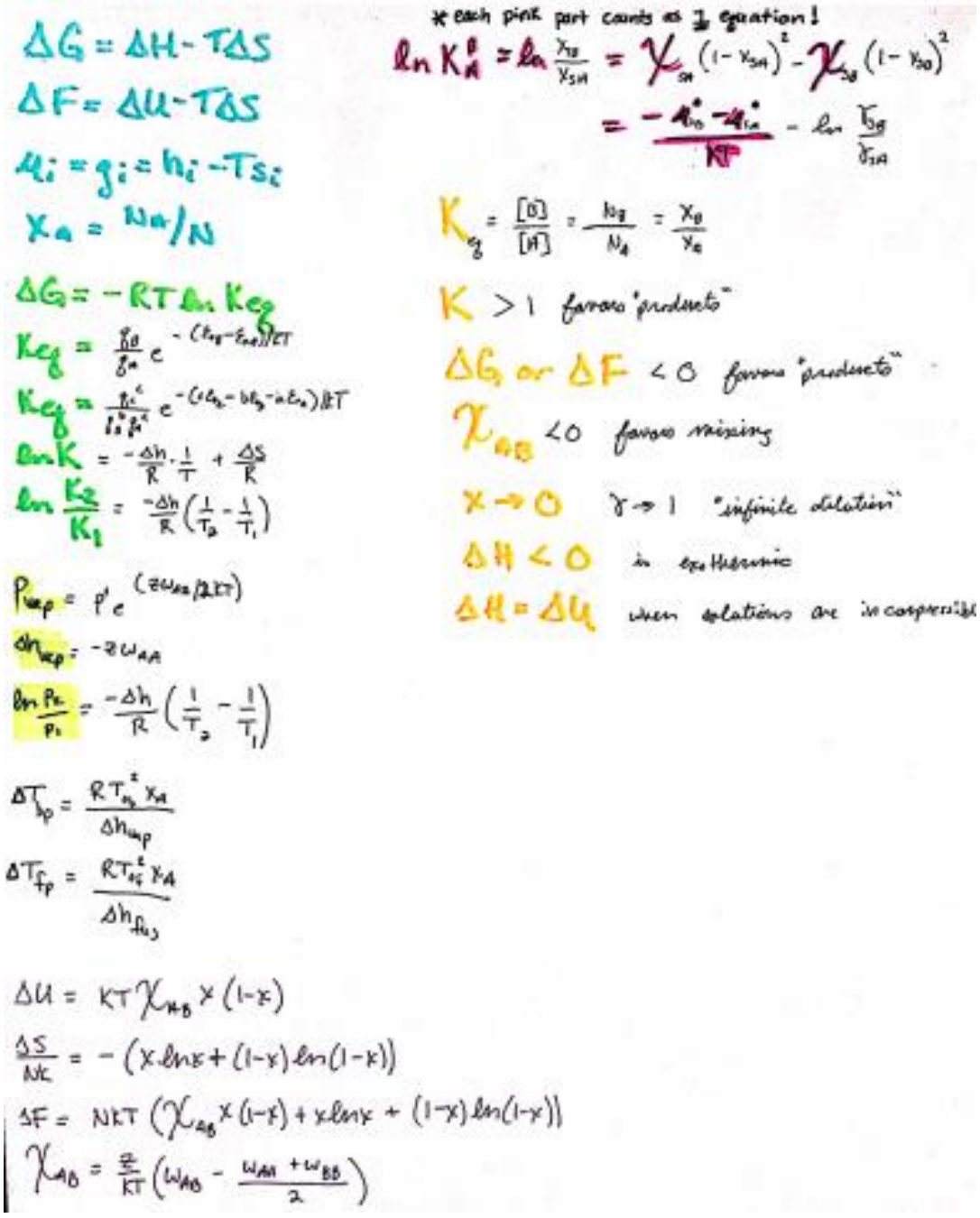

Supporting File S6.6: Challenge Round Three – Rank the options

On the following pages, you fill find the Rank the Options Questions for all the groups. The students will find this information at the end of the Color Coded Equation Challenge from the envelope matrix on the board. The question I picked here required students to take notice of the direction of solute movement and the subsequent sign of the various components. Switching the signs would result in a reversal of the order, and the selection of the incorrect answer, although the rest of the math was quite simple.

Each team has two options that can solubilize the solute and two that will not. I asked students to select the second-best option so that they would need to do all the problems out instead of just guessing. Below is a table of the two most effective solvents for each group – the ineffective solvents are not listed but are different for each group.

Group	Best Option	Second-Best Option
1	F	B
2	F	H
3	I	B
4	I	B
5	I	B
6	I	F
7	H	B
8	F	H
9	I	F
10	H	B

Before the game: The half sheets below will need to be printed single sided in duplicate and stuffed in the Color Coded Equation envelopes. Each envelope should be labeled on the front with the correct letter from the Color Coded Challenge and on the back with the team number. You'll need to create and label the bins for the students to find their answers for this round in. The bins should be labeled and placed facing the wall so that the answers can't be seen. Here, there are three correct answer bins (B,H,F) and you could pick any number of incorrect options (C and J are the two most common second worst options that would result from getting the sign incorrect). The correct bins should contain slips of paper with the challenge for the next round (Find the Antidote) and the incorrect bins should contain slips of paper that direct students to try again and think about the key concept of the question (in this case sign) that are included with the question sheets in S6.7.

Group 1

You need to find a way to neutralize or remove the zombie plasmid from both the water and the blood of the zombies. Thankfully, water and blood both behave as similar chemicals when it comes to thermodynamics.

Rank, from best to worst, which of the 4 chemicals listed below will **be able to get the plasmid out of the water** at 37 C. W = water phase and C = "chemical" phase. The second best one will tell you which bin contains your next challenge.

Chemical	$h_W - h_C$	$s_W - s_C$	$\mu_w - \mu_c$
B	-340	-5	
D	-50	75	
G	100	25	
F	250	-15	

Group 2

You need to find a way to neutralize or remove the zombie plasmid from both the water and the blood of the zombies. Thankfully, water and blood both behave as similar chemicals when it comes to thermodynamics.

Rank, from best to worst, which of the 4 chemicals listed below will **be able to get the plasmid out of the water** at 37 C. W = water phase and C = "chemical" phase. The second best one will tell you which bin contains your next challenge.

Chemical	$h_W - h_C$	$s_W - s_C$	$\mu_w - \mu_c$
C	-500	50	
G	100	25	
H	800	-10	
F	250	-15	

Group 3

You need to find a way to neutralize or remove the zombie plasmid from both the water and the blood of the zombies. Thankfully, water and blood both behave as similar chemicals when it comes to thermodynamics.

Rank, from best to worst, which of the 4 chemicals listed below will **be able to get the plasmid out of the water** at 37 C. W = water phase and C = "chemical" phase. The second best one will tell you which bin contains your next challenge.

Chemical	$h_W - h_C$	$s_W - s_C$	$\mu_w - \mu_c$
B	-340	-5	
E	-1000	-2	
G	100	25	
I	10	-100	

Supporting File S6.7: Challenge Round Four – Find the antidote

Below you will find the questions and information for the students to solve which of two possible antidotes will be the best option for halting the zombie virus in its tracks. Whatever you decide to put for this question, you should make an answer key similar to the one below.

Group	Round 4
	Antidote Name
1	Zombie Slayer
2	Brain Food
3	Zombie Slayer
4	Brain Food
5	Zombie Slayer
6	Drink Me
7	Zombie Slayer
8	Brain Food
9	Drink Me
10	Zombie Slayer

Before the Game: You should select 4 suitable boxes or containers and label them with chemical letter answers from Challenge Round 3. You should print out at least 10 copies of the following sheets so that each group can get two half sheets to look at and all the containers will still look viable for the last groups. The Find the Antidote sheets should be printed single-sided.

Finishing the Game: Once the students have answered this question they have completed the whole Challenge and have saved the town from certain doom! They should fill out all their answers on the sheet and you should reward bonus points or prizes as you previously determined.

Chemical B

Now that you know which chemical will pull the plasmid out of the blood/water of the city, you need to figure out which antidote to use to break it down and destroy it.

You have two options,

Walking Live	**Zombie Slayer**
$\Delta H^{\pm}$ = 10 kcal/mol	E_A* = 15 kcal/mol
$\Delta S^{\pm}$ = 2 cal/mol	ΔH = 7 kcal/mol
	A = 5 x 10^{12}

1) Calculate the forward rate coefficient for "Walking Live" and "Zombie Slayer" at 27 °C.
2) Which of these two antidotes will go to work the fastest on the plasmid?

Chemical F

Now that you know which chemical will pull the plasmid out of the blood/water of the city, you need to figure out which antidote to use to break it down and destroy it.

You have two options,

Eat Me	**Drink Me**
$\Delta H^{\pm}$ = 10 kcal/mol	E_A* = 15 kcal/mol
$\Delta S^{\pm}$ = 2 cal/mol	ΔH = 7 kcal/mol
	A = 5 x 10^{12}

3) Calculate the forward activation energy and rate coefficient for "Eat Me" and "Drink Me" at 27 C.
4) Which of these two antidotes will go to work the fastest on the plasmid?

Chemical H

Now that you know which chemical will pull the plasmid out of the blood/water of the city, you need to figure out which antidote to use to break it down and destroy it.

You have two options,

More Gutz	Brain Food
$\Delta H^{\pm}$ = 10 kcal/mol	E_A* = 15 kcal/mol
$\Delta S^{\pm}$ = 2 cal/mol	ΔH = 7 kcal/mol
	A = 5 x 10^{12}

1) Calculate the forward activation energy and rate coefficient for "More Gutz" and "Brain Food" at 27 C.
2) Which of these two antidotes will go to work the fastest on the plasmid?

Better luck next time…

You made a crucial error in your calculations! Go back and re-evaluate your work especially your assumptions about which way the solute was traveling.

You have two options,

Throw in the Towel	I Believe I Can Fly